Molybdenum-95 and nitrogen-15 as probes in nitrogen fixation related nuclear magnetic resonance studies

Thesis

MOLYBDENUM-95 AND NITROGEN-15 AS PROBES IN NITROGEN FIXATION RELATED NUCLEAR MAGNETIC RESONANCE STUDIES

A Thesis presented in the
Department of Chemistry of the Open University
for the degree of
Doctor of Philosophy

by

Mark Hughes B.Sc.

December 1984

Date of Submission: 28th October 1985
Date of Award: 30th April 1986

To My Parents

CONTENTS

ACKNOWLEDGEMENTS

I wish to thank my supervisors, Dr. R.L. Richards (AFRC) and Dr. J. Mason (OU) for their help, encouragement and guidance throughout this study. I should also like to express my gratitude to all my friends and colleagues in the Unit of Nitrogen Fixation for making the three years of this project both enjoyable and productive. Special thanks go to Miss Caroline Shortman for her excellent proof-reading and help with the final stages, and to Drs. Richard Henderson and David Stanley for helpful discussions. Finally, I am indebted to Miss Beryl Scutt for her speedy and efficient typing of this thesis, to the AFRC for providing excellent facilities and the SERC for support and high-field NMR services.

STATEMENT

The work described in this thesis, carried out largely in the AFRC Unit of Nitrogen Fixation from October 1981 to November 1984, is that of the author and has not been submitted in any form for any other degree.

Signed .....

Mark Hughes

ABSTRACT

This thesis examines the application of ^{15}N and ^{95}Mo Nuclear Magnetic Resonance Spectroscopy in studies relevant to nitrogen fixation and describes further development of technique.

Chapter 1 provides a general introduction to the study of nitrogen fixation but with reference to some specific examples of areas of interest.

Chapter 2 is in two sections, the first dealing with the practical aspect of NMR spectroscopy and particularly the problems involved with the study of ^{15}N and ^{95}Mo. The second section gives a general introduction to nuclear magnetic shielding theory and shows some of the ways in which this has been applied.

Chapter 3 describes the effect of change in co-ligands on the physical properties of some nitrosyl and diazenido-complexes.

Chapter 4 discusses a possible spectrochemical series of ligands based on the ^{95}Mo NMR parameters of complexes.

Chapter 5 deals with the use of ^{15}N NMR spectroscopy to probe the structure of nitrogenous ligands which show some form of structural isomerism.

Chapter 6 is a compilation of data obtained by NMR spectroscopy on protonation reactions involving dinitrogen and hydrazido(2-)-complexes, with some possible interpretations.

Chapter 7 mentions initial enzyme studies by ^{95}Mo NMR spectroscopy and concludes with some general comments and suggestions for the direction of future work.

ABBREVIATIONS

Å	Angstrom (10^{-10} M)
Ar	general aryl group
Bu^t	tertiary butyl - $(CH_3)_3C$
Br	broad
Cp	cyclopentadienyl - η^5-$C_5H_5^-$
C.T.	charge transfer
δ	chemical shift
dArpe	$Ar_2PCH_2CH_2PAr_2$
depe	$Et_2PCH_2CH_2PEt_2$
dppe	$Ph_2PCH_2CH_2PPh_2$
dtc	general dithiocarbamate
dme	dimethoxyethane
dmf	N,N-dimethylformamide
EDTA	ethylenediaminetetraacetic acid
EPR	electron paramagnetic resonance
Et	ethyl - CH_2CH_3
$E_{\frac{1}{2}}^{ox}$	half-wave oxidation potential
ν	frequency
Hz	Hertz
HOMO	highest occupied molecular orbital
i.r.	infra-red
I	spin quantum number
J	coupling constant
L	neutral ligand
LUMO	lowest unoccupied molecular orbital
M	metal

MO	molecular orbital
Me	methyl - CH_3
γ	magnetogyric ratio
NMR	nuclear magnetic resonance
NOEF	Nuclear Overhauser Enhancement Factor
P	general tertiary phosphine
P P	chelating ditertiary phosphine
ppm	parts per million
Ph	phenyl - C_6H_5
Pr^i	iso-propyl - $CH(CH_3)_2$
Pr^n	normal propyl - $CH_2CH_2CH_3$
R	general alkyl group
r.f.	radio frequency
r.m.s	root mean square
σ	shielding term
s.c.e.	saturated calomel electrode
thr	tetrahydrofuran
TMP	trimethylphosphite
X,Y	anionic ligand

CHAPTER 1

The Study of Nitrogen Fixation

1.1 Introduction

The field of nitrogen fixation covers a very wide area of science, from industrial processes to the detailed study of the genetics of nitrogen-fixing microorganisms. The extent of research in the field is exemplified by the regular appearance of comprehensive reviews of advances in the chemistry,[1,2,3] the biochemistry,[1,3] and the biology[1] and genetics[1,3,4] of nitrogen fixation. There are also several texts dealing with more general aspects *e.g.* Postgate in reference 5. It is not the intention below to present another such detailed review of the field, but instead to expound some of the basic principles and select various examples of the work in the AFRC Unit of Nitrogen Fixation which help to put the present study into context.

1.2 The sources of fixed nitrogen

The abundant dinitrogen molecule may be converted into forms available to plants in a variety of ways. Oxidative processes mainly involve lightning and combustion, generating NO_x species (increasingly an occupation of man, through pollution). Reductive processes include man's more deliberate contribution to fixation via the well-known Haber Process. The large scale production of ammonia from nitrogen and hydrogen involves extremes: pressure, temperature, and cost, the latter because of the necessity

of fossil fuel feedstocks to provide the hydrogen, and also the expense of the complex plant required. The conditions are harsh even with the presence of a catalyst as shown in reaction (1.1), conversion is low and the mechanism of reaction is still not clear.

$$N_2 + 3H_2 \xrightarrow[350\text{-}1000\ \text{atm.}\ 300\text{-}400^\circ C]{\text{promoted iron-alumina catalyst}} 2NH_3 \qquad (1.1)$$

The increasing world population and demand for food mean that even larger amounts of NH_3 must be made by the Haber Process. In fact, total input of fixed nitrogen into the environment is one of the few areas where this process competes with microorganisms, providing ca. 50% of that provided by the biological mechanisms. It is also worth noting that addition of fertiliser to the land does not guarantee it reaching the plant, and raises the growing problem of nitrate leaching into water supplies.

The major source of fixed nitrogen is through micro-organisms, either free-living (e.g. Klebsiella pneumoniae, Kp) or in association with higher plants (e.g. Rhizobia). The latter types are important in agriculture as they provide fixed nitrogen directly at the site of need, as in the root nodules of the legumes.

1.3 Enzymatic reduction of dinitrogen

1.3.1 The structure of the enzyme

Only certain microorganisms are endowed with the capability to reduce N_2 and responsible for this function is an enzyme system: nitrogenase. The system consists of two types of protein, the Fe protein (component I) and the MoFe protein (component II). Both of these proteins are necessary for the reduction of N_2 and both are irreversibly damaged by oxygen. The Fe protein has a molecular weight of ca. 60,000 and contains one Fe_4S_4 cluster. It is involved in the transfer of electrons to the MoFe protein in a reaction involving MgATP (ATP = adenosine triphosphate). The MoFe protein, with a molecular weight in excess of 200,000, contains the site at which substrates are reduced. The protein of Kp contains 2 molybdenum atoms, 32±3 Fe atoms and more than 15 acid-labile sulphur atoms.[5] Each Mo is arranged in a MoFeS cluster which can be extracted from the protein as the iron-molybdenum cofactor or FeMoco. This cofactor has been much studied and recent evidence confirms that it contains the active site.[6] One of the elements of this research is interesting as it emphasises the contribution that genetics can make to solving essentially biochemical problems. Briefly, a mutant strain of Kp was produced which synthesises a form of nitrogenase that can reduce acetylene better than N_2. The FeMoco extracted from this mutant when used to reconstitute another mutant nitrogenase, this time containing no FeMoco, confers its substrate specificity to the host enzyme.

Several spectroscopic techniques have been employed in attempts to probe the structure of FeMoco including electron nuclear double resonance (ENDOR),[7] electron paramagnetic resonance (EPR),[8] Mössbauer[9] and extended X-ray absorption fine structure (EXAFS) spectroscopy.[10] The latter technique is particularly useful as it can give information about the general type, number and distance of ligand atoms around the Mo centre in the cofactor. The technique depends on comparison with model complexes and indicates that the Mo is surrounded by 2-3 Fe atoms, 3-4 proximal S atoms and 1-2 more distant S atoms.[10]

EPR provides information about the paramagnetic centres in the FeMo protein. The signals observed have been shown to be associated with the Fe atoms of the protein and during turnover under ethylene certain signals assignable to Fe atoms of FeMoco have been detected.[11]

Mössbauer spectroscopy of ^{57}Fe atoms in the FeMo protein shows that 6 Fe atoms are associated with the paramagnetic centre discussed above.[9]

ENDOR spectroscopy involves observation of EPR while a nuclear spin transition is saturated and has provided evidence that Mo may also be involved in the FeMoco EPR-active species.[7]

When the nitrogenase enzyme is turning over, the EPR signals of the FeMo protein are greatly diminished in intensity.

From this sort of evidence a general picture of the FeMo protein can be built up and a schematic diagram is shown in Figure (1.1).

Figure (1.1):

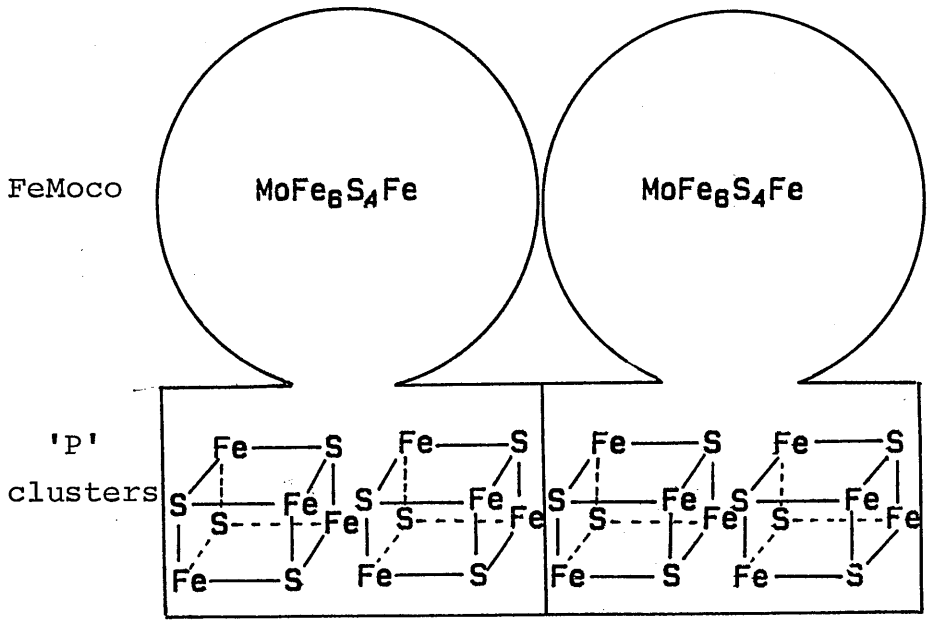

It is important to point out that no unequivocal proof exists that the substrate binds to the Mo atom in FeMoco, although a mass of circumstantial evidence and comparison with chemical models makes this is a commonly-held belief.

1.3.2 Nitrogenase mode of action

The essential task of the enzyme system is to channel electrons from an external reductant to the substrate and this is achieved by the route shown in Scheme (1.1).

Scheme (1.1):

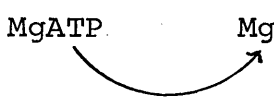

Reductant ⟶ Fe protein ⟶ MoFe protein ⟶ Reducible substrate e.g. N_2

The process is driven by the hydrolysis of MgATP and the reaction follows the stoichiometry shown in reaction (1.2).

$$N_2 + 8H^+ + 8e^- + 16MgATP \longrightarrow 2NH_3 + H_2 + 16MgADP + 16P_i \quad (1.2)$$

Nitrogenase is also capable of reducing other, mainly triply-bonded, substrates as summarised in Table (1.1).

Table (1.1): Examples of Nitrogenase Substrates (from ref. 8)

Substrate	Formula	Products
Dinitrogen	N_2	NH_3
Acetylene	$HC\equiv CH$	C_2H_4
Hydrogen cyanide	$HC\equiv N$	$CH_4 + NH_3 + CH_3NH_2$
Acrylonitrile	$CH_2=CH-C\equiv N$	$CH_3CH=CH_2 + NH_3$
Methyl isocyanide	$CH_3-\overset{+}{N}\equiv\overset{-}{C}$	$CH_3NH_2 + CH_4$ + traces of C_2 products
Vinyl isocyanide	$CH_2=CH-\overset{+}{N}\equiv\overset{-}{C}$	CH_4 + ?
Cyanogen	$N\equiv C-C\equiv N$	CH_4 + ?
Hydrogen azide	$H-\overset{-}{N}-\overset{+}{N}\equiv N$	$N_2 + NH_3 + N_2H_4$
Nitrous oxide	$N\equiv\overset{+}{N}-\overset{-}{O}$	$N_2 + H_2O$
Hydrogen thiocyanate	$H-S-C\equiv N$	CH_4 + ?
Methyl isothiocyanate	$CH_3-\overset{+}{N}\equiv C-\overset{-}{S}$	CH_4 + ?
Cyclopropene		 + $CH_3CH=CH_2$
Hydrogen ion	H^+	H_2

Besides these substrates, which are reduced, the enzyme may also bind carbon monoxide (CO) and nitric oxide (NO) which inhibit reduction of N_2 but are not themselves reduced.

Nitrogenase has some features which set it apart from many other enzymes. It is very slow, taking ca. 150 ms to transfer a single electron to the substrate, and this feature means an active nitrogen-fixing microorganism may contain nitrogenase in a proportion as large as 20% of cell protein. It may be also noted that H^+ is reduced to H_2 as a by-product of N_2 reduction. Evolution of H_2 is proportionately greater in the absence of N_2 and even proceeds when CO is present. This H_2 production appears to be very wasteful of energy but seems to be a consequence of the mechanism that nitrogenase adopts in the reduction of N_2.

A detailed computer model of the kinetics and mechanism of nitrogenase action has been developed by Thorneley and Lowe[12] from studies by stopped-flow spectrophotometry and rapid quench techniques. The cycle pertaining to the MoFe protein is shown in Figure (1.2) and highlights the complexity of the mechanism.

Figure (1.2): MoFe protein cycle
(adapted by R. Jones from ref. 12).

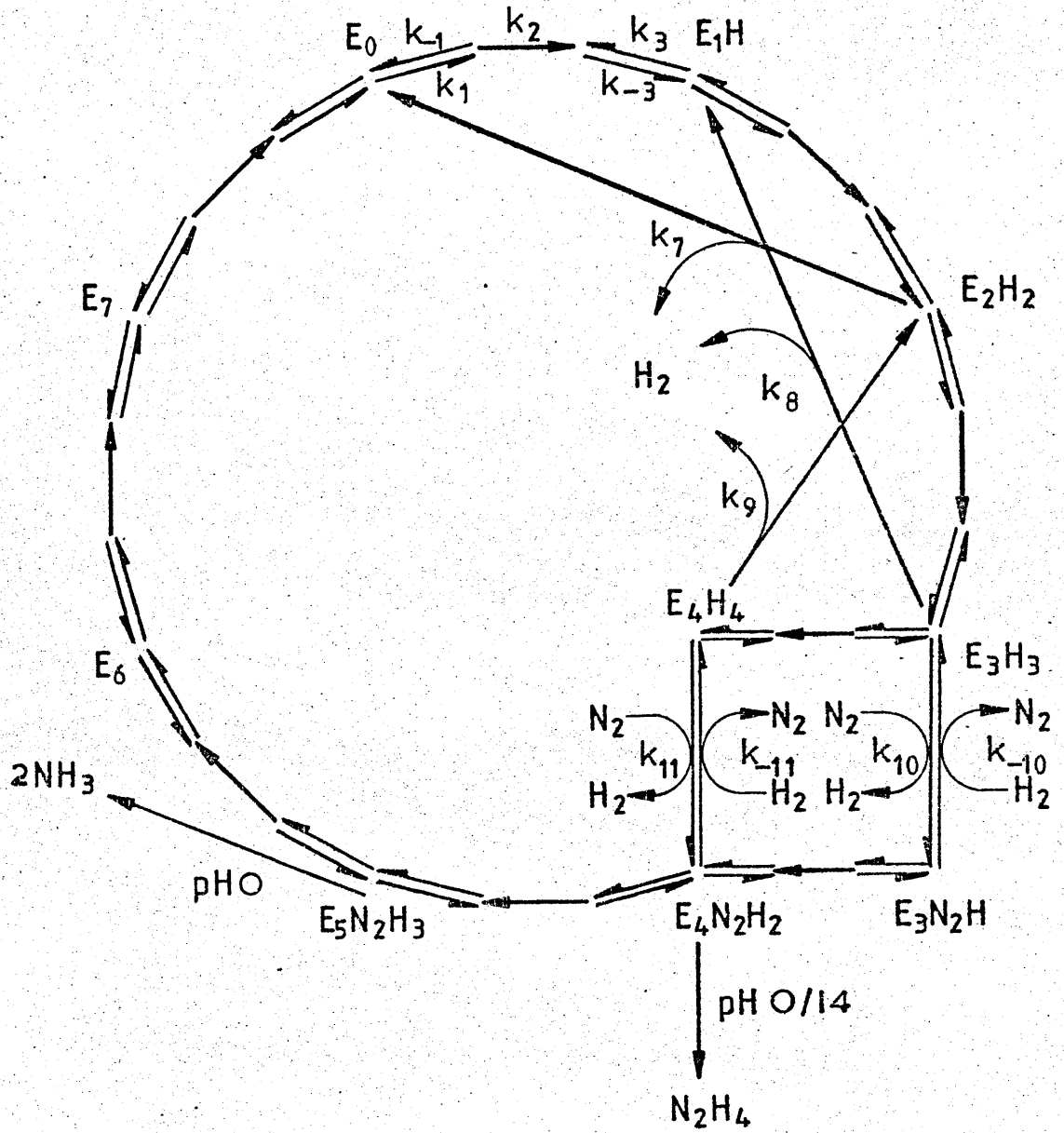

Reaction (1.2) shows that $8e^-$ are needed to reduce one N_2 molecule. The species E_o to E_7 in Figure (1.2) represent the number of times the MoFe protein has received an electron, in a 3 step cycle, from the Fe protein. No free intermediates are observed in the reduction of N_2 but acid or alkali quench leads to the formation of hydrazine. N_2H_4 is shown as derived from the $E_4N_2H_2$ intermediate in the cycle and this species may then contain a bound hydrazido(2-)-group [$M=N-NH_2$, M = metal (Mo) site]. It is envisaged that N_2 binds by displacing H_2 from the site at either the E_3H_3 or the E_4H_4 stage. E_3H_3 and E_4H_4 are regarded as metal dihydrides with respectively one or two protons on adjacent sites. The kinetics of NH_3 release are not yet clear but two molecules of NH_3 are probably released from species E_5 and/or E_6. The cycle depends on the assumption that each FeMoco binds only one N_2 and that each FeMoco operates independently of the other. It has been postulated that E_5 may be similar to a hydrazido(2-) species ($M = N-NH_3^+$) and E_6 to a nitrido-derivative ($M\equiv N$). It is interesting to note that when nitrogenase, actively involved in N_2 reduction, is quenched with acid, the first product released is H_2 followed by N_2H_4 and finally 2 moles of NH_3.[13]

1.4 Chemical models and catalytic cycles of nitrogen fixation

The assignment of intermediates in the enzymatic reduction of dinitrogen must at present be based on species

observed in model systems. Some of these possible assignments have already been mentioned and are included in the general scheme shown below.[2]

Scheme (1.2): Pathways for the stepwise reduction of N_2 to NH_3 and N_2H_4.

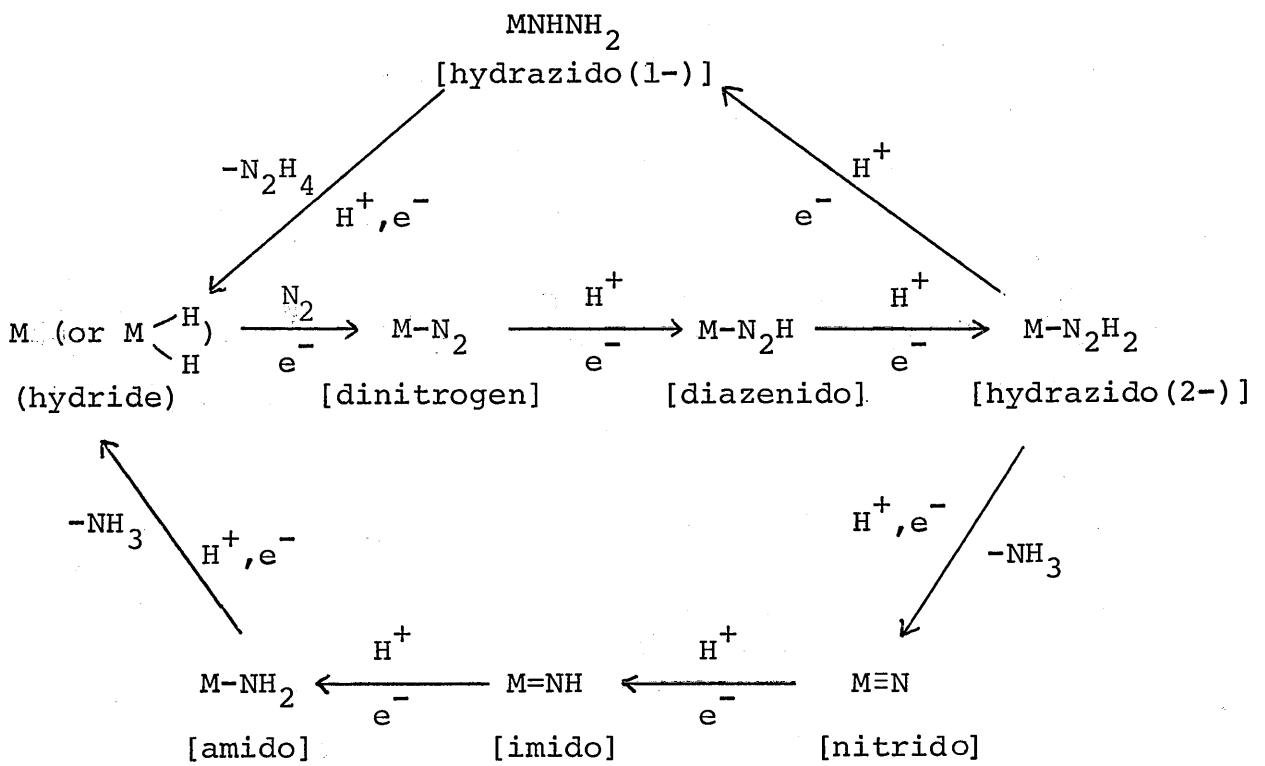

Such a scheme is based on protonation of N_2 bound at a mononuclear metal site, reduction occurring through one or two-electron transfer steps via the metal to the coordinated N_2. This type of scheme, although favoured by many, is not the only one proposed. Two other schemes, amongst others, have been put forward based on catalytic cycles involving molybdenum in a protic solvent.

The first is derived from such systems as that involving $MoCl_5$ and sodium amalgam in methanol.[14] Reduction may also be achieved electrolytically using a mercury cathode in a buffered solution. Such systems typically operate at high pressures of N_2 and produce only low yields of nitrogen hydrides, in this case N_2H_4. These reactions are thought to proceed via binuclear Mo(III) intermediates and this forms the basis of the Scheme (1.3) below, proposed by Shilov for nitrogenase.[14]

Scheme (1.3): A binuclear mechanism for nitrogenase

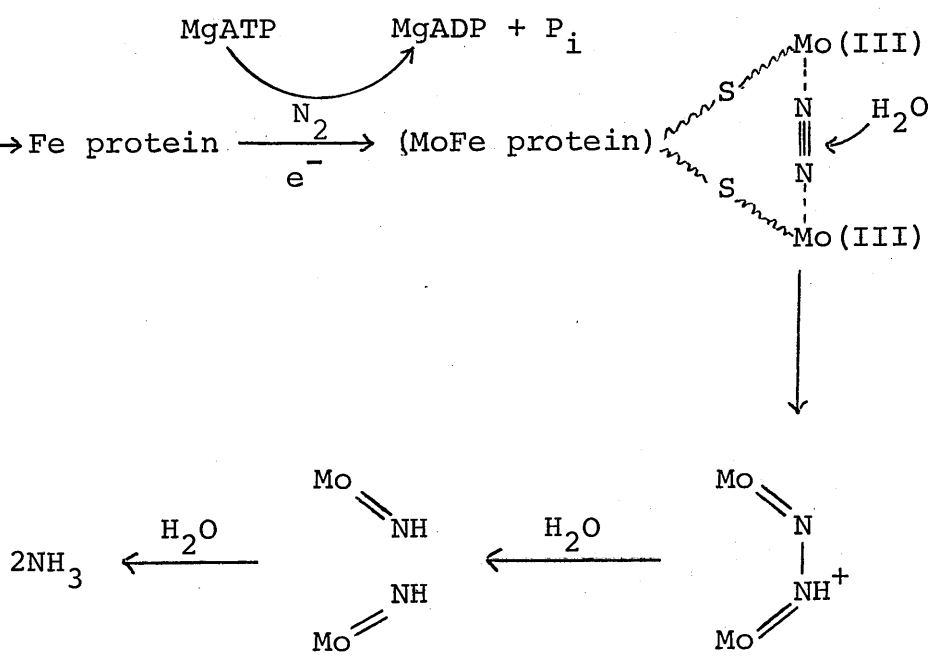

A second scheme proposed by Schrauzer[15] is derived from work on aqueous catalytic systems. The most efficient example is provided by a mixture of molybdate with reduced bovine serum albumin in a borate buffer. The disrupted

enzyme is thought to bind Mo via thiolate groups. Systems such as this work best at low dilution under a pressure of N_2 and may show up to 5% the efficiency of nitrogenase (moles NH_3 per Mo atom basis).

The basic premise to arise from this work is that N_2 is bound sideways at the mononuclear nitrogenase active site and that reduction occurs via a cis-diazene (HNNH) intermediate. It is envisaged that diazene accumulates in a "pocket" around the active site, then it either disproportionates to give N_2H_4 and N_2 which are then further reduced at the site or decomposes to give N_2 and H_2. These ideas are summarised in Scheme (1.4).

Scheme (1.4): A dinitrogen reduction mechanism involving diazene

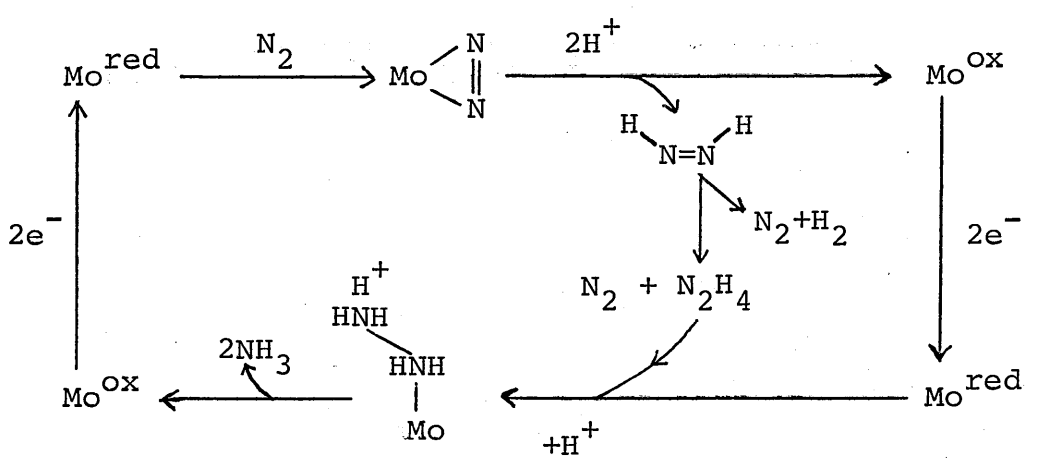

The catalytic cycles from which these two schemes are derived are very difficult to characterise by normal spectroscopic or analytical techniques. The nature of the reacting species in many of the systems is thus uncertain and in some cases the subject of controversy.

Returning to the cycle presented earlier [Scheme (1.2)] it may be noted that no catalytic chemical system yet exists based on this mechanism. However, all the forms of $M\text{-}N_xH_y$ or analogous $M\text{-}N_xR_y$ species have been isolated in some way. As demonstrated in Chapter 6, certain $M\text{-}N_2$ model complexes can be protonated to give NH_3 or N_2H_4, although again, not catalytically.

One area of research that has rendered part of the cycle close to catalytic, provides an interesting example of the use of model complexes.[16] The various steps are summarised in Scheme (1.5). The cycle involves alkylated nitrogen species and not $M\text{-}N_xH_y$ and thus the products are organonitrogen $N_xH_yR_z$-type compounds.

Scheme (1.5): Steps towards a catalytic cycle for synthesis of organonitrogen products[16]

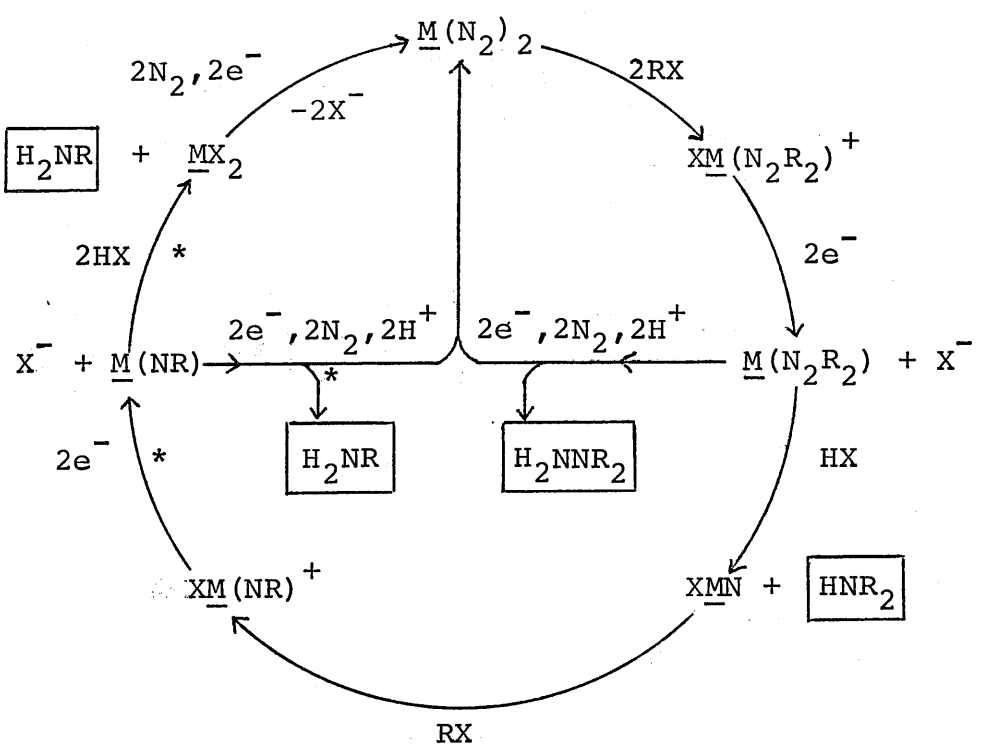

M = Mo(dppe)$_2$; X = halide; R = alkyl;
* = pathway not completely established.

Not all of the steps in the scheme are completely established and many have been studied only in isolation. Despite this, such work shows great promise of achieving the goal of a completely catalytic cycle.

1.5 The synergic bonding of dinitrogen in its complexes

When N_2 binds in an end-on fashion at a transition metal site it utilises two sets of orbitals in an attempt to form a stable bond to the metal. The N_2 molecule donates electrons via a filled σ-orbital into a vacant metal orbital of σ-symmetry. The metal back-donates electron density from its filled dπ orbitals into the two orthogonal empty N_2 π* orbitals. This is known as synergism and is depicted in Figure (1.3).

Figure (1.3):

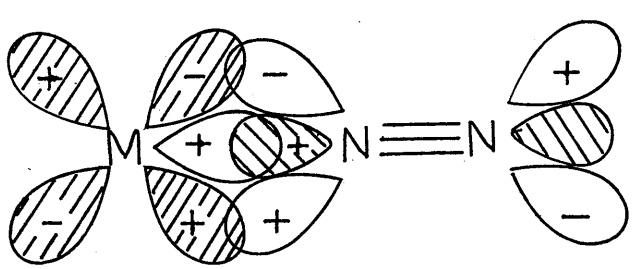

Such bonding is not unique to N_2 and many other ligands e.g. CO and NO also show synergism. Ligands involved in side-on bonding may also exhibit a similar interaction, the

common example being ethylene. In this case it is the filled ligand π-orbitals that donate, the empty π* orbital again acting as the acceptor as shown in Figure (1.4).

Figure (1.4):

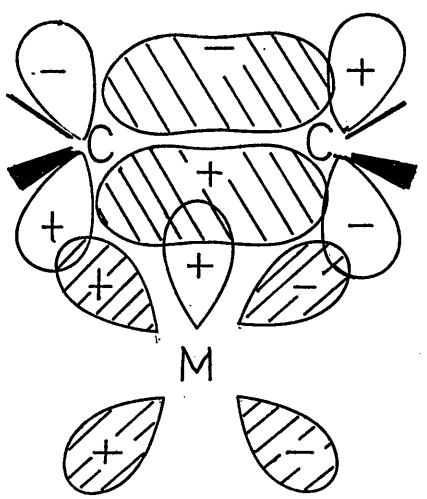

1.6 Characterisation of intermediates and model systems

There are various techniques that may be used for identification and characterisation of nitrogen-containing complexes, among their number being the commonly-used infra-red and U.V.-visible spectroscopy and more and more frequently, electrochemical methods. For isolated complexes such methods as elemental analysis and in some cases X-ray crystallography can be used. Complementary to all of these techniques is NMR spectroscopy. Proton NMR has, of course, been a vital tool of the chemist for many years and gradually as techniques have improved the less sensitive nuclei have been upgraded from mere curiosities to useful NMR probes.

Progress is now rapid and ^{15}N NMR has reached the level of a useful tool for the characterisation of many metal complexes. Chemical shift regions of ^{15}N resonances of several of the nitrogenous species postulated in the N_2 reduction cycle have been mapped out at relevant points in this thesis, and are discussed later. Pioneering work has also been carried out on ^{15}N NMR of nitrogenase actively reducing N_2.[17] No intermediates were detected in these experiments but with the advances in techniques likely over the next few years similar investigations in the future are likely to yield valuable information about the nature of bound intermediates.

In the biological nitrogenase system and in several other catalytic and model processes, molybdenum appears to be crucial for the reduction of N_2. A direct probe of this nucleus would then be an advantage. ^{95}Mo NMR spectroscopy provides a possibility but as yet is untested in such a rôle.

1.7 Aim of the present work

Bearing in mind the points mentioned above, the aim of this work is:

1) To assess the use of ^{15}N NMR spectroscopy of probe ligands as a means of obtaining information on changes in co-ligands at a metal site.

2) To develop the use of ^{15}N NMR spectroscopy as an indicator of ligand geometry.

3) To initiate work on ^{95}Mo NMR spectroscopy with a view to defining shift ranges of complexes relevant to nitrogen fixation and to increase understanding of the ways

in which ligands effect metal shielding.

4) To provide the ground-work for the study of molybdo-enzymes by ^{95}Mo NMR spectroscopy.

5) To extend existing information concerning protonation reactions in model systems and to assess the scope of NMR spectroscopy in studying general reactions of this type.

CHAPTER 2

^{95}Mo and ^{15}N NMR

2A. Techniques

2A.1 Introduction

The contrasting fields of ^{15}N and ^{95}Mo NMR spectroscopy provide interesting examples of the state of the art in the study of less abundant, quadrupolar and less NMR-sensitive nuclei. The techniques for study of ^{15}N NMR are now well established and are almost routine for many organic molecules.[1-3] ^{15}N NMR of transition metal complexes is now attracting more attention[4,5] with the increasing availability of high-field (high-sensitivity) ^{15}N NMR spectrometers. ^{95}Mo NMR however is in its infancy and by far the largest portion of work has been carried out, by various groups, during the period covered by this thesis. Again, the availability of spectrometers with ^{95}Mo capability coupled with the attraction of a direct probe of chemical environment has made ^{95}Mo NMR an increasingly useful tool. Both techniques however still have problems associated with the nature of the nucleus under study. The work in this thesis was carried out using Pulsed Fourier Transform (PFT) NMR methods which are described in both theoretical and practical detail in many standard texts.[7-11] Particularly useful for the practical multinuclear NMR spectroscopist is the text by Brevard and Granger.[6]

2A.2 Nuclear properties of ^{15}N and ^{95}Mo

Summarised in Table (2.1) are various properties of the nuclei ^{15}N and ^{95}Mo as compared with ^{14}N, ^{13}C and ^{1}H. ^{15}N has a nuclear spin of $I = \frac{1}{2}$ and therefore no quadrupole moment. Both ^{95}Mo ($I = \frac{5}{2}$) and ^{14}N ($I = 1$) have reasonably small quadrupole moments and thus in coordination environments where there is a small electric field gradient (EFG) at the resonant nucleus, quadrupole broadening may be small and signals acceptably narrow. ^{14}N is not often found in such environments and thus linewidths are often quite large, although narrow resonances may be observed in groups with cylindrical symmetry such as M-N≡C [12] and M-N≡CR [13] in sufficiently small molecules, as will be discussed. In molybdenum complexes of appropriate symmetry (to give a low EFG at ^{95}Mo) quite narrow lines can sometimes be observed.

For studies requiring accurate measurement of chemical shift and coupling constants, ^{15}N is the preferred nucleus. Its major drawback is the low natural abundance and sensitivity making it ca. 50 times less sensitive than the more familiar spin-dilute nucleus ^{13}C, when measured in natural abundance. The receptivity of a given nucleus is determined by the magnetogyric ratio γ, the natural abundance N, and the spin quantum number I, as shown in the relationship below:

$$\text{Receptivity} \propto \gamma^3 N I (I+1) \qquad (2.1)$$

TABLE 2.1: Comparison of Nuclear Properties

Nucleus	^{95}Mo	^{14}N	^{15}N	^{13}C	^{1}H
Nuclear spin (I)	$\frac{5}{2}$	1	$\frac{1}{2}$	$\frac{1}{2}$	$\frac{1}{2}$
Natural abundance/%	15.720	99.635	0.365	1.108	99.985
Magnetogyric ratio (γ)/ 10^{-7} rad $T^{-1}sec^{-1}$	1.743	1.933	-2.711	6.726	26.751
Quadrupole moment (Q)/ 10^{-24} cm^2	0.011	0.016	-	-	-
NOEF (η_{max})	-	-	-4.93	1.99	0.5
Relative sensitivity (equal number of nuclei)	0.21	0.06	0.07	1.00	62.9
Relative receptivity (natural abundance)	2.88	5.68	0.02	1.00	5.68×10^3
NMR frequency[a] ∋ /MHz	6.542	7.228	10.137	25.145	100.000

[a]Resonance frequency in a magnetic field such that protons in TMS (Me_4Si) resonate at exactly 100 MHz.

Thus ^{95}Mo with a low γ is ca. 3 times more receptive than ^{13}C because of its higher natural abundance and spin.

The value of γ has further consequences for the nuclei under study. After a r.f. (radio frequency) pulse in the PFT NMR experiments, for ^{15}N, the main processes by which the magnetisation of a nucleus is equilibrated during relaxation are dependent on γ^2. Relaxation then, can be slow for ^{15}N as γ is relatively small and so long delays are required between pulses, leading to long accommodation times. A summary of the various relaxation mechanisms is given in Appendix 1. When proton coupling is removed from the signal of a spin $\frac{1}{2}$ nucleus X in a decoupling experiment, the strong irradiation of the proton frequencies causes a Nuclear Overhauser Effect (NOE) which can lead to changes in the X nucleus signal intensity. This factor (NOEF) is dependent on the magnetogyric ratio of X and also on the proton-X dipole-dipole (DD) contribution to relaxation of X. The maximum η_{max}, is given by equation (2.2), for purely DD relaxation [Table 2.1)].

$$\eta_{max} = \frac{\gamma_H}{2\gamma_X} \qquad (2.2)$$

For ^{13}C with γ positive the NOEF is always favourable (or zero) and NMR signals are upright. γ for ^{15}N is negative, giving $\eta_{max} = -4.93$. If non-dipolar relaxation mechanisms are present also, $0 \geqslant NOEF > -4.93$. For $0 \geqslant NOEF > -1$ a diminished upright signal is observed. If the NOEF = -1 then the signal is nulled. The range $-2 > NOEF \geqslant -4.93$ gives an inverted resonance of enhanced intensity.

^{95}Mo relaxation is wholly quadrupolar as shown later.

Since the characteristic resonance (Larmor) frequency ν_o of a nucleus is directly dependent on γ, equation (2.3) holds:

$$\nu_o = \frac{\gamma}{2\pi} B_o \qquad (2.3)$$

where B_o = magnetic field

The low value of ν_o for ^{95}Mo presents special problems, as will be seen.

2A.3 Strategy for ^{15}N NMR

In the light of the problems outlined above, several solutions are possible. Many of the difficulties can be overcome by the use of isotopic labelling with ^{15}N up to 99% which can increase sensitivity by a factor of ca. 270 and thus reduces the spectrometer accumulation time required for a given signal to noise ratio by ca. 7×10^4 as given by the relationship (2.4)

$$N_s \alpha \frac{1}{n^2} \qquad (2.4)$$

where N_s = number of scans

n = number of ^{15}N nuclei involved in NMR experiment.

This relation also shows the benefit of wide-bore NMR instruments to allow large sample volume. The present work has used a wide-bore spectrometer (Bruker WH180, taking 25 mm sample tubes) as well as standard-bore (Bruker WM360, WH400,

CXP300 and Jeol FX90Q) instruments, taking 10 mm tubes. The importance of using a high field spectrometer arises from the dependence of the signal intensity on B_o^2 (where B_o is the magnetic field strength) whereas the noise is proportional to $B_o^{\frac{1}{2}}$:[7]

$$\frac{S}{N} \alpha B_o^{3/2} \qquad (2.5)$$

$\frac{S}{N}$ = ratio of signal to r.m.s. noise

Sensitivity can also be increased by lowering the temperature. This occurs because the NMR experiment is dependent on unequal populations of the nuclear energy levels in a magnetic field and this inequality is disrupted by thermal motion.

Combining the various factors discussed above a general relation for the NMR sensitivity of a given nucleus can be derived:

$$\text{Sensitivity} \quad \alpha \quad \frac{\gamma^3 I(I+1) B_o^{3/2}}{T} \qquad (2.6)$$

Both field strength and temperature have effects on relaxation times via the mechanisms shown in detail in Appendix 1. High magnetic fields have a pronounced influence on shielding anisotropy (SA) relaxation through the dependence on B_o^2. $\Delta\sigma$, the shielding anisotropy, can be large for multiply bonded nitrogen[4] and therefore the SA mechanism may dominate ^{15}N relaxation at high field strengths for complexes

containing nitrogen ligands without directly bonded protons. This has been shown often to be the case for dinitrogen in complexes.[5] From the above argument it is apparent that the NOEF, as discussed earlier, may be unfavourable for many ligands in this study, and therefore proton decoupling was only employed for the purposes of structure determination.

NMR pulse sequences such as INEPT (Insensitive Nuclei Enhanced by Polarisation Transfer) operate by transferring the magnetisation of the sensitive proton to ^{15}N, but are only useful where the coupling constant J_{NH} is of sufficient magnitude and this largely is unsuitable for this work. In cases where very long relaxation times are expected, a relaxation agent such as $[Cr(pd)_3]$ (pd = 2,4-pentanedionate) provide a more efficient route for relaxation via its paramagnetic interaction. $[Cr(pd)_3]$, in moderate amounts, does not give appreciable line-broadening or change the chemical shift of signals of interest.[14]

Optimisation of spectrometer parameters is obviously important to keep accumulation times to a minimum. One such parameter is the flip angle θ. In the PFT NMR experiment a single pulse of r.f. power excites all nuclei within a given frequency range. The maximum signal intensity is given by a pulse which flips the magnetisation through 90° after which relaxation occurs before the next pulse is applied. For a 90° pulse a long wait between pulses is required to prevent saturation of the magnetisation and thus a smaller value is chosen, determined by the relaxation

time (T_1) and the delay between pulses (t). In practise the time t is the acquisition time (A_t), dependent on the spectral resolution required. The optimum value of θ, θ_M or the Ernst angle,[7] is given by equation (2.7).

$$\theta_M = \text{arc cos } [\exp(\frac{-t}{T_1})] \qquad (2.7)$$

In the present work T_1 values were assumed to be of the order ca. 10 seconds at a field strength of 8.456 T (WM360 instrument), from previous studies of metal dinitrogen complexes.[5] A_t was ca. 0.8 seconds for reasonable resolution giving $\theta_M = 22.5°$.

2A.4 ^{95}Mo: Problems associated with a quadrupolar nucleus

2A.4.1 The nature of quadrupole broadening

Nuclei with $I > \frac{1}{2}$ have an electric quadrupole moment as they have a non-spherical distribution of nuclear charge. 2I+1 energy levels arise from this situation and thus several transitions are possible in a magnetic field, with the selection rule $\Delta_m = \pm 1$. An asymmetric distribution of electron density around the nucleus produces an electric field gradient at the nucleus which fluctuates at a frequency suitable to induce transitions, in a rapidly tumbling molecule. Molecular electric fields are much larger than corresponding magnetic fields and this then provides an efficient mechanism for relaxation of the nuclear spin. The quadrupolar relaxation time (T_q), for "extreme narrowing" conditions (see Appendix 1), is given by equation (2.8).

$$\frac{1}{T_q} = \frac{3}{40} \frac{(2I+3)}{I^2(2I-1)} \chi^2 \left(1+\frac{\eta^2}{3}\right) \tau_c \qquad (2.8)$$

[A. Abragam "The Principles of Nuclear Magnetism" Oxford 1961 p.314]

χ is the nuclear quadrupole coupling constant and measures the strength of the interaction between the quadrupole moment (Q) and the field gradient (q): $\chi = \frac{e^2qQ}{\hbar}$. η is the asymmetry parameter for q, and τ_c is an effective correlation time which characterises the rotation of the molecule. The Stokes-Einstein theory gives τ_c as

$$\tau_c = \frac{\eta' V f}{kT} \qquad (2.9)$$

η' = viscosity of the medium

V = Volume of solute molecule (assumed spherical)

f = microviscosity factor (0.16 for pure liquids)

k = Boltzmann constant

T = absolute temperature.

Under "extreme narrowing" conditions, $T_q = T_1 = T_2$ and the NMR linewidth at half-height is given by equation (2.10)

$$W_{\frac{1}{2}} = \frac{1}{\pi T_2} \qquad (2.10)$$

This is a statement of the Heisenberg Uncertainty Principle and predicts that small values of T_q will give broad lines.

Considering the above factors for ^{95}Mo, Q is relatively small [Table (2.1)] and has recently been revised downwards by an order of magnitude.[16] The spin of $\frac{5}{2}$ gives ^{95}Mo linewidths ca. 16 times narrower than for I = 1 (e.g. ^{14}N) all other factors being equal. The dependence on q^2 is reflected in the wide range of linewidths found for ^{95}Mo in complexes of differing symmetry. Qualitative analysis of linewidths in ^{59}Co NMR spectra of octahedral complexes, based on a point charge model gives the following results:[17]

TABLE (2.2): Linewidth analysis of octahedral complexes

Complex geometry	Linewidth formula
MA_6	0
MAB_5	$4(\gamma_A'-\gamma_B')^2$
cis-MA_2B_4	$4(\gamma_B'-\gamma_A')^2$
trans-MA_2B_4	$16(\gamma_A'-\gamma_B')^2$
fac-MA_3B_3	0
mer-MA_3B_3	$9(\gamma_A'-\gamma_B')^2 + 3(\gamma_B'-\gamma_A')^2$
trans-MAB_4C	$4(\gamma_A'+\gamma_C'-2\gamma_B')^2$

where γ' = line broadening factor of particular ligand.

On purely symmetry grounds trans > cis linewidth is difficult to visualise but it is the nature of the EFG tensor which determines this. A recent paper by Akitt[18] discusses the factors and various ligand stereochemistries which lead to zero or low EFG values. It is concluded that the highly

symmetrical tetrahedral and octahedral complexes are only special cases of low EFG and complexes of apparently low symmetry may also give narrow lines. The importance of the local EFG is shown for ^{95}Mo by the narrow lines observed for complexes of the type $[(\pi\text{-Arene})Mo(CO)_3]$[19] e.g. figure (2.1).

Figure (2.1):

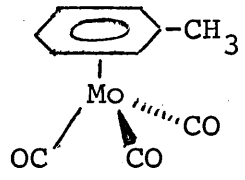

$W_{\frac{1}{2}} = 5Hz$

For octahedral ^{95}Mo complexes the general rules outlined above are obeyed although the trans linewidth is seldom 4 times larger than the cis e.g. ref. 20.

The τ_c term in equation (2.8) has important consequences in ^{95}Mo NMR. Linewidth usually increases with molecular size although this is not always so as internal rotation may reduce the local correlation time at the quadrupolar nucleus. This has been observed for ^{17}O in phosphates bound to the enzyme Ribonuclease A[21] and also for ^{95}Mo in molybdenum(VI) complexes $[MoO_3L]$ (L = various polydentate nitrogen / oxygen ligands e.g. EDTA).[23] These studies are relevant to the work on Xanthine Oxidase discussed in Chapter 7 as is also the observation of relatively narrow lines for $^{43}Ca^{2+}$ bound to various proteins.[22] Increasing temperature and decreasing solvent viscosity[24] can reduce the linewidth although choice of solvent is usually based on maximum complex solubility and temperature increases have

been avoided in this work as this can lead to changes in chemical shift (see later) or complex decomposition. Large linewidths have consequences for the detection of quadrupolar nuclei in the PFT NMR experiment.

2A.4.2 Instrumental drawbacks

The relaxation of nuclear spins to an equilibrium distribution after the r.f. pulse in the PFT NMR experiment is observed during the acquisition time as a free induction decay (FID). For quadrupolar relaxation this decay can be very fast as shown in figure (2.2a) compared to that of a spin $\frac{1}{2}$ nucleus. The power of the r.f. exciting pulse is very large and is supplied by the same coil, in the NMR probe, as that which detects the very small current induced by the decaying magnetisation. There is therefore a delay between transmission and reception, called the "deadtime", to allow the r.f. pulse to die away and so not saturate the receiver. At low frequency with sensitive receiver circuitry (high quality factor Q) the deadtime may be quite large. The problem is exacerbated by "acoustic ringing" in which the r.f. pulse sets up a standing wave in the material of the probe which then re-emits at a frequency similar to that of the NMR signal. This problem is also worse for low frequency nuclei such as ^{95}Mo. The "ring-down" pattern thus produced, shown in figure (2.2b), when Fourier transformed, gives rise to rolling baselines and/or spurious signals in the NMR spectrum. Such anomalies may be removed by using large delays

Figure (2.2): Probe ringing at low frequencies

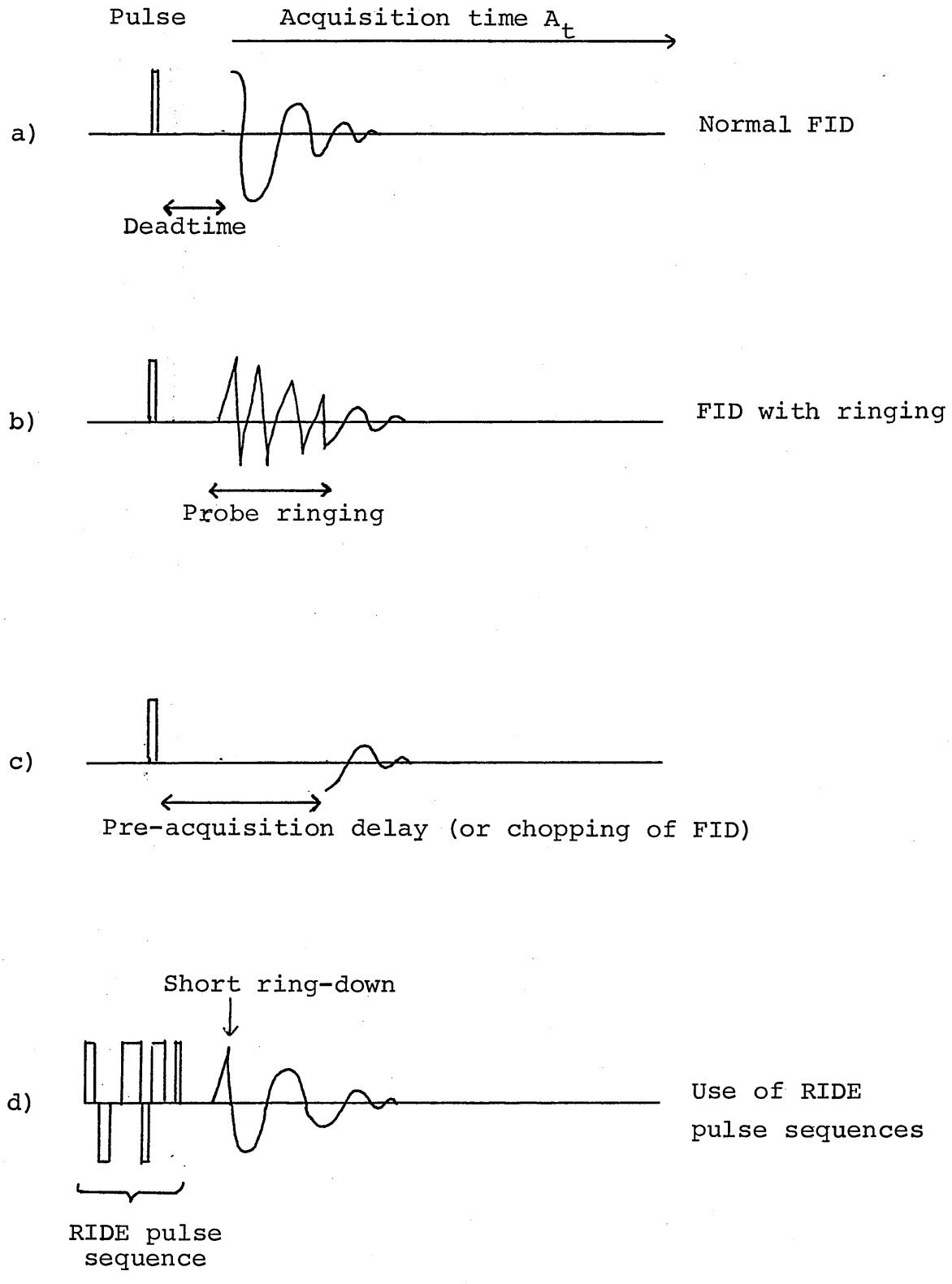

before turning on the receiver and acquiring the FID, and/or collecting the ring-down and chopping off the offending data before Fourier transformation [figure (2.2c)]. These methods invariably lead to loss of signal intensity or for very broad lines complete loss of signal and some distortion of resonance lines observed. The effect of these above treatments, for various ring-down times in the literature or experienced in this study, on differing linewidth signal is shown in Table (2.3).

TABLE (2.3): Signal loss through probe ringing

Ring-down time/ μs	Signal remaining after delay for various $W_{\frac{1}{2}}$ (%)			Reference
	5000 Hz	1000 Hz	100 Hz	
20	73	94	>99	t.w., 25
60	39	83	98	25
200	4	53	94	24
300	0.9	39	91	22
350	0.4	33	89	26
600	8×10^{-3}	15	82	t.w., 27
800	3×10^{-4}	8	77	26

t.w. = this work.

Recently pulse sequences have been used which rely on the fact that the FID due to the sample depends on the types of pulse which precede it while the ring-down does not. By alternating the phase of series of pulses the ringing may be subtracted from the FID. Such a sequence is RIDE[25] (RIng Down Elimination) which reduces the ring-down time to 20 μs on a high power, wide-line, NMR spectrometer (Bruker CXP300). Unfortunately this type of treatment shown in figure (2.2d) is not widely applicable as instruments of the wide-line type with high power and very accurate pulse length and timing are required. Treatment at source through better design of receivers[28] and selection of materials used in probe construction[11,26] is a better but obviously more expensive solution.

2A.4.3 Advantages of a quadrupolar nucleus

With short relaxation times, very rapid pulsing regimes may be used with concomitant reduction of accumulation time. The broad lines obviate the need for high resolution spectra and therefore the sample need not be spun (as is usually required to offset effects of field inhomogeneity). For superconducting magnet spectrometers with stable fields a field frequency lock is not required (often provided in the form of deuterated solvent or in a reference capillary). ^{95}Mo referencing is provided by substitution of the sample by a standard 2M aqueous solution of sodium molybdate at pH 11. Low resolution, high sensitivity transverse probes[25,26]

may also be used as on the CXP300 instrument mentioned above. Detailed instrumental parameters are given in the experimental section.

2B. Nuclear Magnetic Shielding: qualitative theory and application

2B.1 Introduction

The detailed theoretical treatment of nuclear magnetic shielding is complex and thus various approximations and assumptions have been evolved to allow the original concepts put forward by Ramsey[29] to be adapted for use by the practising chemist. The application of such approximate terms in a qualitative sense, to the chemical shift behaviour of nuclei in some metal complexes, will be discussed below, together with correlations with other physical properties. The general fields of nuclear magnetic shielding theory have been reviewed[15,30,31] and more specialised treatments on nitrogen[3-5] and the transition metals[32] have appeared recently.

The inferences drawn from a consideration of the magnetic shielding theory will be discussed in the context of the metal complexes studied under the relevant chapter heading. Comparisons of ^{15}N with ^{13}C as second row elements and ^{95}Mo with other metal nuclei will be made.

2B.2 The origin of nuclear magnetic shielding

The measured quantity in the NMR experiment is the energy of a transition between nuclear spin states which is determined

by the effective magnetic field at the nucleus. This field (B) is related to the applied field (B_o) by equation (2.11).

$$B = B_o\ (1-\sigma) \qquad (2.11)$$

σ represents the extent to which a nucleus is screened from the magnetic field. This shielding term arises from the induced circulation of electrons about the nucleus X and may be split into two terms:-

$$\sigma(X) = \sigma_d(X) + \sigma_p(X) \qquad (2.12)$$

The diamagnetic term, σ_d opposes the applied field and is due to isotropic rotation of charge whereas σ_p, the paramagnetic term originates from the asymmetric circulation of valence electrons induced by, and augmenting, the applied field. The Ramsey equations for σ_d and σ_p involve summation of the term over the whole molecule and can be greatly simplified by considering the "Atom in a Molecule" approximation.[33] In this, only effects of electrons in the locality of the atom are considered in σ_d and σ_p and a third term due to contributions from other atoms Y is invoked:-

$$\sigma(X) = \sigma_d^{loc}(X) + \sigma_p^{loc}(X) + \Sigma\sigma'(XY) \qquad (2.13)$$

The σ_d^{loc} term is now dependent on the radius and population of atomic orbitals on X and is little perturbed by ligands.

σ_d^{loc} then is effectively constant for a given nucleus in similar series of complexes. σ' represents long range effects which are expected to be small,[33] and so the term σ_p dominates the chemical shift differences in complexes (a special case is proton NMR in which all the terms may be important). The paramagnetic shielding involves the mixing of excited electronic states with the ground state, the Ramsey expression requiring summation over all such states. To simplify matters an average or effective excitation energy $\overline{\Delta E}$ may be selected to represent such states[34] as in equation (2.14).

$$\sigma_p = -\text{const.}\ \overline{\Delta E}^{-1} \langle r^{-3} \rangle \ \Sigma Q \qquad (2.14)$$

where r is the expectation value for the radius of the orbitals contributing to the shielding (2p in the case of ^{15}N, 4d for ^{95}Mo). The ΣQ term is given by elements of the charge-density, bond-order matrix produced by a M.O. treatment of the bonding of X to other atoms Y and consists of two components:-

$$\Sigma Q = Q_{XX} + \sum_{Y \neq X} Q_{XY} \qquad (2.15)$$

where Q_{XX} depends on the electron density at X and Q_{XY} on the extent of π-bonding to Y.

2B.3 Trends in chemical shifts

2B.3.1 Second row elements: ^{15}N

2B.3.1.1 Application of shielding terms to ligands in metal complexes

Variation of the σ_d and σ' terms is usually assumed to be negligible compared with changes in σ_p in series of complexes in which changes in the coordination environment are small and remote from the probe nucleus X. This, however, does not make prediction or analysis of such effects much simpler due to the complex interdependence of the components making up σ_p. This problem can be exemplified by reference to work in the literature and by comparing ^{13}C and ^{15}N NMR.

Many studies have involved transition metal carbonyl complexes[35-41] and interpretations of ^{13}C chemical shifts have been adapted as further data have come to light.

In general, as the metal site becomes electron-rich due to increased donation from co-ligands, and thus π-back-bonding to the CO π^* orbital increases, the ^{13}C nucleus is deshielded. This has been rationalised in several ways. Where the ΔE term is assumed to be dominant[35,36] deshielding is envisaged as a lowering of this energy separation with increasing metal to CO back-donation. It has been pointed out[39] that such donations will in fact raise the energy of the CO π^* orbitals relative to the σ orbital and that the situation is far from simple with the probability that several excited states contribute to σ_p besides that from the $\sigma \rightarrow \pi^*$ transition. Studies on the same types of complexes show an opposite trend in ^{17}O shifts to that of ^{13}C shifts.[38,41] This has been

TABLE (2.4): ^{15}N NMR, i.r., Hammett σ_p and $^{1}E_{\frac{1}{2}}^{ox}$ data for *trans*-$[Mo(NCR)(N_2)(dppe)_2]$

Complex *t*-$[Mo(NCR)(N_2)(dppe)_2]$	$\delta^{15}N$ (ppm) N_α	N_β	$^{1}E_{\frac{1}{2}}^{ox}$ (V)	$\nu(N_2)$ (cm^{-1})	σ_p
R = Pr^n	-32.2	-35.9	-0.57	1925	-
Me	-31.2	-34.0	-0.58	1920	-
C_6H_4OMe-4	-28.6	-33.7	-0.53	1935	-0.27
C_6H_5	-24.0	-33.0	-0.48	1945	-0.00
C_6H_4F	-24.8	-35.1	-0.47	1951	+0.06
C_6H_4OCMe-4	-7.0	-34.8	-0.41	1965	+0.5

From ref. 42.

is gross changes in the bond order of the nucleus X.[4] This is observed in both ^{13}C and ^{15}N NMR and operates when ΣQ is dominant. ΣQ is lowest for carbon and nitrogen when they are singly bonded, e.g. in CH_4, C_2H_6, NH_3 and N_2H_4 and low also when they are triply bonded, e.g. in C_2H_2, C≡O, CN^-, N_2 and NO^+. Asymmetry in the electronic charge close to the resonant nucleus increases for double bonds e.g. in C_2H_4, C=O, C=N, N=N and N=O and also for groups such as CO_2 and NO_3^-. In fact although ΣQ may be dominant above, it has a direct bearing on the ΔE term, this decreasing with greater asymmetry. It is the interdependence of terms such as these that form the basis of many qualitative discussions of shielding dependent simply on changes of ΔE.

An important distinction for nitrogen but not carbon arises in the presence of a lone pair in a delocalised system;

attributed to effects of electron density changes on carbon and oxygen, increasing at oxygen while decreasing at carbon as donation to CO increases. The respective decrease and increase in $\langle r^{-3} \rangle_{2p}$ shields ^{17}O and deshields ^{13}C.[38] Recently[40,41] these ideas have been challenged and the ΣQ term considered. Calculations suggest differences in ^{13}C and ^{17}O shielding to be due to contributions from the π-bonding of the metal to carbon, Q_{MC} dominating the ΣQ term of ^{13}C whereas Q_{CO} dominates the ^{17}O shielding. As π-back-bonding increases Q_{MC} becomes greater and the shielding decreases, the converse being true for Q_{CO}.[40]

Dinitrogen, isoelectronic with CO, can show different shielding behaviour in its complexes. It has been noted[4] that both N_α and N_β may be deshielded as back-donation to N_2 decreases. However in the series of complexes <u>trans</u>-$[MoL(N_2)(dppe)_2]$ (L = N_2, NCR; R = Me, Pr^n, C_6H_4B-4; B = H, MeO, MeCO or F)[42] when L = N_2 is replaced by MeCN, a poorer π-acceptor, both N_α and N_β are deshielded and this is rationalised in a similar way to the ΔE argument for ^{13}C of carbonyls. When L = RCN and R is varied the ^{15}N shift of N_α only, is shielded with increasing donor power of R. This is envisaged to operate via only a σ influence on N_α shielding, N_β being relatively unaffected. A set of data for these complexes is given in Table (2.4).

Fortunately in some situations a particular component of the σ_p term becomes dominant and this greatly facilitates interpretation of the shielding behaviour. One such case

this allows low energy n(N)→π* transitions which are very effective in deshielding the nucleus. Particular manifestations are shown in the large downfield shifts of nitrogen in nitrosyl or diazenido ligands when these become bent, through the localisation of a lone pair and the upfield shifts on protonation when a lone pair is used in bonding. Such effects will be discussed in Chapter 5.

This lone pair effect for delocalised systems should be contrasted with the situation in systems such as $\ddot{N}H_3$ where there is no π-system and only high energy n→σ* transitions are available, explaining the high-field position of ammonia.

The lone pair effect on nitrogen and the larger ΣQ values found account for the much greater shielding range of nitrogen shifts than that predicted from the increase of $\langle r^{-3} \rangle_{2p}$ over carbon.[4]

The $\langle r^{-3} \rangle_{2p}$ term is responsible for the deshielding observed from NH_3 to NH_4^+ as an increase in cationic charge decreases r so increasing $\langle r^{-3} \rangle_{2p}$; this is a generally observed phenomenon.

2B.3.1.2 Correlations with other physical methods

A common practise in NMR studies is to compare shielding data with that from other physical measurements. In many cases good correlations have been observed and some examples are given below. Caution should be used to avoid over-interpretation of results as stressed in the concluding remarks [Section 2B.3.1.2e].

2B.3.1.2a Infra-red

Infra-red stretching frequencies are often used as an indicator of bond-strength in ligands such as CO, CN^-, N_2 and NO^+ although the force constant (k) is a more accurate measure as stretching frequencies can be distorted by vibrational coupling.

Correlations are found between ^{13}C shifts and k_{CO} in many studies of carbonyl complexes.[35] Deshielding of ^{13}C with lowering of k_{CO} is observed as back-bonding increases. Interestingly in complexes such as $[LM(CO)_5]$ (M = Cr, Mo or W; L = e.g. phosphine, phosphite) $\delta^{13}CO^{cis}$ shows a good negative linear correlation with $k_{CO}{}^{cis}$ whereas $\delta^{13}CO^{trans}$ gives only a poor correlation with $k_{CO}{}^{trans}$. Similar trends are also observed for $\delta^{13}C$ and $\delta^{15}N$ with k_{CN} in complexes of the type $[M(CN)_x]^{\ell-}$ as the transition metal M is varied.[43] The J_{CN} coupling constant generally increases with shielding of ^{13}C or ^{15}N. For closely related compounds $\delta^{15}N$ has been shown to increase linearly with increase in $\nu(N_2)$ as in the trans-$[Mo(N_2)(NCR)(dppe)_2]$ series of complexes discussed earlier[42] and shown in Table (2.4).

2B.3.1.2b Electrochemistry

For the alkyl and aryl nitrile complexes mentioned above a linear relationship is also shown between $\delta^{15}N$ for N_α and $^1E_{\frac{1}{2}}^{ox}$, the reversible first oxidation potential. $E_{\frac{1}{2}}^{ox}$ is a measure of the relative energy of the H.O.M.O. in a closely similar series of complexes. Such electrochemical measurements have been used to probe the overall donor ability ($\sigma+\pi$) of various

ligands.[44] As the nitrile group above becomes more electron releasing, oxidation is more facile as the level of the H.O.M.O. rises and thus $E_{\frac{1}{2}}^{ox}$ falls. The equivalent change in $\delta^{15}N$ for N_α is to higher shielding. Reverse behaviour is observed for a series of carbonyl complexes $[Cr(CO)_5L]$ (L = phosphine or nitrogen based ligands)[45] and although some of the electrochemical data is in error,[46] ^{13}C is deshielded with increasing ease of oxidation. The reduction potential for the series $[(\eta^5\text{-}C_5H_5)Fe(CO)_2X]$ (X = various alkyl and aryl groups or CN) when plotted against $\delta^{13}CO$ gives a straight line.[37] Here the energy of the L.U.M.O. is being probed. Reduction becomes easier as increasingly electron withdrawing groups are ligated and this correlates with shielding of the ^{13}C nucleus.

2B.3.1.2c U.V.-visible spectra

Correlations are expected between shielding and U.V.-visible transition energies when these correspond to a dominant effective ΔE separation in σ_p for the resonant nucleus. Paramagnetic excitation must be magnetic dipole allowed i.e. charge must rotate (e.g. $\sigma_x \rightarrow \sigma_y^*$) whereas U.V.-visible transitions must be electric dipole allowed, (to have) much intensity) i.e. charge moves in a linear path (e.g. $\pi \rightarrow \pi^*$) and often these conditions are mutually exclusive. However the $n \rightarrow \pi^*$ transition has both magnetic ($p_x \rightarrow p_y$) and electric ($s \rightarrow \pi$) dipole allowed components[4] and a clear correlation is often observed as in organic nitroso and diazene compounds, which have a nitrogen carrying a lone pair in a delocalised system.[4]

Correlations are also observed between shielding data and U.V.-visible transitions which have no magnetic components as the energy of these excitations can reflect that of the effective ΔE separation. This is common in the study of complexed ligands.

Transitions assigned as metal to ligand (M→L) charge transfer (CT) have been observed in the U.V.-visible spectra of $[M(CO)_5L]$ (M = Mo or W; L = various phosphine ligands).[36] As the energy of this transition, ascribed as transfer from the metal to cis-carbonyl π^* orbitals, rises, so the shielding of $^{13}CO^{cis}$ increases. This is brought about by ligation of successively better π-acceptors L which lower the metal $d\pi$ orbitals in relation to the CO π^*. A more approximate trend is shown by $[Fe(CN)_5L]^{n-}$ (L = a range of π-acceptors) for $\delta^{13}C$ of cis-cyanide with a d-d transition.[47] Deshielding occurs with increasing ligand field splitting.

2B.3.1.2d Other parameters

Mössbauer spectroscopy, restricted mainly to ^{57}Fe among the transition metals so of limited applicability, probes electron density at iron and reflects the relative donor power of ligands. A similar trend to that mentioned above for cyanide complexes is also observed with the isomer shifts of the ^{57}Fe nucleus.[47] Similarly many techniques which depend on the electronic environment at the metal centre give relationships with nuclear magnetic shielding, the proviso being that this technique gives results in some way connected with charge

density at the resonant nucleus. In these cases parameters which reflect the electron withdrawing or donating power of a substituent in the same coordination sphere as the resonant nucleus, may correlate with chemical shift. Examples are the Hammett substituent constants σ[48] which are derived from the effect of a group X, via a linear free energy relationship, on the reactivity of a system [Equation (2.16)].

$$\log \frac{k}{k_o} = \sigma\rho \qquad (2.16)$$

where k_o = rate constant for X = H

k = rate constant for X in place of H

ρ = constant for a given reaction

Hammett σ_p measures the effect of an X group on a benzene ring para to the site of interest, a positive value indicates electron withdrawal, and a negative value, electron donation, relative to the proton. More complex terms such as Hammett σ^+ are often used when an X substituent is thought to be in direct resonance with the site.

2B.3.1.2e Conclusions

Linear correlations are to be expected where a particular physical technique probes an energy level or difference directly related to the ΔE term, this term dominating the shielding. Indirect effects may be observed where a measured parameter mirrors the changes in effective ΔE and this can give rise to more general trends in shielding with data from a particular

technique although this is less likely to respond to subtle or complex behaviour and may reflect only gross changes. Where a linear correlation is observed it should not be concluded necessarily, that energy differences involved in shielding are being probed directly, especially in techniques such as electrochemistry where it is often the relative energy of a single level that is being measured.

2B.3.2 Transition elements

The transition elements occupy a special position in the consideration of chemical shielding. This arises from the dominant influence of the d-electrons which have a large orbital angular momentum when unquenched by a magnetic field. This property is primarily responsible for the large ranges of chemical shift in the transition series. Variations in σ^d and σ' are again taken as negligible and this is a good approximation as changes in σ_p are relatively large. A modified term for σ_p can be used derived from equation (2.14) [Equation (2.17)].

$$\sigma_p = -\text{const.}\ \overline{\Delta E}^{-1} \langle r^{-3} \rangle_{nd} (C_{M_{nd}})^2 \qquad (2.17)^{48}$$

$C_{M(nd)}$ is a coefficient derived from a M.O. treatment representing the metal character of molecular orbitals involved in the paramagnetic shielding and allows for the covalent bonding of ligands. In a crystal field model this factor may be formulated as k, the orbital expansion factor and is used to adapt the equation of Griffith and Orgel originally

formulated for cobalt d^6 complexes.[52]

$$\sigma_p = -\text{const.} \quad \frac{\langle r^{-3} \rangle_{3d}}{\Delta_o} \quad \langle O|L^2|O\rangle \qquad (2.18)$$

where Δ_o = crystal field splitting

$\langle O|L^2|O\rangle$ = ground state angular momentum term.

In transition metal complexes of high symmetry there are fewer excited states of the correct symmetry to contribute to σ_p than in a low symmetry system. In such cases ΔE is effectively the ligand field splitting (Δ_o),[52] circulation of charge occurring between t_{2g} and e_g orbitals in the octahedral case i.e. $d_\pi \rightarrow d_\sigma^*$. Such circulations are important as long as Δ_o is not overly large. It is the dependence on ΔE that produces the often large temperature dependence found for the shielding of transition metals with incomplete d shells. As the temperature increases shielding decreases as thermal excitation lowers the effective ΔE.[52] These effects range from ca. 3 ppm per °C for ^{57}Co, 1 ppm per °C for ^{103}Rh, to ca. 0.4 ppm per °C for ^{183}W.[60]

The various features of the shielding term can be demonstrated by considering ^{59}Co complexes on which much work has been done.[32] Co^{III} (d^6) forms octahedral complexes with a large variety of ligands which split the d orbitals according to their various σ and π electronic effects. The relative effect of ligands is probed by electronic absorption spectroscopy and allows them to be ordered ordered in the spectrochemical series.[50] Roughly, it is the ligating atom

of a particular ligand which determines Δ_o the ligand field splitting, so the order of increasing ligand effect is:-

$$I < Br < Cl < S < F < O < N < C$$

For 2p elements ligated to cobalt a linear correlation of chemical shift with $\frac{1}{\Delta_o}$ is observed and indicates that ΔE and $\langle r^{-3} \rangle$ terms are acting in concert.

Complexes containing ligating atoms from further down the periodic table often do not show such behaviour.[51] This can be attributed to their greater polarisability which allows them to interact with the metal d orbital in such a way as to expand the electron cloud. This nephelauxetic effect then changes the $\langle r^{-3} \rangle$ term in equation (2.17) and acts in opposition to changes in ΔE. Each ligand has its own such effect and it is not so much a function of the ligating atom thus the order of increasing influence for some general ligands is:-

$$F^- < H_2O < NH_3 < \underline{N}CS^- < Cl^- \sim CN^- < Br^- < I^-$$

An alternative expression for the nephelauxetic effect is the C_M term which reflects the degree of covalency of metal-ligand interactions. In practice this is difficult to separate from the $\langle r^{-3} \rangle$ term as both operate in the same direction and have similar origins. For qualitative arguments the two parameters are often considered in concert.[31]

From an inspection of the various components of σ_p it is apparent that a metal nucleus will be more shielded as:-

1) ΔE increases by lowering $d\pi$ or raising σ^* levels (or both) through changes in π-acceptor or σ-donor properties of ligands or changes in local symmetry.

2) $\langle r^{-3} \rangle$ is reduced by more nephelauxetic ligands.

3) C_M^2 is decreased by greater covalent ligand interaction.

Although the range of ligands bound by Co(III) is large, the types encountered are often not representative of the ligation found in low oxidation state systems. As the ^{95}Mo NMR studies of this thesis are predominantly of Mo(0) compounds it is pertinent to examine shielding trends in complexes of this type. For low oxidation state cobalt complexes, e.g. Co(-I) higher metal shielding is observed than for most Co(III) compounds.[53] Cobalt is highly shielded by ligands such as PF_3, H^- and CO; η^5-C_5H_5 is to medium field and halides and NO^+ cause deshielding.[32] In Co(-I) (d^{10}) complexes, d-d circulations are (formally) absent or arise through s, p, d mixing. In fact excitations involving the $4p/d\pi^*$ orbitals have been used to account for shielding changes.[53]

Low oxidation states with partially filled d orbitals are found earlier in the transition series as for V(-I), V(I) Nb(-I) and Mn(I) systems and these have been studied to various degrees by NMR.[49,54-59] Data on η^5-cyclopentadienyl complexes such as $[CpV(CO)_3PZ_3]$[54] and $[CpV(NO)_2L]$[57] (L = PZ_3, various Lewis acids; Z = F, OMe, alkyl and aryl) shows deshielding of ^{51}V in the order: PF_3 > CO > $P(OMe)_3$ > PR_3 > nitriles > amines > O-donors > I^- > Br^- > Cl^- > F^-.

For compounds in the series $[CpMn(CO)_2L]$ (L = various phosphines and phosphites) there is little variation of $\delta^{55}Mn$ with change in L and this is attributed to the large ΔE in these complexes. Nephelauxetic terms become dominant and these in turn are "equilibrated" by the π-bonding of the cyclopentadienyl ligand.[54] In complexes $[Mn(CO)_5L]^+$ [59] the ΔE term is more important and thus more variation in ^{55}Mn shielding is observed but the ordering of some ligands is reversed as compared to ^{51}V.[54]

Simple rationalisation of shielding effects due to some ligands, and particularly multiple substitution, may be difficult in $[CpV(CO)_{4-n}L_n]$ complexes due to the low symmetry and therefore the presence of several transitions in the 3d manifold which can contribute to σ_p. Higher symmetry complexes such as $[V(CO)_5L]^-$ and <u>cis</u>-$[V(NO)_2L_4]^-$ should present a more consistent picture and are also comparable with the Mo(0) complexes discussed in Chapters 3 and 4. For the former series shielding decreases in the order:-

$$CO > CNR \sim SbR_3 > PR_3 > AsR_3 > BiR_3 > DMSO \text{ (S-coordinated)} > NCR > \text{pyridine} > O \text{ donors.}[56]$$

Similar behaviour is observed for the dinitrosyl complexes where it is also found that I > Br > Cl.[55] Inspection of the trends shown reveals a dependence on the electronegativity of the ligating atom. As this decreases and π and σ donor ability is enhanced the metal σ^* orbitals are destabilised,

electron density is increased at the metal atom and this promotes back-bonding to the CO or NO ligand so stabilising the metal $d\pi$. A π-accepting ligand L will further stabilise the $d\pi$ orbitals so increasing the metal shielding. Such synergic interaction, or the presence of polarisable ligands will work to decrease σ_p by lowering $\langle r^{-3} \rangle_d C_{M_d}^2$. Interestingly the shielding order:-

$$[V(CO)_5L]^- > [V(CO)_{5-n}(NO)L_n] > [VX(NO)L_4]^+ > [V(NO)_2L_4]^+$$

(L = same ligand throughout, X = halide)

shows that the linear NO ligand is relatively deshielding towards vanadium and has been placed in the same class as NCR type ligands.[55] Investigations of this type provide the basis for the classification of ligands through their effect on metal shielding. The principles involved are generally applicable to other transition metals and will be further expanded when considering ^{95}Mo NMR in Chapters 3 and 4.

2B.4 A note on coupling constants

Spin-spin coupling can be observed in the spectrum of a probe nucleus X when it interacts with another magnetic nucleus Y. The magnitude of the coupling constant so produced is dependent on the extent of the interaction and also on γ_X and γ_Y. This $^nJ_{XY}$ quantity, where n is the number of bonds separating X and Y, may be directly compared with that for other nuclei by using the reduced coupling constant K_{XY} in equation (2.19).

$$K_{XY} = \frac{2\pi}{h\ \gamma_X\gamma_Y}\ J_{XY} \qquad (2.19)$$

The dominant influence on K_{XY} is usually the Fermi Contact Term which expresses the interaction of the nuclear moments of X and Y via the electron spins in s-orbitals. Coupling constants may be used for structure determination but can also give information about the bonding of X to Y as discussed in Chapters 4 and 5.

The coupling constants for two isotopes are related by their γ values and this gives a relation between ^{14}N and ^{15}N shown in equation (2.20).

$$J_{^{15}NX} = 1.403\ J_{^{14}NX} \qquad (2.20)$$

For J_{NX} couplings a particularly interesting feature is that contributions from the lone pair electrons on a nitrogen atom can be opposite to those due to the bonding electrons and can lead to much smaller coupling constants than otherwise predicted.[61]

CHAPTER 3

^{15}N and ^{95}Mo NMR Studies of Molybdenum Nitrosyl- and Diazenido-Complexes

3.1 Introduction

The linear nitrosyl ligand, formally NO^+, is isoelectronic with N_2 and adopts a similar synergic bonding mode in its complexes. In the context of nitrogen fixation, free NO is important as a potent inhibitor of nitrogenase probably binding to the same site in the enzyme that also interacts with dinitrogen. In chemical systems NO^+ is found at many metal sites which can also bind N_2 and has a rich coordination chemistry forming many varied complexes including complex cluster compounds. The nitrosyl ligand is of interest in its own right especially with its ability to change geometry between the linear $3e^-$ and the bent $1e^-$ donor configuration (formally NO^-) which is considered in more detail in Chapter 5. Nitrosyls may also be used to probe changes in the chemical environment at the metal site via NMR spectroscopy and comparison of such data with other physical properties may also yield useful information on the nature of the metal-ligand and ligand-ligand interactions.

Similar considerations apply to the diazenido-ligand NNR. This may be singly-bent, formally N_2R^+ (analogous to NO^+) or doubly-bent, formally N_2R^- (analogous to NO^-). Consideration of this geometrical transformation will be postponed until Chapter 5. An important example of the

diazenido-moiety is the NNH-ligand, a postulated intermediate in the reduction pathway for N_2 at a metal site.

Finally, the direct measurement of NMR parameters at the metal centre via ^{95}Mo NMR can provide complementary data concerning the effects of changes in the coordinating ligands.

The complexes chosen for this study were the octahedral, 18-electron, d^6 molybdenum complexes trans-$[MoX(NA)(dppe)_2]$ and trans-$[Mo(NCR)(NA)(dppe)_2]^+$ (A = O or NEt; X = a variety of anionic ligands; R = methyl or aryl; dppe = $Ph_2PCH_2CH_2PPh_2$). These complexes which formally contain Mo(0) are shown below:

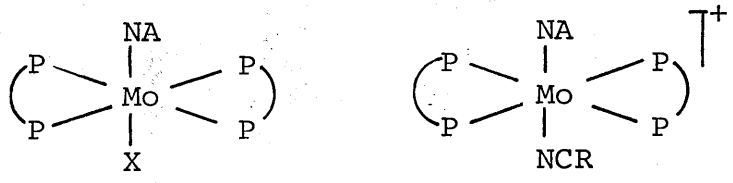

(A = NEt or O)

(X = a variety of ligands)

(R = methyl or aryl)

3.2 Preparation

3.2.1 Nitrosyl complexes

Some members of the series trans-$[MoX(NO)(dppe)_2]$ (3A; X = F, Cl or Br) were originally prepared by reaction of trans-$[MoX(N_2H)(dppe)_2]$ (obtained indirectly from trans-$[Mo(N_2)_2(dppe)_2]$) with NO gas.[1] This is summarised in Scheme (3.1).

Scheme (3.1)

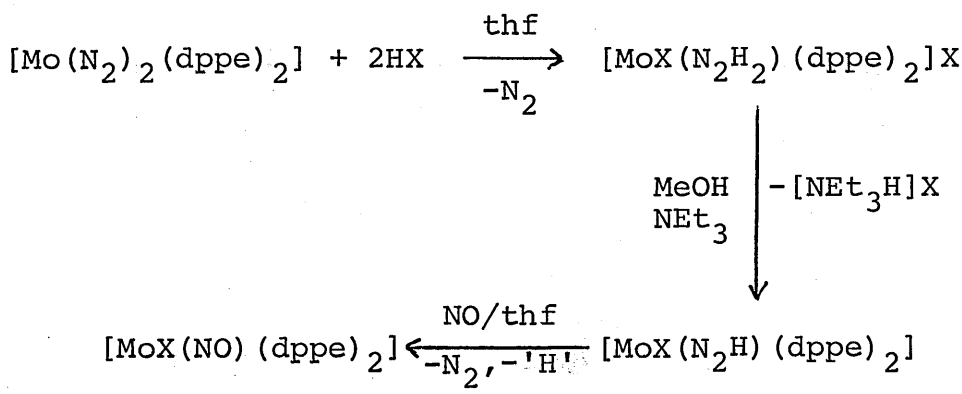

[X = Br, Cl or F (derived from BF_4^-)]

The complexes (3A; X = NCO) and (3A; X = H or OH) were originally isolated by the reaction of $[Mo(N_2)_2(dppe)_2]$ with $MeN(NO)C(O)NH_2$ and Et_2NNO respectively.[2] The complexes (3A; X = OH or H) may be metathesised as shown in (3.1)

$$[MoX(NO)(dppe)_2] + Y^- \xrightarrow[\text{reflux}]{\text{thf/MeOH}} [MoY(NO)(dppe)_2] + X^- \quad (3.1)$$

(X = OH or H; Y = SCN, NCO or N_3)

and converted (3A; X = OH) to $[Mo(NCMe)(NO)(dppe)_2][BF_4]_2$ as in reaction (3.2) where $AgBF_4$ acts as the oxidant.

$$[Mo(OH)(NO)(dppe)_2] \xrightarrow[\substack{\text{MeCN}\\\text{reflux}}]{AgBF_4} [Mo(NCMe)(NO)(dppe)_2][BF_4]_2 \quad (3.2)$$

A combination of the reactions shown in Scheme (3.1) and reactions (3.1) and (3.2) has been modified to introduce a

^{15}N label into the nitrosyl ligand by the use of ^{15}NO gas, as shown in Scheme (3.2). $TlBF_4$ is used as a non-oxidising halide abstractor to produce the common synthetic intermediate, $[Mo(NCMe)(^{15}NO)(dppe)_2][BF_4]$ (3B). The BF_4^- anion interferes with subsequent metathesis through formation of $[MoF(NO)(dppe)_2]$ and was therefore replaced by BPh_4^-.

Scheme (3.2)

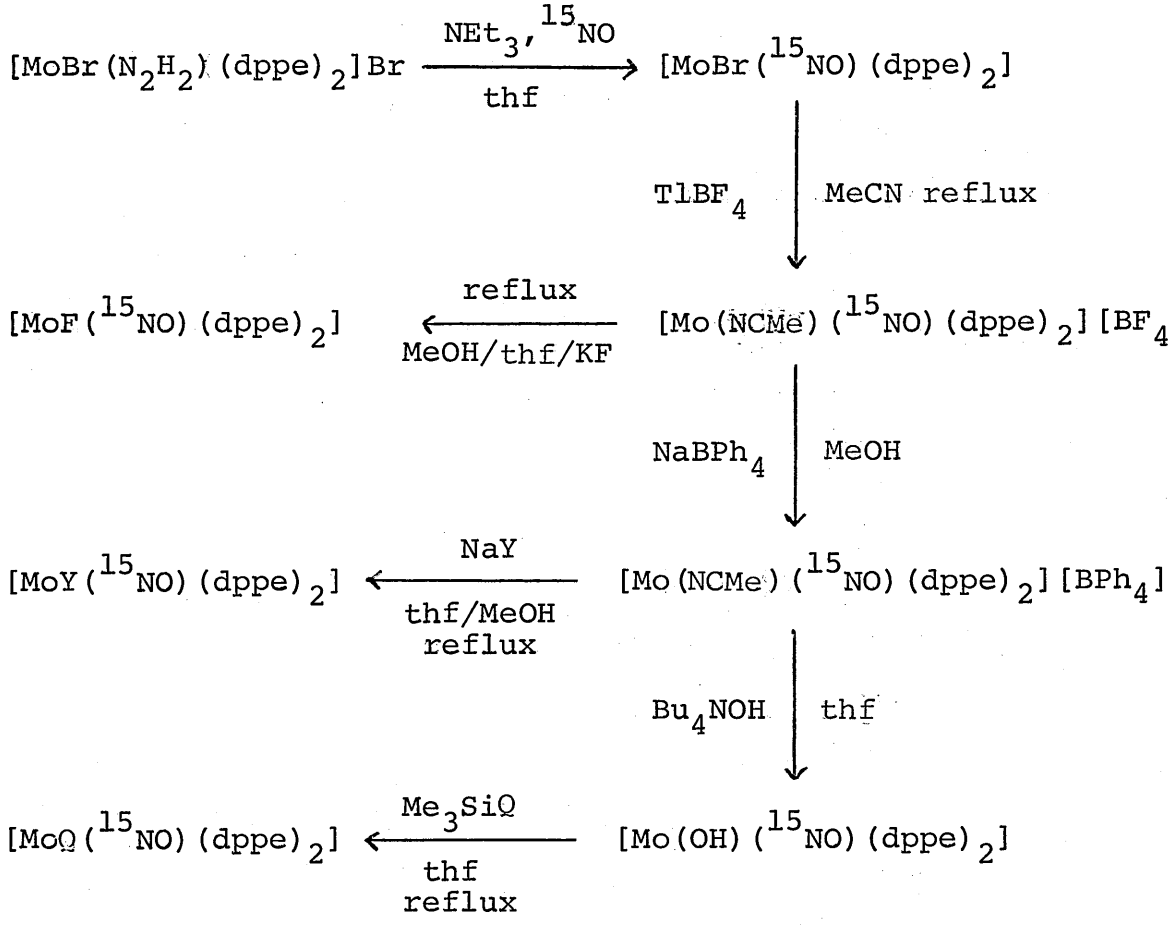

(Y = I, NCO, N_3, SCN or OPh; Q = SPh or CN)

Despite numerous attempts, the complex (3A; X = H) could not be made although it has been reported.[2] The

compounds synthesised were all yellow or orange crystalline samples stable in the solid state and in anaerobic solution but slowly decomposing in solution in air.

3.2.2 Diazenido-complexes

The compounds trans-$[MoBr(N_2R)(dppe)_2]$ (R = CH_3, NC_4H_9 and $(CH_3)_2CCH_2{=}CH_2$) have been prepared by George et al.[3] using reaction (3.3) and metathesised in a similar manner to

$$[Mo(N_2)_2(dppe)_2] \xrightarrow[\text{Benzene}]{\text{RBr, h}\nu} [MoBr(N_2R)(dppe)_2] \qquad (3.3)$$

(3.1) to give $[MoY(N_2R)(dppe)_2]$ (3C; Y = N_3 or SCN). In the present work ^{15}N isotopic labelling was introduced through $[Mo(^{15}N_2)_2(dppe)_2]$ which was converted to $[MoBr(^{15}N_2Et)(dppe)_2]$ by the action of EtBr. Convenient metathesis in high yield and purity was provided by Scheme (3.3), similar to that for the nitrosyl complexes.

Scheme (3.3):

$$[MoBr(^{15}N_2Et)(dppe)_2] \xrightarrow[\substack{\text{MeCN}\\\text{reflux}}]{TlBF_4} [Mo(NCMe)(^{15}N_2Et)(dppe)_2][BF_4]$$

$$\downarrow \text{MeOH} \mid NaBPh_4$$

$$[MoY(^{15}N_2Et)(dppe)_2] \xleftarrow[\substack{\text{thf/MeOH}\\\text{reflux}}]{NaY} [Mo(NCMe)(^{15}N_2Et)(dppe)_2][BPh_4]$$

$$\downarrow \text{RCN} \mid \text{thf, reflux}$$

$$[Mo(NCR)(^{15}N_2Et)(dppe)_2][BPh_4]$$

(R = C_6H_4Z-4; Z = H, MeO, MeCO; Y = I, NCO, N_3 or SCN).

The complex $[Mo(OH)(N_2Et)(dppe)_2]$ could not be made in an analogous way to the nitrosyl (3A; X = OH) [Scheme (3.2)] although it has been reported, in very low yield, as a side-product during chromatography of (3C; X = I; R = C_6H_{11}) on alumina.[4] Apparently the basic conditions required to introduce the OH substituent promote decomposition of the starting material. The complexes $[Mo(NCR)(^{15}N_2Et)(dppe)_2][BPh_4]$ (R = C_6H_4/Z-4; Z = H, MeO, MeCO) were made by simple replacement of MeCN in $[Mo(NCMe)(^{15}N_2Et)(dppe)_2][BPh_4]$ All complexes were isolated as micro-crystalline solids and are slightly less stable than the equivalent nitrosyl complex in solution in air but are quite stable in anaerobic solution.

3.3 ^{15}N NMR spectroscopy

3.3.1 Nitrosyl complexes

The complexes $[MoX(^{15}NO)(dppe)_2]$ (X = Br, I, N_3, NCS, NCO, CN, OPh, F, SPh and OH) and $[Mo(NCMe)(^{15}NO)(dppe)_2][BPh_4]$ labelled to 95%, in CH_2Cl_2 solution, all gave ^{15}N signals close to that of the reference CD_3NO_2 [Table (3.1)]. When resolved, the $^2J_{NP}$ coupling constants are ca. 6 Hz as shown in Figure (3.1). The shifts are in the region typical of linear nitrosyls[5] showing only a small upfield co-ordination shift from the free nitrosonium NO^+ ion at ca. +3 ppm.[6] The range of chemical shift is ca. 25 ppm. This may be compared with a range of ca. 4 ppm for the ^{13}C shifts of the trans-carbonyl ligands in a series of d^6 complexes

TABLE (3.1): ^{15}N NMR, U.V.-visible, electrochemical and infra-red data for nitrosyl complexes *trans*-[MoX(NO)(dppe)$_2$]

Complex	$\delta^{15}N$ (ppm)	λ_{max} (nm)	$E_{\frac{1}{2}}^{ox}$ (V)	$\nu(^{14}NO)$ (cm^{-1})
[Mo(CN)(NO)(dppe)$_2$]	-16.2	288	0.27	1575
[Mo(NCO)(NO)(dppe)$_2$]	-23.1	295	0.23	1553
[Mo(NCS)(NO)(dppe)$_2$]	-17.6	290	0.34	1572
[MoN_3(NO)(dppe)$_2$]	-20.2	306	0.25	1552
[Mo(OH)(NO)(dppe)$_2$]	-30.7	318	0.06	1510 (b)
[Mo(OPh)(NO)(dppe)$_2$]	-19.8	298	0.19	1533
[Mo(SPh)(NO)(dppe)$_2$]	-23.4	298	0.24	1552
[MoF(NO)(dppe)$_2$]	-22.8 (a)	310	0.15	1533
[MoBr(NO)(dppe)$_2$]	-22.0	302	0.24	1558
[MoI(NO)(dppe)$_2$]	-23.3	306	0.27	1566
[Mo(NCMe)(NO)(dppe)$_2$][BPh_4]	-5.8		0.53	1595

Notes for Tables 3.1 and 3.2:

All measurements in CH_2Cl_2 solution unless otherwise stated.

$\delta^{15}N$ relative to external $CD_3NO_2/Cr(pd)_3$, ±0.1 ppm, 298 K.

$E_{\frac{1}{2}}^{ox}$ relative to s.c.e. in thf with [NBu_4][BF_4] (0.2 M) carrier electrolyte, Pt electrode, ±10 mV.

λ_{max} ±2 nm; i.r. ν(NO) ±2 cm^{-1}, $\nu(N_2Et)$ ±5 cm^{-1}

(a) $^2J_{NF}$ *ca.* 53 Hz; (b) nujol mull.

Figure (3.1): ^{15}N NMR spectrum of trans-$[Mo(NCMe)(^{15}NO)(dppe)_2][BPh_4]$

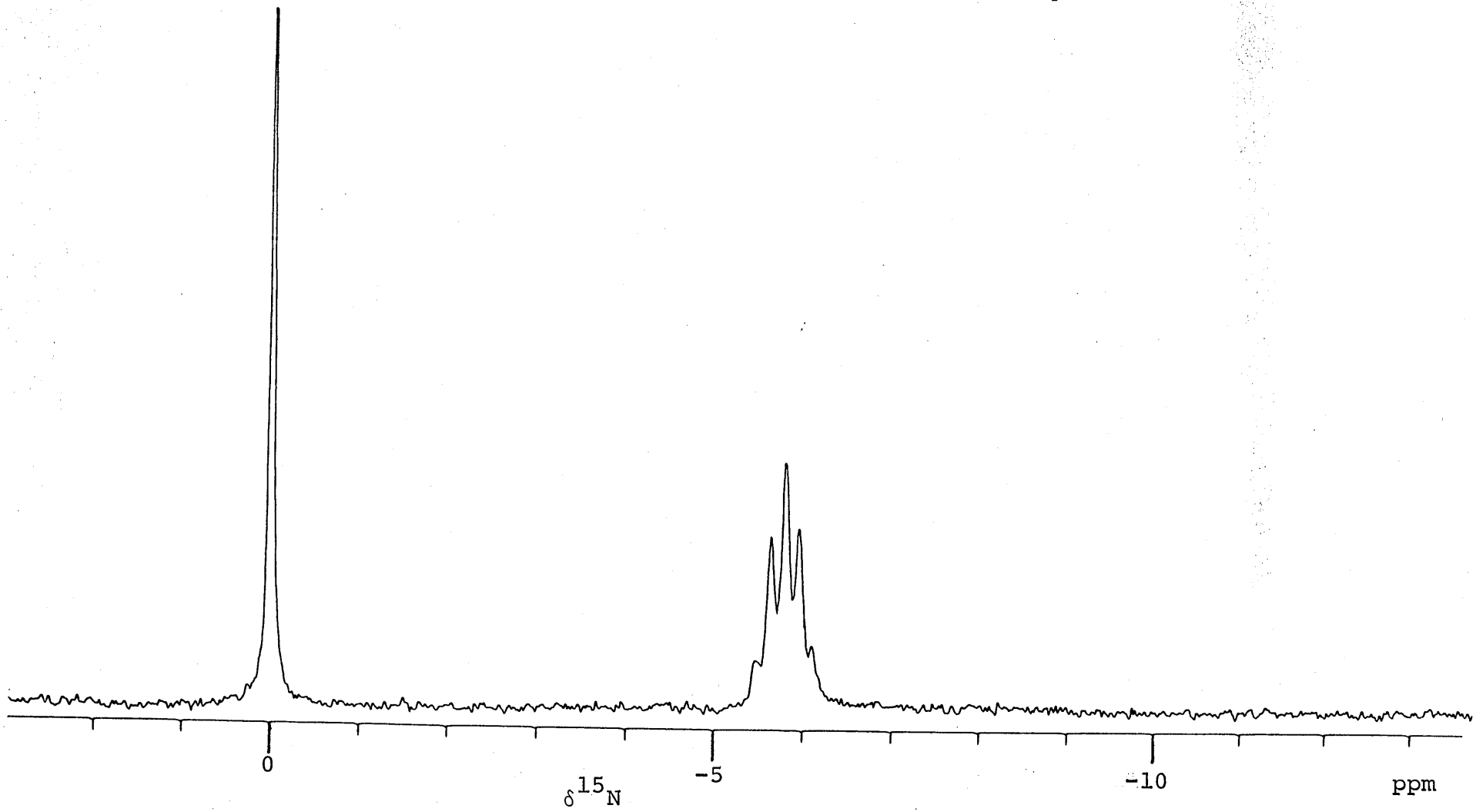

$[W(CO)_5L]^{n-}$ (L = neutral donor, n = 0; L = anionic donor, n = 1). The shielding order is $MeCN > CN^- > NCS^- > Br^- > I^- > SH^-$ [7] and although there are fewer ligands to compare, this is the reverse of the trend for ^{15}N in the nitrosyl complexes: i.e.

$$OH^- >> SPh^- > I^- > NCO^- > F^- > Br^- > N_3^- > OPh^- > NCS^- > CN^- >> MeCN.$$

This is similar to the situation found in complexes $[(\eta^5\text{-}C_5H_5)Mo(CO)L(NO)]$ (L = PPh_3 or CO).[8] As L is changed from CO, a good π-acceptor, to PPh_3, a poor π-acceptor, the ^{13}C of the carbonyl ligand is deshielded while ^{15}N of the nitrosyl is slightly shielded. Of course, some caution should be used in comparing the effects with trans-$[MoX(^{15}NO)(dppe)_2]$ as the coordination environments and geometries are somewhat different.

Rationalisation of shielding changes in terms of changing levels of molecular orbitals is difficult because of the complexity of the factors involved, as shown in Chapter 2. Some general observation can, however, be made. It was mentioned in Chapter 2 that $\sigma \leftrightarrow \pi$ circulations have been proposed as the main contribution to the deshielding of ^{13}C in metal carbonyls. Evidence for this comes from ^{13}C shielding tensor measurements.[9] Studies of ^{15}N shielding tensors in nitrosyl complexes have led to similar conclusions for the deshielding of ^{15}NO.[10] The relative importance of $\sigma \rightarrow \pi^*$ and $\pi \rightarrow \sigma^*$ components of the $\pi \leftrightarrow \sigma$ circulation may, however, be different for the CO and NO ligands, because of

differences in their orbital energies with respect to the metal d orbitals.

The general trends in shielding for ^{13}CO and ^{15}NO, shown above, seem to suggest that changes in the donor-acceptor properties of the co-ligands may have opposite effects on the shielding. In case this behaviour should be found to be generally observed, it is interesting to examine how it might arise. In the free NO molecule the π^* orbital is at least 3.7 eV more stable than that in CO and the lone pair 2.5 eV more stable (i.e. 2.5 eV further away in energy from the metal d-orbitals).[11] It is likely, therefore, that the π and π^* orbitals are stabilised in M-NO, as compared with M-CO, relative to the σ orbitals. A crude assumption from this argument is that the $\sigma \rightarrow \pi^*$ energies are likely to decrease and $\pi \rightarrow \sigma^*$ energies to increase from CO to NO. A further consequence is that the π^* (NO) orbital is brought closer in energy to the $d\pi$ orbitals, substantially increasing the interaction.[12] The interaction of the ligand and metal π orbitals is, however, greatly reduced as compared with M-CO.

Normally, discussion of synergic behaviour is confined to $d\pi \leftrightarrow \pi^*$ (XY) interaction but the $d\pi \leftrightarrow \pi$ (XY) interaction has been invoked to explain the difference in behaviour of the NO, NS and CO, CS pairs of ligands, in their complexes.[13]

A schematic (qualitative) drawing is shown below [Figure (3.2)] showing the possible differences in interaction of NO and CO π and π^* orbitals with the metal $d\pi$ orbitals.

Figure (3.2):

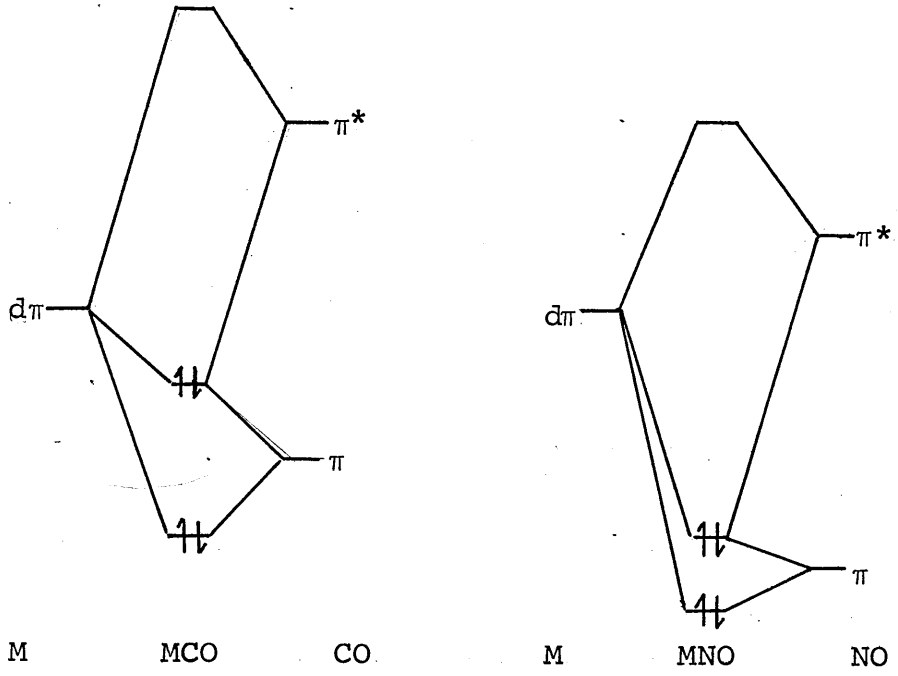

Considering the possible components of $\sigma \leftrightarrow \pi$ circulation: the $\pi \rightarrow \sigma^*$ possibly involves the π HOMO and a high lying σ^* orbital. The $\sigma \rightarrow \pi^*$ components might involve the π^* LUMO shown in the diagram, the HOMO being some relatively high lying σ orbital. In terms of changes in π levels only, a good π-donor <u>trans</u> to XY (NO or CO) will raise the π and π^* (MXY) orbitals and so tend to lower $\pi \rightarrow \sigma^*$ and raise $\sigma \rightarrow \pi^*$ energies. Herein may lie a possible difference between NO and OC since changes in π(MXY) will be more important for CO, which has the greater (repulsive) π-interaction between filled $2p\pi$ and $d\pi$ orbitals. Thus a good π-donor in the <u>trans</u>-position may deshield ^{13}CO by decreasing $\pi \rightarrow \sigma^*$

energies but increase ^{15}NO shielding by increasing $\sigma \rightarrow \pi^*$ energies. Although this type of argument is a gross over-simplification it may serve as a starting point for predictions of other shielding correlations which can be verified by experiments and calculation.

General trends in the ^{15}N shielding of the molybdenum nitrosyl complexes are consistent with the argument put forward above. Thus OH^-, a good π-donor, shields ^{15}NO whereas at the other extreme MeCN is a relatively good π-acceptor resulting in deshielding. The large downfield shift is also partly due to the positive charge of $[Mo(MeCN)(NO)(dppe)_2]^+$.

CN^- can also accept charge from the metal resulting in deshielding of ^{15}N. The order $OH^- > OPh^-$ might be expected as the oxygen 2p orbitals in OPh^- are somewhat delocalised into the aromatic system, decreasing π-donation to the metal. Between the obvious extremes there is a range of shielding behaviour determined by the relative σ-donor and π-acceptor/donor power of the ligand and perhaps also the degree of overlap of ligand orbitals with the metal orbitals. This is probably reflected in the observed ordering $I^- > F^- > Br^-$. Similarly the other ligands are difficult to compare with each other but comparisons may be made with data from other sources (*vide infra*). In the series *trans*-$[MoX(NNH_2)(dppe)_2]^+$ shielding also decreases with X in the order $I^- > F^- > Br^-$ for both nitrogens of the hydrazido(2-)-ligand.[14] Interestingly in the complexes *trans*-$[MoX(NH)(dppe)_2]^+$ the oxygen donor ligand OMe^- shields the imido-ligand by *ca.* 70 ppm with respect to Br^-.[14]

3.3.2 Diazenido-complexes

These complexes are all very soluble in CH_2Cl_2 and ^{15}N NMR data for these solutions are shown in Table 3.2. Enrichment to 50% in ^{15}N was employed. A representative range of ligands X in the series *trans*-[MoX($^{15}N_2$Et)(dppe)$_2$] (X = NCO, Br, N_3 or SCN) was studied for comparison with the nitrosyl analogues and also the complexes *trans*-[Mo(NCR)($^{15}N_2$Et)(dppe)$_2$] (R = Me, C_6H_4Z-4; Z = H, MeO or MeCO) were examined. These complexes contain two ^{15}N probe nuclei, the N_α and N_β of the singly-bent diazenido-ligand:

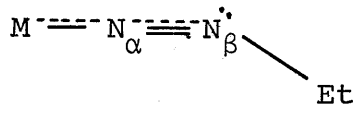

Two signals are observed in the ^{15}N NMR spectrum in the region characteristic of this ligand type (N_α *ca.* 0 ppm and N_β *ca.* 150 ppm) and close to that for aryl diazonium ions.[15] $^1J_{NN}$ couplings are *ca.* 10 Hz where resolved but no J_{NP} couplings could be resolved from the broad N_α resonance [Figure (3.3)]. Comparison with other diazenido-systems is made in Chapter 5. N_α of the diazenido-ligand shows the same trend in ^{15}N shielding as for the nitrosyl ligand:- $NCO^- > Br^- > N_3^- > NCS^- >> MeCN$, and it may be envisaged that similar effects are operating in both systems. This is further substantiated by the trend in N_β which is similar to that above for N_α, effects being transmitted through the M-N-N fragment. Electron withdrawing ligands such as MeCN will lower the π^* level for N_α and N_β. Shielding of N_β will decrease as n(lone pair)$\rightarrow\pi^*$ excitations are important

TABLE (3.2): ^{15}N NMR, electrochemical and infra-red data for diazenido-complexes *trans*-$[MoX(N_2Et)(dppe)_2]$

Complex	$\delta^{15}N$ (ppm) N_α	N_β	$E_{\frac{1}{2}}^{ox}$ (V)	ν^{14}_{NN} (cm^{-1})
$[Mo(NCO)(N_2Et)(dppe)_2]$	-5.1	-154.1	0.09	1520
$[Mo(NCS)(N_2Et)(dppe)_2]$	+2.4	-148.8	0.17	1535
$[MoN_3(N_2Et)(dppe)_2]$	-0.8	-148.7	0.07	1520
$[MoBr(N_2Et)(dppe)_2]$	-2.6	-153.6	0.09	1530
$[Mo(NCMe)(N_2Et)(dppe)_2][BPh_4]$	+12.9	-136.6	0.40	1570
$[Mo(NCC_6H_4MeO\text{-}4)(N_2Et)(dppe)_2][BPh_4]$	+13.3	-135.2	0.39	1575
$[Mo(NCC_6H_5)(N_2Et)(dppe)_2][BPh_4]$	+13.7	-134.2	0.41	1580
$[Mo(NCC_6H_4CH_3CO\text{-}4)(N_2Et)(dppe)_2][BPh_4]$	+14.7	-132.1	0.43	1580

For notes see Table (3.1)

Figure (3.3): ^{15}N NMR spectrum of trans-$[MoN_3(^{15}N_2Et)(dppe)_2]$

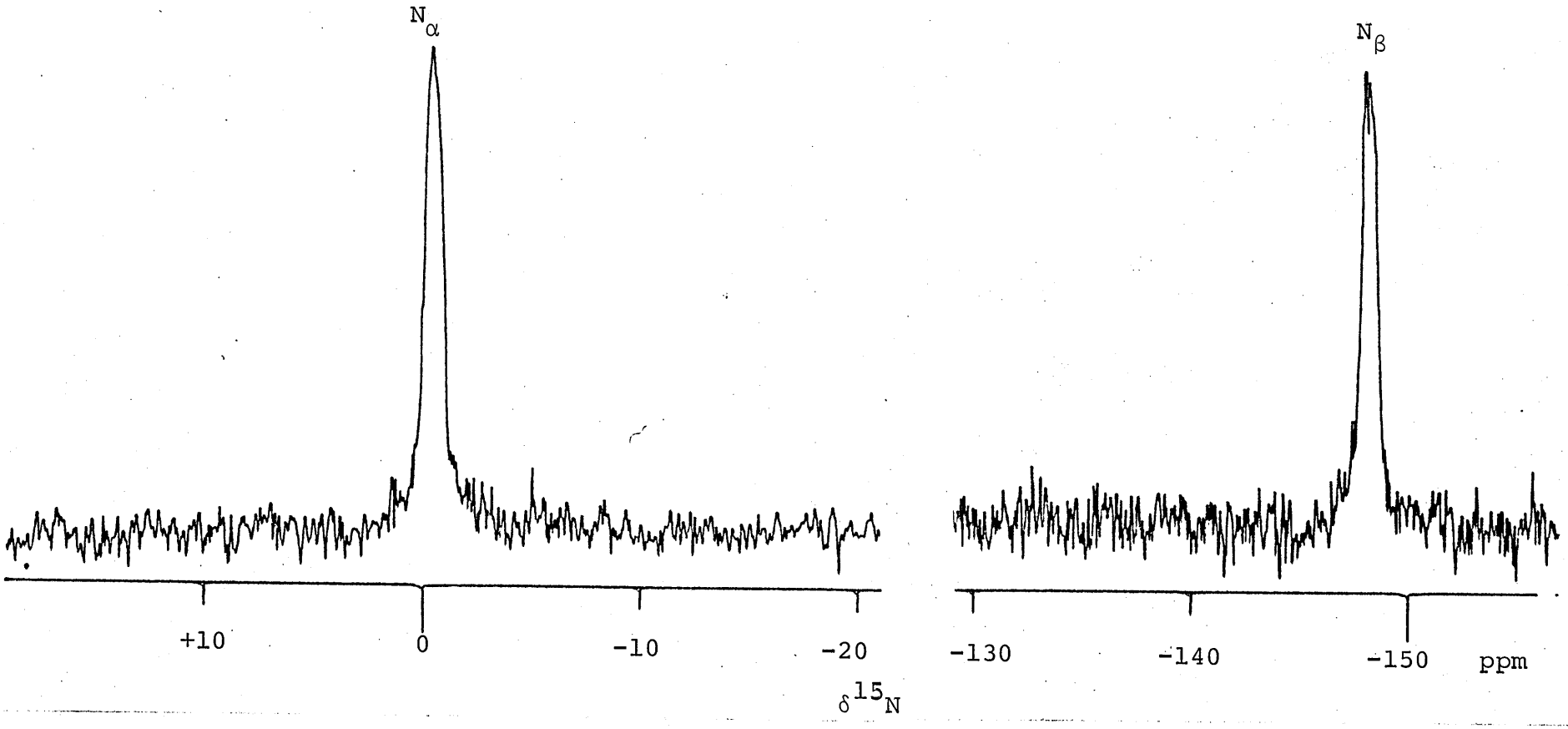

for the terminal nitrogen. This is indicated by the large upfield shift of N_β on protonation to give the hydrazido(2-)-complexes with $Mo{=}N{-}N\begin{smallmatrix}H\\Et\end{smallmatrix}$ [Table (3.3)] in which protonation of the lone pair removes the low energy $n\rightarrow\pi^*$ contribution to deshielding. This effect, commonly observed for such systems, will be further discussed in Chapter 5.

TABLE (3.3): ^{15}N NMR data for hydrazido(2-)-complexes trans-$[MoX(N_2HEt)(dppe)_2]Br$

Complexes	$\delta^{15}N$ (ppm) N_α	N_β
$[Mo(NCO)(N_2HEt)(dppe)_2]Br$	-73.5	-219.4
$[Mo(NCS)(N_2HEt)(dppe)_2]Br$	-67.2	-215.1
$[MoN_3(N_2HEt)(dppe)_2]Br$	-75.4	-221.8

The complexes $[Mo(NCR)(N_2Et)(dppe)_2]^+$ provide a comparison with the previously studied $[Mo(NCR)(N_2)(dppe)_2]$ series mentioned in Chapter 2 and Table (2.4). The shielding of $^{15}N_\alpha$ (of N_2Et or N_2) decreases for both sets of complexes with decreasing overall donor ability of R, although for the dinitrogen complexes larger changes are observed. For these complexes, however, $\delta^{15}N_\beta$ is almost invariant whereas for the diazenido-series, $\delta^{15}N_\beta$ varies, with change in R, in the same direction and also slightly more markedly than does N_α. This shows the obvious differences between shielding in the N_2 ligand compared with

N_2R. Differences in the deshielding contributions in the two systems are to be expected; for example it has been shown that π^* is much lower in energy for N_2R^+ than for N_2 in similar complexes.[16]

3.4 Interpretation of data from electrochemical measurements, infra-red and U.V.-visible spectroscopy

3.4.1 Oxidation potentials

The nitrosyl and diazenido-complexes all show reversible one-electron oxidation in thf when studied by cyclic voltammetry; an example is shown in Figure (3.4).

Figure (3.4): Cyclic voltammogram of trans-$[Mo(NCO)(N_2Et)(dppe)_2]$

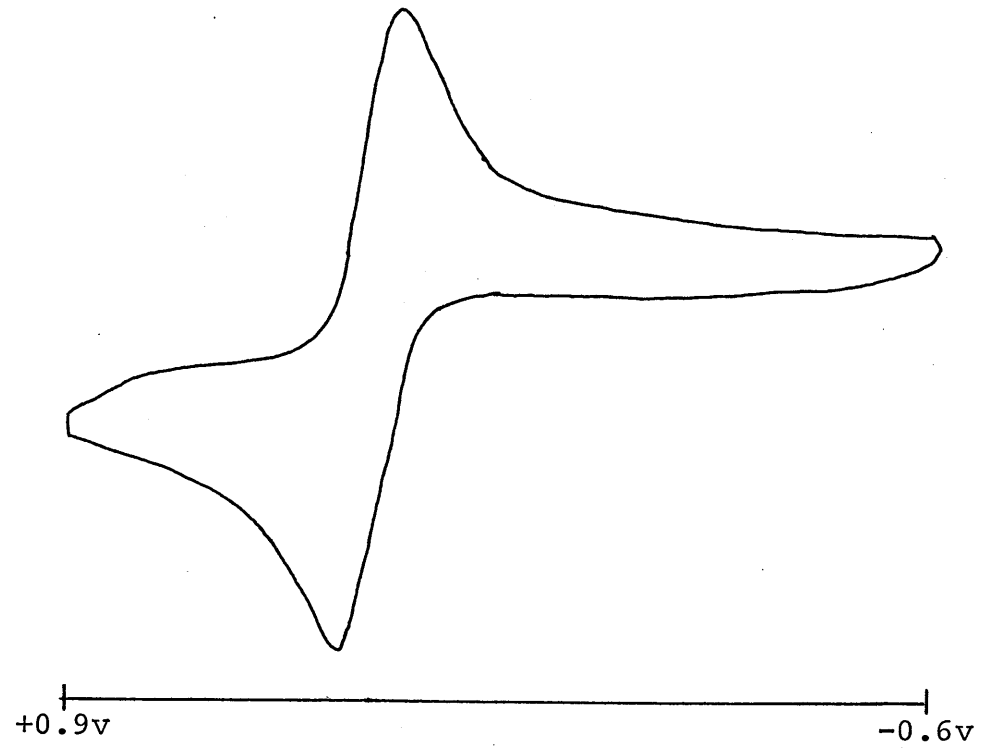

The half-wave oxidation potentials ($E_{\frac{1}{2}}^{ox}$) are shown in Tables (3.1) and (3.2). For these closely related series of compounds a low $E_{\frac{1}{2}}^{ox}$ indicates ease of oxidation from a relatively high energy H.O.M.O. produced by a decreased effective nuclear charge at the metal.[17] This is shown by the ordering of the ligands with increasing complex oxidation potential:- $OH^- < F^- < OPh^- < NCO^- \leqslant Br^- \sim SPh^- \leqslant N_3^- < CN^- < I^- < NCS^- << MeCN$. The first point to note is that OH^- and MeCN are at the extremes as for ^{15}N shielding, as determined by their gross donor or acceptor properties. The ordering of the rest of the ligands reflects the response of $E_{\frac{1}{2}}^{ox}$ to the relative charge at the metal, the H.O.M.O. probably having little X ligand character.[17] It has been suggested that $E_{\frac{1}{2}}^{ox}$ is a measure of the total ($\sigma+\pi$) donor properties of the ligand X towards the site.[17] It appears in the present study that ligands containing more electronegative atoms reduce $E_{\frac{1}{2}}^{ox}$ and so OPh < SPh, $F^- < Br^- < I^-$ and $NCO^- < NCS^-$. Clearly this pattern is distinct from that for ^{15}N shielding, the difference stemming from the mixing of ligand X character into orbitals involved in the σ_p shielding term. Comparing the series of compounds $[Mo(NCR)(L)(dppe)_2]$ ($L = N_2Et$) with ($L=N_2$), once again $E_{\frac{1}{2}}^{ox}$ changes in the same direction for both, but less markedly for $L = N_2Et$, reflecting the greater π-accepting capability of this ligand compared to N_2, effectively "buffering" the charge on the metal. A similar analysis has been made for NO in nitrosyl complexes.[17]

Attempts to probe the L.U.M.O. by studying reduction potentials of the various complexes in thf were unsuccesful, reduction occurring at more negative potentials than that at which the solvent is reduced, ca. -2.5 V vs. S.C.E. This potential gives a lower limit to the energy of the L.U.M.O.

3.4.2 Infra-red spectroscopy

Ligand stretching frequencies $\nu(^{14}NO)$ or $\nu(^{14}NN)$ were generally measured in CH_2Cl_2 solution but for [Mo(OH)(NO)$(dppe)_2$] a very broad band was found, probably due to hydrogen bonding, and so this spectrum was recorded as a nujol mull. The error in measurement of $\nu(^{14}NN)$ is large due to broadening of the band through vibronic coupling with CH_2 bending modes of the ethyl group.[3] Isotopic labelling, places $\nu(^{15}NO)$ ca. 30 cm^{-1} to lower frequency and $\nu(^{15}N^{15}N)$ lower by ca. 40 cm^{-1} compared to the unlabelled ligand. The data in Tables (3.1) and (3.2) show all ν(NO) and ν(NN) to be below 1600 cm^{-1} which is relatively low for linear nitrosyl and singly-bent diazenido-ligands and may be explained by substantial back-donation from the electron rich molybdenum centre to the ligand π^* orbitals.[2] If the empirical rules developed by Haymore and Ibers[18] (see also Chapter 5) are employed, to apply a correction factor to the NO and NN stretching frequencies, the corrected frequencies all come above 1650 cm^{-1} and thus in the required range for linear nitrosyl-

and singly-bent diazenido-ligands. There is a correlation of stretching frequency with $E_{\frac{1}{2}}^{ox}$, showing that a metal-ligand π-donation as probed by ν(N=A) has a simple relation with electronic charge at the metal[17] and so does not reflect the competitive ligand effects shown by ^{15}N NMR.

3.4.3 U.V.-visible spectroscopy

Typical U.V.-visible spectra of the nitrosyl and diazenido-complexes are shown in Figure (3.5). The essential features of the spectra are superimposed on the broad, very strong absorption assigned to the dppe ligands[4] which rises to a maximum at ca. 250 nm. In both the nitrosyl and diazenido-systems a shoulder at ca. 350 nm is observed with ε ca. 6000 $M^{-1}cm^{-1}$. This band has been assigned as metal to ligand charge transfer (MLCT), Mo→P, in diazenido-complexes[3] and a similar assignment is reasonable for the analogous nitrosyls. A band observed in the nitrosyl but not the diazenido-compounds occurs as a shoulder in the region 320 to 285 nm with ε ca. 10,000 $M^{-1}cm^{-1}$. This band varies with the trans-ligand X [Table (3.1)] and this behaviour, coupled to its absence in the diazenido spectrum, points to it being MLCT or LMCT (Mo←→NO). The strong OH^- donor causes a shift to lower energy, whereas more withdrawing groups such as NCS^- or CN^- cause a blue shift. In the MeCN complex the absorption is shifted to sufficient energy to be lost under the dppe band. This may be explained by donor ligands raising the energy of the metal π level relative to the ligand π* level as in a Mo→NO MLCT. In the diazenido-

Figure (3.5a): U.V.-visible spectrum of trans-$[Mo(SCN)(NO)(dppe)_2]$

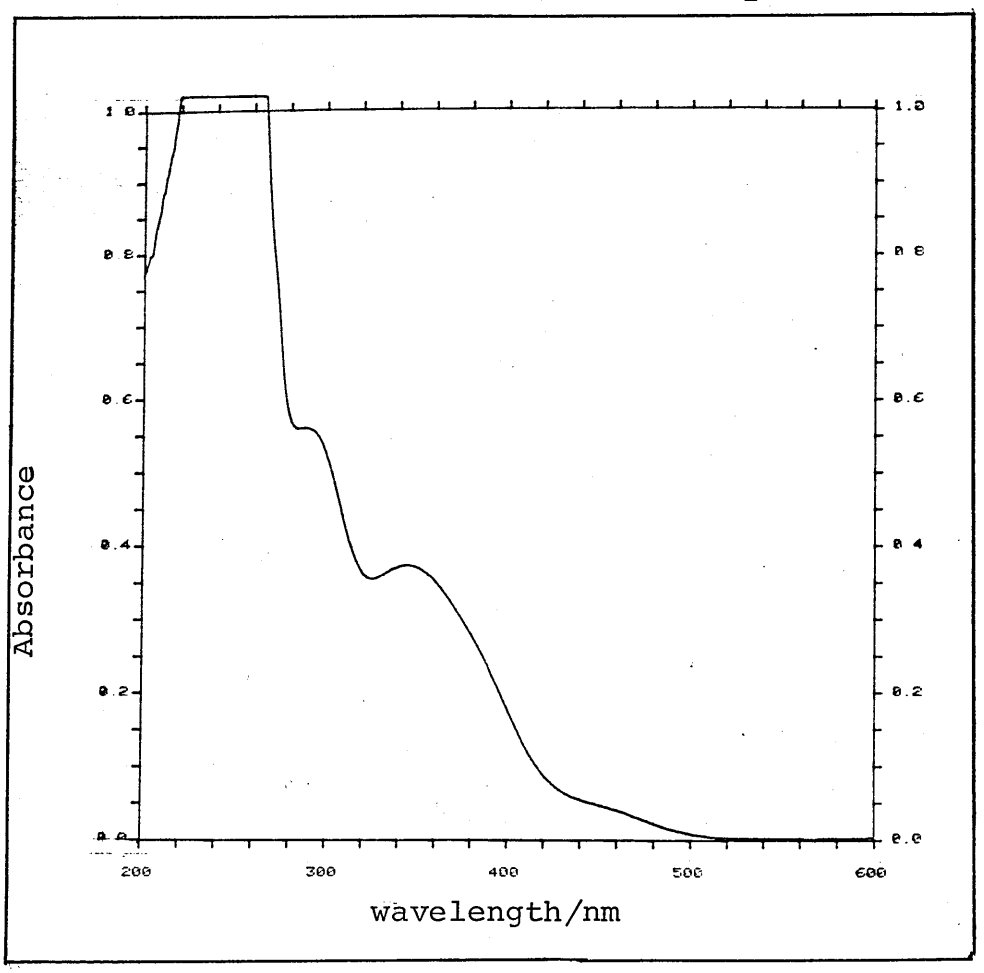

Figure (3.5b): U.V.-visible spectrum of trans-$[Mo(SCN)(N_2Et)(dppe)_2]$

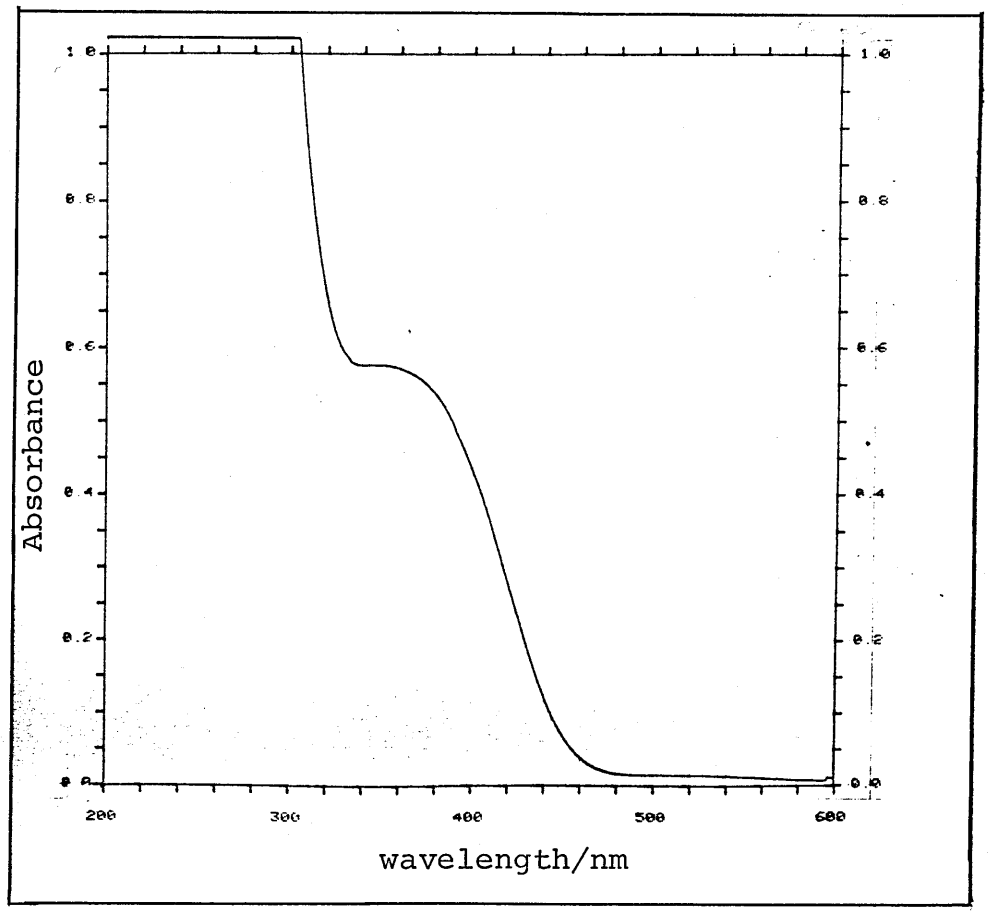

complexes d-d transitions at ca. 500 nm were observed but were too broad to be measured accurately.

3.5 Trends in ^{95}Mo and ^{31}P NMR data

The ^{95}Mo and ^{31}P chemical shifts of some of the diazenido- and nitrosyl complexes are presented in Table (3.4). The typical ^{95}Mo NMR spectrum in Figure (3.6) shows a quintet from coupling to four equivalent phosphorus nuclei $^{1}J_{MoP}$ coupling constants were ca. 170 Hz where resolved. ^{31}P spectra are all singlets expected from the trans geometry.

A comparison of the data in Tables (3.1) and (3.2) with that in Table (3.4) clearly shows that trends in the ^{95}Mo and ^{31}P data differ substantially from those in the $E_{\frac{1}{2}}^{ox}$, i.r., U.V.-visible, and ^{15}N NMR measurements. This is similar to the situation found in complexes containing the cis-$\{Mo(NO)_2\}^{2+}$ unit where small changes in co-ligand give shielding effects on ^{95}Mo as discussed below, but show no relation to trends in U.V.-visible or ν(NO) infra-red measurements.[19]

The ^{95}Mo chemical shifts of complexes containing nitrosyl or diazenido-ligands, in terms of a spectrochemical series of ligands, will be discussed in the next chapter. The ^{95}Mo shifts for the nitrosyl complexes cover a range of ca. 300 ppm and this reflects the sensitivity of this nucleus to small changes in coordination environment, the corresponding change in ^{31}P shifts being only ca. 10 ppm. In fact a linear, inverse relationship is found between ^{95}Mo and ^{31}P shifts for both the diazenido- and nitrosyl complexes [Figure (3.7)],

TABLE (3.4): ^{95}Mo and ^{31}P NMR data for nitrosyl and diazenido-complexes

Complex	$\delta^{31}P$ (ppm)	$\delta^{95}Mo$ (ppm)
$[Mo(CN)(NO)(dppe)_2]$	-81.8	-777
$[Mo(NCO)(NO)(dppe)_2]$	-84.1	-636
$[Mo(NCS)(NO)(dppe)_2]$	-83.8	-629
$[MoN_3(NO)(dppe)_2]$	-84.8	-614
$[Mo(OH)(NO)(dppe)_2]$	-85.4	-572
$[Mo(NCMe)(NO)(dppe)_2][BF_4]$	-81.2	-553
$[MoI(NO)(dppe)_2]$	-86.9	-526
$[Mo(SPh)(NO)(dppe)_2]$	-87.0	-521
$[MoBr(NO)(dppe)_2]$	-89.3	-514
$[Mo(OPh)(NO)(dppe)_2]$	-89.0	-493
$[Mo(NCS)(N_2Et)(dppe)_2]$	-80.3	-206
$[Mo(NCO)(N_2Et)(dppe)_2]$	-80.5	-201
$[MoN_3(N_2Et)(dppe)_2]$	-81.7	-180
$[Mo(NCMe)(N_2Et)(dppe)_2][BPh_4]$	-77.7	-140
$[MoBr(N_2Et)(dppe)_2]$	-83.6	-89

All measurements in CH_2Cl_2 solution at 298 K.

$\delta^{31}P$ relative to external $P(OMe)_3/C_6D_6$

$\delta^{95}Mo$ relative to external 2M aqueous Na_2MoO_4 at pH 11.

Figure (3.6): ^{95}Mo NMR spectrum of trans-[Mo(OPh)(NO)(dppe)$_2$]

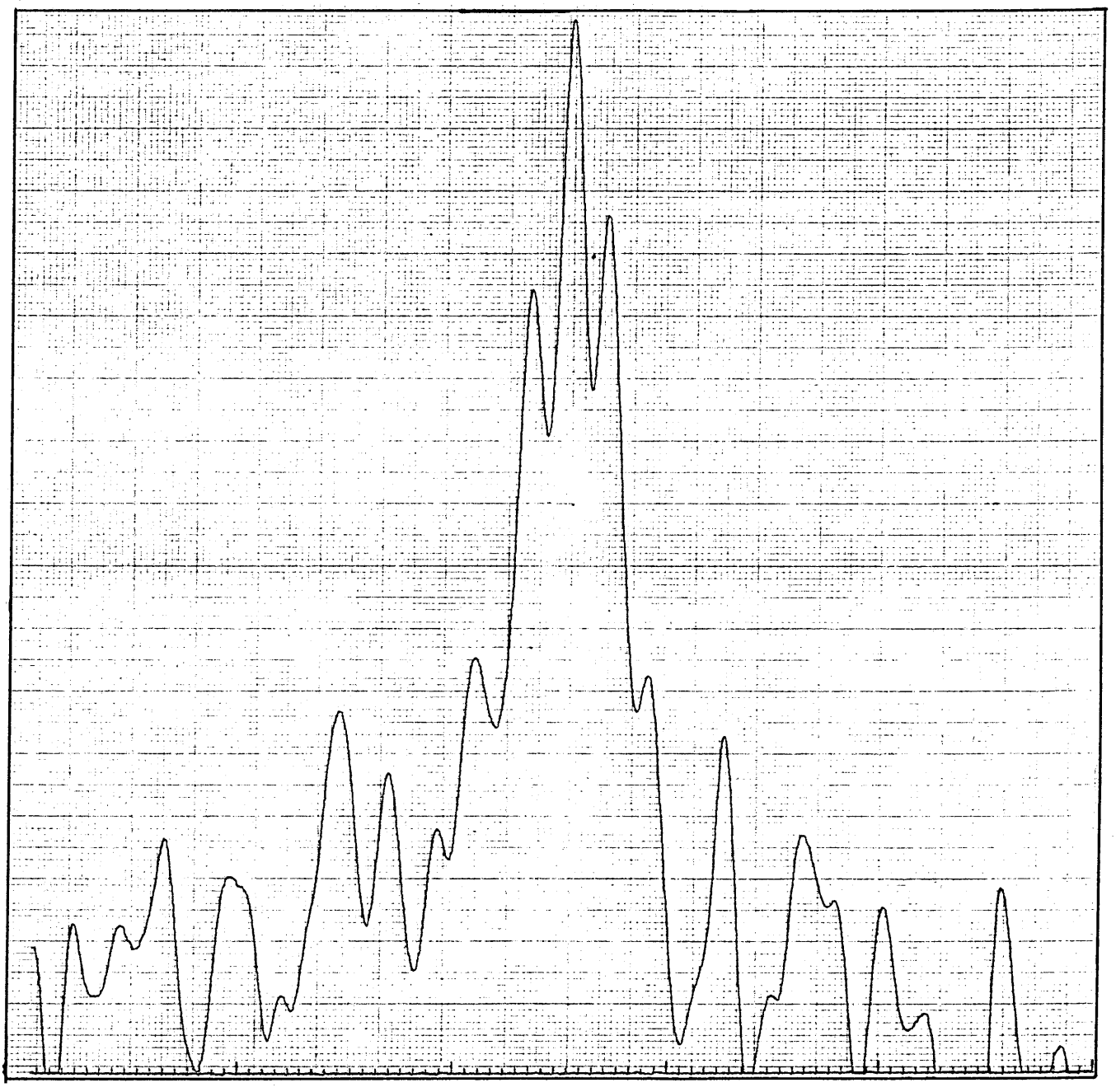

Figure (3.7): Graph to plot ^{31}P vs. ^{95}Mo chemical shift for trans-$[MoX(L)(dppe)_2]$ (L = NO or N_2Et)

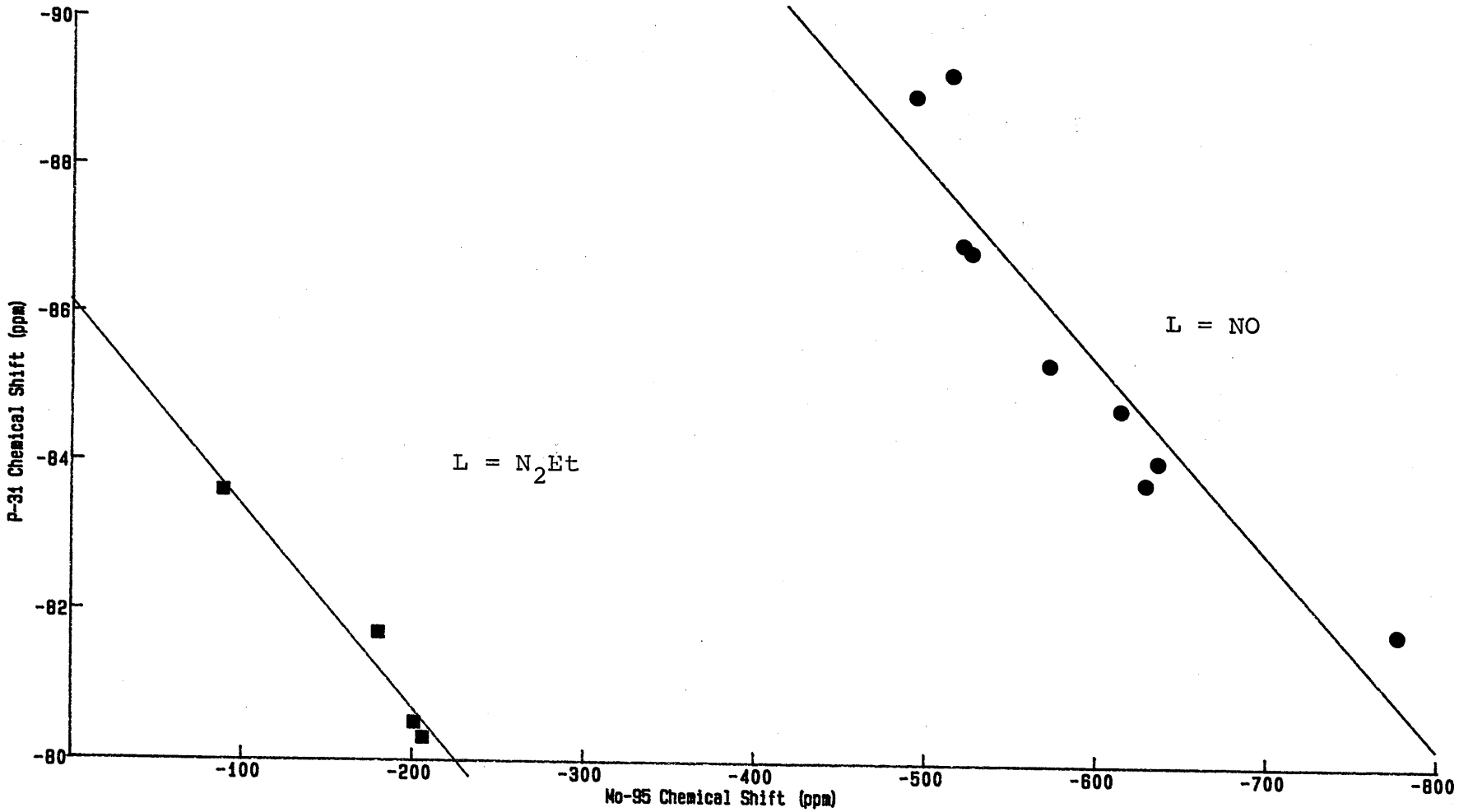

shielding of the ^{31}P nuclei of the dppe ligands increasing as ^{95}Mo is progressively deshielded. An explanation of this trend may arise from considering the factors determining changes in ^{95}Mo shifts for these complexes. The discussion of shielding found in Chapter 2 is relevant to these systems. The order of increasing shielding of the ^{95}Mo nucleus with change in X ligand is:-

$OPh^- < Br^- < SPh^- < I^- < OH^- < N_3^- < NCS^- < NCO^- < CN^-$

This bears an interesting resemblance to the spectrochemical series based on the ligating atom, discussed before, which for the above ligands is:- I < Br < S < O < N < C, reflecting the increase in the ΔE separation. Therefore it would seem the chemical shifts can be explained largely by the ΔE formalism. Some of the ligand orderings, however, are not as predicted by the above, notably the order $Br^- < I^-$ and $OPh^- < SPh^-$. Here the effects due to the nephelauxetic property of the ligand are important. Thus I^- and SPh^- are more polarisable than Br^- and OPh^- respectively, increasing the radius of the d-orbitals and perhaps inducing more covalent character into the M-X bond, thus decreasing σ_p by a decrease in $\langle r^{-3} \rangle_{4d}$ and $C^2_{M_{4d}}$. This may also contribute to the ordering of ligands with the same ligating atom, i.e. N_3^-, NCS^- and NCO^-. As mentioned before, it is not possible to measure d-d transitions for these systems, therefore correlation with ligand field splitting ($t_{2g} \rightarrow e_g$ transitions) cannot be examined.

The complexes with X = MeCN do not fall on the lines drawn in Figure (3.7), consistent with the further deshielding of ^{95}Mo relative to ^{31}P because of the positive charge on the complex. This is a further manifestation of the nephelauxetic effect, cationic charge increasing $\langle r^{-3} \rangle_{4d}$.

Re-examining the relationship in Figure (3.7), some interesting points arise. ^{31}P magnetic shielding has received scant attention in the field of metal complexes with few attempts to separate the contributions to σ_p for this nucleus.[20] As with other nuclei, a rationale based on ΔE for charge circulation at the nucleus might be invoked, but it is difficult to see how this might be related to the ^{95}Mo shielding and particularly why the ^{31}P shielding is in the opposite direction. As noted above, the ^{95}Mo shielding order for the various ligands X arises through a combination of terms in $\sigma_p^{\S}$ and so ^{31}P shielding cannot be related simply to only the ΔE term or the $\langle r^{-3} \rangle C_{M_{4d}}^2$ term at ^{95}Mo. Similar inverse correlations are found between ^{95}Mo and ^{13}C shifts in $[Cp_2MoH_2]$ and $[Cp_2MoH_3]^+$.[21] Such observations at first glance resemble results found for metal hydrides by Buckingham and Stevens[22] who put forward a theory which explains the inverse relationship of ^{195}Pt with ^{1}H shifts in <u>trans</u>-$[Pt(PEt_3)_2HX]$ (X = various anionic ligands).[23] It must be stressed however that this theory is <u>only</u> applicable to the proton and not to heavier elements such as ^{31}P. This is demonstrated by the fact that in the above Pt system a positive relation is found between ^{195}Pt and ^{31}P shifts.[23]

Clearly further work is required to understand the relationships between metal and heavy element ligand shieldings although it has been shown for the trans-[MoX(NA)(dppe)$_2$] system, that a correlation does exist between ^{95}Mo and ^{31}P shifts.

3.6 General comparisons and conclusions

It is apparent that the nature of the trans-ligand X in the systems studied has various effects on the components of the orbital manifold. When this ligand is changed, relatively good correlations are observed between those parameters with origins which are broadly similar. Such a case is found between $E_{\frac{1}{2}}^{ox}$ and the nitrosyl or diazenido-stretching frequency, reflecting build-up of charge at the metal centre provided by both σ and π donor effects. Extremes of δ^{15}N, $E_{\frac{1}{2}}^{ox}$, U.V.-visible and i.r. parameters are consistent with the strong π-donor effect of OH^- and similarly the π-acceptor power of the MeCN ligand. Evidence has been provided, however, that simple shielding arguments based on electron density should be treated with caution.

^{95}Mo NMR (and to a lesser extent ^{31}P) provides information about the character of the metal site and importantly, predictive criteria for determining ligand influences on the overall orbital manifold. The value of ^{95}Mo as a chemical probe is evident and will be further developed in the following chapter.

CHAPTER 4

Ligand Parameters from ^{95}Mo NMR Spectroscopy

4.1 Introduction

The discussion in Chapter 2 highlights the usefulness of transition metal NMR spectroscopy in the study of complexes through its inherent sensitivity to coordination environment and the large ranges of chemical shift found for many d-block elements. This will now be extended to ^{95}Mo NMR spectroscopy for which the relatively simple shielding principles have already been exemplified in the preceding chapter. The object is to build up a ligand series, using the diverse systems studied in the literature together with the more systematic examination in the present work, based on substituent effects of ligands on the ^{95}Mo shift. Of particular interest is the classification of ligands important in nitrogen fixation or model studies, e.g. N_2, CO, RNC, RCN, NO^+, N_2R^+, amines etc. via the ^{95}Mo shift scale and thus allow this technique to be used in a predictive sense for structure determination. An overview of ^{95}Mo NMR up to early 1981 has appeared[1] and a comprehensive review of ^{95}Mo NMR applications in inorganic chemistry is in press.[2]

4.2 The range of ^{95}Mo chemical shifts

The ^{95}Mo chemical shift scale covers a range of ca. 7000 ppm which is represented by a diverse selection of complexes, both mono- and polynuclear with oxidation states of Mo(0), (II), (IV), or (VI). The ranges covered by these formal

oxidation states are shown in Figure (4.1) together with the various regions in which particular complex types are found. It can be seen that ^{95}Mo NMR spectroscopy does not provide a good method to distinguish oxidation states in complexes, as the regions of mononuclear Mo(0), d^6; Mo(II), d^4; and Mo(IV), d^2 overlap, but these are explained below. A detailed discussion of the many complexes studied by ^{95}Mo NMR is beyond the scope of this thesis but a brief consideration of the shielding in the general types of complex is useful in the context of this chapter.

The Mo(VI) systems studied are of particular importance to the investigation of molybdoenzymes such as xanthine oxidase in Chapter 7. The simplest complexes are the $[MoX_4]^{2-}$ (X = O, S or Se) tetrahedral species which were studied first because of their high solubility and narrow ^{95}Mo NMR lines. The reference complex $[MoO_4]^{2-}$ resonates to highest field but successive substitution of oxygen by other chalcogenides (S or Se) leads to downfield shifts with $[MoSe_4]^{2-}$ at lowest field.[3] This is a good example of a general trend shown by d^o systems, with shielding decreasing as the group of the ligating atom is descended. Similar effects are found for e.g. VOX_3 (X = halide) and in this case is known as the inverse halogen dependence (IHD)[4] and is in contrast to the so-called normal halogen dependence (NHD) (and also chalcogen dependence) found in many complexes with partially filled d shells.[5] In the formally d^o complexes it is low energy circulations of ligand electrons in the d orbitals which deshield the metal nucleus. Corresponding effects are

Figure (4.1): ^{95}Mo shift ranges (see text for assignments)

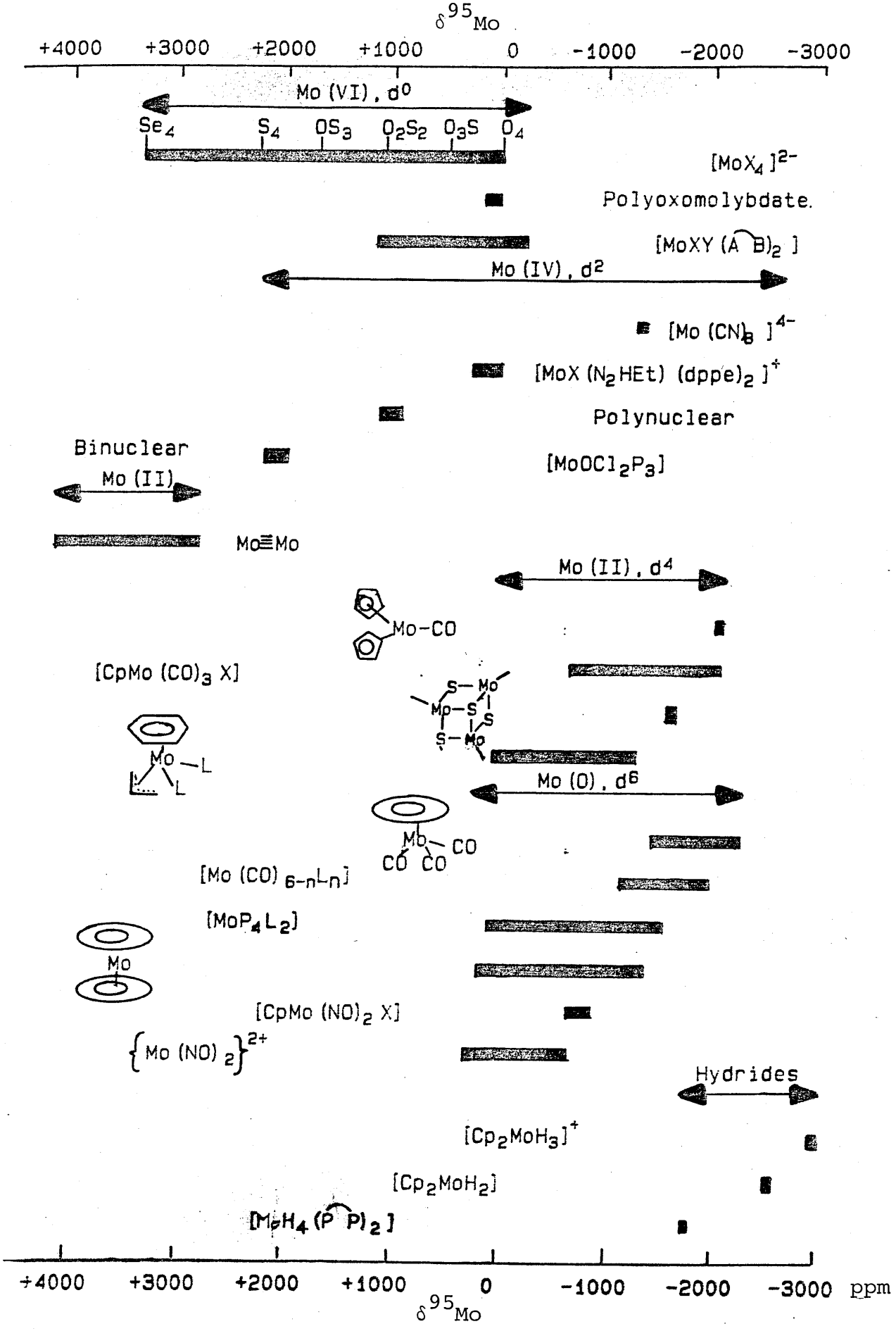

observed in the 6-coordinate complexes $[MoXY(\overset{\frown}{A\ B})_2]$ (X,Y = O, S or Se; $\overset{\frown}{A\ B}$ = various S, N or O chelating ligands)[3,6a] are particularly important as models for the xanthine oxidase active site and have the general stoichiometry shown in Figure (4.2).

Figure (4.2):

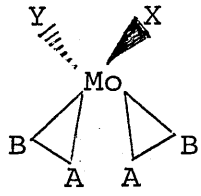

They fall into the typical region for Mo(VI) with O and Se ligands toward the high and low field extremes respectively. IHD is also found for a series of complexes $[MoO_2LX]$ (X = halide, L = $HB[3,5\text{-}Me_2Pz]_3$).[6b]

The large range of Mo(IV) shielding is covered by mononuclear oxo-cyano-complexes, and the polynuclear aqueous formally Mo(IV) species.[7] At lowest field are the $[MoOCl_2(phosphine)_3]$ complexes at ca. 2000 ppm described at the end of Chapter 5. The hydrazido(2-) complexes trans-$[MoX(N_2HEt)(dppe)_2]Br$ resonate as low as +300 ppm and are discussed later. Formally d^2, is the complex $[MoH_4(dppe)_2]$ which resonates to relatively high field (-1805 ppm)[9], to be expected for the strong, highly shielding, hydride ligand.[4] This is also shown by $[Cp_2MoH_2]$ and its protonation product $[Cp_2MoH_3]^+$ which at -2953 ppm is the highest field ^{95}Mo signal yet detected.[10]

The main work on Mo(II) has involved the complexes shown in Figure (4.3).

Figure (4.3):

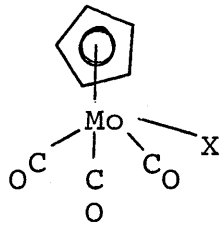

(X = halide, hydride, substituted benzyl or a metal fragment.)

Molybdenum is highly shielded in compounds with X = hydride but the shielding decreases in the halides, and I > Br > Cl.[11] The ^{95}Mo shift in these systems has great sensitivity to changes removed from the metal nucleus as shown by a range of 40 ppm for the series with X = variously substituted benzyl groups.[12] The $[Cp_2MoCO]$ resonance occurs at relatively high field[10] but significantly, is at lower field than the hydride analogue $[Cp_2MoH_2]$. A set of complexes with π-arene and π-allyl coordination has been studied.[10] These $[(\eta^6\text{-}C_6H_6)Mo(\eta^3\text{-}C_3H_5)L_2]$ complexes contain various ligands L_2 ranging from phosphine chelates to nitrogen donors and ^{95}Mo shifts cover ca. 1300 ppm.

Also of interest is the cubane cluster complex $[Mo(\mu^3\text{-}S)(C_5H_4Pr^i)]_4$ at -1643 ppm.[10] A special group of Mo(II) compounds worthy of mention are the binuclear systems containing Mo-Mo quadruple bonds, an example of which is shown in Figure (4.4).

Figure (4.4):

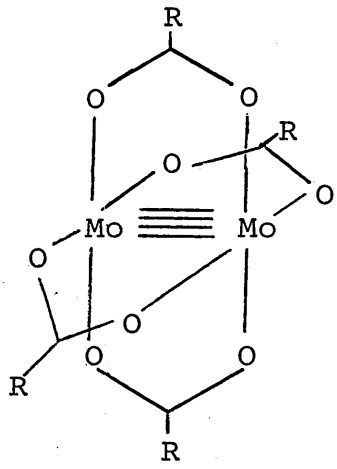

R = alkyl

These complexes give ^{95}Mo lines at exceptionally low field and in fact define the low field extreme for ^{95}Mo shielding e.g. for R = CF_3, δ = +4026. Surprisingly (considering only the size and shape of this molecule) the linewidth ($W_{\frac{1}{2}}$) found for this complex was only 250 Hz.[7]

By far the largest proportion of study has been devoted to the extensive range of Mo(0) complexes containing carbonyl or phosphine co-ligands. Some of the earliest work in this latter category involved the [(π-arene)Mo(CO)$_3$] "piano stool" complexes shown below [Figure (4.5)].

Figure (4.5):

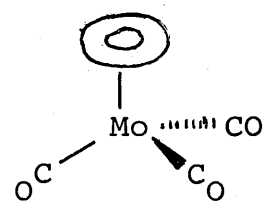

π-arene = substituted benzene or η^5-$C_5H_5^-$

These compounds have high solubility, very narrow lines and give a large shielding range, δ = -1684 to -2123 ppm.[13] More recently the π-arene complexes shown in Figure (4.6) have been studied and a correlation of ΔE (the HOMO-LUMO gap for circulation of charge at ^{95}Mo, estimated from photoelectron spectroscopy) with ^{95}Mo shielding is observed as the π-arene group is changed,[10] ^{95}Mo is deshielded with decrease in ΔE.

Figure (4.6):

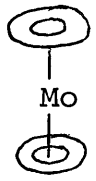

π-arene = non- or variously substituted aromatic ligand.

The series mentioned at the end of Chapter 3 containing the $[Mo(NO)_2]^{2+}$ core exhibits a large range of ^{95}Mo shifts. The complexes of the type $[CpMo(NO)_2X]$ (X = halide) give higher field resonances (typical of η^5-C_5H_5 complexes) whereas at lower field are the compounds $[Mo(NO)_2X_2L_2]$ (X = halide, anionic, C, O or S donors; L = neutral donor ligands) extending $\delta^{95}Mo$ for Mo(0) to ca. +200 ppm.

Several reports deal with the octahedral complexes $[Mo(CO)_{6-n}L_n]$ (n = 0, 1, 2, 3; L = a variety of P, As, Sb, O, N and C donor ligands)[8,9,14-20] and the anionic compounds $[Mo(CO)_{6-n}X_n]^-$ (n = 1 or 2; X = halide or S donor).[21] This range of ^{95}Mo shifts covers ca. 800 ppm and within each series the shielding is sensitive to change in ligand

substituent,which allows comparison of ligand properties as discussed below.

The present work involves complexes of the type $[MoLL'P_4]$ (L,L' = various donor ligands; P = mono- or chelating tertiary phosphine ligands) which extend over a 1600 ppm range downfield from $[Mo(CO)_2(dppe)_2]$ at ca. -1500 ppm, and includes the nitrosyl and diazenido-compounds of Chapter 3.

4.3 ^{95}Mo NMR spectroscopy of molybdenum phosphine complexes

4.3.1 General features

The systems studied fall into two main categories, those with monophosphine co-ligands such as PMe_3, PMe_2Ph, $PMePh_2$ or $PPr^n{}_2Ph$ and those containing chelating phosphines $Ar_2PCH_2CH_2PAr_2$ (dArpe; Ar = C_6H_4Y; Y = OMe, Me, H, Cl or CF_3) [Figure (4.11)] or $Et_2PCH_2CH_2PEt_2$ (depe). The complexes with monophosphine or depe ligands are generally much more soluble than the corresponding dArpe compounds which makes them more amenable to study. The latter systems, however, generally show more versatile bonding to a variety of substrates L and the resulting complexes are often more stable than those with monophosphines. All the types of $\{MoP_4\}$ core give complexes with dinitrogen.

4.3.2 Dinitrogen complexes

4.3.2.1 Spectra

^{95}Mo NMR data for the N_2 complexes studied are shown in Tables (4.1) and (4.2). The complexes in Table (4.1), being very soluble in THF,could be studied with a low field

TABLE (4.1): ^{95}Mo NMR data for dinitrogen complexes

Complex	$\delta^{95}Mo$[a,c] ppm	$W_{\frac{1}{2}}$[d] Hz
c-$[Mo(N_2)_2(PMe_2Ph)_4]$	-455	25
t-$[Mo(N_2)_2(PMePh_2)_4]$	-464[e]	25
c-$[Mo(N_2)_2(PMe_3)_4]$	-637[b]	20
$[Mo(N_2)(PMe_3)_5]$	-718	15
t-$[Mo(N_2)_2(depe)_2]$	-1022[e]	65
t-$[Mo(N_2)_2(depe)(dppe)]$	-899[e]	65
t-$[Mo(N_2)_2(PMe_2Ph)_2(dppe)]$	-701	20
m-$[Mo(N_2)_3(PPr^n{}_2Ph)_3]$	-392	10

a) Measured in THF ± 1 ppm at 23.47 MHz 298K or b) at 5.80 MHz.
c) $^1J_{MoP}$ = 170 to 190 ± 5 Hz. d) ±5 Hz. e) from ref. 20 at 5.80 MHz.

TABLE (4.2): NMR data and Hammett σ_p values for substituted aryldiphosphine dinitrogen complexes

Complex t-$[Mo(N_2)_2(dArpe)_2]$	$\delta^{95}Mo$[a,b] ppm	$W_{\frac{1}{2}}$[c] Hz	$\delta^{31}P$ ppm	Hammett σ_p
Ar = C_6H_4OMe-4	-798	30	-78.4	-0.27
C_6H_4Me-4	-793	50	-77.8	-0.17
C_6H_5	-787	50	-75.5	0.00
C_6H_4Cl-4	-785	130	-77.2	0.23
$C_6H_4CF_3$-4	-774	170	-74.7	0.54
C_6H_4Me-3	-795	50	-75.8	-

a) Measured in THF at 26.08 MHz 298K; ±1 ppm.
b) $^1J_{MoP}$ = 175 to 185±5Hz; c) ±10 Hz. All ^{95}Mo shifts relative to 2M $Na_2[MoO_4]$ at pH 11.

spectrometer,[22] but the series of aryl diphosphine complexes [Table (4.2)] needed higher sensitivity and were studied at higher field. All of the $\{MoP_4\}$ complexes give quintets in their ^{95}Mo NMR spectra. This is expected for trans-P_4 complexes with all ^{31}P nuclei equivalent but in the cis-complexes, trans-$[Mo(N_2)_2(PMe_2Ph)_2(dppe)]$ and trans-$[Mo(N_2)_2(depe)(dppe)]$, a $2P_A$, $2P_B$ system is present, although a quintet still results as $^1J_{MoP_A}$ is nearly equal to $^1J_{MoP_B}$ for these compounds. The spectrum of trans-$[Mo(N_2)_2(PMe_2Ph)_2(dppe)]$ in Figure (4.7) shows the typical quintet structure. A similar equivalence exists in the complex $[Mo(N_2)_3(PPr^n{}_2Ph)_3]$ which has a mer-configuration and the ^{95}Mo spectrum shows a simple quartet [Figure (4.8)]. $^1J_{MoP_A}$ is also close to $^1J_{MoP_B}$ for the complex $[Mo(N_2)(PMe_3)_5]$ which has a unique phosphine trans to N_2:

Figure (4.9):

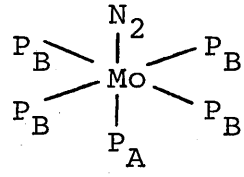

(P = PMe_3)

$^1J_{MoP}$ ranges from 170 to 190 Hz in all of the dinitrogen complexes. It may be noted that Wedd and co-workers report the shift of trans-$[Mo(N_2)_2(dArpe)_2]$ (Ar = $C_6H_4CH_3$-4) to be -776 ppm and $^1J_{MoP}$ as 205 Hz in THF solution at 328K.[9] In the present work, at ambient temperature (298K), $\delta^{95}Mo$ = -793 ppm. This is a good example of the care that should

Figure (4.7): ^{95}Mo NMR spectrum of trans-$[Mo(N_2)_2(PMe_2Ph)_2(dppe)]$

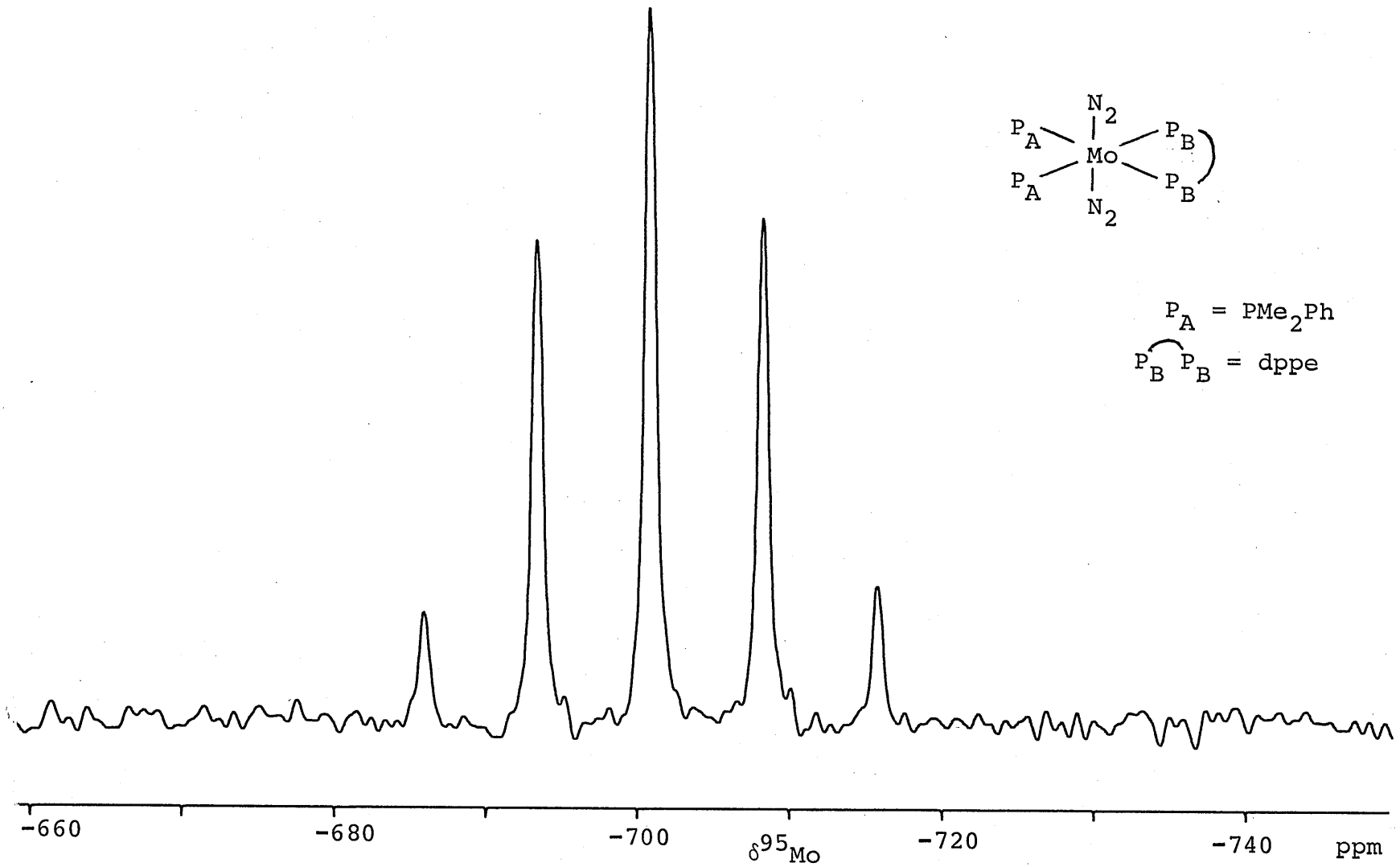

Figure (4.8): ^{95}Mo NMR spectrum of mer-$[Mo(N_2)_3(PPr^n{}_2Ph)_3]$

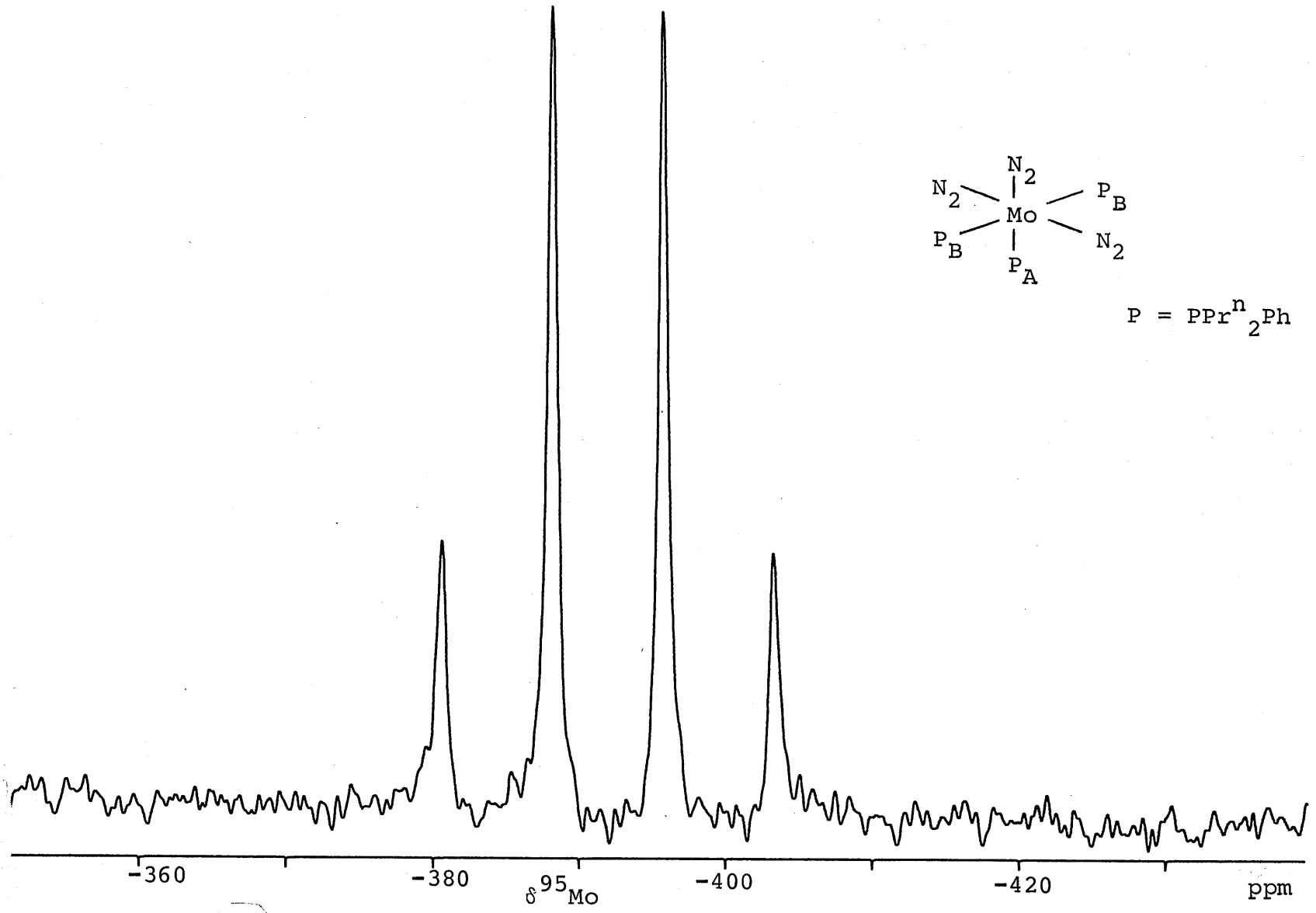

be taken to compare spectra at consistent temperatures. The difference between the reported shift and ours corresponds to a temperature dependence of ca. 0.5 ppm per °C.

Both complexes cis-$[Mo(N_2)_2(PMe_3)_4]$ and $[Mo(N_2)(PMe_3)_5]$ were examined ca. 50% labelled with $^{15}N_2$. The ^{95}Mo NMR spectra show coupling of ^{15}N to ^{95}Mo but the $^1J_{Mo}{}^{15}N$ coupling constants are not easily measured due to an isotope shift upfield from the unlabelled complex. This is demonstrated in Figure (4.10), where the sextet due to $[Mo(N_2)(PMe_3)_5]$ is superimposed on the sextet of doublets due to the labelled complex. $^1J_{Mo}{}^{15}N$ is estimated at ca. 30 Hz and the isotope shift at ca. 0.5 Hz. The coupling constant can be compared with that reported for $[(\eta^5\text{-}C_5H_5)Mo(CO)_2NO]$, the value of $^1J_{Mo}{}^{14}N$ is estimated at ca. 46Hz[23] corresponding to a $^1J_{Mo}{}^{15}N$ coupling of 64 Hz (see end of Chapter 2).

Isotope effects are dependent on the shift range of the resonant nucleus and the percentage change in the mass of the isotope of the coordinated atom. They are expressed as $^n\Delta X(Y)$ where X is the resonant nucleus, Y is the substituted isotope and n is the number of bonds between them.[24] In the present case the $^1\Delta\ ^{95}Mo(^{15}N)$ value is ca. 0.5 ppm which compares with a value of $^1\Delta\ ^{95}Mo(^{18}O)$ of 0.25 ppm for the MoO_4^{2-} ion. The sensitivity of ^{95}Mo is again highlighted if the above effects are contrasted with e.g. $^1\Delta\ ^{13}C(^{15}N)$ for the CN^- ion which is 0.03 ppm.[24]

Figure (4.10): ^{95}Mo NMR spectrum of $[Mo(N_2)(PMe_3)_5]$ ca 40% labelled with $^{15}N_2$

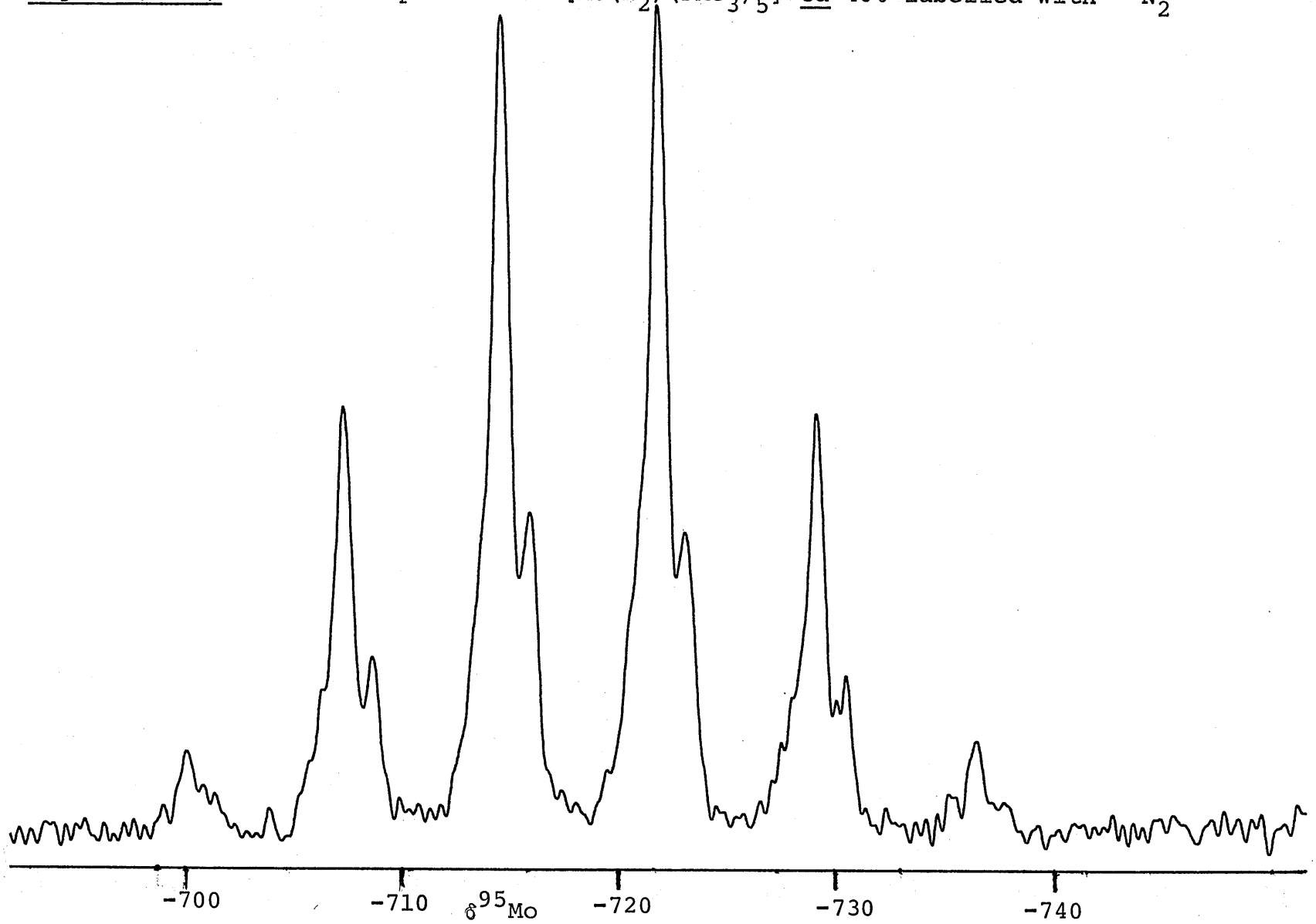

The linewidth $W_{\frac{1}{2}}$ is small for the lower molecular weight monophosphine complexes. $W_{\frac{1}{2}}$ increases for the complexes with bulkier chelating phosphines and is largest for the compound with highest molecular weight, $[Mo(N_2)_2(dArpe)_2]$ (Ar = $C_6H_4CF_3$-4). As expected, $[Mo(N_2)(PMe_3)_5]$ has a narrow ^{95}Mo resonance but unusually mer-$[Mo(N_2)_3(PPr^n{}_2Ph)_3]$ has the narrowest lines which normally would indicate a fac-stereochemistry; the meridional ligand arrangement has been confirmed by ^{15}N NMR (Chapter 6), ^{31}P NMR and a crystal structure determination.[25]

4.3.2.2 Trends in shielding

Several features are evident from comparison of the data in Tables (4.1) and (4.2). Replacement of monophosphines with bidentate diphosphine ligands increases the ^{95}Mo shielding and is an example of a chelate effect observed for ^{51}V and other metal nuclei[26], as well as ^{95}Mo.[15,17] This effect is not strictly additive: substitution of $2PMe_2Ph$ by dppe in $[Mo(N_2)_2(PMe_2Ph)_4]$ shields ^{95}Mo by 246 ppm but a further replacement of $2Me_2Ph$ to give $[Mo(N_2)_2(dppe)_2]$ increases shielding by only 86 ppm.

Substitution of a more basic phosphine ligand such as PMe_3 for the weaker $PMePh_2$ or PMe_2Ph increases the ^{95}Mo shielding. This is also evident for the series $[Mo(N_2)_2(diphos)_2]$ in which the ordering of shielding follows the strength of the diphosphine $(depe)_2 > (depe)(dppe) \geq (dppe)_2$. Each replacement of a depe ligand by dppe deshields ^{95}Mo

by ca. 100 ppm. In fact, the shielding is not simply dependent on electronic effects: steric influences may operate with bulky phosphines, which tend to deshield ^{95}Mo [19] as with other metals,[26] probably because of angular distortion in the coordination sphere. cis-configurations are expected to be to low field of trans-, from symmetry arguments,[8] which may explain why ^{95}Mo in cis-$[Mo(N_2)_2(PMe_2Ph)_4]$ is deshielded relative to trans-$[Mo(N_2)_2(PMePh_2)_4]$ even though PMe_2Ph is more basic than $PMePh_2$.

When steric influences are minimal, clear electronic factors are observed as is shown by the data in Table (4.2). The complexes trans-$[Mo(N_2)_2(dArpe)_2]$ show a linear increase of ^{95}Mo shielding with increase in electron donating power of the substituent on the aryl group, as evidenced by a decreasing Hammett σ_p value. A plot of the data is given in Figure (4.11) and a similar straight line is given for a graph of the oxidation potential $E_{\frac{1}{2}}^{ox}$ against Hammett σ_p.[27] Oxidation becomes easier as Hammett σ_p is lowered, reflecting increased charge at the metal. Hammett σ_p^+ does not give good correlations and this indicates that in the $[Mo(N_2)_2(dArpe)_2]$ system, trends in ^{95}Mo and $E_{\frac{1}{2}}^{ox}$ are determined primarily by changes in inductive effects transmitted through the phosphine ligands. The N_2 infra-red stretching frequency, however, does correlate with σ_p^+,[27] $\nu(N_2)$ decreases as σ_p^+ decreases reflecting increased π back-bonding from metal to N_2 as the phosphine substituents donate more charge, via conjugation.

Figure (4.11): Graph of δ^{95}Mo against Hammett σ_p for complexes $[Mo(N_2)_2(dArpe)_2]$

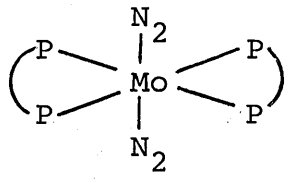

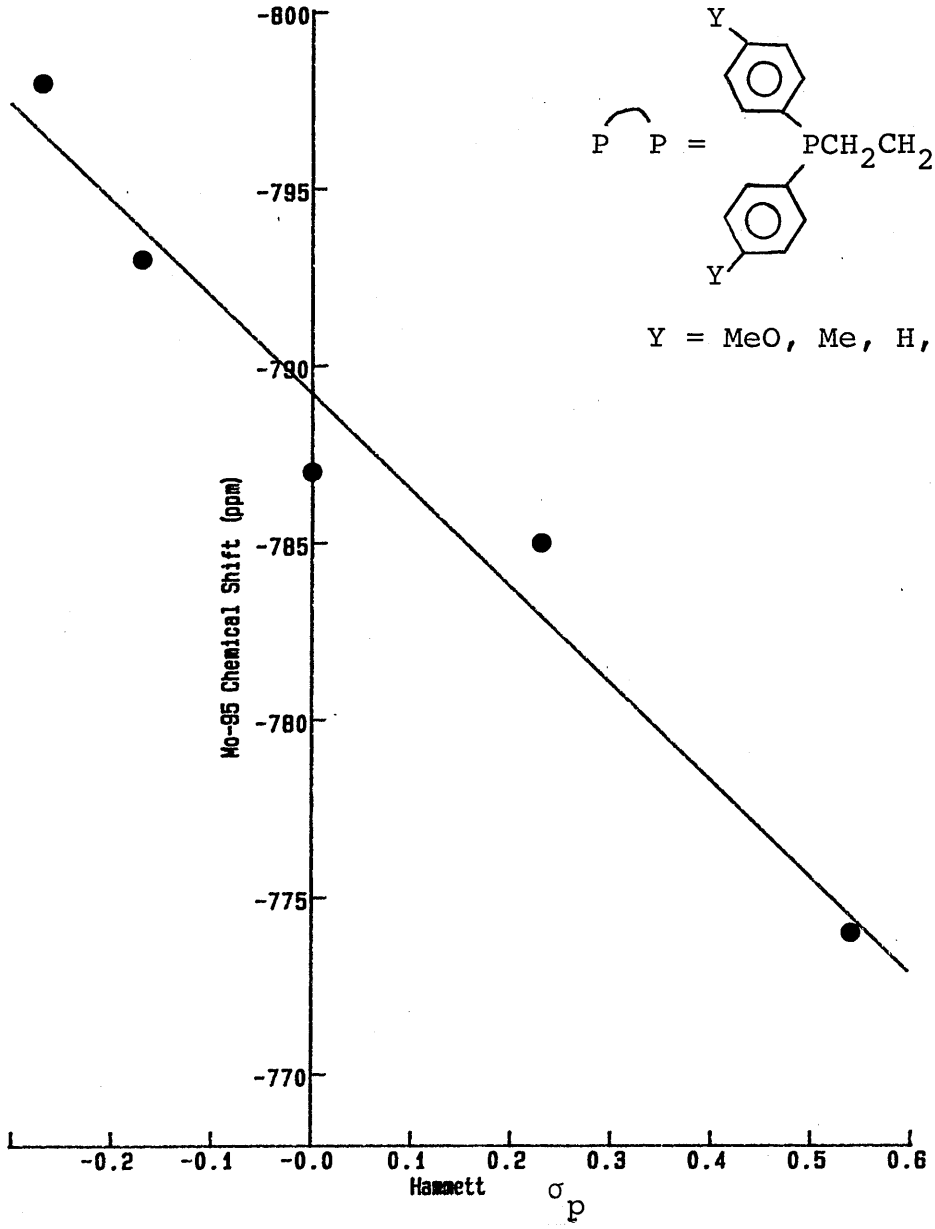

Y = MeO, Me, H, Cl, CF_3

Interestingly the ^{31}P NMR shifts of the coordinated dArpe ligands change in the same direction as the ^{95}Mo shifts, in opposition to the trend observed for nitrosyl and diazenido-complexes in Chapter 3. For the $[Mo(N_2)_2(dArpe)_2]$ complexes, however, a linear relation of ^{95}Mo with ^{31}P chemical shift is not found and this may be explained by differing steric effects of substituents on the aryl groups, to which ^{31}P shielding is known to be very sensitive.[28]

Replacement of PMe_3 by N_2 in the complexes $[Mo(N_2)(PMe_3)_5]$ deshields ^{95}Mo by *ca.* 80 ppm. The *mer*-$[Mo(N_2)_3(PPr^n{}_2Ph)_3]$ complex resonates at lowest field agreeing with the other evidence of the relative deshielding effect of dinitrogen.

4.3.2.3 Conclusions

The dinitrogen complexes are excellent probes for the effect of the phosphine co-ligand on ^{95}Mo chemical shift. The simple relationship between ^{95}Mo shielding and phosphine basicity or Hammett σ_p parameters indicates that major effects involve the σ orbital system, increasing phosphine donor power causing an increase in the ΔE term. It is apparent from this that alkyl phosphine > aryl phosphine in a ^{95}Mo spectrochemical shielding series. In phosphines with other substituents, increasing effects of π-bonding become important as shown below. The $[Mo(N_2)_2(dArpe)_2]$ complexes provide a good example of a system in which nuclear magnetic

shielding may be directly related to charge density at the metal.

The relatively low position of dinitrogen in a ^{95}Mo spectrochemical series, compared with phosphine ligands has been demonstrated, and will be discussed further.

4.3.3 Various complexes with a {Mo(phosphine)$_4$} core

4.3.3.1 Complexes available for study

The complexes [Mo$(N_2)_2$(phosphine)$_4$] can be converted to a variety of compounds in which one or both dinitrogens are substituted by a range of ligands, maintaining the {Mo(phosphine)$_4$} core. trans-[Mo$L_2$$(PMe_3)_4$] (L = CO_2, C_2H_4) are derived from cis-[Mo$(N_2)_2$$(PMe_3)_4$] by direct displacement of dinitrogen by carbon dioxide[29] or ethylene[30] gases at ambient temperature. Reaction with other ligands such as CO, CNR etc., can give mixtures of compounds often with loss of the {MoP_4} site due to the lability of PMe_3[30,31]. trans-[MoL_2(dppe)$_2$] (L = C_2H_4, RNC; R = Me or Bu^t) may be derived from [Mo$(N_2)_2$(dppe)$_2$], although more forcing conditions are required for both the C_2H_4[32] and RNC[33] preparations as N_2 is bound more strongly than in the monophosphine complexes. The first N_2 ligand is labile and may be exchanged at room temperature to give trans-[Mo(N_2)(NCR)(dppe)$_2$] (NCR = various nitriles). Complexes of the type trans-[Mo(CO)L(dppe)$_2$] (L = N_2, CO, NCR and various other donor ligands; R = C_6H_4Y-4; Y = OMe, H or OCMe) can be synthesised from the bis-dinitrogen complex via the 5-coordinate, coordinatively unsaturated,

16e$^-$ complex $[Mo(CO)(dppe)_2]$[34], as shown in the Scheme (4.1) using a modification[35] of the method of Hidai et al.[36]

Scheme (4.1):

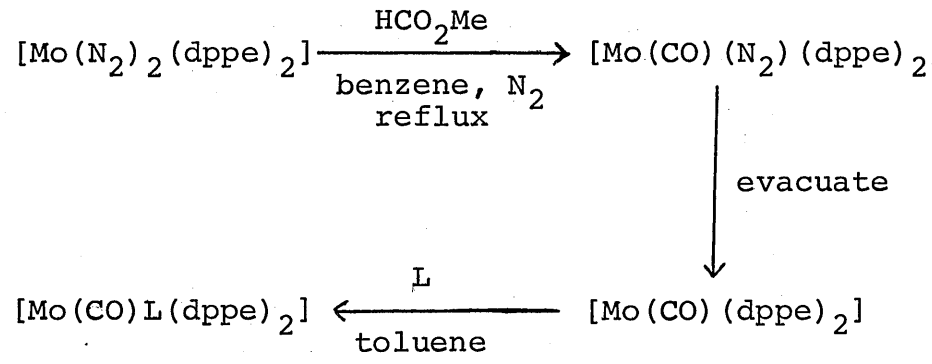

Several complexes synthesised by this route such as $[Mo(CO)L(dppe)_2]$ (L = dimethylformamide, ethylamine, thiophene, pyridine, imidazole or ethylene) were not amenable to ^{95}Mo NMR study either through poor solubility or instability in solution. The complex trans-$[Mo(CO)_2(dppe)_2]$ isomerises to give the cis-complex, and so was generated in situ by treatment of trans-$[Mo(CO)(NCC_6H_4OMe\text{-}4)(dppe)_2]$ with CO gas, the ^{95}Mo spectrum being collected immediately.

4.3.3.2 ^{95}Mo NMR spectra

Table (4.3) shows the chemical shift data for the $\{MoP_4\}$ complexes. These shifts cover a range of ca. 1500 ppm. The high field boundary is given by the cis-dicarbonyl complexes $[Mo(CO)_2(dArpe)_2]$ (Ar = C_6H_5 or C_6H_4OMe-4) which have very similar shifts. The spectrum of cis-$[Mo(CO)_2(dppe)_2]$ is somewhat complex [Figure (4.12)] and is unlike the quintets

TABLE (4.3): ^{95}Mo NMR data for Mo(0) complexes containing the $\{MoP_4\}$ unit

Complex	δ^{95}Mo (ppm)
c-[Mo(CO)$_2$(dArpe)$_2$]	
Ar = C_6H_5	-1486[a]
Ar = C_6H_4OMe-4	-1484
t-[Mo(CO)$_2$(dppe)$_2$]	-1451[a]
t-[Mo(CNBu^t)$_2$(dppe)$_2$]	-1351[b]
t-[Mo(C_2H_4)$_2$(dppe)$_2$]	-1262
t-[Mo(CO)(N_2)(dppe)$_2$][c]	-1167
t-[Mo(CO)(NCAr)(dppe)$_2$]	
Ar = C_6H_4OMe-4	-1126
C_6H_5	-1118
C_6H_4OCMe-4	-1089
t-[Mo(C_2H_4)$_2$(PMe_3)$_4$][d]	-884[a,g]
t-[Mo(N_2)(NCAr)(dppe)$_2$]	
Ar = C_6H_4OMe-4	-667[b,f]
t-[Mo(CO_2)$_2$(PMe_3)$_4$][e]	+1[a]

Spectra measured at 26.08 MHz except
a) 23.47 MHz and b) 19.54 MHz and at 298K.
In solution in THF except
c) toluene, d) hexane and e) methanol.
Referenced to aq. 2 M Na_2MoO_4, pH 11.
f) $^1J_{MoP}$ = 170 Hz, $W_{\frac{1}{2}}$ = 170 Hz.
g) $^1J_{MoP}$ = 140 Hz, $W_{\frac{1}{2}}$ = 45 Hz.

observed for the cis-bis dinitrogen complexes. The probable indication is that $^{1}J_{MoP_{cis}} \neq {}^{1}J_{MoP_{trans}}$ and the spectrum should be an overlapping triplet of triplets although it is not immediately apparent how these may combine to give the observed spectrum.

Figure (4.12): ^{95}Mo spectrum of cis-$[Mo(CO)_2(dppe)_2]$

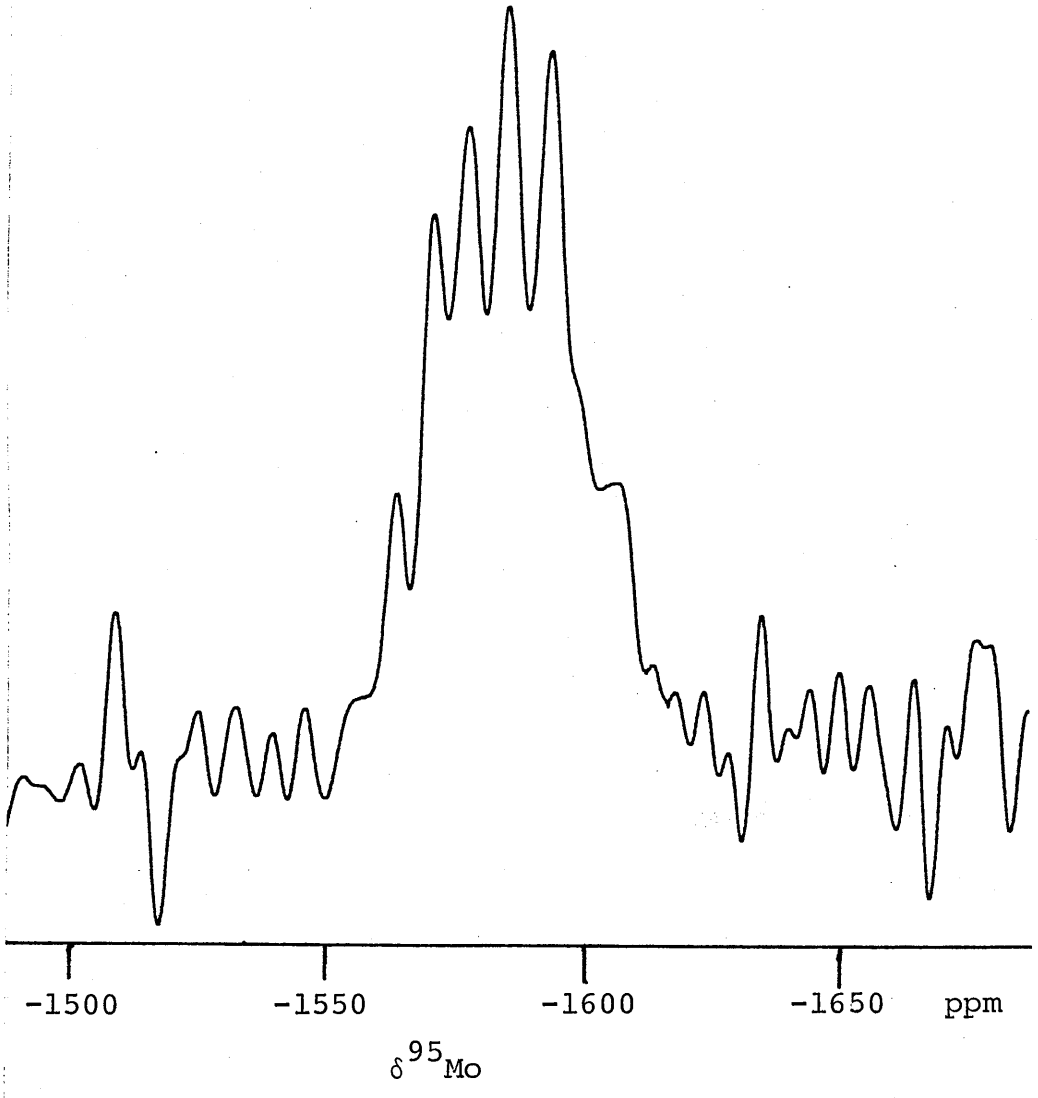

Distortion may arise through the large pre-acquisition delay used in this experiment (see Chapter 2).

The spectrum of cis-$[Mo(CO)_2(dArpe)_2]$ (Ar = C_6H_4OMe-4) is somewhat broadened by unresolved coupling. The shift values may be compared with the literature value for cis-$[Mo(CO)_2(dArpe)_2]$ (Ar = $C_6H_4CH_3$-4) -1475 ppm (THF soln., 330K).[9] This spectrum also shows incompletely resolved coupling. When couplings cannot be resolved and $^1J_{MoP}$ is unknown the signal linewidth $W_{\frac{1}{2}}$ is difficult to estimate as the unresolved components contribute to the overall width of the signal envelope.

The complex trans-$[Mo(CO)_2(dppe)_2]$ resonates some 35 ppm to lower field than the cis-isomer. This position is in stark contrast to the literature value for trans-$[Mo(CO)_2(dArpe)_2]$ (Ar = $C_6H_4CH_3$-4) at -1802 ppm (THF soln., 330K).[9] It should be noted, however, that $[MoH_4(dArpe)_2]$ (Ar = $C_6H_4CH_3$-4) has been measured at -1805 ppm (toluene, 338K)[9] and is a possible decomposition product of the trans-dicarbonyl when this is heated in THF.[37] The resonance due to trans-$[Mo(CO)_2(dppe)_2]$ is broad and so $^1J_{MoP}$ could not be resolved. This is the case for many of the spectra of the complexes in Table (4.3) and is often associated with poor signal-to-noise, preventing the application of significant resolution enhancement techniques. The complex trans-$[Mo(N_2)(NCC_6H_4OMe\text{-}4)(dppe)_2]$, however, shows the expected quintet structure (only 4 components resolved) [Figure (4.13)] as does trans-$[Mo(C_2H_4)_2(PMe_3)_4]$ [Figure (4.14)].

Figure (4.13): ^{95}Mo NMR spectrum of trans-$[Mo(N_2)(NCC_6H_4OMe\text{-}4)(dppe)_2]$

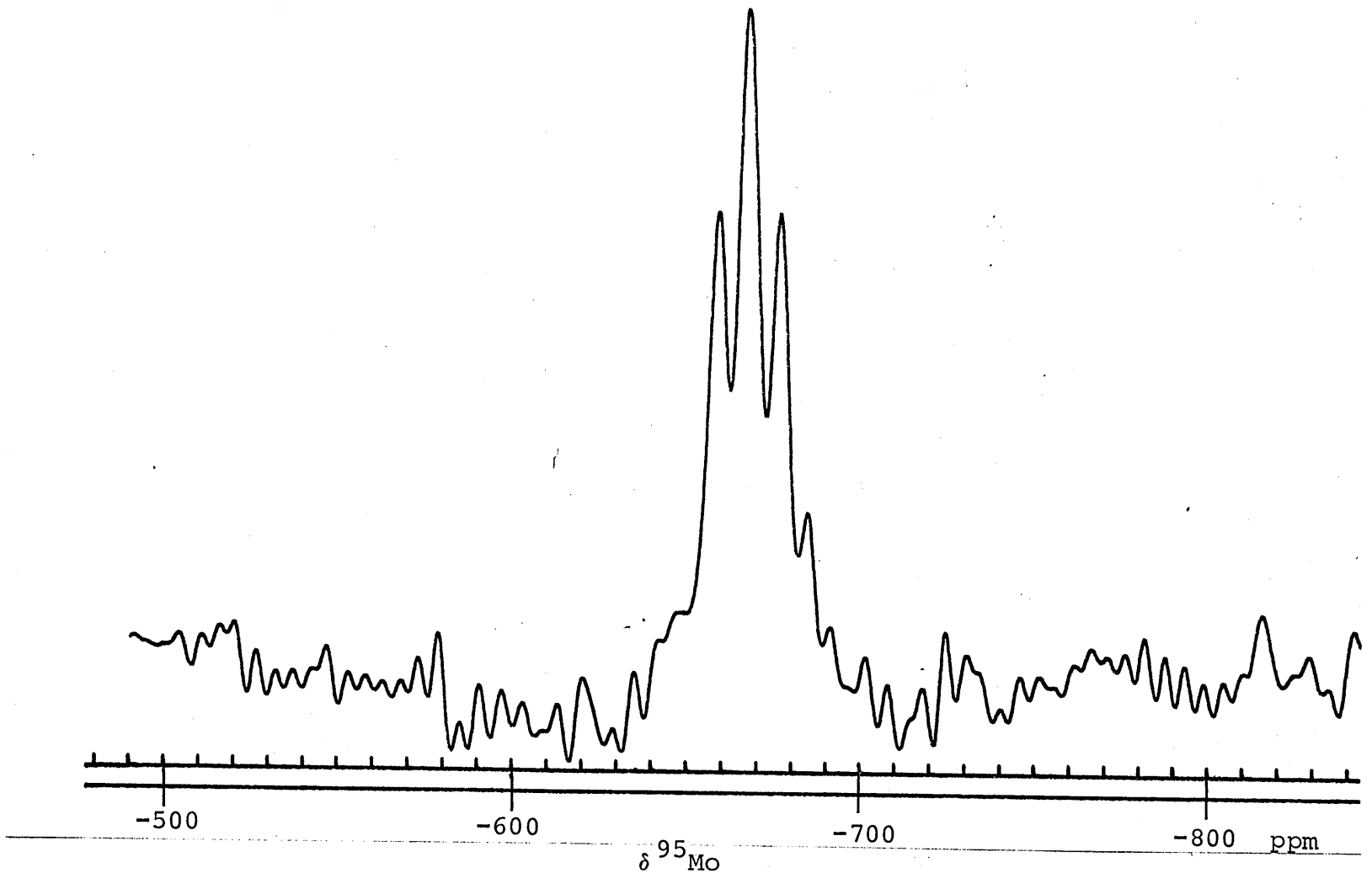

Figure (4.14): ^{95}Mo NMR spectrum of trans-$[Mo(C_2H_4)_2(PMe_3)_4]$

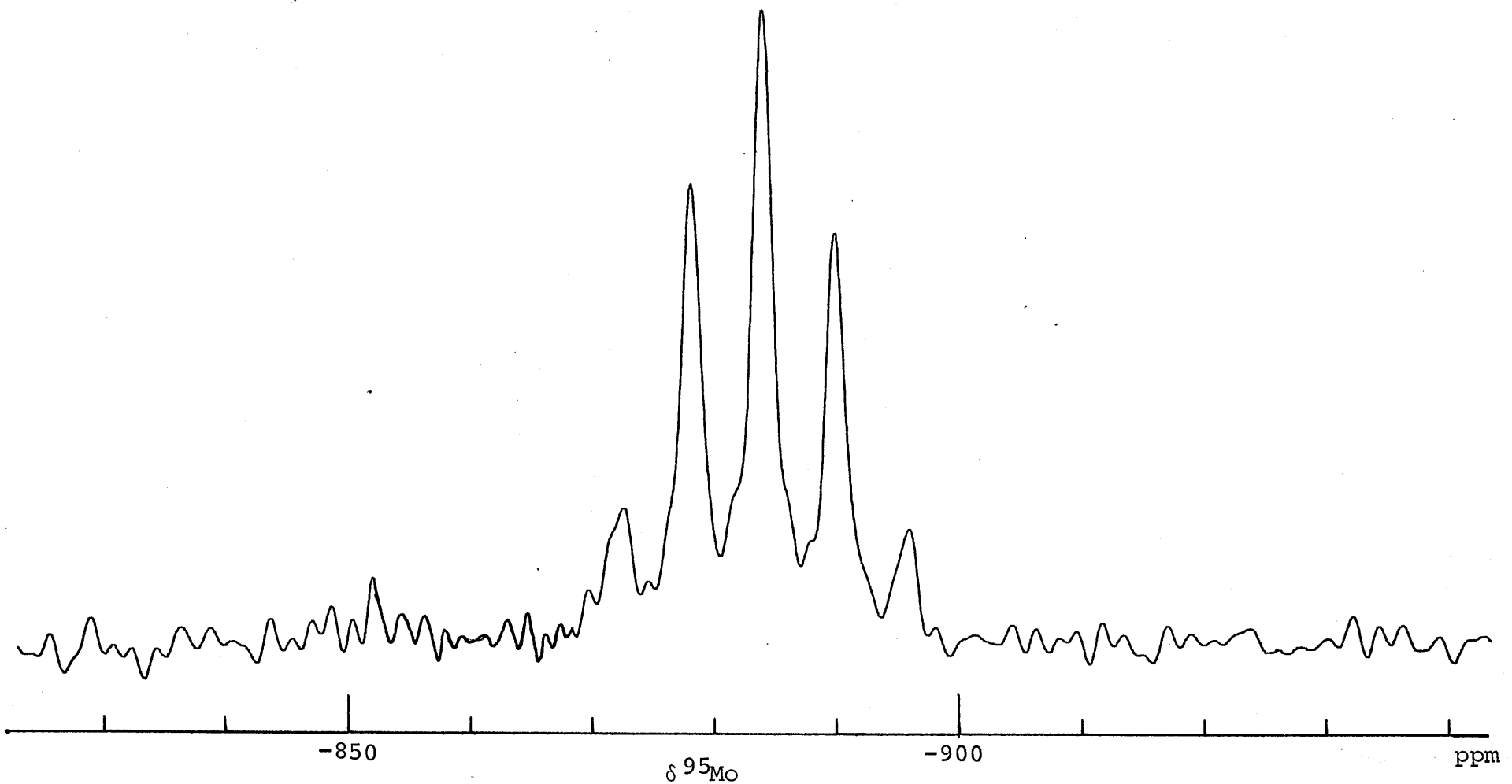

4.3.3.3 Discussion

The position of the bis-carbonyl complexes with the highest ^{95}Mo shielding, is to be expected from the influence of the CO ligand, a good π-acceptor and also a fair σ-donor. A small deshielding is observed on going from cis- to trans-$[Mo(CO)_2(dppe)_2]$. For many Mo(0) carbonyl-monophosphine complexes a small upfield shift is usually observed (e.g. ref. 17), expected on symmetry grounds.[8] No studies have been made, however, of cis/trans isomers involving chelating ligands such as dppe.

Replacement of CO by N_2 to give trans-$[Mo(CO)(N_2)(dppe)_2]$ leads to a deshielding of ca. 300 ppm, in line with both the lower π-acceptor and σ-donor properties of the dinitrogen ligand. This may be compared with the further downfield shift of ca. 400 ppm on going to trans-$[Mo(N_2)_2(dppe)_2]$. Comparing trans-$[Mo(CO)(N_2)(dppe)_2]$ with the series trans-$[Mo(CO)(NCAr)(dppe)_2]$ (Ar = C_6H_4Y-4; Y = OMe, H or OCMe), a deshielding of 40-80 ppm is observed. Clearly the NCR ligand is lower than N_2 in any spectrochemical series based on ^{95}Mo shifts. Within the nitrile series, changes in aryl substituents may have a pronounced effect on the ^{95}Mo shielding. As the Hammett σ_p value increases in the order OMe < H < OCMe the shielding decreases. This is consistent with decrease in σ-donor power of the nitrile ligand. A further example of the relative position of NCR and N_2 in a ^{95}Mo spectrochemical series is the ca. 100 ppm downfield ^{95}Mo shift from trans-$[Mo(N_2)_2(dppe)_2]$ to trans-$[Mo(N_2)(NCC_6H_4OMe\text{-}4)(dppe)_2]$.

The relative π-acceptor and σ-donor power of the isonitrile Bu^tNC in its complex may be assessed by comparison with trans-$[Mo(CO)_2(dppe)_2]$. The downfield shift of 100 ppm found for trans-$[Mo(CNBu^t)_2(dppe)_2]$ is consistent with the iso nitrile ligand being a poorer π-acceptor than CO, in agreement with known behaviour.[38] A further deshielding by ca. 100 ppm is observed from trans-$[Mo(CNBu^t)_2(dppe)_2]$ to trans-$[Mo(C_2H_4)_2(dppe)_2]$. The η^2-ethylene ligand shows synergic behaviour (see Chapter 1) and the ^{95}Mo shielding gives a measure of the σ + π component of the synergism although the relative importance of "isolated" π and σ effects is, of course, difficult to disentangle.

The downfield shift from trans-$[Mo(C_2H_4)_2(dppe)_2]$ to trans-$[Mo(C_2H_4)_2(PMe_3)_4]$ is an example of the chelate effect as observed in the bis-dinitrogen complexes.

The ordering of ligands so far examined shows $CO > CNBu^t > C_2H_4 > N_2 \geqslant NCR$ in order of decreasing ^{95}Mo shielding. This bears an interesting resemblance to trends from Mössbauer measurements on complexes such as trans-$[FeHL(depe)_2][BPh_4]$[39] and $[CpFe(CO)_2L]^+$ (L = various π-acid ligands).[40] The Mössbauer chemical shift measures relative (σ + π) effects (i.e. the total effect of σ-donation and π-acceptance) for the ligands L, so the ^{95}Mo shielding may be responding to similar influences.

At this point it is pertinent to reconsider the ^{95}Mo shielding of the complexes trans-$[MoX(NA)(dppe)_2]$ (A = O or NEt; X = various anionic ligands) and trans-$[Mo(NCMe)(NA)(dppe)_2]$ (A = O or NEt) discussed in Chapter 3. ^{95}Mo resonances of the nitrosyl and diazenido-complexes appear towards the low field end of the $\{MoP_4\}$ shielding range, for NO^+ ca. -500 to -750 ppm and N_2Et^+ ca. -100 to -200 ppm. Mössbauer[41] and other evidence[42] show the NO^+ ligand to be a very good π-acceptor and the diazenido-(N_2R^+) ligand, analogous to NO^+ should also show good π-acceptor properties. The relative deshielding caused by NO^+ and N_2R^+, compared to e.g. CO, seems to be inconsistent with ^{95}Mo shielding arguments based simply on a $\pi \rightarrow \sigma^*$ ΔE rationale.

The deshielding effect of the nitrosyl ligand seems to be a common feature and is also shown for ^{51}V and ^{59}Co complexes, as mentioned in Chapter 2 but as yet no explanation of this phenomenon has been put forward.

For certain ligands it seems that the metal shielding is probing other substituent effects not based simply on (σ+π) grounds. It is interesting to note, however, that the relative ^{95}Mo shifts of the nitrosyl and diazenido-complexes are consistent, on ΔE grounds, with NO^+ being a better (σ+π) ligand than N_2R^+, in agreement with other evidence.[42]

The ^{95}Mo resonance of trans-$[Mo(CO_2)_2(PMe_3)_4]$ is at lowest field of the $[MoL_2P_4]$ complexes. The structure of this complex has not been determined by X-ray crystallography but can confidently be assumed to have a trans-geometry with staggered CO_2 ligands as shown in the structure of the

analogous complex trans-$[Mo(CO_2)_2(CNMe)(PMe_3)_3]$[43] [Figure (4.15)].

Figure (4.15):

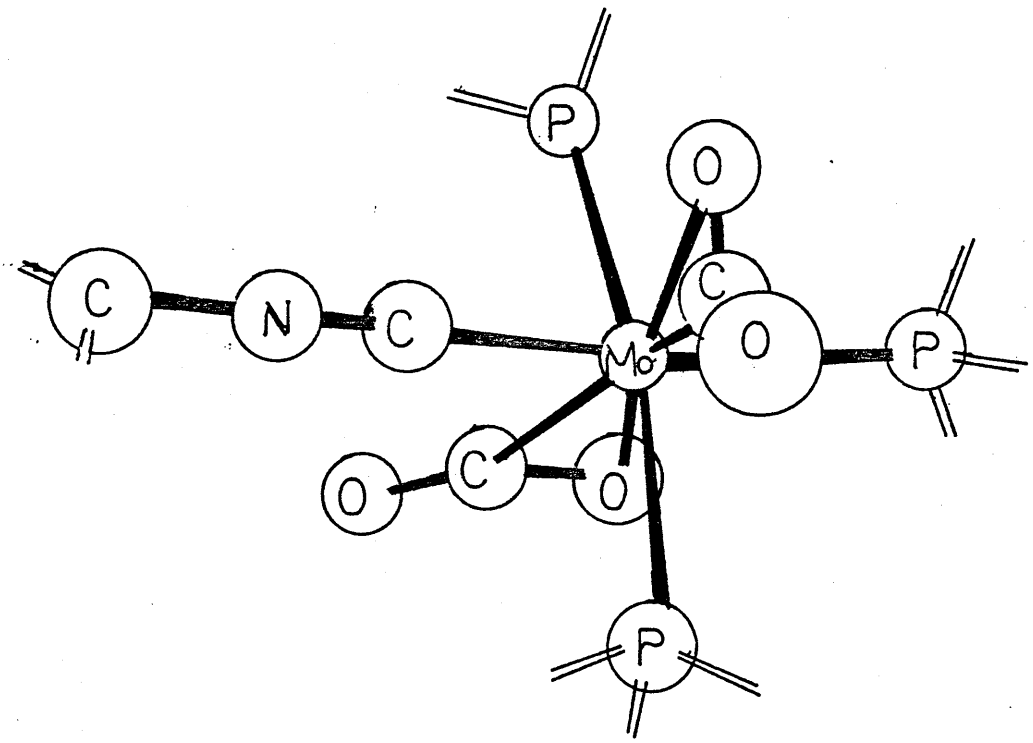

With this η^2-coordination, the CO_2 ligand is showing a synergic interaction with the metal and substantial π-back-donation is proposed.[29] If this is the case, the relatively low field ^{95}Mo shift of trans-$[Mo(CO_2)_2(PMe_3)_4]$ again seems inconsistent but as with the nitrosyl complexes it may be reflecting some other property of the ligand. No other metal NMR data have been obtained for carbon dioxide complexes.

Protonation of the diazenido-complexes mentioned above gives the hydrazido(2-) complexes trans-$[MoX(N_2HEt)(dppe)_2]^+$ (X = SCN, N_3, NCO and Br) discussed in Chapter 3. The formal oxidation state in these complexes is Mo(IV) and ^{95}Mo resonates some 300-400 ppm downfield of the parent

diazenido-complex. The ^{95}Mo shifts are shown in Table (4.4).

TABLE (4.4): ^{95}Mo NMR data for Mo hydrazido(2-)-complexes

Complex	$\delta^{95}Mo$ (ppm)
t-[$MoN_3(N_2HEt)(dppe)_2$]Br	+141
t-[$Mo(NCO)(N_2HEt)(dppe)_2$]Br	+173
t-[$Mo(SCN)(N_2HEt)(dppe)_2$]Br	+200
t-[$MoBr(N_2HEt)(dppe)_2$]Br	+337

Measured at 26.08 MHz in CH_2Cl_2 soln.

Comparing these hydrazido(2-)-complexes with the diazenido-complexes and trans-[$Mo(N_2)(NCC_6H_4OMe\text{-}4)(dppe)_2$] gives some idea of the effect of dinitrogen alkylation and subsequent protonation, on the ^{95}Mo shielding. Thus alkylation of the N_2 ligand to give N_2Et deshields ^{95}Mo by ca. 500 ppm, and protonation to give N_2HEt produces a further deshielding, as noted above, of ca. 300-400 ppm. This trend may in some way be related to the extent of M-N π-bonding which increases in the order: $M\text{-}N{\equiv}N < M\text{-}\overset{\cdots}{N}{=}N^{R} < M{=}N\text{-}N^{R}_{H}$. Although small changes in the trans-ligand in these complexes, and change in overall charge on the complex, must be taken into account in the comparisons, herein lies the basis of defining ^{95}Mo chemical shift ranges for the intermediates postulated in a cycle for N_2 reduction at the metal site.

4.3.3.4 Conclusions

The sensitivity of the ^{95}Mo NMR spectroscopic technique has been demonstrated and the position of N_2 in a spectrochemical shielding series established. The basis of a scale for comparing ^{95}Mo shifts of complexes containing nitrogenous ligands relevant to nitrogen fixation is apparent and this should be extended to other model complexes. Clearly further work is required to explain the shifts of NO^+, N_2R^+ and CO_2 complexes and to see if other ligands show corresponding behaviour at the $\{MoP_4\}$ site.

4.4 Comparison of results from the $\{MoP_4\}$ system with published ^{95}Mo NMR data

The brief survey at the beginning of this chapter shows the diverse nature of complexes studied by ^{95}Mo NMR spectroscopy. Some overall trends in shielding may however be deduced to give a rough spectrochemical series of ligands based on their effect on ^{95}Mo shielding.

Largest shieldings are observed for complexes containing the hydride ligand and the example of $[MoH_4(dArpe)_2]$ (Ar = C_6H_4Me-4)[12] is particularly relevant to the $\{MoP_4\}$ systems. The formal oxidation state of the tetrahydride, Mo(IV), as compared with the $\{MoP_4\}$ oxidation state of Mo(0), may be unimportant in shielding terms as the charge on the metal is probably not very different and the regions of mononuclear Mo(0), (II) and (IV) show a great deal of overlap [Figure (4.1)]. ^{95}Mo in $[MoH_4(diphos)_2]$ is some 350 ppm more shielded than in trans-$[Mo(CO)_2(dppe)_2]$. This trend is further exemplified by the

relative shielding in $[Cp_2MoCO]$ (-1964 ppm) < $[Cp_2MoH_2]$ (-2507 ppm)[13]. The shielding effect of the hydride ligand is due to its very strong σ donor effect, increasing ΔE for charge circulation at ^{95}Mo. Interestingly, protonation of the d^2 complex $[Cp_2MoH_2]$ to give the d^0 complex $[Cp_2MoH_3]^+$ increases the ^{95}Mo shielding by a further 450 ppm. This is consistent with the removal of relatively low energy $\pi \rightarrow \sigma^*$ circulation on coordination of the proton.[10] This forms a clear analogy with the upfield ^{15}N protonation shifts of nitrogen carrying a lone pair in a delocalised system, discussed in the next chapter.

Study of the complexes $[Mo(PF_3)_n(CO)_{6-n}]$[16] shows that PF_3 is very similar to CO in $(\pi+\sigma)$ effects, the whole series covering only a few ppm.

Many similar studies have involved replacement of CO by phosphite ligands $P(OR)_3$ (e.g. refs. 8,9, 15-17, 20) and it has been shown that this type of ligand is only slightly lower than CO in a spectrochemical series. Greater shielding is shown by phosphine PR_3 ligands but as mentioned earlier, steric factors also play a large part in determining the shift of a particular complex. The ordering PF_3 > $P(OR)_3$ > PR_3 is largely due to the electronegative substituent (OR or F) on phosphorus enhancing π-acceptor properties. If the group V element is changed from P to As and then to Sb in the EPh_3 group, a shielding order PPh_3 < $AsPh_3$ < $SbPh_3$ is observed.[8,9] This must be attributed to increasing nephelauxetic effects as influences on ligand field splittings generally decrease down the group. It has been observed that

the isonitrile $CNCMe_2Ph$ deshields ^{95}Mo in the complex $[Mo(CO)_5L]$ less than e.g. L = PPh_3.[14]

Sequential substitution into $Mo(CO)_6$ of MeCN leads to downfield shifts[15] in accordance with the effects of the ArCN ligands in the $\{MoP_4\}$ system. In the case of MeCN the ligand is able to accept π back-donation but this is not so for amines and similar substitution of $Mo(CO)_6$ by pyridine[14], piperidine[8] etc. leads to much greater deshielding of ^{95}Mo.

Various complexes with sulphur chelating ligands e.g. S_2CNR_2 (R = Me, Et etc.) of the type $[Mo(CO)_4\overset{\frown}{L\ L}]$ show increased ^{95}Mo shielding over amine-type donors and this could be attributed to the greater nephelauxetic contribution to the shielding from the more polarisable sulphur.[21]

If the data evident from the literature is combined a rough ordering emerges:

$H^- > PF_3 \sim CO > P(OR)_3 > PR_3 > CNR \geqslant PAr_3 > NCR >$ amines.

If this is then compared with the orderings deduced from the present work i.e. $PR_3 > PAr_3 > N_2$ and $CO > CNR > C_2H_4 > N_2 > NCR$ a rough overall spectrochemical series may be proposed:

$H^- > PF_3 \sim CO > P(OR)_3 > PR_3 > CNR > C_2H_4 > PAr_3 > N_2 > NCR >$ amines.

This places N_2 quite low in the series and among the other nitrogen donor ligands. If the nitrosyl, diazenido- and hydrazido(2-)-ligands were to be included, on the basis of their ^{95}Mo shielding contributions, they would also be so classified.

4.5 Coupling constants

A general observation for J_{XY} coupling constants is that the absolute value increases as substituents on either X or Y become more electronegative (everything else being equal). This is because bonds to electronegative substituents contain more p character and thus leave more s character at the coupled nucleus[44] and also cause some orbital contraction due to increased effective nuclear charge. Both effects increase the important Fermi contact spin-spin coupling term (and increase in $\langle r^{-3} \rangle$ increases other coupling terms). This is found for the $|^1J_{MoP}|$ coupling constant in $[Mo(CO)_5(PX_3)]$ which increases from ca. 125 to 180 Hz in the sequence:

$$PR_3 < PAr_3 < P(NMe_2)_3 < P(OR)_3 < PCl_3 < PF_3$$ [9,16,17,45]

Similar behaviour over a small range is shown for the complexes cis-$[Mo(CO)_4(PPh_2XR)]$ where the ordering for a change in XR is: $SR < NR_2 < OR < Cl$.[18]

Unfortunately for many of the $\{MoP_4\}$ systems coupling constants could not be resolved but when accurate coupling constant data is available valuable information may be obtained about the ability of a ligand to donate σ-electron density to the metal. An example is the comparison between cis-$[Mo(N_2)_2(PMe_3)_4]$ ($^1J_{MoP}$ = 175 Hz) and trans-$[Mo(C_2H_4)_2(PMe_3)_4]$ ($^1J_{MoP}$ = 140 Hz) where the decrease in coupling constant may reflect enhanced σ-donor power of C_2H_4 over N_2.

CHAPTER 5

^{15}N NMR as a Probe of Ligand Structural Isomerism

5.1 Introduction

There exist several important nitrogen containing ligands that show some form of structural isomerism in their complexes. Of particular note are nitrosyl and diazenido-ligands which can change their mode of coordination, depending on the environment at the metal centre, through bending at the ligating atom. These systems are perhaps the best characterised, with structural data available for both geometries of nitrosyl and diazenido-ligands. Such data however are not available for all such complexes and thus distinguishing the various bonding modes must be dependent on spectroscopic techniques. As discussed below information from infra-red stretching frequencies can be ambiguous and assignment difficult especially in the case of the aryl diazenido-ligand. ^{15}N NMR spectroscopy can make a significant contribution to the study of these ligands if distinct shielding criteria can be established for the various bonding modes. Particularly important is the development of such techniques to allow interpretation of data obtained from reacting solutions in which intermediates may not be isolable for structural characterisation. Included in this type of analysis is the study of protonation reactions. The protonation of dinitrogen on the route to ammonia or hydrazine is discussed in the next chapter,

and it is useful to consider postulated intermediates on such pathways, in isolation. This is treated below by use of ^{15}N NMR to examine the products derived from protonation of the diazenido-ligand namely the diazene ligand (-NHNHR) and also the hydrazido(2-) ($-N_2HR$) ligand which itself shows interesting structural isomerism.

It is essential to determine how far ^{15}N NMR criteria follow the solid state structural data where this is available and, where deviations do occur, to try to elucidate the causes. In such cases the solution state probe is important as it is in this phase that the majority of reactions occur and these will be affected by ligand configuration. Such comparisons are made below for diazenido- ($-N_2R$), hydrazido(2-) N_2R_2, imido- (-NR) and nitrido- (-N) systems, several models for intermediates that may be involved in the reduction of N_2 at a metal site.

5.2 The diazenido-ligand

5.2.1 Diazenido bonding modes

The diazenido-ligand is found coordinated to a variety of metals with different ligand environments and stereochemistries and is most commonly found in the (formally) $-N_2R^+$ singly-bent mode shown below:

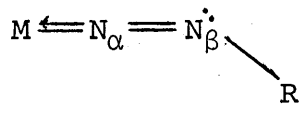

Singly-bent diazenido-ligand

The ligand acts as a 3-electron donor, bonding in the synergic mode mentioned in Chapter 1. The π-acceptor and σ-donor properties are greatly enhanced by the bending at N_β as predicted by a M.O. treatment of the bonding in the diazenido-ligand.[1] There are no structurally characterised examples of the completely linear ligand. Bending at N_α is observed in some complexes and may be visualised as occurring by the localisation of a lone pair on the ligating atom:-

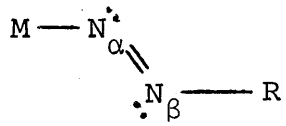

Doubly-bent diazenido-ligand

In this form the ligand acts as a one-electron donor, formally N_2R^-. The N_2R^+, N_2R^- classification is useful but requires that assignment of a singly or doubly-bent geometry be made even where this is uncertain. In such cases and also for the purposes of M.O. discussions[1] ambiguity is avoided by using the $\{MNNR\}^n$ notation, an adaptation of that used for nitrosyls by Enemark and Feltham.[2] n refers to the number of electrons associated with the metal d orbitals and the ligand π* orbitals and is easily calculated by assuming N_2R^+ coordination and counting d electrons on the metal in its formal oxidation state.

The factors governing the bending of nitrosyl and diazenido-ligands have been discussed at length (refs. 1-3).

For 6-coodinate complexes $\{ML\}^n$ (L = NO or N_2R), if $n \leqslant 6$, only bonding and non-bonding orbitals are filled and no bending occurs but for $n > 6$, antibonding orbitals become occupied and bending at the ligating atom occurs to minimise the energy of such unfavourable interactions. In 5-coordinate systems the pattern is more complex as the overall ordering of orbitals in the manifold is determined by the stereochemistry and the donor or acceptor power of the ligands.[3] One general result is that bending is most favoured if the diazenido- or nitrosyl ligand is in the axial position of a square pyramidal (SP) complex:-

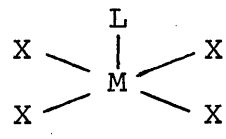

L = NO or N_2R

X = Basal ligands

Bending is encouraged by good π-donors such as Cl^- and discouraged by acceptors like CO. Typical 5-coordinate complexes show either SP or trigonal bipyramidal (TBP) geometry with $\{ML\}^8$.

The situation in 4-coordinate square planar systems is simpler in that $\{ML\}^8$ should give linear coordination and $\{ML\}^{10}$ should induce bending at the ligating atom.[2] It must be mentioned that as well as the end-on ligated form, the diazenido-ligand may also adopt a side-on configuration or bridge between two metals.[4] Complexes containing these types of ligand have not yet been studied by ^{15}N NMR due to the difficulty of introducing a ^{15}N label.

5.2.2 Difficulties with infra-red criteria of ligand structure

The use of infra-red stretching frequencies [ν(NO) or ν(NNR)] for diagnosing the bonding mode of a nitrosyl or diazenido-ligand encounters several problems:

Some bands, especially those at lower frequency, may be obscured by stretching modes due to other ligands, making assignment difficult. A particular problem in aryl-diazenido-systems is vibronic coupling between ν(NN) and the aryl ring deformations. This can give rise to many bands although the correct frequency may be calculated if extensive isotope substitution, using ^{15}N and ^{2}H, is employed (see e.g. ref. 5). Unfortunately the regions of bent and linear ligand stretches also overlap, therefore a set of empirical relations which compensate for the coordination sphere of the complex has been proposed.[6] Application of these rules, however, can still lead to ambiguity in some cases. An example is $[RhCl_2(N_2Ph)(PPh_3)_2]$ the corrected i.r. stretching frequency of which is a borderline value.[6] From the reactivity, and ^{15}N NMR spectrum discussed below, this compound must be doubly-bent.

5.2.3 Examples of singly- and doubly-bent diazenido-ligand systems

Aryldiazenido-complexes dominate the coordination chemistry of the $-N_2R$ ligand and examples may be found for all members of groups VI to VIII of the transition metals, except Ni and Tc. Synthetic and structural data up to 1975

has been reviewed by Sutton.[7] These complexes are of interest for ^{15}N NMR studies as labelling can be achieved via the diazonium cation $Ph^{15}N_2^+$ from which many of the compounds are derived. Unfortunately not all of the complexes amenable to labelling are sufficiently soluble or stable in solution for the purposes of an NMR experiment.

The complex $[RuCl_3(N_2Ar)(PPh_3)_2]$[8] is an example of a $\{MN_2R\}^6$ six-coordinate species containing the singly-bent diazenido-ligand as determined by X-rays.[6] The ligand arrangement [Figure (5.1)] is the same as in the analogous nitrosyl complex and in several cases the structure of a diazenido-complex has been inferred from the known structure of the corresponding nitrosyl complex.

Figure (5.1):

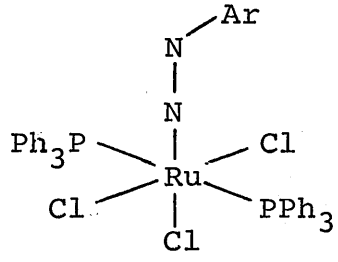

This complex is prepared as shown in reaction (5.1).[8]

$$[RuCl_2(PPh_3)_3] + ArN_2^+ \xrightarrow[\text{Acetone}]{\text{LiCl}} [RuCl_3(N_2Ar)(PPh_3)_2] \quad (5.1)$$

It may be noted that ArN_2^+ (Ar = C_6H_5) can be made labelled at N_α and N_β, but ArN_2^+ (Ar = C_6H_4Me-4, $C_6H_4NO_2$-4, etc.) can be labelled with ^{15}N at N_α only.

The complex $[Ru(CO)_2(N_2Ph)(PPh_3)_2]^+$ may be prepared as shown in reaction (5.2).[5]

$$[Ru(CO)_3(PPh_3)_2] + PhN_2^+ \xrightarrow{\text{Benzene}} [Ru(CO)_2(N_2Ph)(PPh_3)_2]^+ \quad (5.2)$$

This complex is representative of a series of similar compounds of Os or Fe and structures of $[Fe(CO)_2(N_2Ph)(PPh_3)_2]^+$ [9] and $[Os(CO)_2(NO)(PPh_3)_2]^+$ [10] have been determined. These structures should be analogous to that of $[Ru(CO)_2(N_2Ph)(PPh_3)_2]^+$ [Figure (5.2)].

Figure 5.2:

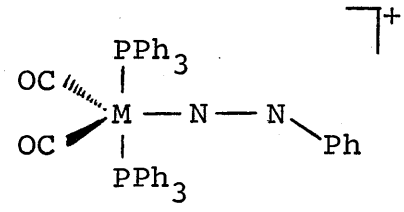

A similar geometry is found for $[OsH(CO)(N_2Ph)(PPh_3)_2]$ [11] which also exhibits an unusually long Os-N bond length [1.867Å]. All of these five-coordinate complexes have the $\{MN_2R\}^8$ configuration. $[Ru(CO)_2(N_2Ph)(PPh_3)_2]^+$ reacts with Cl^- to give the six-coordinate $\{MN_2R\}^8$ complex $[RuCl(CO)_2(N_2Ph)(PPh_3)_2]$ which contains the doubly-bent diazenido-ligand, on the evidence of its low $\nu(NN)$ and its reactivity.[5]

Iridium gives an interesting variety of complexes with the diazenido-ligand. $[IrCl(N_2Ph)(PPh_3)_2]^+$ is derived from Vaska's complex trans-$[IrCl(CO)(PPh_3)_2]$ by the following reaction (5.3).[12]

$$[IrCl(CO)(PPh_3)_2] \xrightarrow[PhN_2^+]{EtOH,\ PhCON_3} [IrCl(N_2Ph)(PPh_3)_2]^+ \quad (5.3)$$

The complex has trans-stereochemistry with a singly-bent diazenido-ligand.[13a,b] The $16e^-$ complex $[IrCl(N_2Ph)(PPh_3)_2]^+$ reacts with a variety of $2e^-$ donors, and with PPh_3 it gives $[IrCl(N_2Ph)(PPh_3)_3]^+$.[12] No X-ray structure determination of this complex is available but the analogue $(IrCl(N_2Ph)(PMePh_2)_3]^+$ has been studied[14] and is interesting for two reasons: the coordination geometry is between square pyramidal and trigonal bipyramidal and the diazenido-ligand adopts a "half-doubly-bent" configuration [Figure (5.3)].

Figure (5.3):

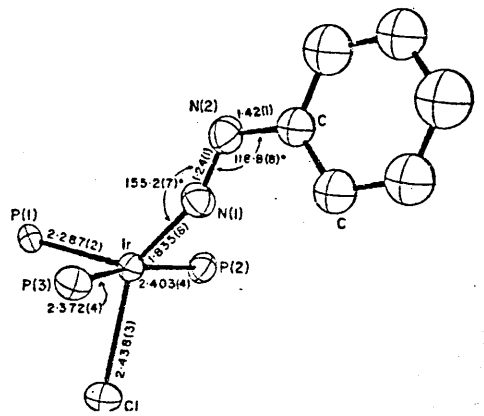

The intermediate geometry of the complex is attributed to the steric constraints of the $PMePh_2$ ligands.[14]

Another variation on the above complexes is $[Ir(N_2Ph)(dppe)_2]^{2+}$ which appears to have a singly-bent N_2Ph ligand, according to the infra-red stretching frequency. This $\nu(NN)$ value is greatly reduced in the derivative $[IrBr(N_2Ph)(dppe)_2]^+$ which contains the doubly-bent diazenido-ligand.[15]

The complex $[IrCl_2(N_2Ph)(CO)(PPh_3)_2]$ can be derived directly from Vaska's complex by a reaction with PhN_2^+ in which CO is retained, followed by coordination of a chloride ion,[16] and has the structure shown [Figure (5.4)] with a doubly-bent N_2Ar ligand.

Figure (5.4):

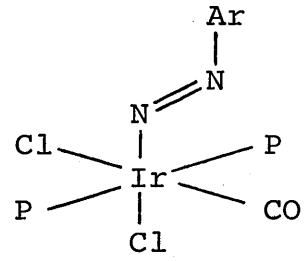

$[RhCl_2(N_2Ar)(PPh_3)_2]$[8] is analogous to $[RhCl(N_2Ph)(PPP)]^+$[15] {PPP = $PhP(CH_2CH_2CH_2PPh_2)_2$} and $[IrCl_2(NO)(PPh_3)_2]$,[17] both of which have a square pyramidal-type geometry, and an apical doubly-bent diazenido- or nitrosyl-ligand. $[RhCl_2(N_2Ar)(PPh_3)_2]$ may be prepared by reaction of $[RhCl(PPh_3)_3]$ with a diazonium salt and lithium chloride[8] and is easily protonated by HCl to give the diazene complex $[RhCl_3(NHNAr)(PPh_3)_2]$. Alternatively, the diazene complexes may be made directly from PhN_2^+ by an "insertion" reaction (5.4) of a rhodium hydride complex.[8]

$$[RhHCl_2P_3] \xrightarrow[Cl^-]{PhN_2^+} [RhCl_3(NHNPh)P_2] + P \qquad (5.4)$$

(P = PPh_3 or $PEtPh_2$)

Reaction with base yields the diazenido-complex of which that with P = $PEtPh_2$ is somewhat unstable.

The Rh and Ir complexes behave as $\{MN_2R\}^8$ systems. A square planar complex of Pt was prepared by Parshall[18] by "insertion" of a diazonium ion into a Pt-H bond in a similar manner to reaction (5.4), followed by deprotonation as in Scheme (5.1).

Scheme (5.1):

$$[PtHCl(PEt_3)_2] + PhN_2^+ \longrightarrow [PtCl(NHNPh)(PEt_3)_2]^+$$

$$\downarrow \text{Base}$$

$$[PtCl(N_2Ph)(PEt_3)_2]$$

The final complex is another example of a doubly-bent diazenido-ligand system and has a four-coordinate $\{MN_2R\}^{10}$ configuration. The structure has been verified crystallographically[19] [Figure (5.5)].

Figure (5.5):

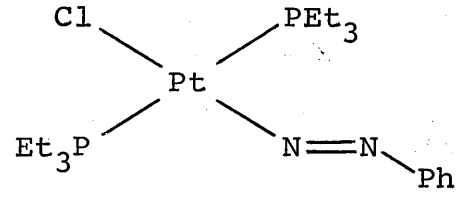

Many diazenido-complexes are derived from reactions with dinitrogen complexes of Mo and W and these invariably contain singly-bent diazenido-ligands[2] for example the trans-$[MoX(N_2Et)(dppe)_2]$ complexes of Chapter 3. These systems are all six-coordinate $\{MN_2R\}^6$ as found for rhenium

with singly-bent diazenido coordination in $[ReCl_2(N_2COPh)(C_5H_5N)(PPh_3)_2]$. This coordination mode is found in the structure of $[ReCl_2(N_2COPh)(PMe_2Ph)_3]$ which has been determined by X-ray analysis.[20] These diazenido-complexes are derived from the chelate complex in Figure (5.6).

Figure (5.6):

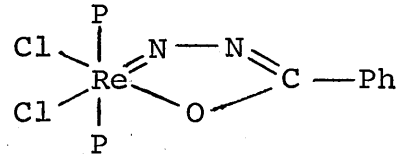

This compound is prepared via a substituted hydrazine[21] and is one of the few complexes so derived that can be ^{15}N labelled. Other Re diazenido-complexes which also contain a protonated diazenido-ligand, will be discussed later.

Finally, $[W(N_2Ph)(S_2CNMe_2)_3]$ is seven-coordinate with a singly-bent diazenido-ligand[22] and constitutes one of the few examples of a $\{MN_2R\}^4$ complex.

5.2.4 ^{15}N NMR of diazenido-complexes

5.2.4.1 Singly-bent and related complexes

Data for singly-bent diazenido- and related complexes are presented in Table (5.1). The measurements for trans-$[MoX(^{15}N_2Et)(dppe)_2]$ are from Chapter 3, and other values of $\delta^{15}N$ for complexes of Mo and also of W and Re are taken from the literature. These complexes are all $18e^-$ singly-bent diazenido-systems and show the following ranges of shielding:-

TABLE (5.1): ^{15}N NMR data for singly-bent diazenido- and related complexes

Complex	$\delta^{15}N$ (ppm)[a] N_α	N_β	$^1J_{NN}$ (Hz)	J_{OTHER} (Hz)	Reference
$[MoX(^{15}N_2Et)(dppe)_2]$[e]	+15 to -5	-132 to -154	10		T.W.
$[MoCl(^{15}N_2COMe)(dppe)_2]$	-35.4[b]	-123.7	12		23
$[WBr(^{15}N_2Et)(dppe)_2]$	-28.2[b]	-164.7	12		23
$[WCl(^{15}N_2COMe)(dppe)_2]$	-32.2[b]	-134.5	12		23
$[WBr(^{15}N_2H)(dppe)_2]$	-25.9[b]	-187.1	14	$^1J_{NH}=60$	24
$[WF(^{15}N_2H)(dppe)_2]$	-24.6[b]	-182.6	14	$^1J_{NH}=60$, $^2J_{NF}=60$	25
$[W(^{15}N_2Ph)(S_2CNMe_2)_3]$	-38.2	-138.0	16	$^1J_{WN}=108$	26
$[ReCl_2(^{15}N_2COPh)(C_5H_5N)(PPh_3)_2]$	-55.9[c]	-148.6	15		23
$[RuCl_3(^{15}NNC_6H_4Me\text{-}4)(PPh_3)_2]$	-46.4	-	-		25
$[RuCl_3(^{15}NNC_6H_5)(PPh_3)_2]$	-46.8	-	-		23

TABLE (5.1): continued

Complex	$\delta^{15}N$ (ppm)[a] N_α	N_β	$^1J_{NN}$ (Hz)	J_{OTHER} (Hz)	Reference
$[RuCl_3(N^{15}NC_6H_5)(PPh_3)_2]$	-	-185.6	-		T.W.
$[RuCl_3(^{15}NNC_6H_4NO_2\text{-}4)(PPh_3)_2]$	-47.7	-	-		25
$[Ru(CO)_2(^{15}N_2Ph)(PPh_3)_2][BF_4]$	+116.8	-25.2	16		T.W.
$[OsH(CO)(^{15}N_2Ph)(PPh_3)_2]$	+98.9	-35.5	17	$^2J_{NP}=6$, $^2J_{NH}=5$	T.W.
$[RhCl(^{15}N_2Ph)(PMePh_2)_3][PF_6]$	+106.3	+2.4	16	$^2J_{NP_A} \simeq {}^1J_{RhN} \simeq 16$ $^2J_{RhN}=30$, $^2J_{NP_B}=3$[d]	T.W. T.W.
$[IrCl(^{15}N_2Ph)(PPh_3)_2][BF_4]$	-92.1	-239.0	8	$^2J_{NP}=4$, $^3J_{NP}=2$	T.W.
$[IrCl(^{15}N_2Ph)(PPh_3)_3][BF_4]$	+59.0	-22.9	14	$^3J_{N_\beta P_A}=8$, $^2J_{N_\alpha P_A}=36$[d] $^2J_{N_\alpha P_B}=5$	T.W., 26

TABLE (5.1): continued

Complex	$\delta^{15}N$ (ppm)[a] N_α	N_β	$^1J_{NN}$ (Hz)	J_{OTHER} (Hz)	Reference
$[IrCl(^{15}N_2Ph)(PMePh_2)_3][BF_4]$	+64.0	-23.6	15	$^2J_{NP_A}$ 35, $^2J_{NP_B}$ =6[d]	T.W.
$[Ir(^{15}N_2Ph)(dppe)_2][PF_6]_2$	+46.4	-38.2	14		T.W.

[a]In CH_2Cl_2 soln. except b) thf or c) toluene; d) see text for assignment. T.W. = this work.
[e]X = various ligands as shown in Chapter 3.

$\{M\text{-}N_\alpha = N_\beta\text{-}R\}^n$ $\quad n = 6,4$

$\delta^{15}N_\alpha$ ca. +15 to -60 ppm

$\delta^{15}N_\beta$ ca. -120 to -190 ppm

These ranges are very similar to those found in aryl diazonium cations for various substituents on the aryl ring:-[27,28]

$N_\alpha \equiv N_\beta^+ - Ar$

N_α ca. -15 to -65 ppm

N_β ca. -120 to -160 ppm

Another series of complexes that fit into the above classification are $[RuCl_3(N_2Ar)(PPh_3)_2]$ (Ar = C_6H_5Y-4, Y = Me, H or NO_2) for which only $\delta^{15}N_\alpha$ values are available.[25] It may be noted that there is a slight upfield shift of the N_α resonance as the substituent on the aryl ring becomes less electron donating. Unfortunately such relationships cannot be explored for N_β as only the $-N_2Ph$ derivative can be synthesised with this nucleus labelled. The $\delta^{15}N$ value for $[RuCl_3(N^{15}NPh)(PPh_3)_2]$ falls within the range designated above. All of these complexes of Mo, W, Re or Ru have $\{MN_2R\}^6$ or $\{MN_2R\}^4$ configurations and it would seem that the shielding range is characteristic of such systems.

This can be contrasted with the five-coordinate $\{MN_2R\}^8$ complexes with singly-bent ligands. The range of shielding found is shown below:-

$\{M - N_\alpha = N_\beta\text{-}R\}^n$ $\quad n = 8$

N_α ca. +120 to +45 ppm

N_β ca. +5 to -40 ppm

These ranges resemble those for certain triazene compounds:

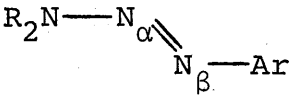

N_α ca. +75 to +70 ppm

N_β ca. -20 to -35 ppm

Considering the complexes individually, certain features emerge: $[Ru(^{15}N_2Ph)(CO)_2(PPh_3)_2][BF_4]$ has the lowest field N_α resonance and may be compared with the isostructural compound $[OsH(^{15}N_2Ph)(CO)(PPh_3)_2]$ which has both N_α and N_β ca. 10-20 ppm to higher field. This shielding may arise through several effects. Changing the metal centre down a group of the periodic table, (Ru to Os in this case), is usually associated with increased shielding in carbonyl (^{13}C and ^{17}O), cyanide (^{13}C and ^{15}N), nitrosyl (^{15}N) and dinitrogen complexes.[29] Moreover a good π-acceptor (CO) has been replaced by a good σ-donor (H^-) with removal of the formal cationic charge, an effect similar to that exhibited by the $[MoX(N_2Et)(dppe)_2]$ complexes in Chapter 3. The general low field N_α resonances of the two Os and Ru complexes may be related to the length of the M-N bond. This is exceptionally long for Os as shown earlier but no structure has been reported for the Ru complex.

The spectrum of $[OsH(^{15}N_2Ph)(CO)(PPh_3)_2]$ is shown in Figure (5.7) and displays both $^2J_{NP}$ and $^2J_{NH}$ coupling which are of similar size. The $^2J_{NP}$ value is typical of the cis-P-N couplings found in these systems (vide infra). [Table (5.1)].

The complexes $[IrCl(^{15}N_2Ph)P_3][BF_4]$ (P = $PMePh_2$ or PPh_3) give very similar spectra (shown for the $PMePh_2$

Figure (5.7): ^{15}N NMR spectrum of $[OsH(^{15}N_2Ph)(CO)(PPh_3)_2]$

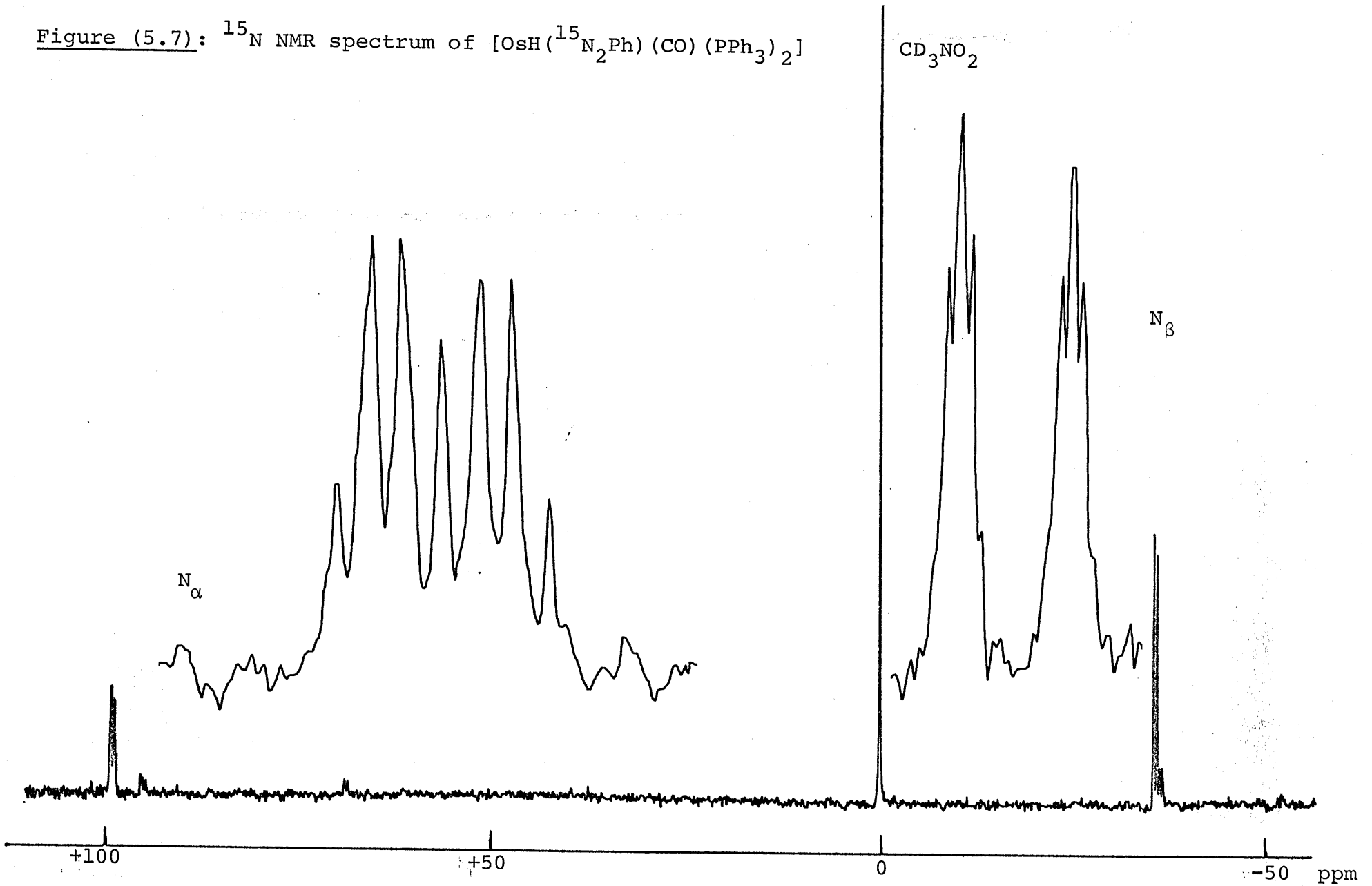

variant [Figure (5.8)]). The N-P coupling pattern is consistent with a pair of equivalent cisoid, (P_A) and one unique transoid (P_B) phosphine ligand. This is not at odds with the intermediate geometry proposed for $[IrCl(N_2Ph)(PMePh_2)_3]^+$ and the ^{31}P NMR spectrum.[14] The similarity of the ^{15}N spectra of the $PMePh_2$ and the PPh_3 analogues, however, coupled with the fact that the $\delta^{15}N_\alpha$ shift is not to abnormally low field, indicates the possibilities:

(a) Both complexes $[IrCl(N_2Ph)P_3]^+$ (P = $PMePh_2$ or PPh_3) may have the same intermediate stereochemistry. This is unlikely due to the steric bulk of the PPh_3 ligand[14] and the relatively shielded N_α resonance, indicative of a normal singly-bent configuration.

(b) More likely, both complexes assume the same geometry in solution with a singly-bent diazenido-ligand, and the "half-doubly-bent" character of the diazenido-ligand in the solid state most probably arises through crystal packing forces.

It is unfortunate that a crystal structure of $[IrCl(N_2Ph)(PPh_3)_3]^+$ is not available for direct comparison.

In $[RhCl(^{15}N_2Ph)(PMePh_2)_3][PF_6]$ the ^{15}N resonances are somewhat downfield of those of its Ir analogues and this may be partly due to the change of metal. The N_β resonance [Figure (5.9)] is simple showing only N-N and Rh-N coupling (^{103}Rh, $I = \frac{1}{2}$, 100% abundance) but for N_α the pattern is more complex. This arises because $^1J_{NP_A}$, the coupling to the unique phosphine (also observed in the ^{31}P NMR spectrum), is approximately equal to both $^1J_{RhN}$ and $^1J_{NN}$ at ca. 16 Hz

Figure (5.8): ^{15}N NMR spectrum of $[IrCl(^{15}N_2Ph)(PMePh_2)_3][BF_4]$

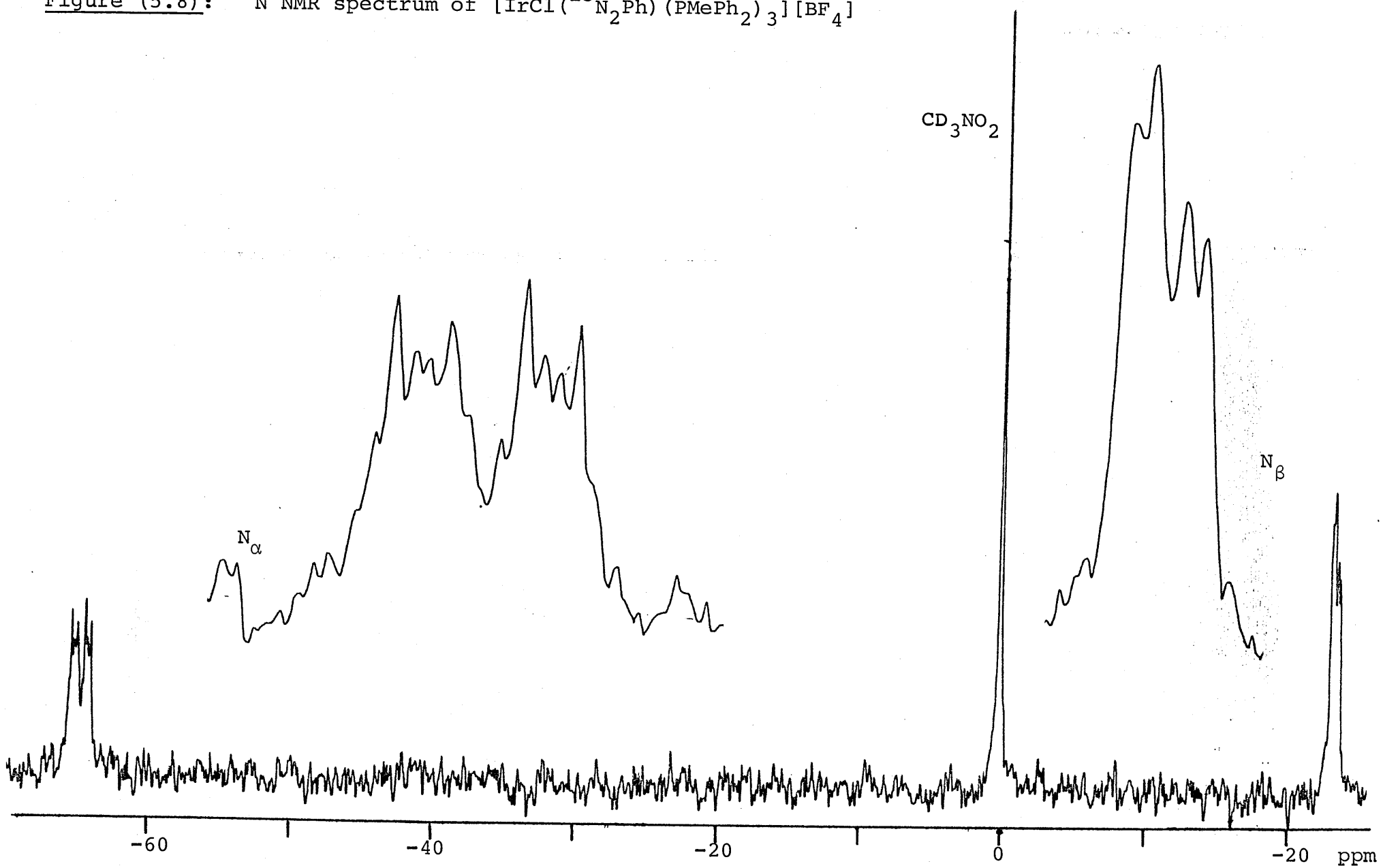

Figure (5.9): ^{15}N NMR spectrum of $[RhCl(^{15}N_2Ph)(PMePh_2)_3][PF_6]$

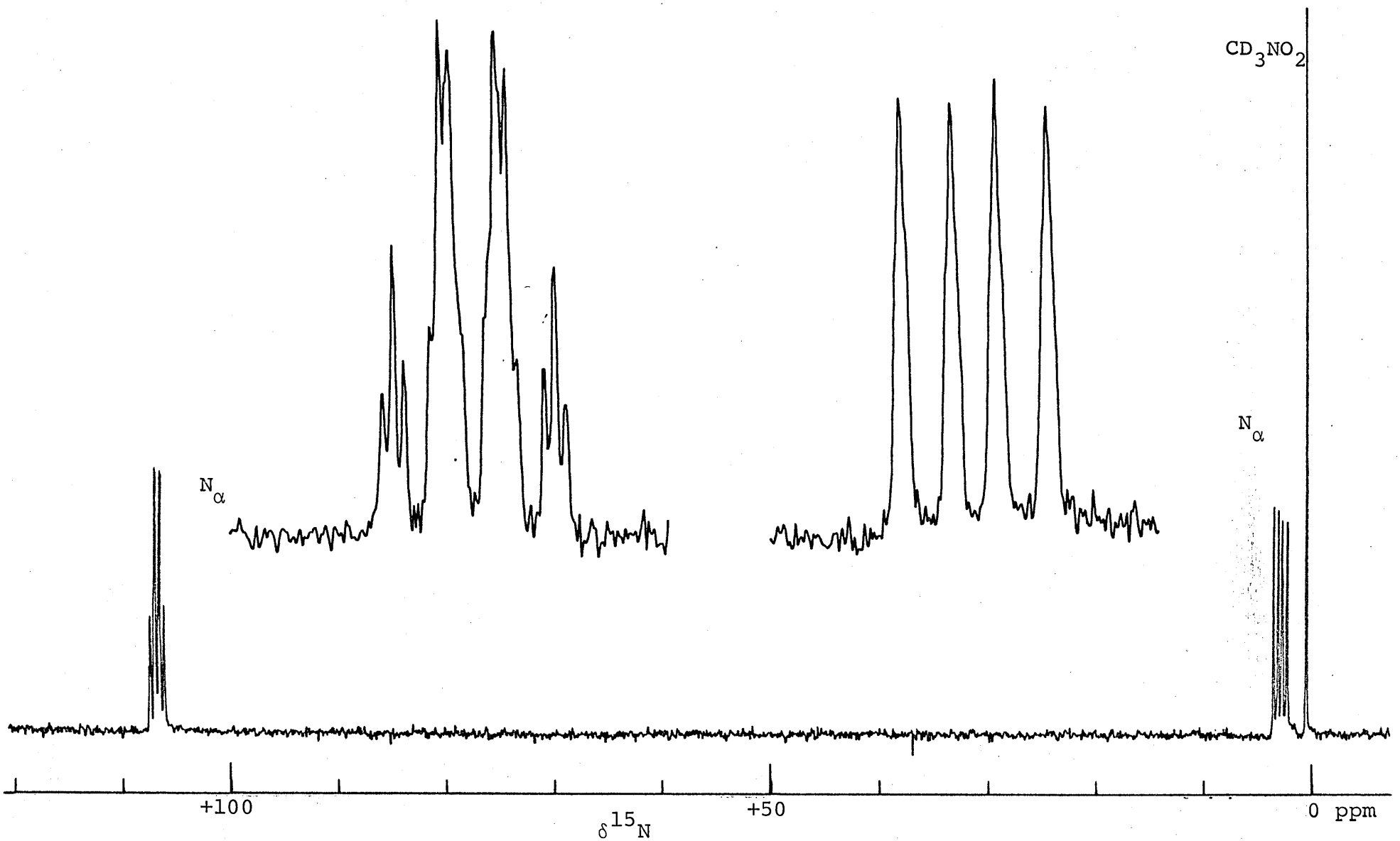

[Table (5.1)]. An interesting feature is that $^{1}J_{RhN} < {}^{2}J_{RhN}$, at variance with the customary ordering $^{1}J >> {}^{2}J$ for a given pair of nuclei. In $[W(^{15}N_2Ph)(S_2CNMe_2)_3]$ with $^{1}J_{WN}$ (^{183}W, $I = \frac{1}{2}$, 14.4% abundance) ca. 100 Hz, $^{2}J_{WN}$ was not observed[26] and in the dinitrogen complex $[RhCl(^{15}N_2)(PPr^{i}_3)_2]$[30] $^{1}J_{RhN}$ (28 Hz) is much larger than $^{2}J_{RhN}$ (4 Hz). The reversal of order in $[RhCl(^{15}N_2Ph)(PMePh_2)_3][PF_6]$ is probably a consequence of the sensitivity of J_{NX} to the hybridisation at nitrogen, in particular the effect of lone pairs as discussed at the end of Chapter 2. This points to some degree of change in hybridisation at the N_α nucleus, possibly involving bending and development of lone pair character. Such effects as well as reducing $^{1}J_{RhN}$, might also be expected to diminish $^{2}J_{NP}$, and a comparison with the Ir systems indeed shows a halving of both $^{2}J_{NP_A}$ and $^{2}J_{NP_B}$ on going from Ir to Rh. It may be noted that the ^{31}P spectra of the complexes $[MCl(N_2Ph)(PMePh_2)_3]^{+}$ (M = Ir or Rh) give similar $^{2}J_{P_AP_B}$ coupling constants: for Ir, $^{2}J_{P_AP_B}$ = 12 Hz [14] and for Rh = 16 Hz.

A tentative conclusion from these data is that $[RhCl(N_2Ph)(PMePh_2)_3][PF_6]$ retains some "half-doubly-bent" diazenido-character in solution.

The complex $[Ir(^{15}N_2Ph)(dppe)_2][PF_6]_2$ shows N_α and N_β resonances consistent with singly-bent diazenido-coordination.

$[IrCl(^{15}N_2Ph)(PPh_3)_2][BF_4]$ was the only four-coordinate $16e^{-}$ complex studied by ^{15}N NMR and it shows unique behaviour. The resonances of both N_α and N_β are to much

higher field than in the $18e^-$ $\{MN_2R\}^8$ complexes and also more shielded than the $\{MN_2R\}^6$ complexes. In fact the ^{15}N shifts are reminiscent of those found for hydrazido(2-) complexes of Mo and W[31], as is the value of $^1J_{NN}$ which is low compared with the other diazenido-complexes. These observations are indicative of the diazenido-ligand changing its hybridisation to maximise its donor power towards the electron-deficient metal centre. The structure of $[IrCl(N_2Ph)(PPh_3)_2]$[+13a,b] shows many similarities to the $\{MN_2R\}^6$ complex $[RuCl_3(N_2Ph)(PPh_3)_2]$, described earlier, with the two trans-chloride ligands removed. If the diazenido-ligand were developing hydrazido(2-) character, a shortening of the $M-N_\alpha$ bond length might be expected, or if lone pair character at N_β were decreasing by delocalisation into the N-N bond (which might be expected to lead to shielding of N_β), a straightening of the $\hat{NNC}$ angle should follow. In fact neither of these effects is observed and thus it appears that ligand structural isomerism is not responsible for the "anomalous shifts". In this context it would be interesting to look at other coordinatively unsaturated singly-bent diazenido-complexes to examine whether the upfield shift is a general phenomenon. Unfortunately this Ir complex is at present unique.

5.2.4.2 Doubly-bent diazenido- and related complexes

Table (5.2) shows data for doubly-bent diazenido-complexes. The ranges of shifts encountered are given below:-

TABLE (5.2): ^{15}N NMR data for doubly-bent diazenido- and related complexes

Complex	$\delta^{15}N$ (ppm)[a] N_α	N_β	$^1J_{NN}$ (Hz)	J_{OTHER} (Hz)	Reference
$[RhCl_2(^{15}N_2C_6H_5)(PEtPh_2)_2]$	+241.0	n.o.	16	$^1J_{RhN} = 8$	T.W.
$[RhCl_2(^{15}NNC_6H_5)(PPh_3)_2]$	+298.4	-	-		23
$[RhCl_2(^{15}NNC_6H_4NO_2\text{-}4)(PPh_3)_2]$	+327.1	-	-		23
$[IrCl_2(CO)(^{15}N_2Ph)(PPh_3)_2]$	+240.2	+148.4	n.o.		T.W.
$[IrBr(^{15}N_2Ph)(dppe)_2][PF_6]$	+220.5	+158.3	18	$^3J_{NP} = 6$	T.W.
$[PtCl(^{15}N_2Ph)(PEt_3)_2]$	+285.0	+162.0[b]	19	$^1J_{PtN} = 157$, $^3J_{NP} = 5$	T.W.
$[PtCl(N^{15}NPh)(PEt_3)_2]$	-	+162.0[b]	-	$^2J_{PtN} = 70$	T.W.
$[RhCl_3(^{15}NH^{15}NPh)(PEtPh_2)_2]$	-37.6	+102.0	16	$^1J_{RhN} = 16$, $^1J_{NH} = 70$, $^2J_{NH} = 3$	T.W.
$[RhCl_3(^{15}NH^{15}NPh)(PPh_3)_2]$	-37.0	+104.0	n.o.		T.W.
$[PtCl(^{15}NHNPh)(PEt_3)_2][BF_4]$	-54.7	+124.5	16	$^1J_{PtN} = 510$, $^2J_{PtN} = 80$, $^1J_{NH} = 75$, $^2J_{NP} = 4$ $^3J_{NP} = 2$, $^2J_{NH} = 2$	T.W.

a) In CH_2Cl_2 soln. except b) thf.

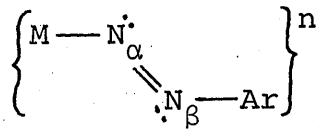

$\delta^{15}N_{\alpha}$ ca. +330 to +220 ppm

δN_{β} ca. +160 to +150 ppm

n = 10,8

The range for N_{β} is similar to that found in alkyl or aryl diazenes:-[32]

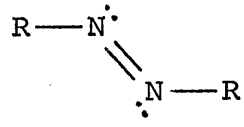

$\delta^{15}N$ ca. +170 to +120 ppm

R = alkyl or aryl

In other azo-type compounds, XN=NX, the chemical shift shows a dependence on the electronegativity of X, with shielding decreasing as X becomes more electropositive.[33] The lower shielding of N_{α} with respect to N_{β} in the $M-N_2R$ system is consistent with this.

The two complexes $[RhCl_2(^{15}NNC_6H_4Y\text{-}4)(PPh_3)_2]$ (Y = H or NO_2), labelled at N_{α} only, were the subject of an earlier ^{15}N NMR study.[23] In the present work, repeated efforts to observe the N_{β} resonance in $[RhCl_2(N^{15}NC_6H_5)(PPh_3)_2]$, failed due to the low solubility and rapid decomposition of the complex. A related compound, $[RhCl_2(^{15}N_2C_6H_5)(PEtPh_2)_2]$, selected for its high solubility, was synthesised.

Unfortunately the more basic phosphines encouraged rapid decomposition and only the N_{α} signal could be identified. The N_{α} resonance in this series of complexes shows a large variation with phosphine co-ligand and with substituent on the aryl ring of the diazenido-ligand. This is often

found in systems with strong deshielding, as small changes in ΔE are important because ΔE itself is small. It is interesting that substitution of Y = H by NO_2 leads to a substantial downfield shift of the N_α resonance, in contrast to the small upfield shift observed in $[RuCl_3(N_2Ar)(PPh_3)_2]$. Such effects are also shown in the aryl diazene compounds:

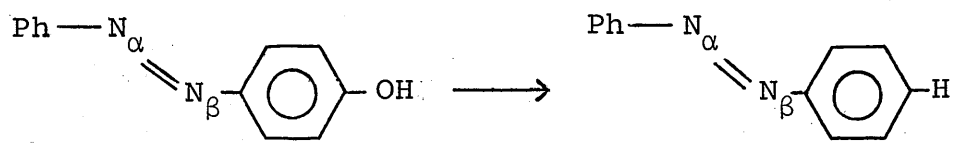

$\delta^{15}N_\alpha$ ca. +110 ppm

$\delta^{15}N_\alpha$ ca. +130 ppm

There is little effect on N_β.

The $^1J_{RhN}$ coupling constant of 8 Hz in $[RhCl_2(^{15}N_2Ph)(PEtPh_2)_2]$ is somewhat smaller than the observed value in $[RhCl(^{15}N_2Ph)(PMePh_2)_3]^+$ and reflects localisation of lone pair character at the N_α atom in the doubly-bent diazenido-ligand. Further evidence for this is shown in the spectrum of the aryl diazene complex $[RhCl_3(^{15}NH^{15}NPh)(PEt_2Ph)_2]$ in Figure (5.10). The N_α resonance shows the expected coupling to the attached proton ($^1J_{NH}$ = 70 Hz), and also a $^1J_{RhN}$ value of 16 Hz. This is larger than that in the unprotonated parent diazenido-complex due to removal of the negative lone pair contribution to the coupling constant on protonation. Also associated with removal of the lone pair character, is the large upfield shift (ca. 300-350 ppm) of $\delta^{15}N_\alpha$, on protonation. The N_α signal is a doublet of doublet of doublets with $^1J_{RhN} \simeq {}^1J_{NN}$ and this appears as a doublet of triplets.

Figure (5.10): ^{15}N NMR spectrum of $[RhCl_3(^{15}NH^{15}NPh)(PEt_2Ph)_2]$

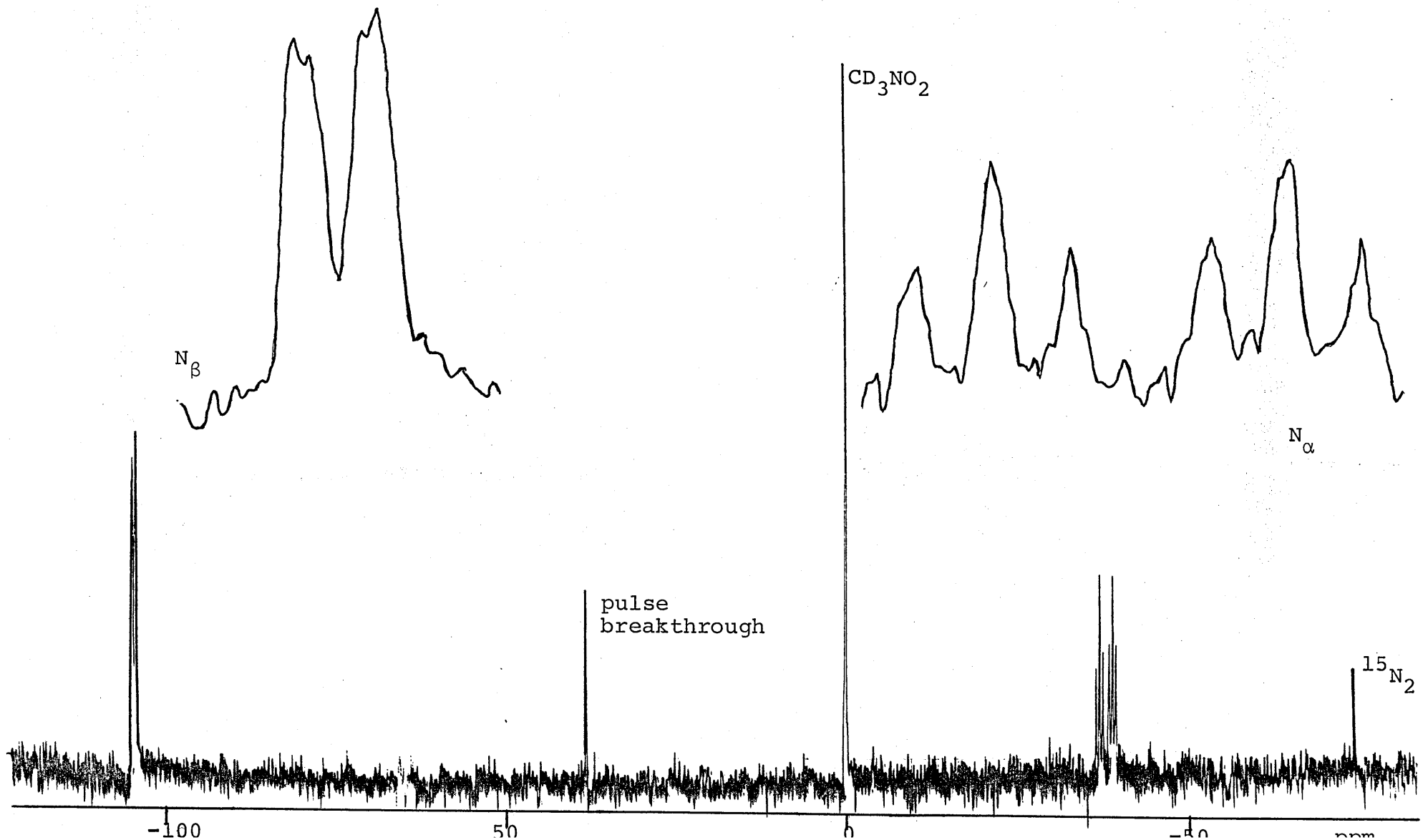

$[PtCl(^{15}N_2Ph)(PEt_3)_2]$ shows similar behaviour, and in this case the effects on N_β can be probed. The ^{15}N NMR spectrum [Figure(5.11)] shows N-N coupling and both $^1J_{PtN}$ and $^2J_{PtN}$ couplings (^{195}Pt, $I = \frac{1}{2}$, 33.8% abundance) with $^1J_{NPt} > {}^2J_{NPt}$. No $^2J_{NP}$ coupling at N_α is observed but a $^3J_{NP}$ coupling at N_β of 5 Hz is apparent. Although this is consistent with the lone pair effect on coupling, the N_α, N_β assignment was checked with singly labelled $[PtCl(N^{15}NPh)(PEt_3)_2]$ and the values of the N_β resonances were found to be in good agreement [Table (5.2)].

The ^{15}N NMR spectrum of the aryl diazene complex $[PtCl(^{15}NH^{15}NPh)(PEt_3)_2]$ [Figure (5.12)], shows a great increase of $^1J_{PtN}$ over that in the diazenido-complex. $^2J_{NP}$ is now observed and this is greater than $^3J_{NP}$. The $^1J_{NH}$ and $^2J_{NH}$ values are similar to those in the Rh diazene complex. $\delta^{15}N_\alpha$ is ca. 350 ppm to higher field with respect to the unprotonated nucleus, similar to the Rh system. Some organic compounds show comparable protonation shifts, an example being diphenyl diazene:-[34]

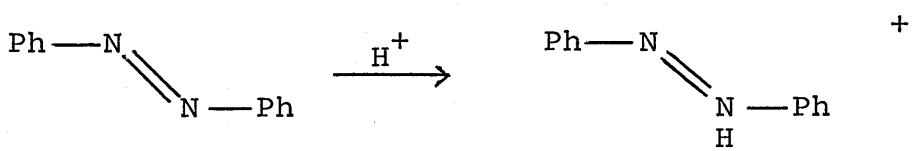

$\Delta\delta^{15}N$ ca. -150 ppm

It may be noted that the $\delta^{15}N_\alpha$ values for the diazene complexes fall in the same region as $\delta^{15}N_\alpha$ for the $\{MN_2R\}^6$

Figure (5.11): ^{15}N NMR spectrum of $[PtCl(^{15}N_2Ph)(PEt_3)_2]$

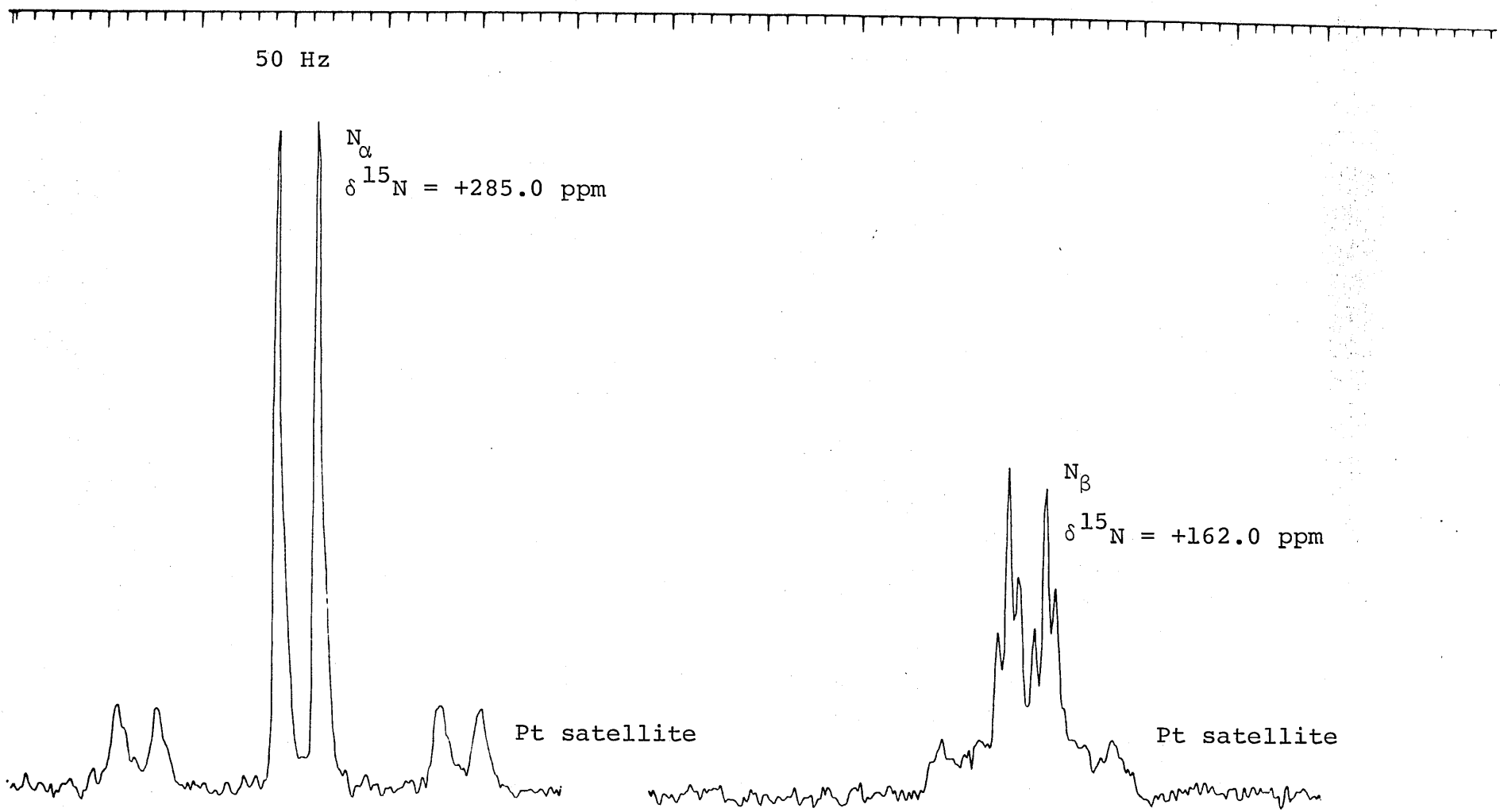

Figure (5.12): ^{15}N NMR spectrum of $[PtCl_2(^{15}NH^{15}NPh)(PEt_3)_2][BF_4]$

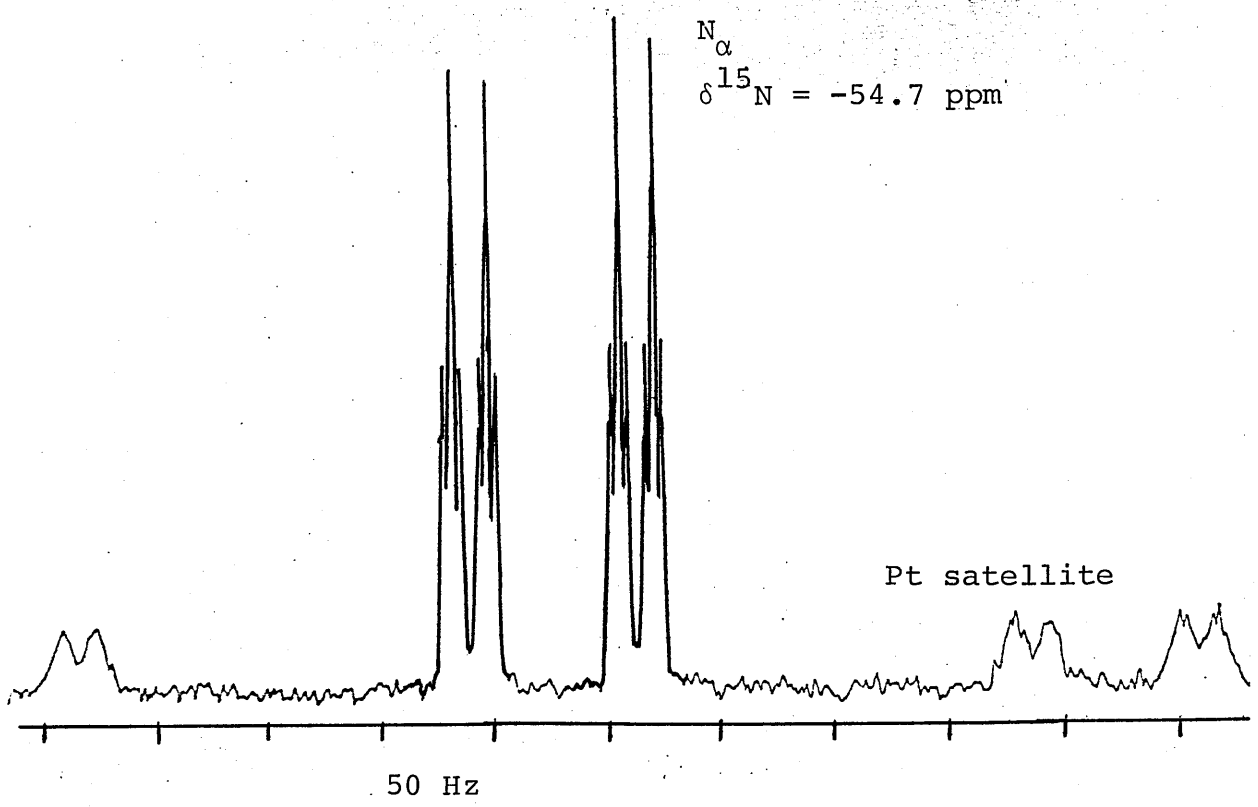

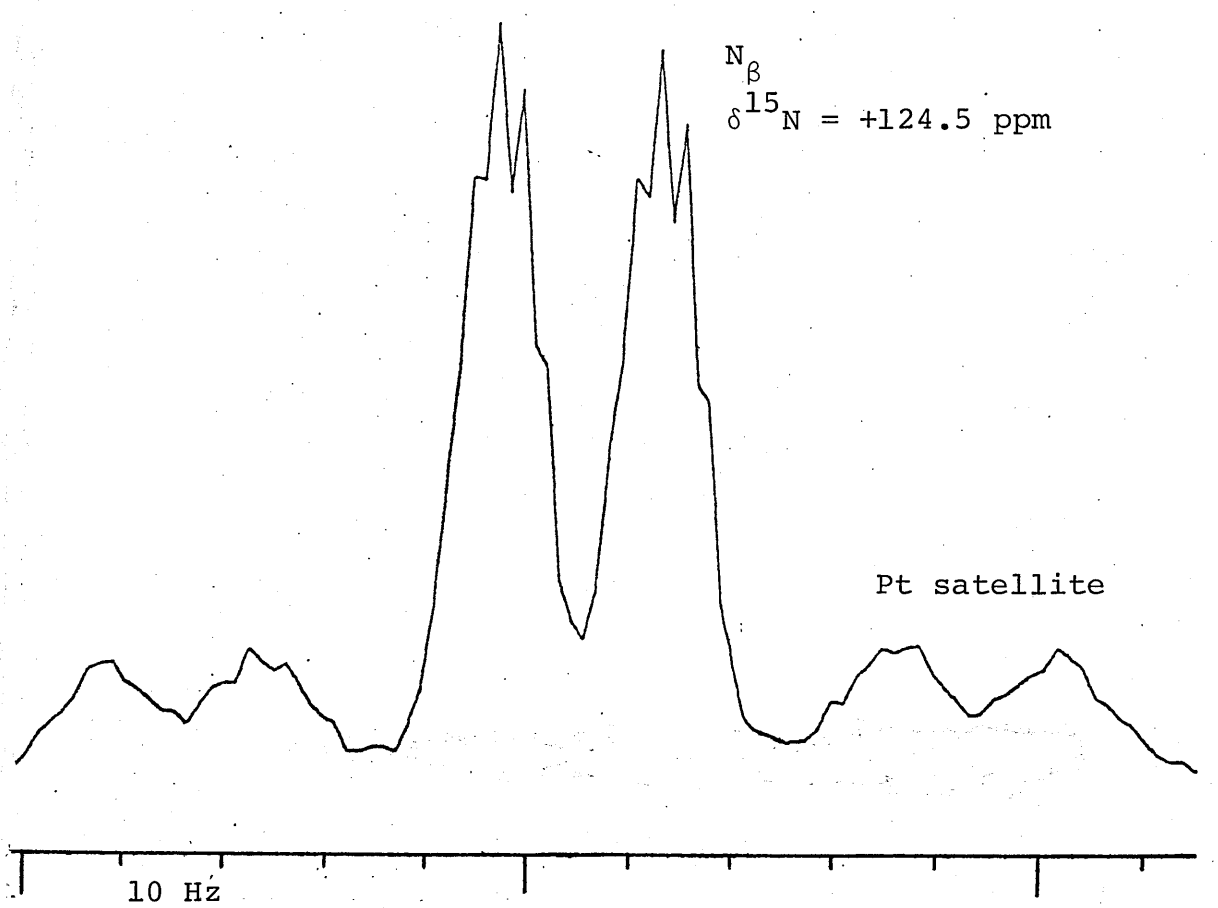

complexes. The Pt diazene complex shows a $\delta^{15}N_{\beta}$ resonance ca. 40 ppm to higher field than that in the diazenido-complex.

$[IrBr(^{15}N_2Ph)(dppe)_2][PF_6]$ shows the N-P coupling expected from four equivalent phosphorus nuclei [Figure (5.13)], however, this is only observed for N_{β}, as in the Pt diazenido-complex. No couplings could be measured from the spectrum of $[IrCl_2(^{15}N_2Ph)(CO)(PPh_3)_2]$ due to its low solubility and gradual decomposition in solution. Several attempts were made to measure the ^{15}N NMR spectrum of the 'doubly-bent' complex $[RuCl(CO)_2(^{15}N_2Ph)(PPh_3)_2]$ but this seems to protonate rapidly in CH_2Cl_2 solution to give a complex mixture of compounds.

5.2.5 General discussion and comparison with nitrosyl complexes

The data considered above show the clear demarcations between the various classes of diazenido-complex, and emphasises the sensitivity of ^{15}N chemical shifts to the precise electronic structure of this ligand in solution. The dominant effect observed, of course, is that produced by $n \rightarrow \pi^*$ circulation of the lone pair electrons, but more subtle changes such as that on going from a $\{MN_2R\}^{4,6}$ to a $\{MN_2R\}^{8}$ singly-bent diazenido-system can be observed. Within the $\{MN_2R\}^{8}$ system there is also some possibility of intermediate behaviour, whether this be bending at N_{α} or lengthening of the M-N bond. This type of phenomenon has been interpreted as indicative of the "readiness"[11] of

Figure (5.13): ^{15}N NMR spectrum of $[IrBr(^{15}N_2Ph)(dppe)_2][PF_6]$

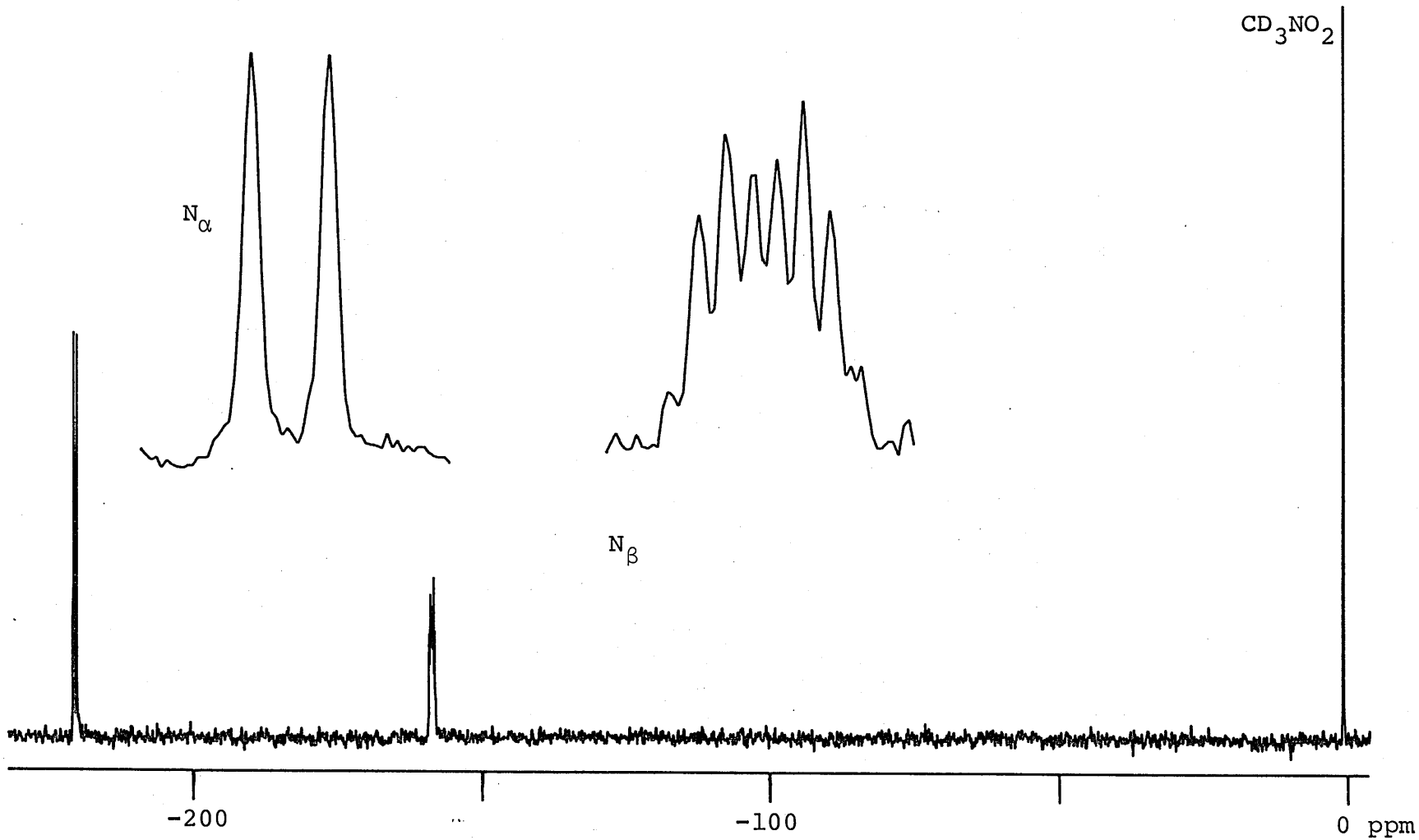

singly-bent $\{MN_2R\}^8$ systems to become doubly-bent and it is possible that the energy barrier between such extremes is relatively small. Further evidence for this is the induction of bending by simple changes of co-ligand or stereochemistry of the complex.

Nitrosyl complexes show many similar features to diazenido-complexes, and the downfield shift on going from a linear to a bent nitrosyl complex is apparent from several studies.[35-37] A detailed comparison with the above data is not possible as some classes of complex have not been studied. Thus the only example of a linear $\{MNO\}^8$ system studied by ^{15}N NMR is $[RhCl(^{15}NO)(PPr^i_3)_2]^+$.[35] This four-coordinate cation is analogous to $[IrCl(^{15}N_2Ph)(PPh_3)_2]^+$ but does not show a similar high field shift at N_α when compared to $\{MNO\}^6$ complexes. All the other $\{MNO\}^8$ complexes are bent, and in agreement with the diazenido-systems, $^1J_{RhN}$ for bent Rh nitrosyls is much less than that for the linear example mentioned above.[36] A particularly noteworthy series of complexes is the bis-nitrosyls (e.g. $[Rh(NO)_2(PPh_3)_2][ClO_4]$) in which there is some interaction between the NO ligands, giving intermediate geometry and downfield ^{15}N chemical shifts.[35] There are few examples of bis-diazenido systems and those that exist have yet to be studied by ^{15}N NMR but they should reveal some interesting results.

In the nitrosyl complexes there is obviously only one ^{15}N probe and as yet few ^{17}O studies have been carried out. This gives the relatively simple picture that bending at N_α is associated with the lone pair localisation and does not

give much information about the NO π system. In the diazenido-complexes, as shown, N_α exhibits the same behaviour as in the NO complexes. However, with the additional ^{15}N probe at N_β, extra information can be obtained in diazenido-complexes. A particularly striking observation is found on going from a singly- to a doubly-bent diazenido-system where both N_α and N_β are deshielded by roughly equivalent amounts. This arises from the presence of adjacent "lone pairs" of similar energy. These "non-bonding" orbitals can interact, to some extent, to give bonding and antibonding combinations. In this way a delocalised system with the transition metal is found over the (M-N-N) fragment. Associated with the bending at N_α are changes in orbital energies over this whole fragment, changes which are reflected in the chemical shifts. In organic nitroso-compounds[38] the overlap of n_N with n_O non-bonding orbitals ("lone-pairs") gives a π' and π'^* pair of orbitals. In this way the $n_N \rightarrow \pi^*$ and $n_O \rightarrow \pi^*$ excitations can be described as $\pi'^* \rightarrow \pi^*$ and $\pi' \rightarrow \pi^*$. It is concluded that each $n \rightarrow \pi^*$ transition shields both nuclei, to some extent,[38] and correspondingly in the diazenido-complexes.

Further evidence of this effect is given by the upfield shift of both N_α and N_β on protonation at N_α, as shown for the diazene complexes. It has also been noted that protonation of a singly-bent diazenido-ligand at N_β to give a hydrazido(2-) complex, produces an upfield shift at both N_α and N_β.[39]

5.3 Hydrazido(2-)-complexes

Complexes containing the linear hydrazido(2-)-ligand are common for Mo and W and are important as intermediates in the protonation of N_2 at metal sites as shown in Chapter 6.

The linear ligand has been studied by ^{15}N NMR[31] and shows well defined regions of shielding:

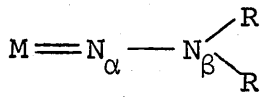

(R = H, alkyl or aryl)

$\delta^{15}N_\alpha$ ca. -45 to -100 ppm

$\delta^{15}N_\beta$ ca. -200 to -250 ppm

The ligand may, however, adopt an alternative geometry by bending at N_α, as found in complexes where the electron count would be $20e^-$. A few examples of complexes showing this type of arrangement have been structurally determined by Sutton and co-workers.[40] These complexes are of the type $[CpRe(CO)_2(NNRR')]$ (R = Me; R' = aryl) and also $[Cp_2WH(NNRR')]$ (R = H; R = aryl) for which $\delta^{15}N_\beta$ has been measured [Table (5.3)]. Several Re complexes containing the bent hydrazido(2-)-ligand have been synthesised by Haymore[26] and also by Dilworth and co-workers, who have determined the crystal structure[41] noted below. These complexes are of the type $[ReX_2(A)(N_2HPh)L_2]$ (X = Br, Cl or H; A = N_2Ph or NO; L = phosphine). The structure determined is that of $[ReBr_2(N_2Ph)(NNHPh)(PPh_3)_2]$ which has a singly-bent diazenido- and a bent hydrazido(2-)-ligand [Figure (5.14)].

Figure (5.14):

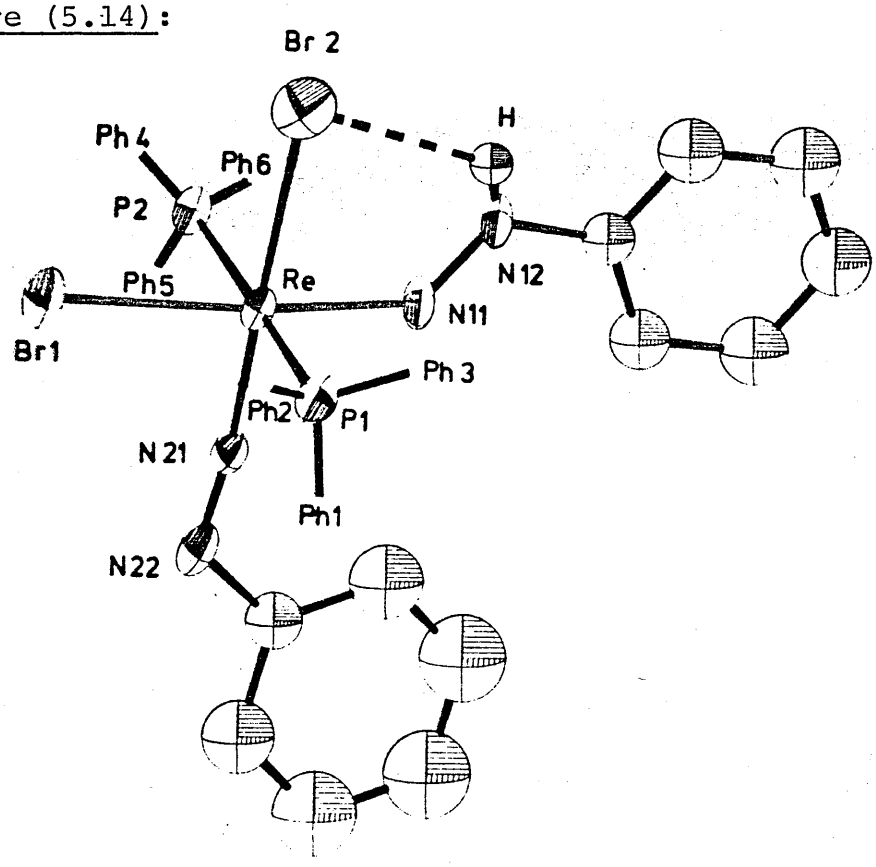

When A = NO in the above complexes, they may exist in two forms, with the proton at N_β in the bent hydrazido(2-) form:

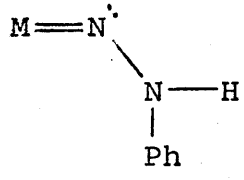

or at N_α, in the diazene form:

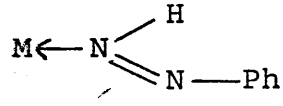

These forms arise in the preparation, and do not interchange in solution. Haymore[26] has studied several of these complexes by ^{15}N NMR and these results together with those from the present study are shown in Table (5.3).

The presence of the isomeric bent hydrazido(2-)- and the diazene complex in solution is shown by the spectrum of $[ReCl_2(NO)(B)(PPh_3)_2]$ (B = $^{15}N_2HPh$ or $^{15}NH^{15}NPh$) [Figure (5.15)].

TABLE (5.3): ^{15}N NMR data for bent hydrazido(2-) and related complexes

Complex	$\delta^{15}N$ (ppm)[b] N_α	N_β	$^1J_{NN}$ (Hz)	J_{OTHER} (Hz)	Reference
$[Cp_2WH(N^{15}NHPh)][BF_4]$[a]	-	-167	-	$^1J_{NH} = 99$	42
$[ReBr_2(NO)(^{15}N_2HPh)(PPh_3)_2]$	+238.7	-135.5	13.6	$^1J_{NH} = 93$, $^2J_{NP} = 1.3$	26
$[ReCl_2(NO)(^{15}N_2HPh)(PPh_3)_2]$	+239.5	-143.4	13	$^1J_{NH} = 94$	T.W.
$[ReHCl(NO)(^{15}N_2HPh)(PPh_3)_2]$	+218.1	n.o.	13		T.W.
$[ReBr_2(NO)(^{15}NH^{15}NPh)(PPh_3)_2]$	-27.0	+44.0	16.1	$^1J_{NH} = 66$, $^2J_{NP} = 1.8$ $^2J_{NH} = 3.3$, $^3J_{NP} = 1.2$	26
$[ReCl_2(NO)(^{15}NH^{15}NPh)(PPh_3)_2]$	-24.8	+37.4	15	$^1J_{NH} = 64$	T.W.
$[ReHCl(NO)(^{15}NH^{15}NPh)(PPh_3)_2]$	+2.7	+54.1	17	$^1J_{N_\alpha H} = 60$ $^2J_{N_\alpha H} = 16$	T.W.
$[ReBr_2(^{15}N_2Ph)(^{15}N_2HPh)(PPh_3)_2]$ (A, B)	A -3.7 B +190.3	-124.7 -159.2	13 12	$^1J_{NH} = 95$	T.W.[c]/26

a) Double resonance in MeCN, originally referenced to NH_4Cl, b) In CH_2Cl_2 soln.
c) Measured at 213K, ref. 26 at 293K gave broad lines but ca. same position.

Figure (5.15): ^{15}N NMR spectrum of $[ReCl_2(NO)(^{15}N_2HPh)(PPh_3)_2]$(1) and $[ReCl_2(NO)(^{15}NH^{15}NPh)(PPh_3)_2]$(2)

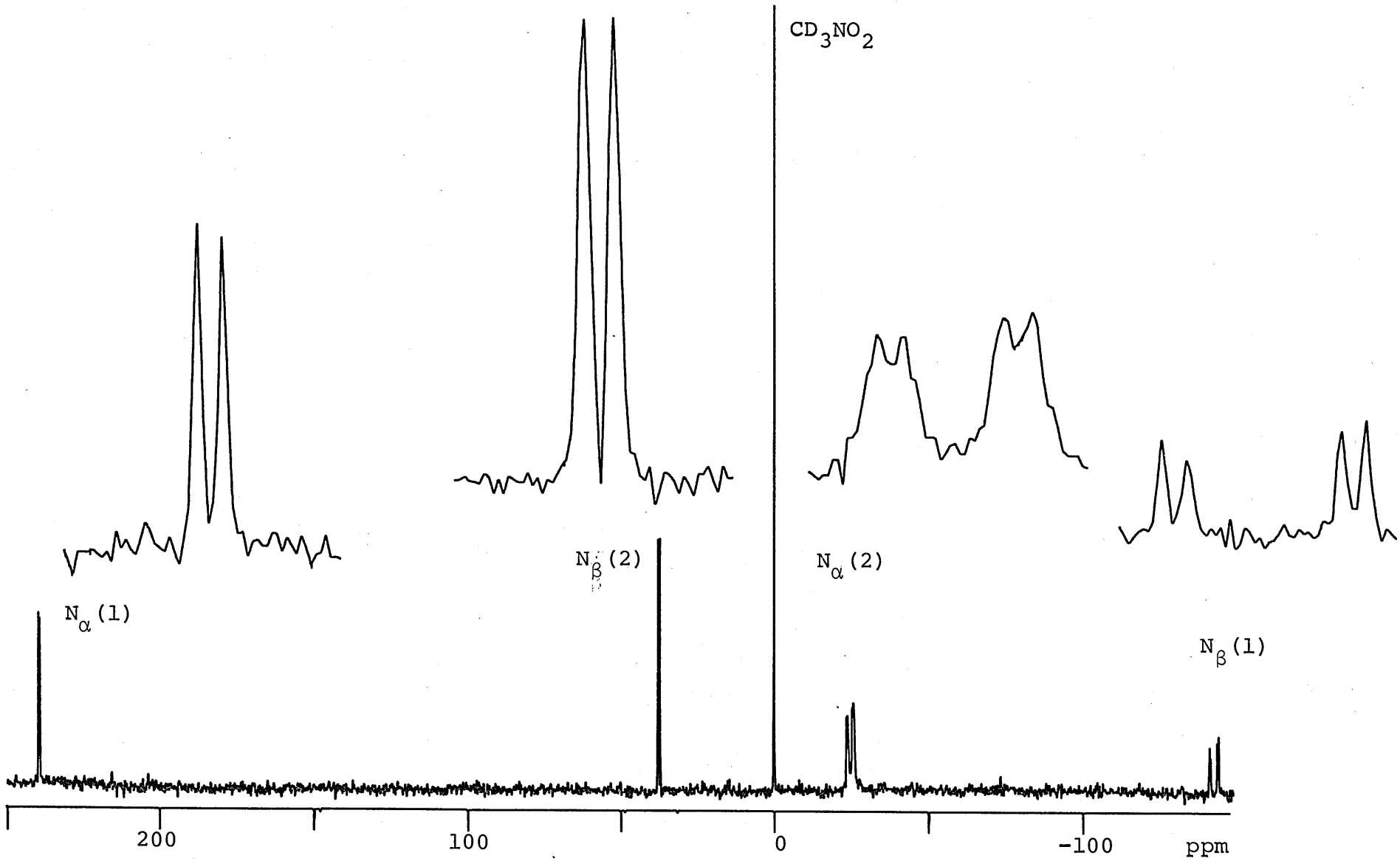

The relative intensities of the signals indicate that the complex with B = $^{15}NH^{15}NPh$ is present in ca. twice the concentration of B = $^{15}N_2HPh$. In $[ReHCl(NO)(B)(PPh_3)_2]$, however, there is very little of the bent-hydrazido(2-) complex and only the N_α resonance could be observed.

$[ReBr_2(^{15}N_2Ph)(^{15}N_2HPh)(PPh_3)_2]$ gave broad lines when studied by ^{15}N NMR at room temperature[26] but the present work has shown that, when cooled to 213K, the lines sharpen and additional peaks characteristic of another bent hydrazido(2-) species can be observed. These are very close to the original resonances, at +184.2 (N_α) and -155.5 (N_β) ($^1J_{NN}$ = 12, $^1J_{NH}$ = 95). This has similarities to the situation observed for the hydrazido(1-) complex $[CpRe(CO)_2(NHNRR')][BF_4]$ (R = Me, R' = aryl) which has been studied by proton NMR.[43] Here, two sets of resonances are observed at room temperature which coalesce at higher temperatures (328K). These are ascribed to the two isomers shown in figure (5.16).

Figure (5.16):

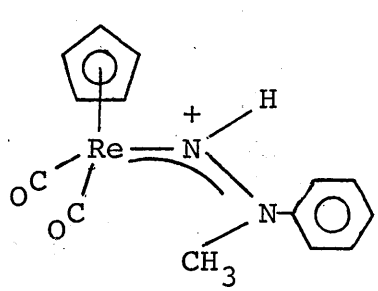

(I)

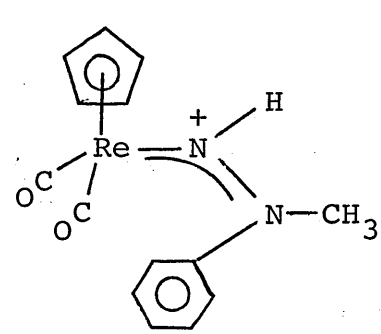

(II)

(I) is the form in the solid state[43] but rotation about the N-N bond (activation energy $\Delta G^{\ddagger}$ ca. 70 kJ mol^{-1}) gives (II) in solution.

Similar behaviour could occur in the bent hydrazido(2-) complex, which has the solid state structure already shown in Figure (5.14), analogous to (I), and could also undergo rotation about the N-N bond:

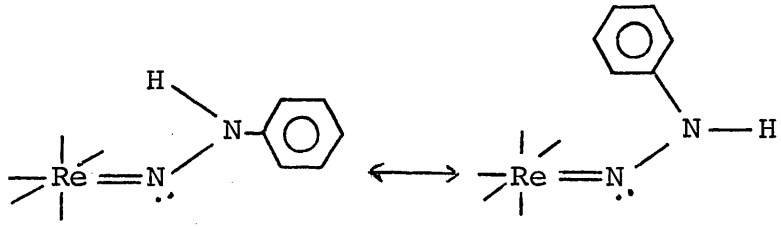

One set of resonances is observed at 298K and although a variable temperature analysis has not been obtained, the fact that coalescence has already occurred at this temperature suggests that the activation energy for rotation about the N-N bond is somewhat less than the 70 kJ mol^{-1} found for the hydrazido(1-)-complex. This might be expected as the hydrazido(2-)-complex has a proton at N_β compared with a more bulky methyl group in the hydrazido(1-)-complexes. It has been observed that the structural parameters of the hydrazido(1-)- and bent-hydrazido(2-)-ligands are similar in the Re cyclopentadiene complexes.[43] This suggests the two ligands could then have similar fluxional properties in solution. However no such behaviour has been reported for the bent hydrazido(2-)-complex $[CpRe(CO)_2(N_2RR')]$.

^{15}N NMR can clearly identify the bent hydrazido(2-)-ligand with its low field N_α and high field N_β resonances. The N_β resonance is somewhat downfield of that expected for the linear hydrazido(2-)-ligand, and this may be attributed to the influence of the lone pair at N_α as

discussed earlier and it thus appears to be a general phenomenon. The $^{1}J_{NH}$ coupling constants are typical of hydrazido(2-)-species.[31] The quite drastic effects of shifting a proton from N_{α} to N_{β}, on the ^{15}N shifts, is ably demonstrated by the change from a bent hydrazido(2-)- to a diazene-system. Clearly these interesting features are worthy of further study.

5.4 Imido-complexes

5.4.1 Structure and bonding

The imido-ligand -NR (R = H, alkyl or aryl) is another postulated intermediate in the reduction of N_2 at metal centres. A review of imido-complexes has appeared.[44]

The most frequently encountered imido-complexes have a linear or near-linear -NR grouping. In valence-bond terms the bonding of such a ligand may be described thus:

4-electron donor, linear imido-ligand

However complexes containing a bent imido-ligand have been reported which could be formulated:

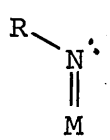

2 electron donor, bent imido-ligand

For the purposes of investigating the possible effect of bending at an imido-nitrogen on the ^{15}N shielding, useful systems are those that have both bent and linear imido-ligands at similar sites. This criterion is met by several complexes which were chosen for study by ^{15}N NMR.

The rhenium complexes trans-$[ReX(NR)(S_2CNR'_2)_2]$ (X = Cl or OEt, R = aryl; R' = CH_3 or C_2H_5) can be synthesised[45] as shown in Scheme (5.2).

Scheme (5.2):

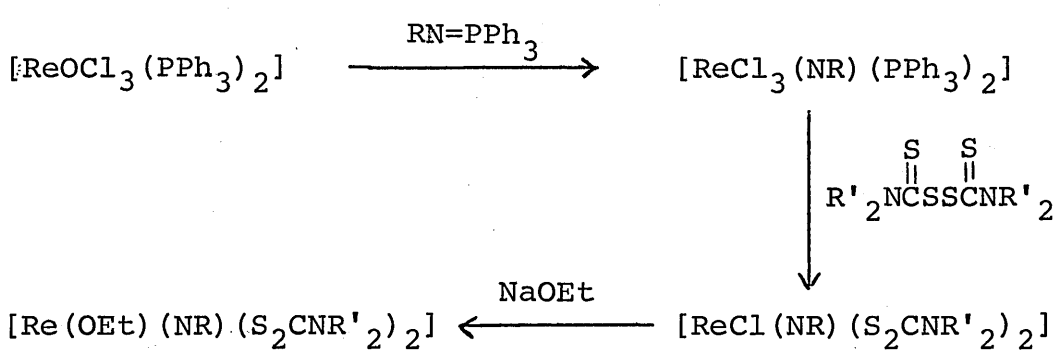

The ^{15}N label was introduced into trans-$[ReX(^{15}NPh)(S_2CNEt_2)_2]$ (X = Cl or OEt) via the phosphinimine $Ph^{15}N{=}PPh_3$ prepared as below:

Scheme (5.3):

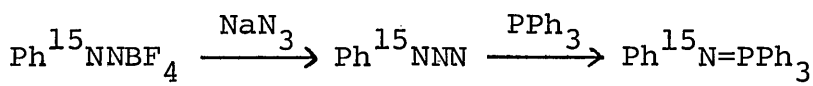

The crystal structure of trans-$[Re(OEt)(NC_6H_4CH_3\text{-}4)(S_2CNMe_2)_2]$ has been determined[15] [Figure (5.17)].

Figure (5.17):

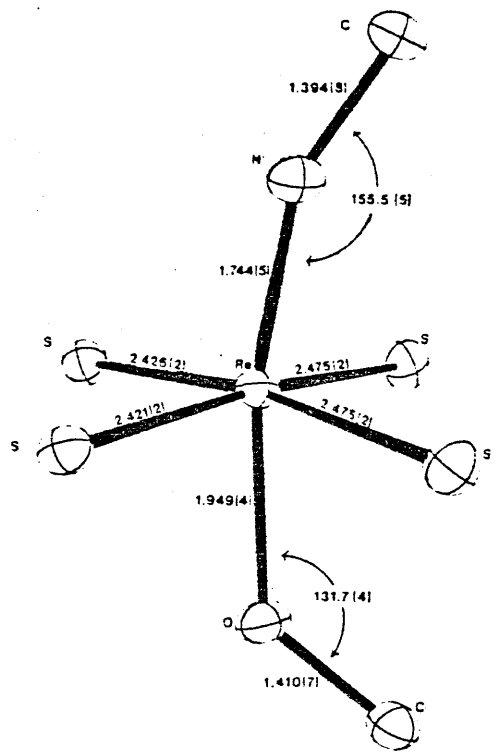

The important features are the long Re-N bond compared with other Re imido-complexes, and the Re-N-C bond angle of 155.5°. The complex with X = Cl instead of OEt has not been structurally characterised but is assumed to have the normal linear imido-coordination.[45]

It has been proposed that whereas $[ReCl(NR)(dtc)_2]$ can mainly be described by the valence bond formulation (III), shown below, $[Re(OEt)(NR)(dtc)_2]$ has contributions from (IV) and (V) the difference being the better π-donor properties of OR^- compared with Cl^-.[45]

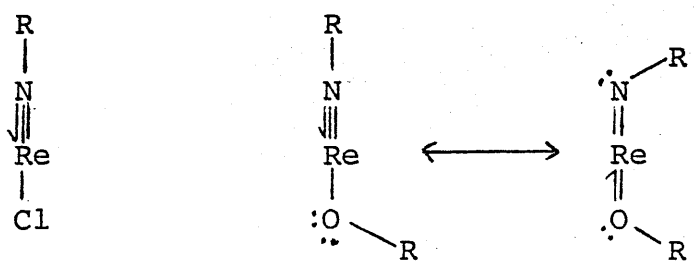

(III) (IV) (V)

Bending of the imido-ligand occurs to maintain the complex $18e^-$ count.

The complex cis-$[Mo(NPh)_2(S_2CNEt_2)_2]$ contains two imido-ligands and is prepared by reaction (5.5).[46]

$$[Mo(CO)_2(S_2CNEt_2)_2] \xrightarrow{PhN_3} [Mo(NPh)_2(S_2CNEt_2)_2] \qquad (5.5)$$

The ^{15}N labelled derivative with S_2CNMe_2 ligands was prepared from $Ph^{15}NNN$ for the purposes of NMR study.

A structural determination [Figure (5.18)] shows the presence of both a bent and a linear imido-ligand.[46] The bent imido-ligand has a longer Mo-N bond than the linear imido-ligand.

Figure (5.18):

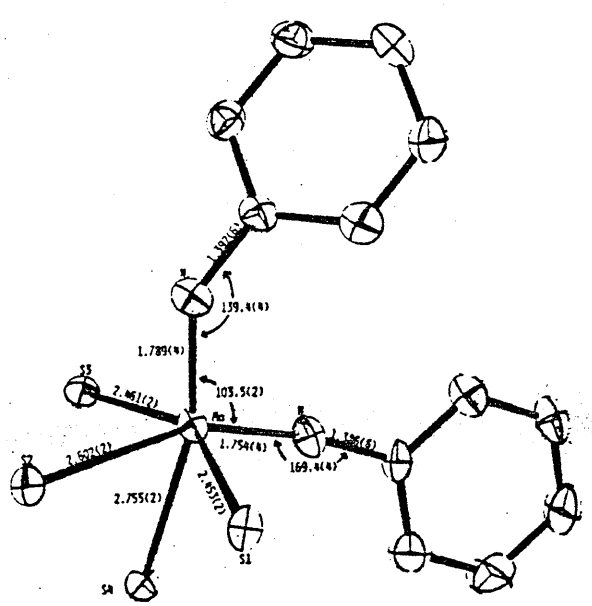

If both imido-ligands acted as four-electron donors this would give a 20-electron count to the complex. A formal 18-electron count can be achieved by the two extreme structures shown in (VI) and (VII).

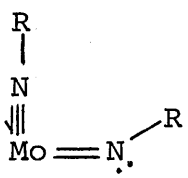

(VI)

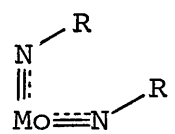

(VII)

In fact the structure observed indicates something between these two extremes.[46]

5.4.2 ^{15}N NMR spectroscopy of imido-complexes

Table (5.4) shows the data from the present study together with those from the literature for purposes of comparison. The shielding range covers ca. +85 to -90 ppm and is represented by some very varied complex types.

The ^{15}N NMR spectrum of trans-[ReCl(^{15}NPh)(S_2CNEt_2)$_2$] consists of a singlet at the high end of the shielding range. The spectrum of trans-[Re(OEt)(^{15}NPh)(S_2CNEt_2)$_2$] shows two singlets, the high field signal having an intensity ca. one third that of the other, both resonances showing higher shielding than that of the chloro-complex. The ^{15}N NMR spectrum of cis-[Mo(^{15}NPh)$_2$(S_2CNMe_2)$_2$] also shows a simple singlet, at the low field end of the shielding range.

TABLE (5.4): ^{15}N NMR data for imido-complexes

Complex	$\delta^{15}N$[a]	Reference
$[Ta(^{15}NPh)(THF)_2Cl_3]$[b]	-12.9	47
$[Ta(^{15}NPh)(PEt_3)_2Cl_3]$	-28.9	47
$[Ta(^{15}NPh)(dmpe)_2Cl]$	-78.9	47
$[Ta(^{15}NPh)(PMe_3)_4Cl]$	-77.9	47
t-$[MoCl(^{15}NH)(dppe)_2]Cl$	+33.3	31
t-$[MoBr(^{15}NH)(dppe)_2]Br$	+10.6	31
t-$[Mo(OMe)(^{15}NH)(dppe)_2]BPh_4$	-58.6	31
t-$[MoCl(^{15}NMe)(dppe)_2]I$	-24.4	31
c-$[Mo(^{15}NPh)_2(S_2CNMe_2)_2]$	+9.6	T.W.
t-$[WBr(^{15}NH)(dppe)_2]Br$	-25.2	31
t-$[WF_4(NMe)(NCMe)]$	+18.8[e]	48
t-$[WF_4(NMe)\{MeC(O)(OEt)\}]$	+9.8[e]	48
t-$[WF_4(NMe)\{Os(OMe)_2\}]$	+10.1[e]	48
$[WCl_2(NPh)(PMe_3)_3]$[c]	+82.0[d]	49
t-$[ReCl(^{15}NPh)(S_2CNEt_2)_2]$	-62.2	T.W.
t-$[Re(OEt)(^{15}NPh)(S_2CNEt_2)_2]$	-81.1	T.W.
	-92.0[f]	T.W.

a) Shifts converted to the neat nitromethane scale (see experimental).

b) $M\hat{N}R$ = 173.3° in $[Ta(NPh)(THF)(PEt_3)Cl_3]$, ref. 50

c) $M\hat{N}R$ = 179.5°, ref. 51. d) natural abundance ^{15}N by INEPT.

e) measured in ^{14}N resonance. f) less intense signal.

T.W. = this work: in CH_2Cl_2 solution.

5.4.3 Discussion

The increased shielding on going from X = Cl to X = OEt in $[ReX(^{15}NPh)(dtc)_2]$ seems to be inconsistent with greater lone pair character at the nitrogen as predicted by the crystal structure, since from earlier arguments some deshielding might be expected. In fact the shift is more reminiscent of the upfield shift from X = Cl to OMe in *trans*-$[MoX(^{15}NH)(dppe)_2]^+$.

There are several possible explanations for this behaviour. It may be argued that the deviation from linearity shown in the crystal structure could be due to packing forces, which are removed in solution allowing the imido-ligand to straighten. However, Haymore and Goeden[45] insist that the bending is real and "not a result of intramolecular steric effects" or "intermolecular contacts". Alternatively the ^{15}N NMR shift could be insensitive to the bending at nitrogen, but this is unlikely in light of the evidence from the work with diazenido-, nitrosyl and bent hydrazido(2-)-complexes. Most likely is the possibility of some fluxionality of the imido-ligand in solution, the observed resonance position would be an average between the linear and bent forms. This is also implied by the observation that replacement of Cl by OMe in $[MoX(NH)(dppe)_2]^+$ results in a *ca.* 90 ppm shift to high field whereas replacement of Cl by OEt in the Re complex results in only a *ca.* 20 ppm upfield shift.

Similar fluxionality provides an explanation of the observation of only one resonance from $[Mo(^{15}NPh)_2(dtc)_2]$ when two would be expected from the crystal structure. A precedent for this type of mechanism is provided by ^{15}N NMR studies on $[RuCl(^{15}NO)_2(PPh_3)_2]^+$.[52] Solid state ^{15}N NMR[53] confirms the crystal structure information that the complex contains both a linear and a bent nitrosyl ligand. In solution, however, one average resonance is observed. This may be thought of as being produced by the process shown in Figure (5.19). The situation is complicated slightly by a contribution from another isomer (VIII).

Figure (5.19):

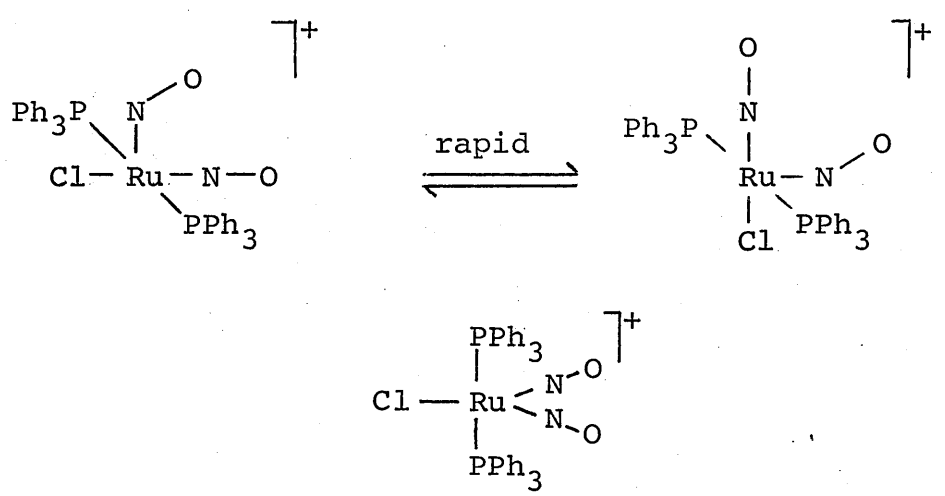

(VIII)

The active fluxionality has been confirmed by observation of an equilibrium isotope effect which operates in the partially labelled complex.[52] Two resonances are observed due to $(^{15}NO)_2$ and $(^{14}NO)(^{15}NO)$, the effect operating because

^{15}N is slightly favoured in the linear geometry. Interestingly the fluxionality is still present even at low temperature. Applying this type of argument to the imido-systems we get the possible mechanisms in Figure (5.20).

Figure (5.20):

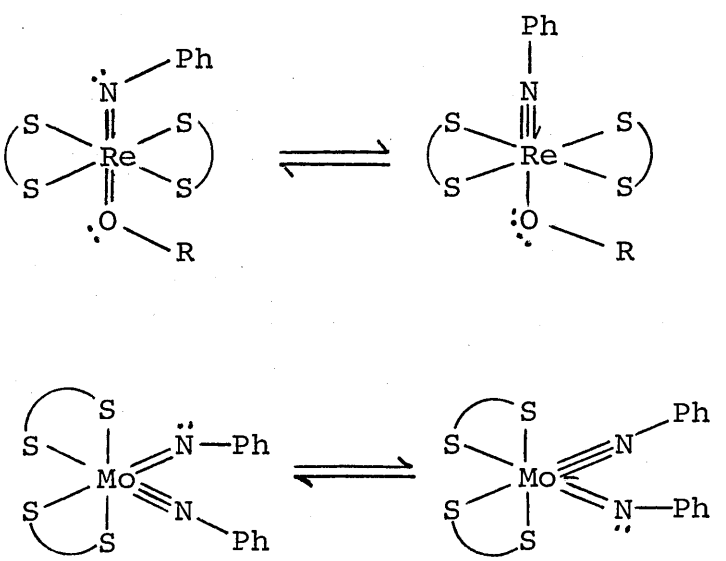

The intermediate geometries observed in the solid state mean that the extremes shown above are probably not true representatives of the limiting forms in the fluxional process. The validity of this type of mechanism could be verified in a similar manner to the nitrosyl case using solid state ^{15}N NMR, or possibly by looking for an equilibrium isotope effect (any such effect is likely to be small as the shielding difference between the "bent" and "linear" imido-groups is probably somewhat less than in the nitrosyl system).

Finally, the two resonances observed in the spectrum of $[Re(OEt)(^{15}NPh)(dtc)_2]$ may be caused in a similar way to the two

sets of peaks seen in the ^{1}H NMR spectra of the various complexes [Re(OR)(^{15}NR')(dtc)] (R = Me, Et; R' = Me, Ph or $C_6H_4CH_3$-4).[45] Two isomers are postulated which could arise in several ways. One possibility is provided by the non-axial disposition of the -OR and -NR groups [see Figure (5.18)] giving rise to the two isomers shown below [Figure (5.21)].

Figure (5.21):

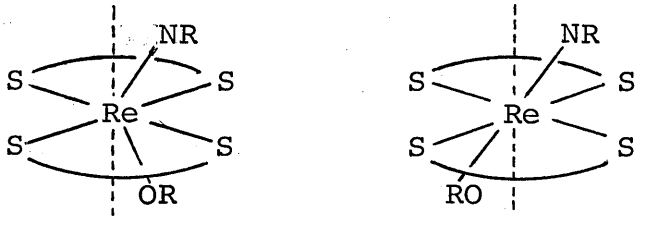

The isomers are separated by ca. 10 ppm in the ^{15}N NMR spectrum, a further indication of the sensitivity of the technique (compare with the ^{1}H spectrum in which the NPh resonances of the isomers are separated by only 0.1 ppm).[45]

5.4.4 Conclusions

When rapid fluxionality is possible, the solution ^{15}N NMR spectrum may not give information about the solid state structure but can still be used to follow changes with an appropriate time scale, in solution. With the advent of solid state ^{15}N NMR techniques, even rapid fluxional processes may be probed, as shown in the example of the bent ⟷linear dinitrosyl complex.

5.5 Nitrido-complexes

5.5.1 Nitride bonding modes

In contrast to the various types of structural isomerism discussed so far in this Chapter, involving bending at the ligating atom, there exists also a structurally characterised effect involving the length of metal-nitrogen bonds. This effect, found in nitrido-complexes, could be referred to as a type of "electronic isomerism". The bulk of nitrido-complexes (which do not contain other strong π-donors) show M-N bond lengths which may be described by this simple valence representation:[54]

(IX)

The bond lengths associated with (IX), characteristic of a triple bond, fall into a relatively narrow range dependent on the size of the metal M.[55]

There are, however, rare examples of nitrido-complexes which do not fit this range or the formalism (IX). These may be described by:

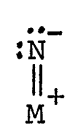

(X)

and possess long M-N bonds, closer to that expected for a double bond.[44]

5.5.2 ^{15}N NMR and crystal structure data

^{15}N NMR data for nitrido-complexes and M-N bond lengths, where determined, are given in Table (5.5).

TABLE (5.5): ^{15}N NMR and metal-nitrogen bond length data for nitrido-complexes

Complex	$\delta^{15}N$ [a] (ppm)	Ref.	d(M-N)[b] (Å)	Ref.
$[Mo(^{15}N)(S_2CNEt_2)_3]$	+40.0	24	1.64	57
$[ReCl_2(^{15}N)(PMe_2Ph)_3]$	+68.2	24	1.66	58
$[ReCl_2(^{15}N)(PPr^nPh_2)_2]$	+85.8	24	n.d.	
$[ReCl(^{15}N)(dppe)_2]Cl$	+153.4	T.W.	1.76	T.W.
$[MoCl(^{15}N)(dppe)_2]$	+166.8	31	n.d.	
$[MoBr(^{15}N)(dppe)_2]$	+190.6	31	n.d.	
$[MoN_3(^{15}N)(dppe)_2]$	+196.3	T.W.	1.79	56
$[ReCl_2(^{15}N)(PEt_2Ph)_3]$	+267.3	T.W.	1.78	59

a) Corrected to neat CH_3NO_2 scale. (b) n.d. = not determined. T.W. = this work in CH_2Cl_2 soln.

The present study completes the data sets for both long and short nitrido-complexes. The structure of $[ReCl_2(N)(PEt_2Ph)_3]$ has been known for some time[59] and first provoked discussion regarding the M-N bond length.[44] The two extremes of bond length are shown by the complexes $[ReCl_2NP_3]$ (P = PEt_2Ph PMe_2Ph), the PEt_2Ph complex exhibiting the longer Re-N bond. In contrast to the relatively high field signal observed for $[ReCl_2(^{15}N)(PMe_2Ph)_3]$,[24] the PEt_2Ph analogue shows a large

shift to low field. None of the complexes show N-P coupling. The crystal structure of the seven-coordinate compound $[Mo(N)(S_2CNEt_2)_3]$[57] shows a short Mo-N bond and the ^{15}N resonance is at relatively high field.[24] Both $[MoX(^{15}N)(dppe)_2]$ (X = Cl or Br) have low field $\delta^{15}N$ [31] but only the structure of $[MoN_3(N)(dppe)_2]$ is known, it shows a long Mo-N bond.[56] The ^{15}N NMR spectrum of $[MoN_3(^{15}N)(dppe)_2]$ shows a low field singlet as does its Cl and Br analogues. A preliminary X-ray structure determination (carried out by E. Schweda, Tübingen) on $[ReCl(N)(dppe)_2]Cl$ shows an apparently long Re-N bond length of 1.76Å, but the result should be considered with some caution as the molecule is somewhat disordered. A redetermination of the ^{15}N NMR parameters of $[ReCl(^{15}N)(dppe)_2]Cl$ shows the original value (+70.5 ppm v. CH_3NO_2)[24] to be in error; the spectrum shows a single resonance to low field (+153.4 ppm v. CH_3NO_2).

5.5.3 Discussion

Although the crystal structure data for $[ReCl(N)(dppe)_2]Cl$ gives only a tentative value for the Re-N bond length, it is reasonable to assume there is a correlation between the ^{15}N NMR shift and the length of the M-N bond. It can be seen from the doubly-bonded valence structure (X) that the long isomer has increased lone pair character at the nitrogen atom, similar to that at the ligating nitrogen in the bent -NNR, -NO and $-NNR_2$ ligands. Furthermore, the lone pair is part of a delocalised system via the M-N π-system; the nitrogen, is then expected to be less shielded in this isomer. Although

the number of complexes studied is small, the following ranges may be ascribed to the two isomers:

$M{\equiv}N$: short nitrido-distance $\delta^{15}N$ ca. +90 ppm to +40 ppm

$\overset{+}{M}{=}\overset{-}{N}$: long nitrido-distance $\delta^{15}N$ ca. +270 ppm to +150 ppm

More evidence of the structure of the long isomer comes from protonation of $[MoX(^{15}N)(dppe)_2]$ (X = Cl or Br) to give the imido-complexes $[MoX(^{15}NH)(dppe)_2]X$ causing upfield shifts of $\delta^{15}N$ of 130 to 180 ppm [31] [Table (5.4)]. The Re-nitride complexes cannot be protonated but $[ReCl_2N(PEt_2Ph)_3]$ forms adducts with Lewis acids (BY_3; Y = F, Cl or Br) [60] and study of these by ^{15}N NMR spectroscopy should give similar upfield shifts.

It would seem that the short nitrido-metal bond is the norm with the long isomer forming only when a combination of steric (i.e. more bulky co-ligands) and electronic factors is correct. In $[ReNCl_2P_3]$ the less bulky P = PMe_2Ph is associated with the short isomer and P = PEt_2Ph with the long. This difference with simple change of phosphine may indicate that there is a relatively "soft" potential energy surface between the long and short forms. When the phosphine is yet more bulky as in PPh_3 or PPr^nPh five-coordinate complexes are formed e.g. $[ReNCl_2P_2]$ with a short Re-N bond; the binding of only two phosphines relaxes the steric constraint on the nitride. [61]

It appears from the data that the ^{15}N shielding of the long nitrido-ligand is also very sensitive to coordination environment. This is exemplified by comparing the ^{15}N shift of $[ReCl_2(^{15}N)(PEt_2Ph)_3]$ with that of $[ReCl(^{15}N)(dppe)_2]^+$, where replacement of chloride by a tertiary phosphine in the chelated complex induces an upfield shift of ca. 100 ppm.

5.5.4 Conclusions

The nitride system shows the potential of ^{15}N NMR spectroscopy for ligand structure elucidation in solution even in the case where only bond lengths are changing and not bond angles. Obvious extensions of this work involve expanding the range of nitride complexes studied by ^{15}N NMR, to elucidate structures not yet characterised by X-rays. ^{15}N NMR spectroscopy should also be useful for following the chemistry of the nitrido-ligand, which is particularly important in studies relevant to nitrogen fixation.

5.6 Oxo-complexes

Oxo-complexes show very similar structural behaviour to the nitrides[62] and also show long and short forms:

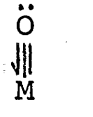

short oxo-ligand

long oxo-ligand

(XI) (XII)

Again it is the short form that predominates. The molybdenum complexes $[MoOCl_2P_3]$ have both short, P = PMe_2Ph,[63] and long, P = PEt_2Ph,[64] forms which also show a difference in colour, blue and green respectively. These forms have been identified crystallographically.[63,64] The complex $[MoOCl_2(PMe_2Ph)_3]$, as well as a stable blue form, also shows an unstable green isomer which has not been structurally characterised, as it rapidly converts to the blue form in solution.[65] This suggests that both long and short isomers of the same complex may be found. A recent report gives details of a complex $[MoOCl_2(PMe_3)_3]$ which also gives both

green and blue isomers on preparation but which do not interconvert in solution.[66] No structures are available for these isomers.

Preliminary ^{17}O NMR studies at natural abundance on the highly soluble complexes $[MoOCl_2P_3]$ (P = PMe_2Ph, PEt_2Ph or PMe_3) were made in CH_2Cl_2 solution. The results are reported in Table (5.6) with the Mo-O bond lengths.

TABLE (5.6): ^{17}O NMR data and molybdenum-oxygen bond lengths in $[MoOCl_2P_3]$ complexes

Complex	^{17}O [a] (ppm)	d(M-O) (Å)	Colour
$[MoOCl_2(PEt_2Ph)_3]$	876	1.80[c]	green
$[MoOCl_2(PMe_3)_3]$	880	-	blue
$[MoOCl_2(PMe_2Ph)_3]$	882[b]	1.67[d]	blue
$[MoOCl_2(PMe_3)_3]$	884	-	green

a) referenced to H_2O; run in CH_2Cl_2 at 48.82 MHz
b) $^2J_{OP_A}$ ca. 150 Hz, $^2J_{OP_B}$ ca. 400 Hz
c) ref. 64, d) ref. 63.

The ^{17}O NMR spectrum of $[MoOCl_2(PMe_2Ph)_3]$, shown in Figure (5.23), consists of an overlapping doublet of triplets consistent with the mer-arrangement of phosphines [Figure (5.22)].

Figure (5.22):

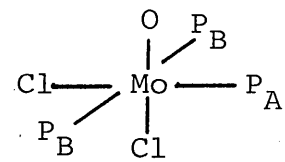

From the spectrum $^{2}J_{OP_B}$ is ca. 400 Hz and $^{2}J_{OP_A}$ is ca. 150 Hz. No couplings could be resolved from the other spectra. Signal linewidths across whole envelopes (including unresolved couplings) at half-height ranged from ca. 100 Hz in the PMe_3 compounds to 400 Hz in the PMe_2Ph and 800 Hz in the PEt_2Ph complexes. Comparison of the data in Table (5.6) show that the ^{17}O shifts for the various complexes fall in a very small range. The ^{17}O shielding appears to be somewhat insensitive to change of phosphine shown by the small downfield shift (8 ppm) between P = PEt_2Ph to PMe_3 in $[MoOCl_2P_3]$. No large downfield shift is observed on going from the short to the long form of the complex, in fact exchanging P = PMe_2Ph for PEt_2Ph gives an upfield shift of 6 ppm. As noted above the Mo-O bond lengths in the PMe_3 isomers have not been determined but might be expected to show the long and short configurations. That the blue and green isomers are different is shown by the difference in their ^{17}O shielding of 4 ppm, however, this is much smaller than predicted from the results from the nitride systems.

In this case ^{17}O NMR does not seem to be diagnostic of bond length. It is clear that further work is required on this type of system to extend these

preliminary observations and to check the applicability of ^{17}O NMR spectroscopy as a structural probe, as ^{15}N NMR spectroscopy is.

Some further information is provided in the form of ^{95}Mo NMR data. The spectra of the complexes $[MoOCl_2P_3]$ (P = PMe_2Ph or PEt_2Ph) in CH_2Cl_2 show resonances at +2020 ppm and +2210 ppm respectively. The difference in shielding of ca. 200 ppm can probably be explained by the change in phosphine co-ligand. No ^{95}Mo studies have yet been carried out on the PMe_3 complexes.

Interestingly comparing these results with those for other mononuclear Mo(IV) complexes (see Chapter 4), the oxo-compounds extend the low-field end of the shielding range by some 2000 ppm.

Figure (5.23): ^{17}O NMR spectrum of $[MoOCl_2(PMe_2Ph)_3]$

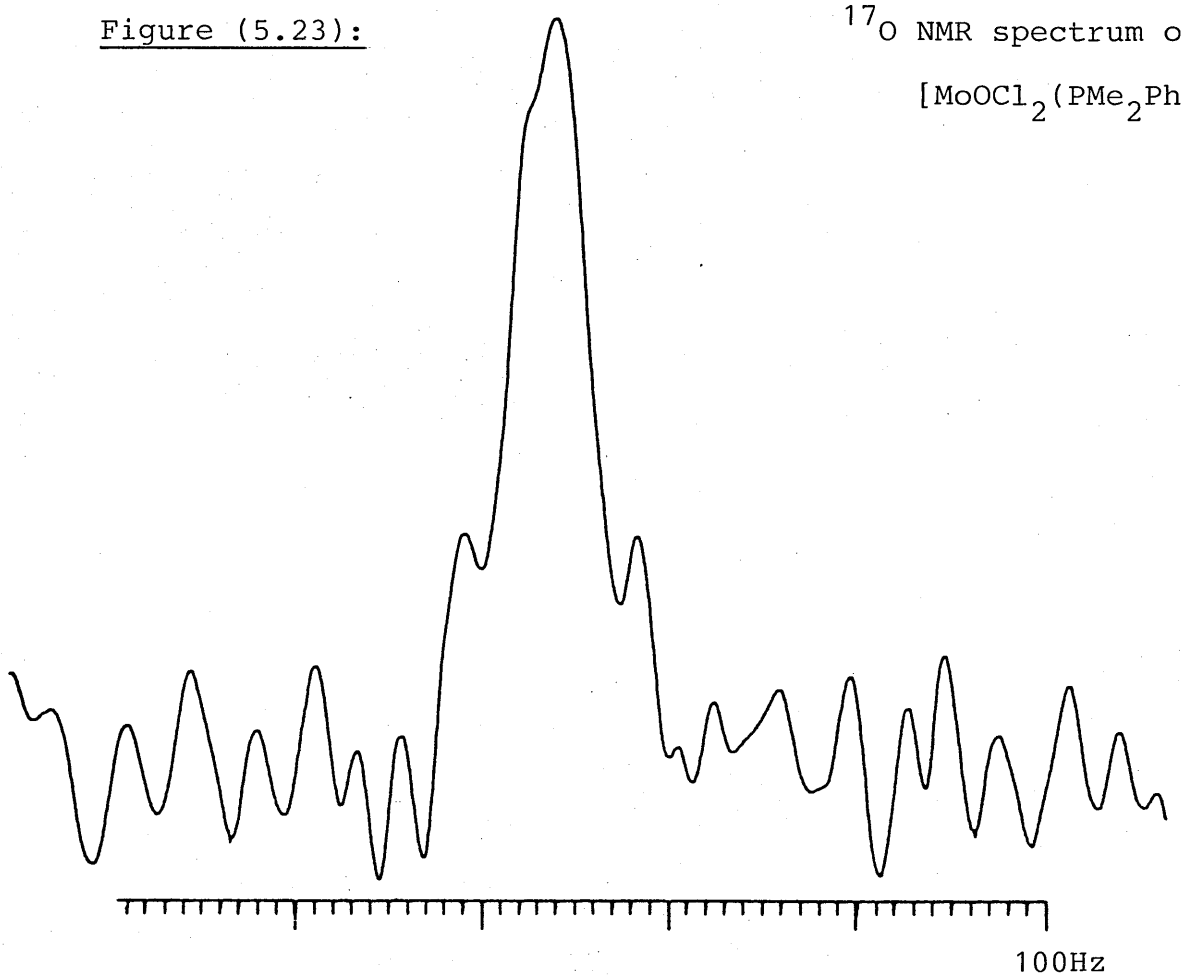

CHAPTER 6

NMR Studies of Protonation Reactions

6.1 Introduction

Essential to an understanding of the mechanism by which dinitrogen is reduced to ammonia in the biological system, is the elucidation of the pathways of protonation of dinitrogen at metal sites in model systems. The cycle proposed in Chapter 1 for reduction of dinitrogen in such systems is based largely on isolated analogues of plausible intermediates in such reactions. Various studies of protonation reactions have been undertaken including kinetic experiments as outlined below. ^{15}N NMR spectroscopy has also been used to probe reacting systems as has ^{31}P NMR spectroscopy. The results from these studies are discussed in relation to the present work which extends these investigations in an attempt to gain more information about intermediates in the reacting solution.

6.2 Protonation of dinitrogen in mononuclear complexes

Despite extensive work since the original report in 1975,[1] molybdenum and tungsten dinitrogen complexes are the sole examples of mononuclear systems from which good yields of ammonia and/or hydrazine may be produced. The subject has been reviewed at length.[2-4]

6.2.1 Diphosphine complexes

Complexes of the type trans-$[M(N_2)_2(\overset{\frown}{P\ P})_2]$ (M = Mo or W; $\overset{\frown}{P\ P}$ = dppe or depe) do not give free nitrogen hydrides on treatment with acids, but typically, hydrazido(2-)-complexes are formed. The reaction with acid, carried out in thf is, however, somewhat dependent on the nature and concentration of the acid. This is exemplified by the mechanism shown in Scheme (6.1) for protonation by HCl in thf.

Scheme (6.1):

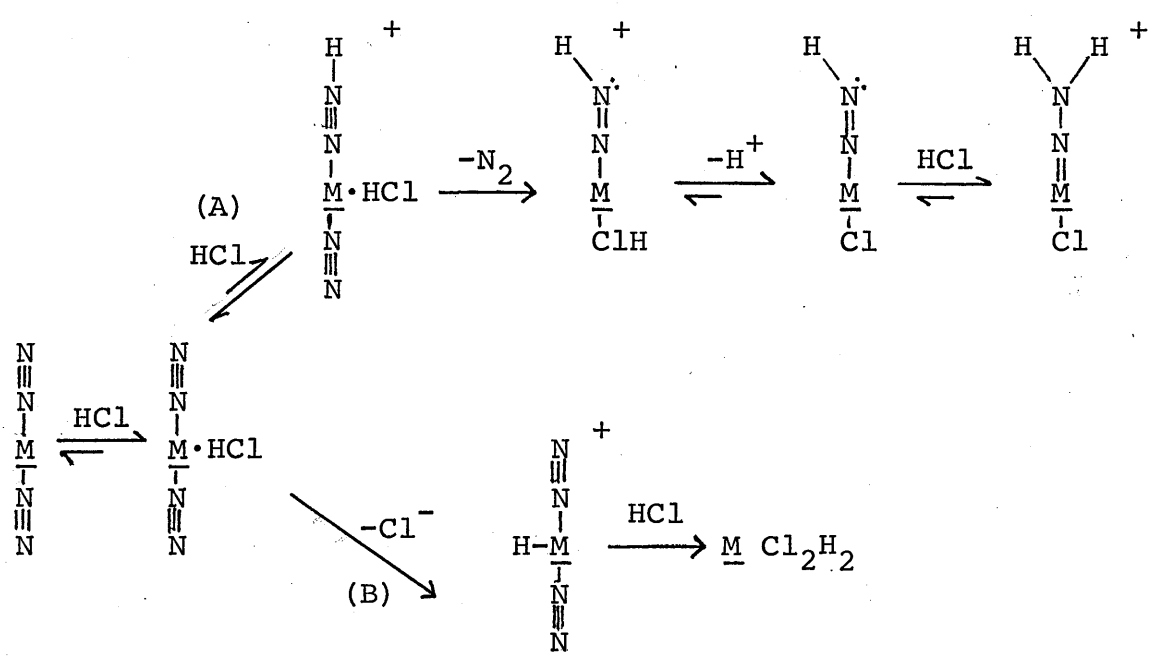

$\underline{M}$ = $Mo(\overset{\frown}{P\ P})_2$ or $W(\overset{\frown}{P\ P})_2$

The two pathways are possible as HCl is a weak acid in thf and associates easily with the bis-N_2 complex. Protonation of the N_2 moiety is necessary for pathway (A) and may be achieved for HCl and M = W at high acid concentration (>6 equivalents) to give the hydrazido(2-)-complex. At

low acid concentration, however, pathway (B) is favoured. For M = Mo, $[MoH_2Cl_2(\widehat{P\ P})_2]$ is the exclusive product at all HCl concentrations due to the lower basicity of N_2 in the Mo system compared to W. With stronger acids (HBr, H_2SO_4) the hydrazido(2-)-complexes are obtained for both metals.

6.2.2 Monophosphine systems

The above situation may be compared with the protonation of cis-$[M(N_2)_2(PMe_2Ph)_4]$ (M = Mo or W) in MeOH shown in Scheme (6.2).

Scheme (6.2):

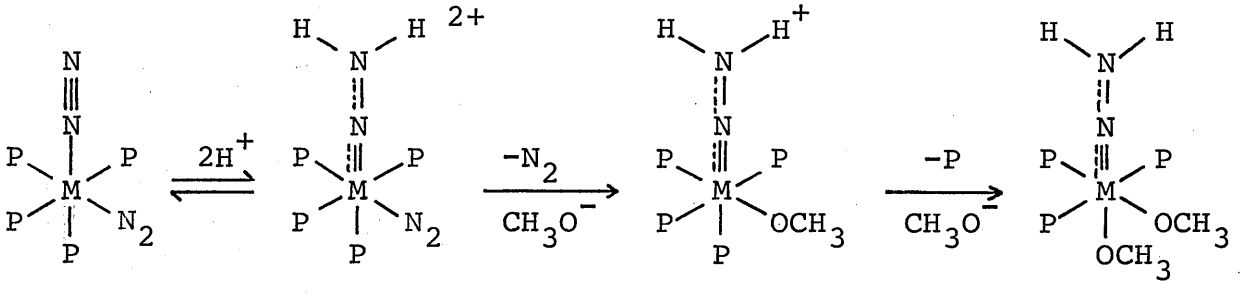

M = Mo or W, P = PMe_2Ph

This scheme, common to the acids HCl, HBr and H_2SO_4, clearly involves participation of the solvent. If two equivalents of acid are used, the intermediate hydrazido-complexes $[MX_2(N_2H_2)(PMe_2Ph)_3]$ can be isolated.

These two examples show the dependence of product on solvent, acid, metal and phosphine. Only when monophosphines are present can the protonation reaction go on to give ammonia or hydrazine and this has been interpreted as showing

the necessary formation of a $\{MP_3\}$ species.[5] The actual necessity is the formation of a site with anionic ligands capable of stabilising higher oxidation states formed during reduction of the $-N_2H_2$ group. The monophosphine dinitrogen complexes have been studied in reactions with various acid/solvent systems and give variable yields of NH_3, N_2H_4 and N_2. Dinitrogen is usually determined by freezing reaction mixtures after protonation is complete, and measuring the gas evolved. NH_3 and N_2H_4 are determined by base distillation of products into an acid trap followed by colourimetric analysis.[5]

There appears to be a clear distinction between W and Mo in these protonation reactions. Thus, protonation of <u>cis</u>-$[W(N_2)_2(PMe_2Ph)_4]$ with an excess of H_2SO_4 in MeOH gives good yields of NH_3[5] and may be represented by reaction (6.1).[4] A trace of hydrazine is also produced.

$$\underline{\text{cis}}\text{-}[W(N_2)_2(PMe_2Ph)_4] \xrightarrow[MeOH]{H_2SO_4} 2NH_3 + N_2 + W(VI) \qquad (6.1)$$

The metal product has not been positively identified.

In thf with the same acid a greater proportion of N_2H_4 is produced. In contrast, Mo gives much lower yields of NH_3 with $MeOH/H_2SO_4$ and follows the stoichiometry of reaction (6.2).

$$\underline{\text{cis}}\text{-}[Mo(N_2)_2(PMe_2Ph)_4] \xrightarrow[MeOH]{H_2SO_4} \tfrac{2}{3}NH_3 + \tfrac{5}{3}N_2 + \text{Mo(IV)?} \qquad (6.2)$$

As indicated, very little is known about the final metal-containing product in this reaction. No hydrazine is detected in this reaction or in that with thf as solvent. Some dinitrogen is evolved in this reaction during the base distillation step.[5] When the acid or solvent is changed this can drastically effect the yields and stoichiometry. This may be shown by reaction (6.3).

$$\underline{cis}\text{-}[Mo(N_2)_2(PMe_2Ph)_4] \xrightarrow[THF]{HBr} NH_3 + \tfrac{3}{2}N_2 + Mo(III) \qquad (6.3)$$

In this case the final metal product has been identified as $[MoBr_3(THF)(PMe_2Ph)_2]$.[6] If the solvent/acid combination is changed it has been reported[7] that significant yields of N_2H_4 may be produced. Thus, in dimethoxyethane (dme) with HCl as acid ca. equal quantities of NH_3 and N_2H_4 are obtained. Study of these protonations has been extended to include reactions of isolated hydrazido(2-)-species of the type $[MX_2(N_2H_2)(PMe_2Ph)_3]$ (M = Mo or W, X = Cl, Br or I) with various acids in several solvents. Again, a range of results is observed. When $MeOH/H_2SO_4$ is used, N_2H_4 is again only observed for M = W and yields of nitrogen hydrides in general are much higher for M = W than M = Mo.[8] The stoichiometry for M = Mo is thought to be as shown in reaction (6.4) for X = Cl.

$$[MoX_2(N_2H_2)(PMe_2Ph)_3] \xrightarrow[MeOH]{H_2SO_4} \tfrac{2}{3}NH_3 + \tfrac{2}{3}N_2 + Mo(IV)? \qquad (6.4)$$

The yield increases to one NH_3/Mo for X = Br or I.[8]

Production of N_2H_4 may again be encouraged by going to the HCl/dme system.[7] This time ca. twice as much N_2H_4 is produced compared with NH_3. It may be added that for M = W, hydride complexes of the type $[WHX_2(NNH_2)(PMe_2Ph)_3]X$ have been isolated from protonation in dme.[7]

In fact the situation is far more complex than shown by the examples above, and in several instances a complete nitrogen balance cannot be achieved, indicating the possibility of unreactive nitrogen species left at the end of the reaction. Some of these problems will be highlighted in discussion of the reactions of $[M(N_2)_2(PMe_3)_4]$ and $[M(N_2)(PMe_3)_5]$ (M = Mo or W) below.

6.2.3 Protonation of $[Mo(N_2)_2(PPh_3)(triphos)]$

The title complex contains both a monophosphine and the tridentate, chelating phosphine $PhP(CH_2CH_2PPh_2)_2$(triphos), and this imparts to the species a degree of reactivity towards protonation.[9] The geometry of the $[Mo(N_2)_2(PPh_3)$ (triphos)] complex is shown in Figure (6.1).

Figure (6.1):

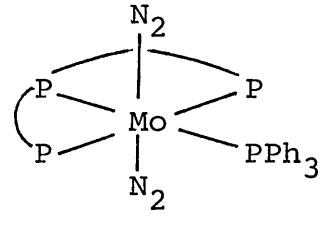

The reaction of this complex in HBr/thf parallels that of the $(PMe_2Ph)_4$ analogue as is shown in reaction (6.5).

$$[Mo(N_2)_2(triphos)(PPh_3)] \xrightarrow[THF]{HBr} NH_3 + \tfrac{3}{2}N_2 + [MoBr_3(triphos)] \qquad (6.5)$$

Time-course studies have shown that 1 mole of N_2 is liberated rapidly per mole of complex on initial protonation, the remaining nitrogen is only slowly evolved as NH_3. It has also been demonstrated[10] that quenching the reaction at an early stage by addition of H_2O/CH_2Cl_2 to the reaction solution leads to the identification of N_2H_4 in the products. If the reaction with HBr is carried out in benzene, the complex $[MoBr_2(N_2H_2)(triphos)]$ is isolated but this will not react further in HBr/thf,[11] in contrast to the mono-phosphine hydrazido(2-)- species discussed above. Reaction (6.5) has been monitored by ^{31}P NMR spectroscopy.[12] Spectra obtained are consistent with the presence of two isomeric hydrazido(2-)-species in the reaction solution immediately after protonation. One set of signals decays over ca. 40 mins with concomitant observation of a signal due to PPh_3. Two compounds corresponding to the hydrazido(2-) isomers have been isolated, and structurally characterised as shown in Figure (6.2).

Figure (6.2):

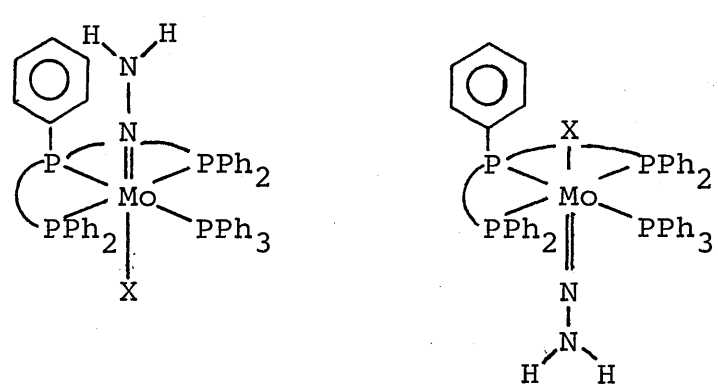

The present work includes a study of this protonation reaction by ^{15}N NMR spectroscopy (vide-infra) which was concluded before the above structures were known.

6.3 Information obtained from ^{15}N NMR studies of protonation reactions

Apart from the ^{31}P NMR work on the triphos system which will be discussed later, several other spectroscopic studies have been reported involving ^{15}N NMR spectroscopy.[8,14] The first study[8] concerned the reaction of cis-$[M(^{15}N_2)_2(PMe_2Ph)_4]$ (M = Mo or W) with H_2SO_4 in thf. The acid was added to a solution of complex in thf, under argon at room temperature, and effervescence of N_2 was allowed to cease before cooling to 243K and spectral accumulation at this temperature. The reaction was then allowed to proceed at 293K for appropriate time intervals followed by cooling and further spectral accumulation. For M = Mo the results are shown schematically in Figure (6.3a). At t = 10 mins, free $^{15}N_2$ and two signals, I and II corresponding to N_α and N_β of a hydrazido(2-)-species are observed. At t = 140 mins a further signal IIa due to N_β of another hydrazido(2-)-species is observed. Both N_β resonances are inverted due to negative NOE from $\{^1H\}$. Because of build up of paramagnetic products, the final spectrum at t = 480 mins shows no signals.[8] No signal due to NH_4^+ was observed.

Figure (6.3a): Schematic ^{15}N NMR spectra (adapted from ref. 8)
Reaction of cis-$[Mo(^{15}N_2)_2(PMe_2Ph)_4]$ with H_2SO_4 in thf.

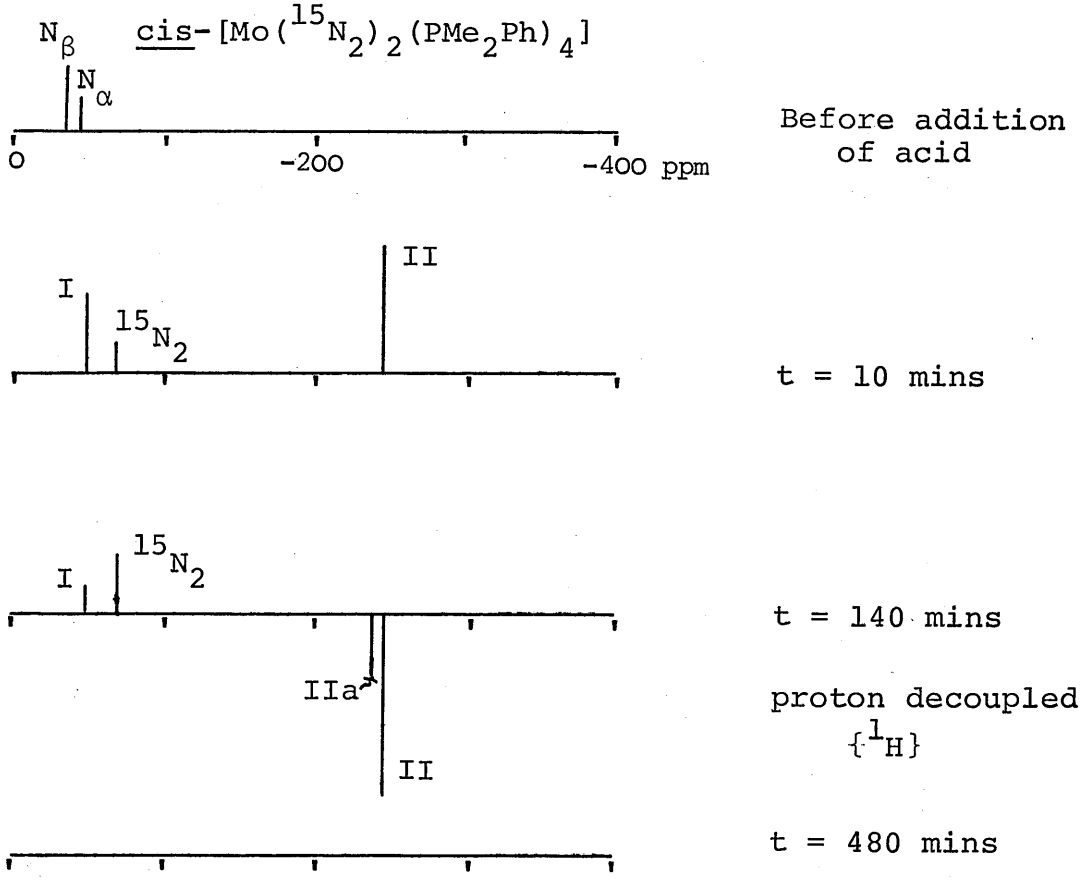

Figure (6.3b): Early stages in reaction of cis-$[W(^{15}N_2)_2(PMe_2Ph)_4]$ with H_2SO_4 in thf

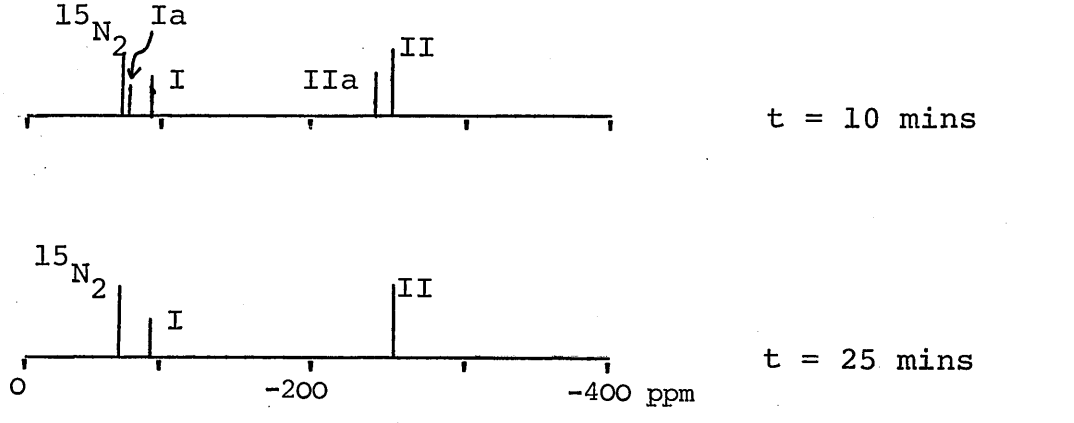

In Figure (6.3b) for M = W at t = 10 mins, signals due to two hydrazido(2-)-species are present but one disappears over 15 mins reaction time to give a single species. After this stage the situation becomes more complicated with the observation of four other signals in the N_β region. At t = 120 mins a single resonance due to NH_4^+ (-364 ppm) is observed but no $N_2H_5^+$.

These two experiments unequivocally confirmed the presence of hydrazido(2-)-species in these protonation reactions in solution.

The reaction of *trans*-$[Mo(N_2)_2(diphos)_2]$ (diphos = dppe or depe) with HBr in THF was monitored by ^{15}N NMR to try to detect species before hydrazido(2-).[14] For the dppe complex, only hydrazido(2-)-species were observed, however, for the depe analogue a transient signal assigned as the N_β resonance of a possible -NNH intermediate was also observed.

^{15}N NMR was used to study the reaction of $[MoI_2(^{15}N_2H_2)(PMe_2Ph)_3]$ with HI in thf.[14] Only the decay of signals due to starting material and the increase of a resonance due to $^{15}NH_4^+$ (at *ca.* -356 ppm)[17] could be observed. These phenomena were monitored with time to give an approximate rate constant for the reaction, $7 \times 10^{-5} s^{-1}$, which compares well with values obtained from time-course studies of NH_3 and N_2 evolution.[15]

6.4 Investigation of some protonation reactions by NMR spectroscopy

6.4.1 Introduction

Several criteria pertain to the choice of systems to study by ^{15}N NMR. Included amongst these are such things as sufficient solubility of starting material and/or intermediates in the reaction solution, to allow important information to be collected in a reasonable accumulation period. Preferably, reactions should not rapidly build up paramagnetic products as this will preclude observation of NMR signals or possibly cause unexpected chemical shift changes. It is also advantageous to look at "clean" systems, i.e. where effects such as solvent decomposition are avoided, as better resolution and more information may be gleaned from such reactions. Unfortunately the acid/thf system may cause problems in this regard as thf is rapidly attacked by the acid to give ring-opened species. Such species, as well as probably being involved in the reaction, can also cause solvent polymerisation.

The protonation studies discussed below were carried out as far as possible under standard conditions, practical details of which are included in the Experimental Section.

6.4.2 ^{15}N NMR study of protonation of $[Mo(^{15}N_2)_2(triphos)(PPh_3)]$

The protonation work of George and co-workers[12] was performed using anhydrous HBr gas. For the present study it was more convenient to use anhydrous HBr generated in situ from Me_3SiBr and MeOH. To check whether this different acid

source would have any effect on the progress of the reaction, the ^{31}P NMR study detailed in reference 12 was repeated, and very good agreement found.

The complex trans-$[Mo(^{15}N_2)_2(triphos)(PPh_3)]$ was made by $^{15}N_2$ exchange with unlabelled material synthesised by the method of George et al.[11] The ^{15}N NMR spectrum in thf at 213K shows two main signals [Figure (6.4a)]. N_β resonates as a sharp doublet ($^1J_{NN}$ = 5 Hz) at -31.9 ppm. N_α gives a much broader signal due to unresolved coupling to phosphorus and is to higher field (-36.3 ppm). Two other signals to high field (-43.7 and -49.7 ppm) are also observed of ca. 20% the intensity of the main resonances. A similar spectrum is given at room temperature (298K). ^{31}P NMR spectra at 298 and 213K both show a normal pattern of resonances for the title complex. On standing, however, free PPh_3 is observed in the spectrum and this decomposition may produce the species responsible for the extra signal in the ^{15}N NMR spectrum.

Addition of ca. 20 mole excess of HBr at ca. 213K caused evolution of N_2 gas and a colour change from orange to light brown. Accumulation at 213K gave the spectrum shown in Figure (6.4b). Free $^{15}N_2$ is observed (-74 ppm) (also used as reference) and two signals assigned to N_α (-63.1 ppm) and N_β (-228.6 ppm) of a hydrazido(2-)-species. No $^1J_{NH}$ coupling is observed probably due to rapid exchange between the protons on the $-N-NH_2$ moiety and the free acid.

The solution was warmed to 298K for 20 minutes and the spectrum re-accumulated at 213K [Figure (6.4c)]. Resolution is poor as most of the acid had reacted with the thf and

Figure (6.4): ^{15}N NMR spectra of protonation of trans-$[Mo(N_2)_2(triphos)(PPh_3)]$ with HBr in thf.

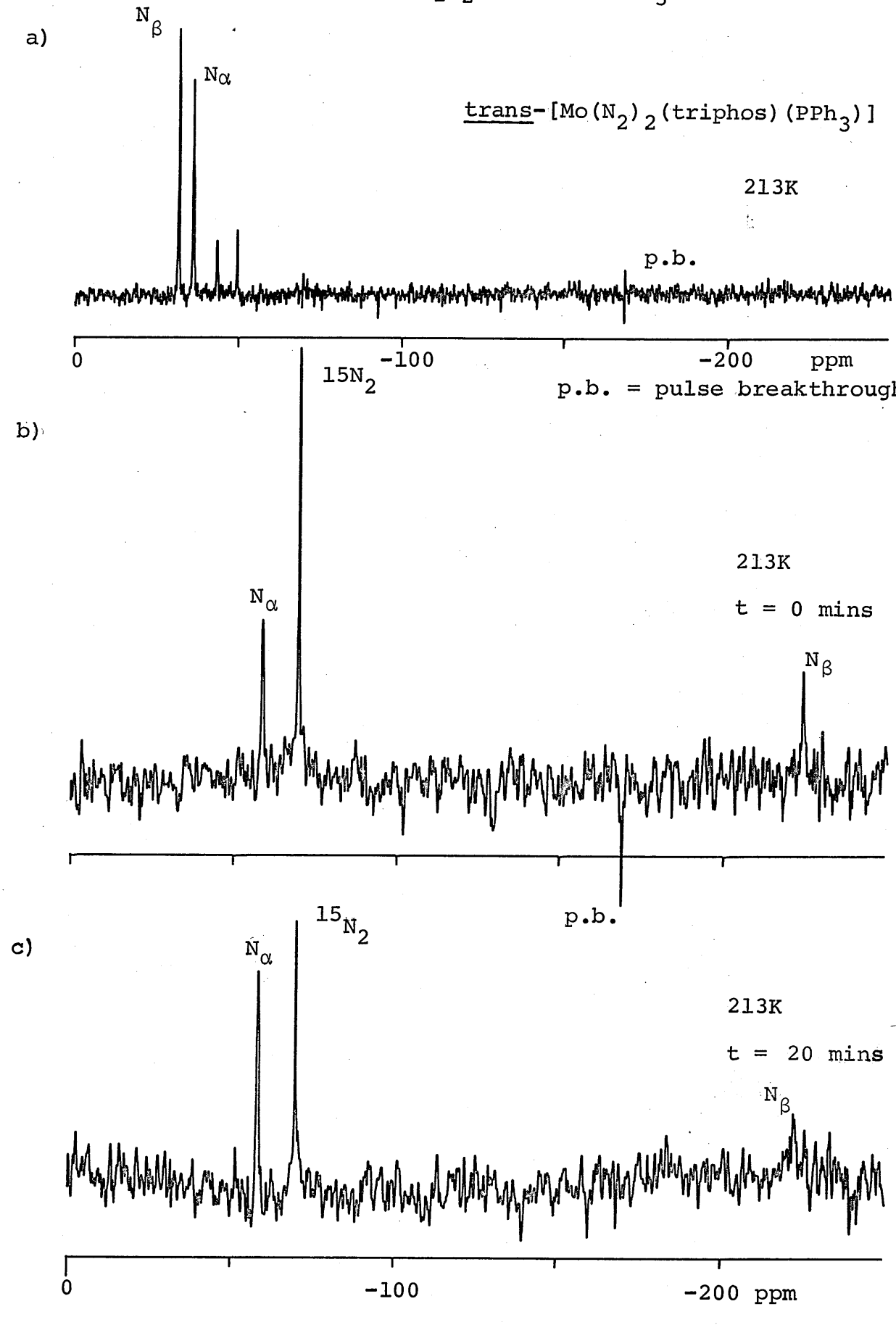

precipitation from solution was occurring. N_α and free $^{15}N_2$ are still visible but N_β is obscured by background noise probably due to the re-establishment of N-H coupling as the acid was consumed. Further spectra after extended times at 298K showed very poor resolution and no further information could be obtained. No NH_4^+ signals were observed.

These observations clearly substantiate the claim that a hydrazido(2-)-species is present in the protonation reaction. The presence of two species in the ^{31}P NMR study but the apparent observation of only one in the ^{15}N NMR experiment is consistent with the now known structures of the hydrazide complexes [see Figure (6.2)]. The different conformation of phenyl groups on the triphos ligand might be expected to have a far larger effect on ^{31}P resonances than on the ^{15}N shifts of the hydrazido(2-) ligand. It is proposed therefore that the resonances of the two species are coincident in the ^{15}N NMR spectrum.

More information could be gleaned about the N_β resonance using proton decoupling. Unfortunately, however, in the experiments detailed, this was not possible due to technical problems.

6.4.3 Protonation of trimethylphosphine molybdenum dinitrogen complexes

6.4.3.1 ^{15}N NMR studies

The complexes cis-$[Mo(^{15}N_2)_2(PMe_3)_4]$ and $[Mo(^{15}N_2)(PMe_3)_5]$ were prepared by exchange of unlabelled compounds with $^{15}N_2$.

Each complex was difficult to obtain free from the other. This is shown in the ^{15}N NMR spectra. The spectrum of cis-$[Mo(^{15}N_2)_2(PMe_3)_4]$ in thf under argon [Figure (6.5)] shows N_β as a sharp doublet, $^1J_{NN}$ = 6 Hz, at -34.3 ppm while N_α is a multiplet at ca. -41.5 ppm. Superimposed on this are signals due to $[Mo(^{15}N_2)(PMe_3)_5]$ at ca. -35 and -41 ppm. These are shown more clearly in the spectrum of $[Mo(^{15}N_2)(PMe_3)_5]$ [Figure (6.6)]. The N_β signal is a doublet, $^1J_{NN}$ = 6 Hz at -41.2 ppm with the broad N_α signal at ca. -35.1 ppm. Also easily seen is the N_β signal of cis-$[Mo(^{15}N_2)_2(PMe_3)_4]$, the N_α resonance of which broadens the base of the resonance of the mono-dinitrogen complex.

These results are interesting as they present an example of the crossover of the N_α and N_β resonances on changing the electronic nature of the metal site, which has been observed for other dinitrogen complexes.[16] In this case, substituting a PMe_3 ligand cis to N_2 for another N_2, shields N_α by ca. 6 ppm and deshields N_β by the same amount. This may be evidence of some type of cis-interaction in solution between N_2 ligands,[16] although such an interaction is not observed in the X-ray structure of cis-$[Mo(N_2)_2(PMe_3)_4]$.[17]

Preliminary investigation of the protonation reactions of $[Mo(N_2)(PMe_3)_5]$ and cis-$[Mo(N_2)_2(PMe_3)_4]$ indicated that maximum yields of NH_3 could be obtained from a HCl/MeOH system (ca. 0.4 mole NH_3 per Mo).[18]

Figure (6.5): ^{15}N NMR spectrum of cis-$[Mo(^{15}N_2)_2(PMe_3)_4]$

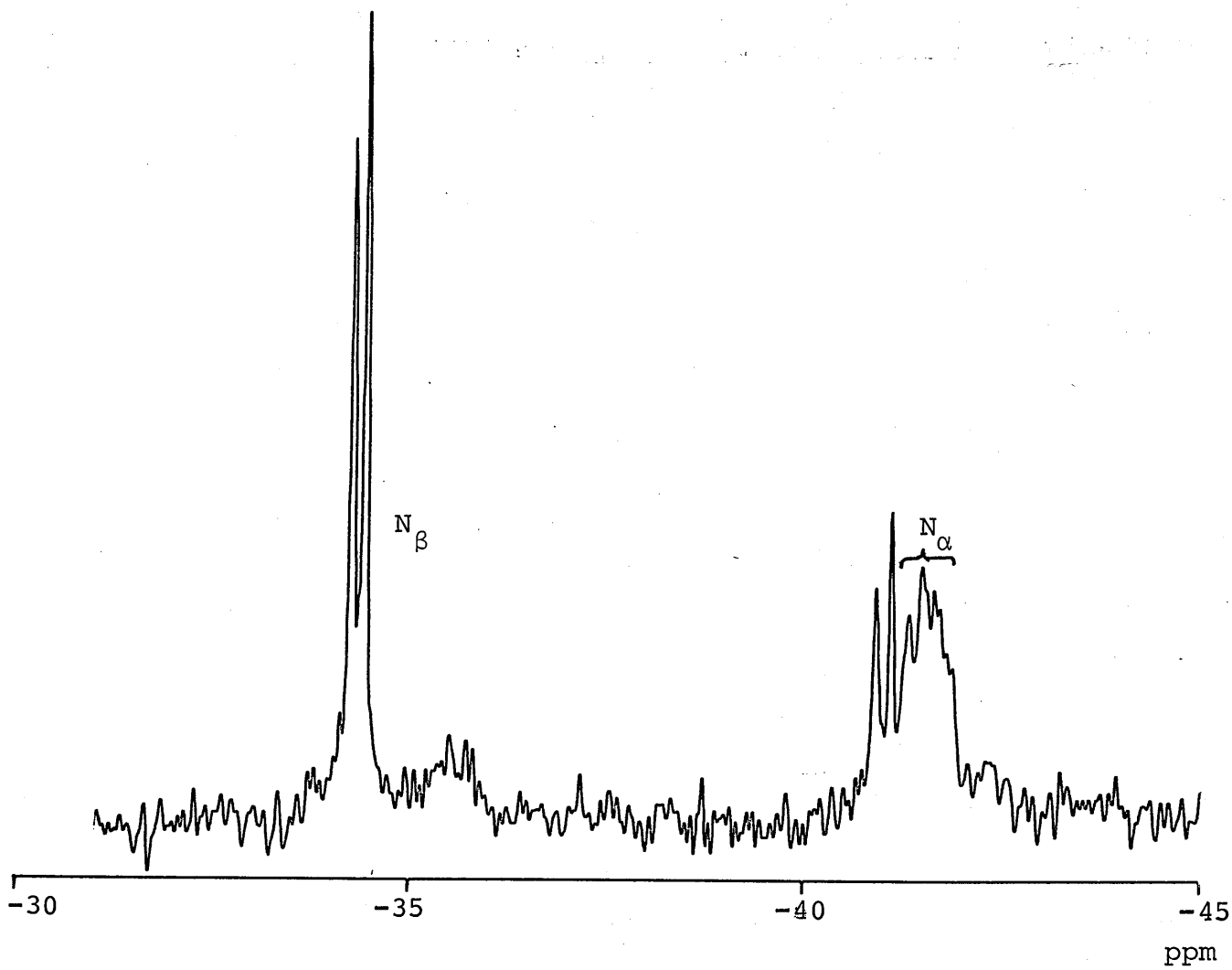

Figure (6.6): ^{15}N NMR spectrum of $[Mo(^{15}N_2)(PMe_3)_5]$

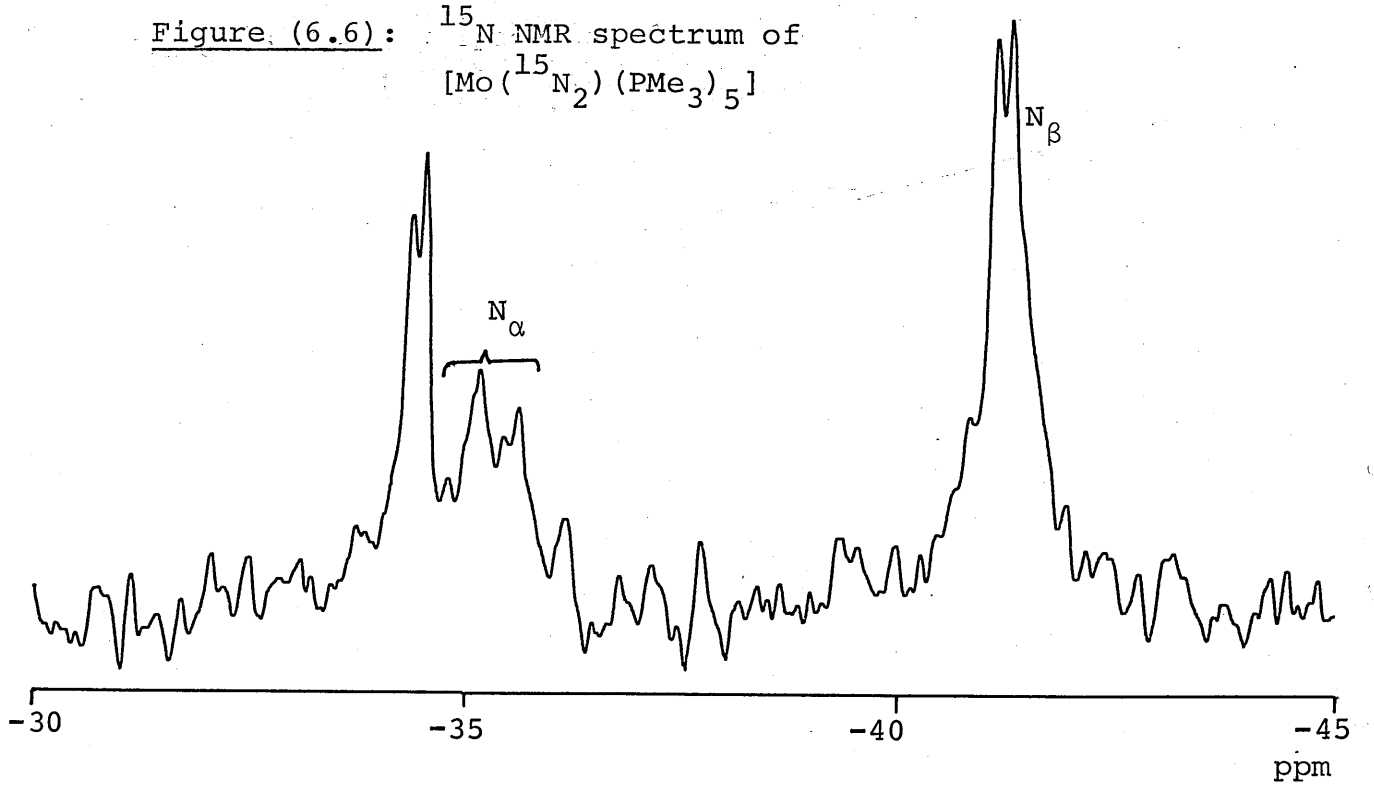

This system was then studied by ^{15}N NMR spectroscopy. Addition of HCl (from Me_3SiCl) to $[Mo(^{15}N_2)(PMe_3)_5]$ in MeOH at 213K caused evolution of nitrogen gas and produced a red solution. Spectral accumulation at 213K gave the spectrum in Figure (6.7a). In this spectrum, apart from a single resonance due to free $^{15}N_2$, two main sets of signals can be seen which are assigned to two hydrazido(2-)-species (A) and (B). Species (A) shows a doublet for N_β with $^1J_{NN}$ = 10 Hz at -236.5 ppm. The N_α signal at -62.9 ppm [Figure (6.7e)] shows a coupling pattern consistent with an overlapping doublet of quintets with $^1J_{NN}$ ca. 10 Hz and $^2J_{NP}$ ca. 8 Hz (4 equivalent phosphorus nuclei). The N_β resonance of species (B) in contrast to (A) shows $^1J_{NH}$ coupling = 92 Hz indicating that these N_β protons are not exchanging with HCl. The resonance is at -223.6 ppm, downfield of that due to (A). The N_α resonance of (B) is a complex multiplet [Figure (6.7e)] showing coupling to ^{15}N and to four or more ^{31}P nuclei, which is at lowest field (-48.2 ppm). Also observed are two signals marked (*) and these are in the regions expected for a diazenido-species with $\delta^{15}N_\alpha$ at -36.0 ppm and $\delta^{15}N_\beta$ at 123.2 ppm. These signals are just above the noise and this may indicate that only a small steady-state concentration of this diazenido-species exists, rapidly going through to hydrazido(2-). Complete conversion probably occurs in a short time and thus, after warming to 298K for 20 mins, spectrum (6.7b) was obtained which shows no resonances of (*) and also none for (B). Species (A) is still present

Figure (6.7): ^{15}N NMR spectra of reaction of $[Mo(^{15}N_2)(PMe_3)_5]$ with HCl in MeOH

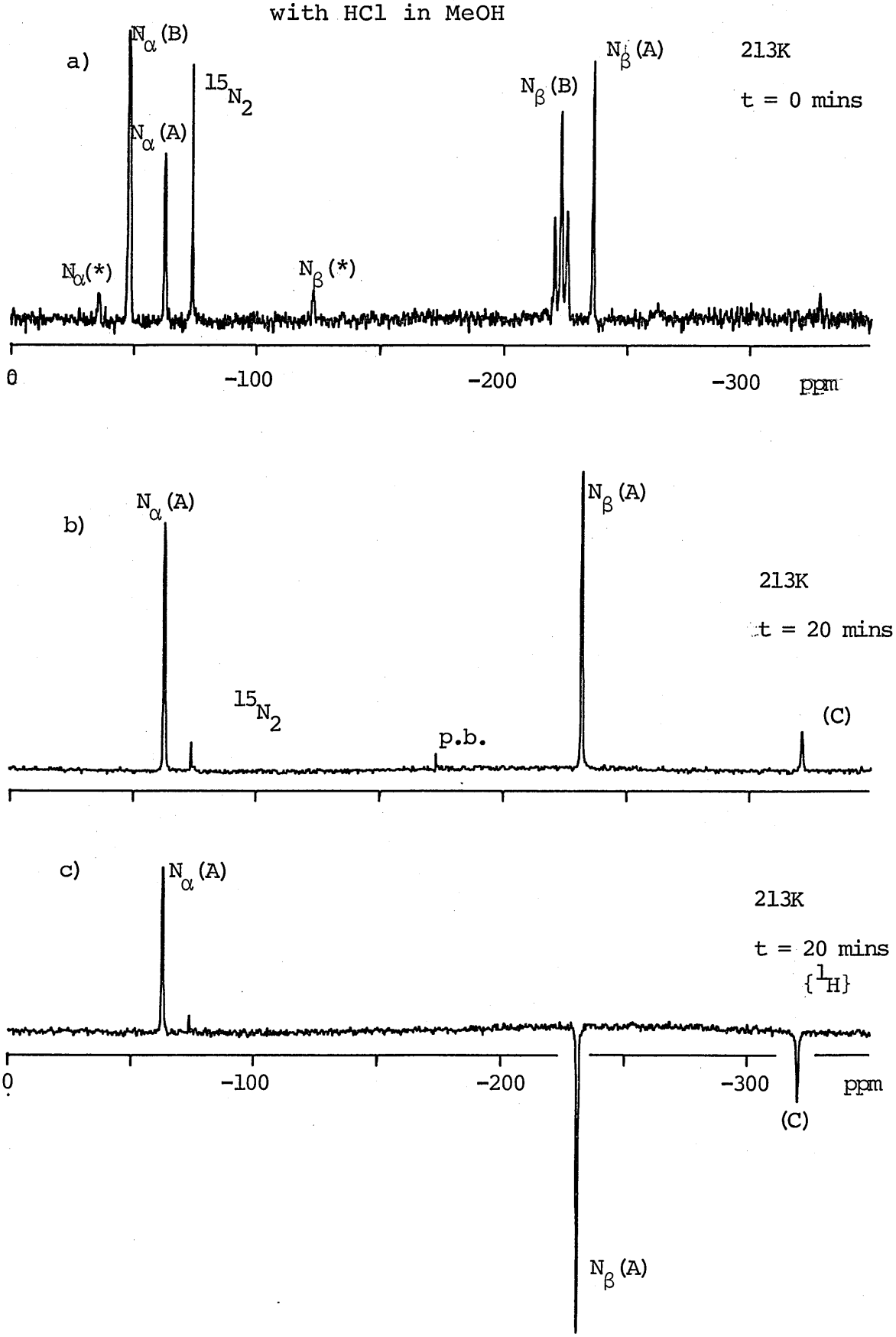

Figure (6.7) continued

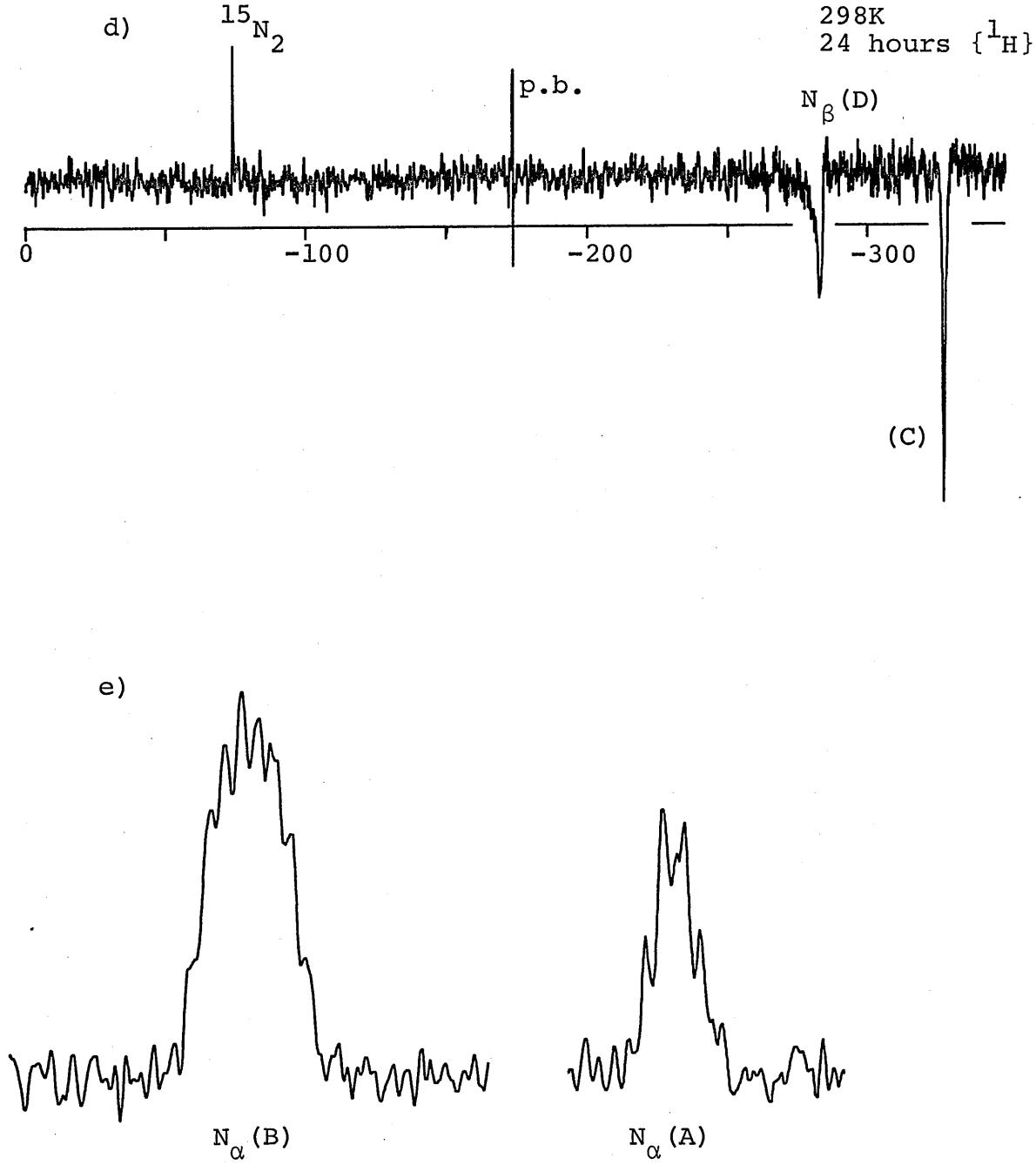

and a further signal at -322.1 ppm (C) is observed. On proton decoupling [Figure (6.7c)] both this signal and that of N_β(A) are inverted due to NOE (see Chapter 2). The new signal (C) is at high field but some 40 ppm downfield of the position expected for NH_4Cl (-365 ppm) in MeOH/HCl solution. Signal (C) appears to have no low field component and thus is probably not an N_β of a M-N-N$\langle$ species, it is, however, protonated as shown by the large NOE observed.

A further spectrum acquired after 3 hours shows an increase in the intensity of (C) and a reduction in N_β(A). After 24 hours at ambient temperature spectrum (6.7d) shows loss of N_β(A) and increase in signal (C). A further broad signal (D) at ca. -278 ppm is also present. The reaction is complete by this time.

The early stages in the similar protonation reaction of cis-$[Mo(N_2)_2(PMe_3)_4]$ are shown in Figure (6.8). Hydrazido(2-)-species (A) is again observed but the second set of hydrazido(2-)-signals (E) at -35.8 (N_α) and -218.4 (N_β) are downfield of those observed for the reaction of $[Mo(N_2)(PMe_3)_5]$. In common with intermediate (B), the species (E) shows $^1J_{NH}$ coupling, in this case of ca. 87 Hz. No signals due to an intermediate (*) are observed.

Species (E) is absent from spectrum (6.8d), after 20 mins. In this case signals due to (C) are not observed at this stage and unfortunately the reaction could not be followed further, due to instrument problems, but might be expected to continue in the same way as that in

Figure (6.8): ^{15}N NMR of spectra of reaction of cis-$[Mo(^{15}N_2)_2(PMe_3)_4]$ with HCl in MeOH

a)

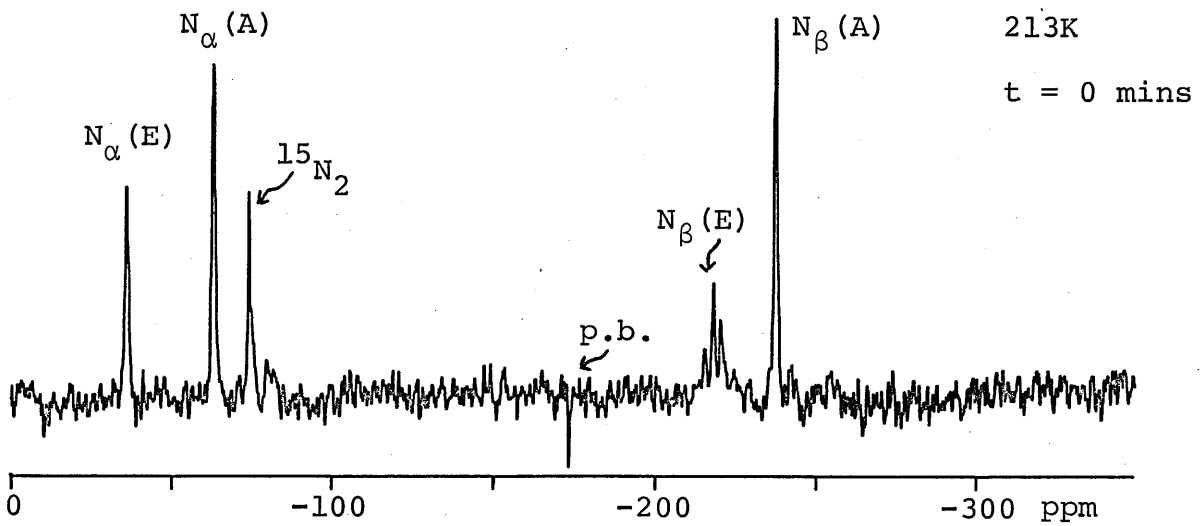

b)

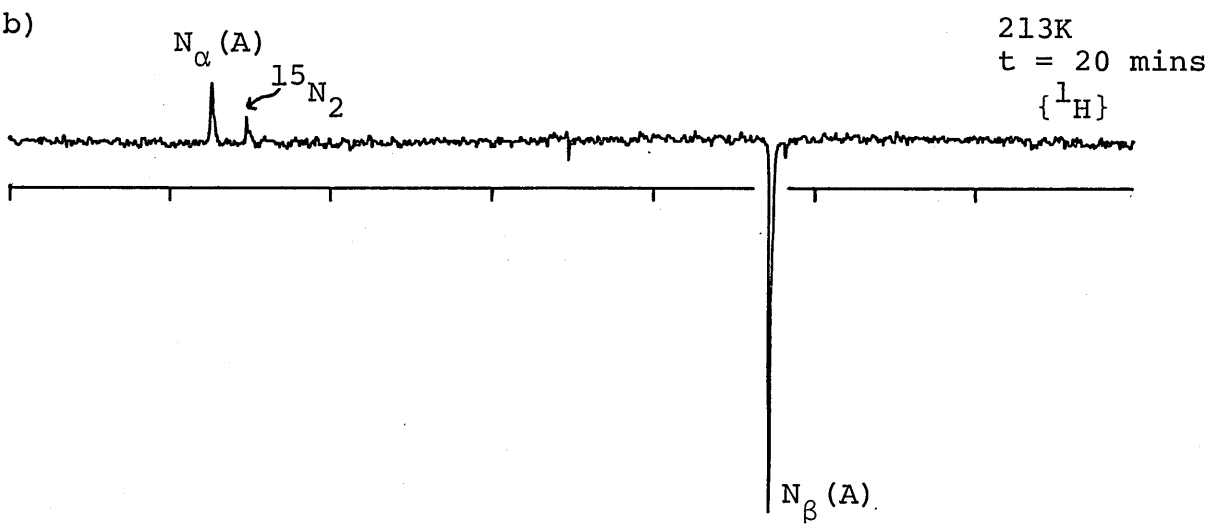

Figure (6.7). The various chemical shifts and possible assignments (see later) are summarised in Table (6.1).

TABLE (6.1): Assignments for Figures (6.7) and (6.8)

Signal	$\delta^{15}N$ (ppm)		Comments
A	-62.9 ($^2J_{NP}$=8Hz)	-236.5 ($^1J_{NN}$=10Hz)	$[MoCl(N_2H_2)(PMe_3)_4]Cl$
B	-48.2	-223.6 ($^1J_{NH}$=92Hz)	$M = N_\alpha - N_\beta H_2$
*	-36.0	-123.2	$M - N_\alpha = N_\beta \diagdown H$
C	-322.1		$[Me_3P-NH_2]^+$?
D	-278(br)		?
E	-35.8	-218.4	$M = N_\alpha - N_\beta H_2$

6.4.3.2 Comparison of ^{15}N NMR results with work on the isolation of intermediates and definition of stoichiometry

The protonation reaction mentioned above, along with others detailed below, have been the subject of an investigation by Mr. A. Galindo, while on study leave from University of Seville, with a view to identifying isolated intermediates and determining yields of nitrogen and nitrogen hydrides.[19] It is found that reaction of either cis-$[Mo(N_2)_2(PMe_3)_4]$ or $[Mo(N_2)(PMe_3)_5]$ with HX (X = Cl or I) in MeOH, hexane or Et_2O leads exclusively to the hydrazido(2-)-complexes $[MoX(N_2H_2)(PMe_3)_4]X$. The complexes precipitate out of hexane or Et_2O for X = Cl or I and out of MeOH in the case of X = I, but for X = Cl the MeOH must be removed to isolate the product.

A typical reaction is shown below [Equation (6.6)].

$$[Mo(N_2)_2(PMe_3)_4] + 2HCl \xrightarrow{\text{hexane}} [MoCl(N_2H_2)(PMe_3)_4]Cl + N_2 \qquad (6.6)$$

The hydrazido(2-)-complexes have the trans-configuration as the ^{31}P NMR spectrum shows only a singlet. These complexes are direct analogues of trans-$[MoX(N_2H_2)(dppe)_2]X$, mentioned earlier, and particularly of trans-$[MoX(N_2H_2)(PMe_2Ph)_4]X$.[20] The latter complexes are intermediates in the formation of $[MoX_2(N_2H_2)(PMe_2Ph)_3]$. In contrast, the PMe_3 systems appear to give exclusively the tetrakis phosphine hydrazido(2-)-complexes. In the ^{15}N NMR studies, hydrazido(2-)-species (A) is thus very likely to be trans-$[MoCl(^{15}N_2H_2)(PMe_3)_4]Cl$. This is confirmed by the ^{15}N NMR spectrum in MeOH of this complex, synthesised by reaction (6.6), which shows resonances identical to those of (A). The isolated complex trans-$[MoCl(^{15}N_2H_2)(PMe_3)_4]Cl$, now designated as (A), undergoes further reaction with an excess of HCl in MeOH. This reaction has been followed by ^{31}P and ^{15}N NMR spectroscopy.

The ^{31}P NMR spectrum of (A) in MeOH shows a sharp singlet at -148 ppm (v. TMP). After addition of acid this signal gradually disappears with the concomitant increase of a broad singlet at ca. -141 ppm. During the reaction time-course, this signal gradually shifts to lower field until it reaches its final position at ca. -126 ppm, when the reaction is complete. These observations, shown in Figure (6.9),

Figure (6.9): ^{31}P NMR spectra of reaction of trans-$[MoCl(N_2H_2)(PMe_3)_4]Cl$ with HCl in MeOH

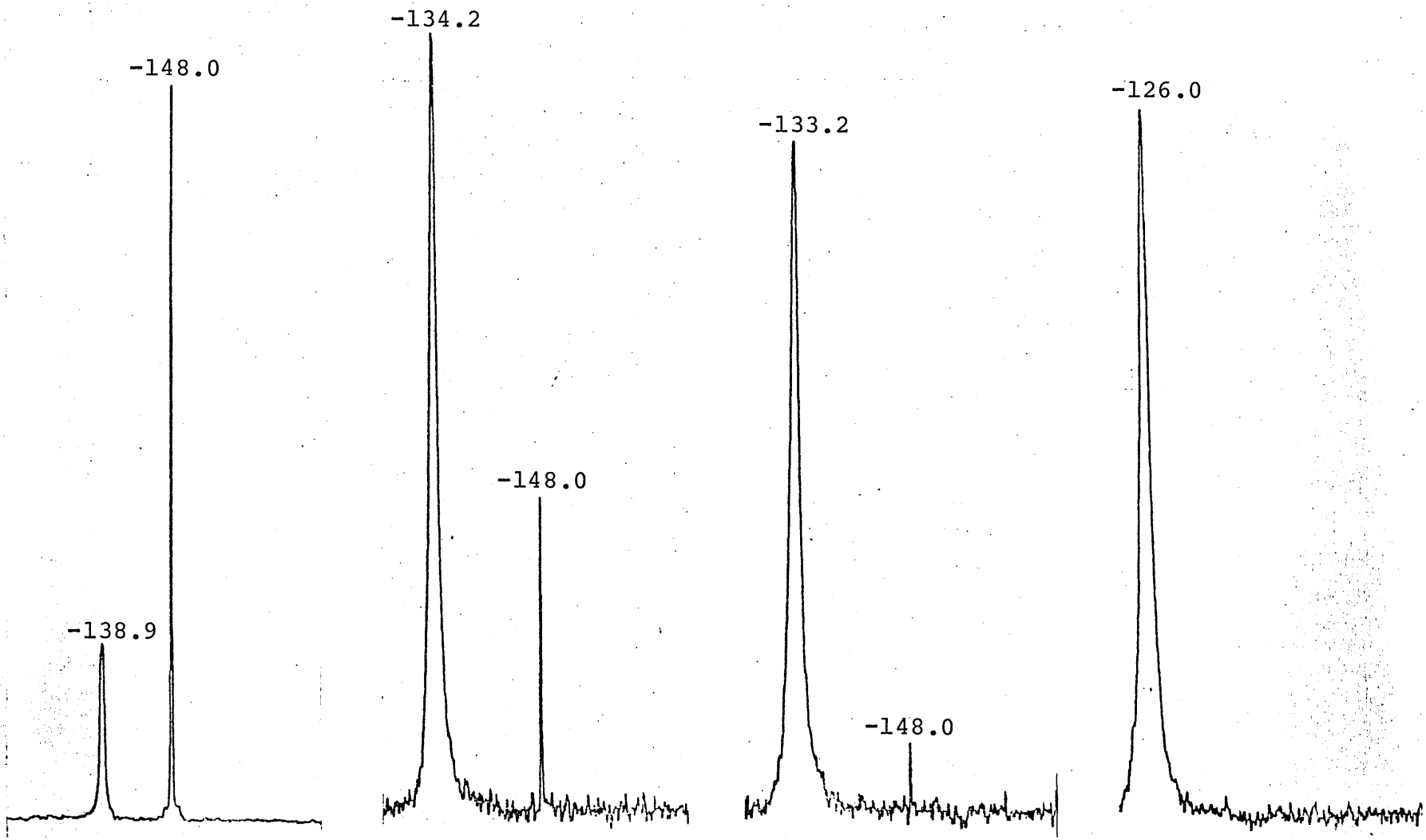

are consistent with the build-up of paramagnetic products in the reaction solution. The initial resonance is close to that found for a solution of PMe_3 in MeOH/HCl, i.e. $HPMe_3Cl$ suggesting phosphine dissociation from (A). The metal-containing product of this dissociation seems to be ^{31}P NMR silent and so may itself be paramagnetic. The equivalent ^{15}N NMR experiment shows the replacement of the signals due to (A) by a broad signal at high field close to the position observed for N_β (D) (vide supra). This signal then decays with evolution of product (C). The positions of the signals over the time-course move downfield slightly as paramagnetic products build up but the final positions of (C) and (D) are as found in the protonation of $[Mo(^{15}N_2)(PMe_3)_5]$.

It can be concluded, therefore, that the reactions of cis-$[Mo(N_2)_2(PMe_3)_4]$, $[Mo(N_2)(PMe_3)_5]$ and trans-$[MoCl(N_2H_2)(PMe_3)_4]Cl$ (A) follow similar pathways and therefore that (A) is a common intermediate in the mechanism of protonation of the dinitrogen complexes.

The steps before formation of (A) are very fast although signals due to a postulated diazenido-species are briefly observed. Different intermediates (B) or (E) are formed by the mono- and bis-dinitrogen complexes respectively. The identities of (B) and (E) can only be conjectured but these intermediates possibly possess the original phosphine stereochemistry and contain a PMe_3 ligand trans to the hydrazido(2-)-group. This moiety then rearranges to form

the (A) geometry. No kinetic studies on these systems have been performed but from comparison with Scheme (6.2), the pathway shown in Scheme (6.3) seems a reasonable suggestion.

Scheme (6.3):

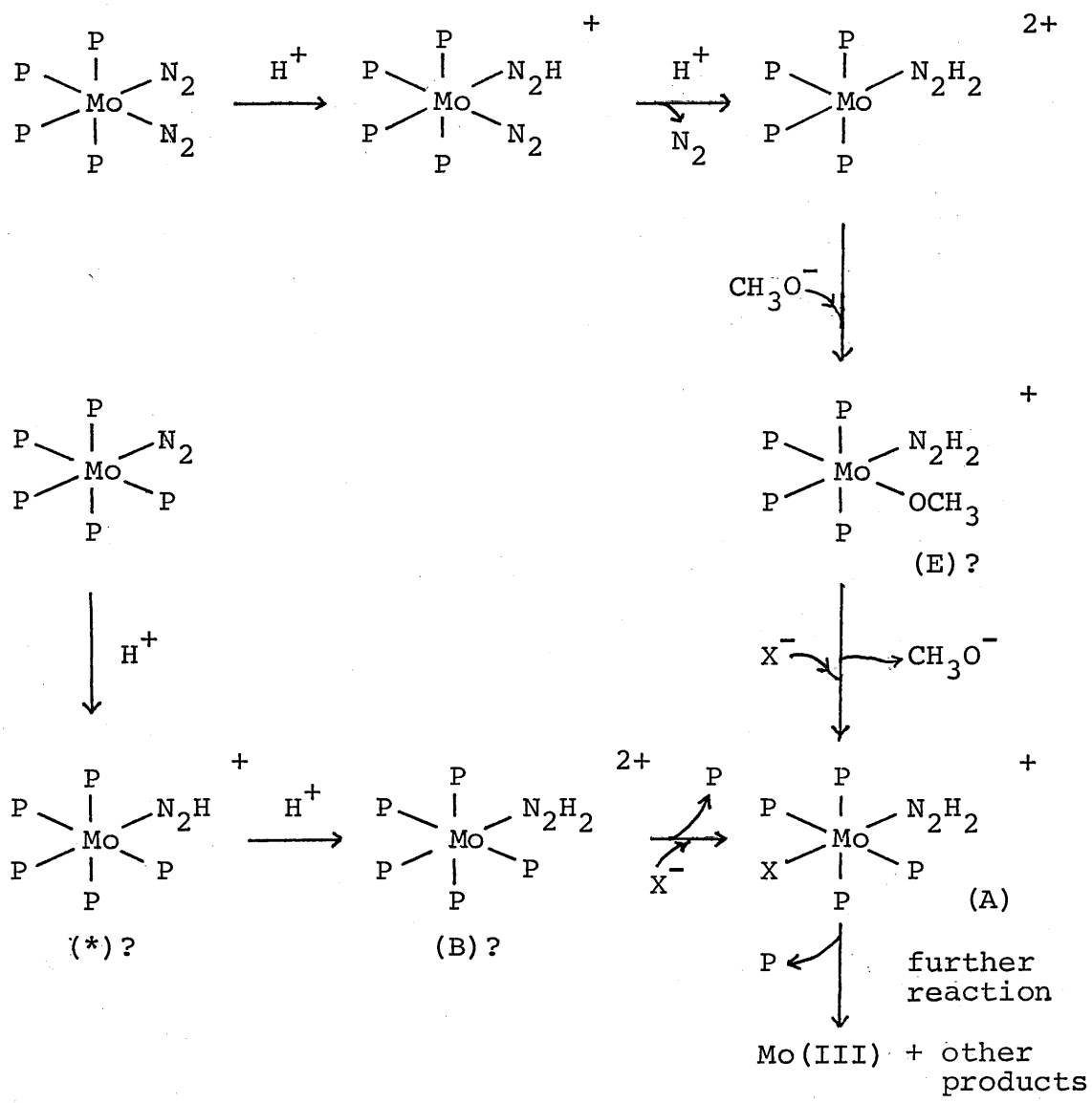

X = halide, P = PMe_3

After trans-$[MoCl(N_2H_2)(PMe_3)_4]Cl$ is formed in Scheme (6.3), further reaction involves loss of phosphine as shown by the ^{31}P NMR experiments. After this, paramagnetic species build up, complicating observation, although species apparently silent in the ^{31}P spectrum can be observed in the ^{15}N NMR spectrum. Species (D) is likely a residual unreacted hydrazido(2-)-complex of some type. Resonance (C), however, presents more of a problem. Reaction stoichiometry determinations[19] show that $[Mo(N_2)(PMe_3)_5]$ gives, at best, 0.4 mole of NH_3 per Mo on base distillation and a total nitrogen balance of 1.48 N_2 per Mo (theoretical = 2). $[Mo(N_2)(PMe_3)_5]$ gives a similar yield of NH_3 and a nitrogen balance of 0.45 N_2 per Mo (theoretical = 1). The "lost" nitrogen may be evolved as N_2 during base distillation, as was found in the protonation studies of $[Mo(N_2)_2(PMe_2Ph)_4]$[5] (vide supra), although a determination has not been carried out in the present case. Product (C) could then possibly be $^{15}NH_4^+$ showing a paramagnetic shift of some 40 ppm or, more likely, a species containing a coordinated nitrogen hydride, possibly an ammine M-NH_3 complex, although these are normally expected to resonate to high field of NH_4^+.[21]

Another candidate is an aminophosphine compound $[Me_3PNH_2]Cl$, for two reasons; the ^{15}N shift of the analogous compound $[Me_3PNHPh]I$ [22] is very close to that of (C) and furthermore, on base hydrolysis this type of compound gives NH_3 and phosphine oxide.[23] The resonance for (C) does not show any resolved N-P coupling but these can be small for aminophosphines (e.g. $[Me_3PNHPh]I$, $^1J_{NP}$ = 4 Hz)[22]. It may

then be suggested that base distillation of (D) yields the missing N_2 and of (C), the NH_3 detected.

Clearly, some further work is required on such systems as these, in order to confirm any of the suggestions above, and ^{15}N NMR should prove to be a useful tool even in apparently paramagnetic systems.

6.4.4 Protonation of trimethylphosphine tungsten complexes

A preliminary ^{15}N NMR investigation has been made of the reaction of cis-$[W(^{15}N_2)_2(PMe_3)_4]$ with HCl in MeOH. A spectrum of the starting material is shown in Figure (6.10).

Figure (6.10): ^{15}N NMR spectrum of cis-$[W(^{15}N_2)_2(PMe_3)_4]$

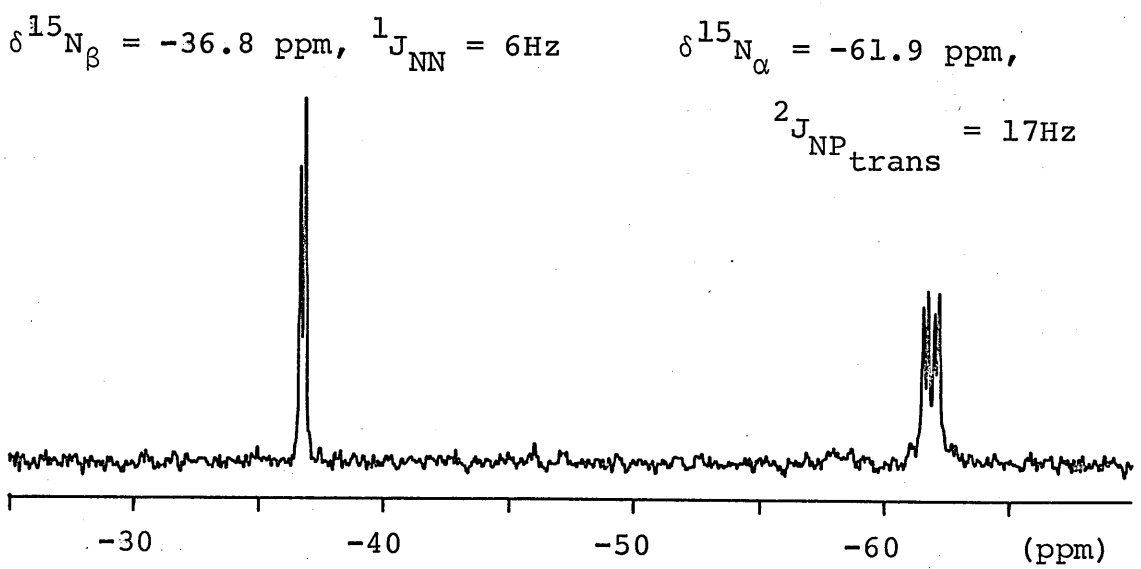

Protonation at 243K yields spectrum (6.11a) showing major hydrazido(2-)-signals at -91.3 ppm [N_α(F)] and -253.4 ppm [N_β(F)] and also small N_β signals (G) and (H) at -234.8 and -237.1 ppm. After 20 mins at 298K a further spectrum (6.11b) shows the (F) and (H) resonances but N_β(G) has disappeared. In fact the spectrum did not change further after 36 hours even after addition of more acid. It appears that in this W system, a hydrazido(2-)-species is formed which does not react further to give NH_3. This is confirmed by the determination of NH_3 yield, ca. 0.09 moles per W and the nitrogen balance of 1.05 N_2 per W (theoretical = 2).[19] A compound analysing as $[WCl(N_2H_2)(PMe_3)_4]Cl_2H$ was isolated from the reaction and this is probably (F). It may be noted that cis-$[W(N_2)_2(PMe_3)_4]$ also gives only traces of NH_3 on reaction with H_2SO_4/MeOH.[19]

These results are in contrast to the cis-$[W(N_2)_2(PMe_2Ph)_4]$ systems which generally give higher yields of NH_3 than the equivalent Mo complexes and to $[W(N_2)(PMe_3)_5]$, which gives 1.6 moles NH_3 per W on treatment with H_2SO_4/MeOH.

6.4.5 Reaction of $[MoI_2(N_2H_2)(PMe_2Ph)_3]$ with HI in dme

Studies by Hidai et al.[7] on $[MoCl_2(N_2H_2)(PMe_2Ph)_3]$ showed that approximately twice as much N_2H_4 is produced compared to NH_3 in the reaction with HCl in dme. Subsequently, it has been observed[24] that $[MoI_2(N_2H_2)(PMe_2Ph)_3]$ reacts with HI (from Me_3SiI/MeOH) in dme to give ca. 0.5 moles N_2H_4 per Mo and negligible NH_3. The reaction of acid with dme is

Figure (6.11): ^{15}N NMR spectra of reaction of cis-$[W(^{15}N_2)_2(PMe_3)_4]$ with HCl in MeOH

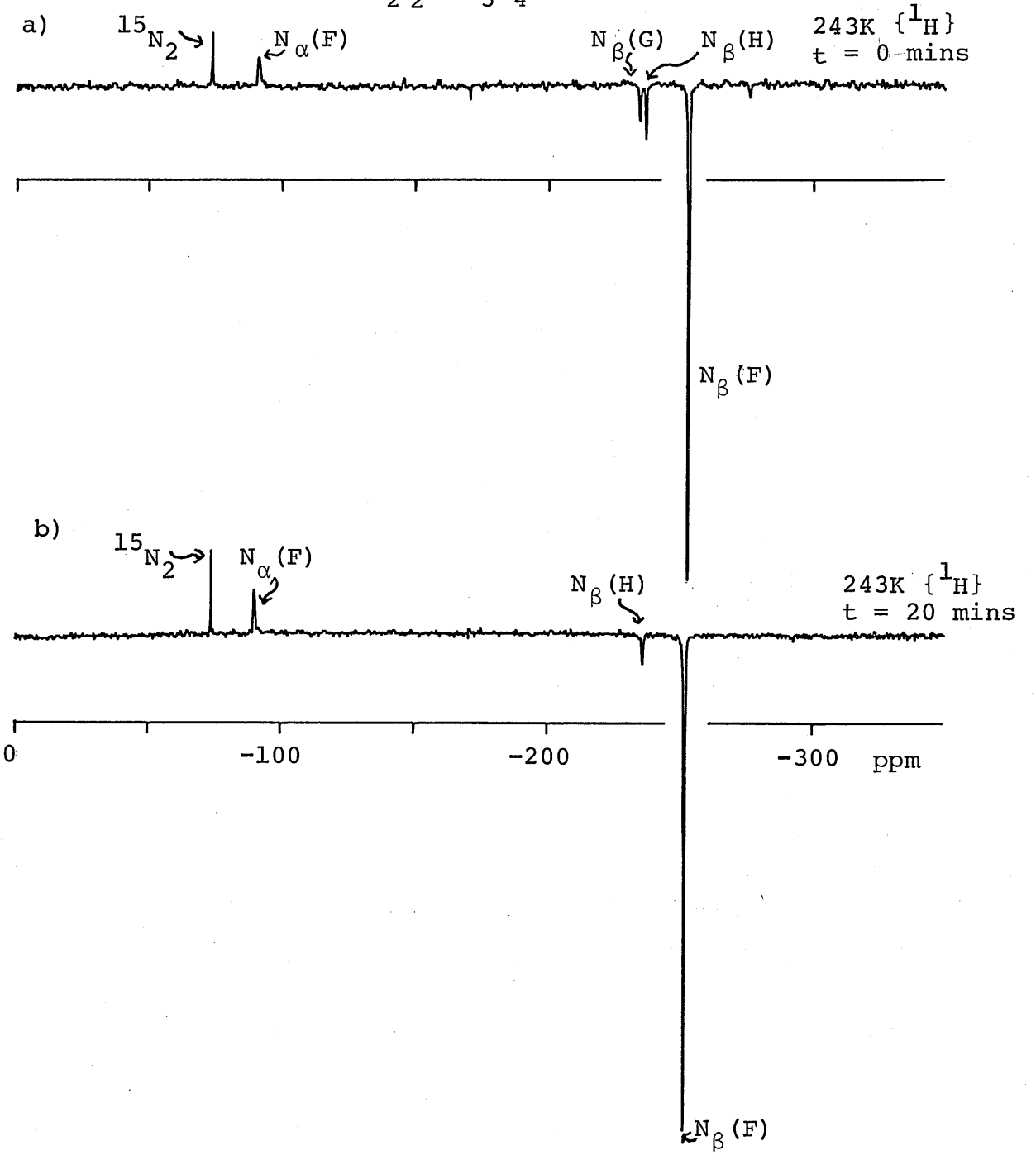

c) Unchanged after 36 hours.

TABLE (6.2): Assignment for Figure (6.11)

Signal	$\delta^{15}N$		Comments
F	-91.3	-253.4	$[WCl(N_2H_2)(PMe_3)_4]^+$?
G		-234.8	$=N-\underline{N_\beta}H_2$
H		-237.1	$=N-\underline{N_\beta}H_2$

slower than that with thf and this system then provides a suitable, "clean", apparently exclusively N_2H_4-producing, reaction for study by NMR spectroscopy.

6.4.5.1 ^{31}P NMR study

A schematic representation of the time-course for reaction of $[MoI_2(N_2H_2)(PMe_2Ph)_3]$ with HI in dme is shown in Figure (6.12). Shortly after protonation (6.12b) a small signal at -136 ppm (I) is observed. This coincides with the conversion of the initially brown solution to an intense dark red colour. After ca. 50 mins (6.12c) a further signal is observed at ca. -112 ppm (J). The reaction was found to be quite slow and so longer time intervals were used. Over the reaction course the red colouration was gradually discharged to give a pale orange solution. After 6 hours [Figure (6.12d)] (I) has gone and an intense signal (K) is present at -111 ppm. The signal due to (J) is now decreasing from some maximum value obtained between 1-6 hours and another signal (L) is just visible at -116 ppm. The further decay of (J) and increase of (L) is shown in Figure (6.12e) at 12 hours. The decay of starting material resonances is now advanced. The reaction is complete by 40 hours [Figure (6.12g)] and both (K) and (L) now have equal intensity.

Compounds isolated from a preparative scale reaction after four days[24] give very similar ^{31}P NMR spectra to those of (K) and (L) and an analysis showed no nitrogen.[24] As (J), (K) and (L) all have singlet spectra, they all could be P_2 species. This is supported by the low carbon and hydrogen

Figure (6.12): ^{31}P NMR spectra of reaction of $[MoI_2(N_2H_2)(PMe_2Ph)_3]$ with HI in dme. (Schematic representation.)

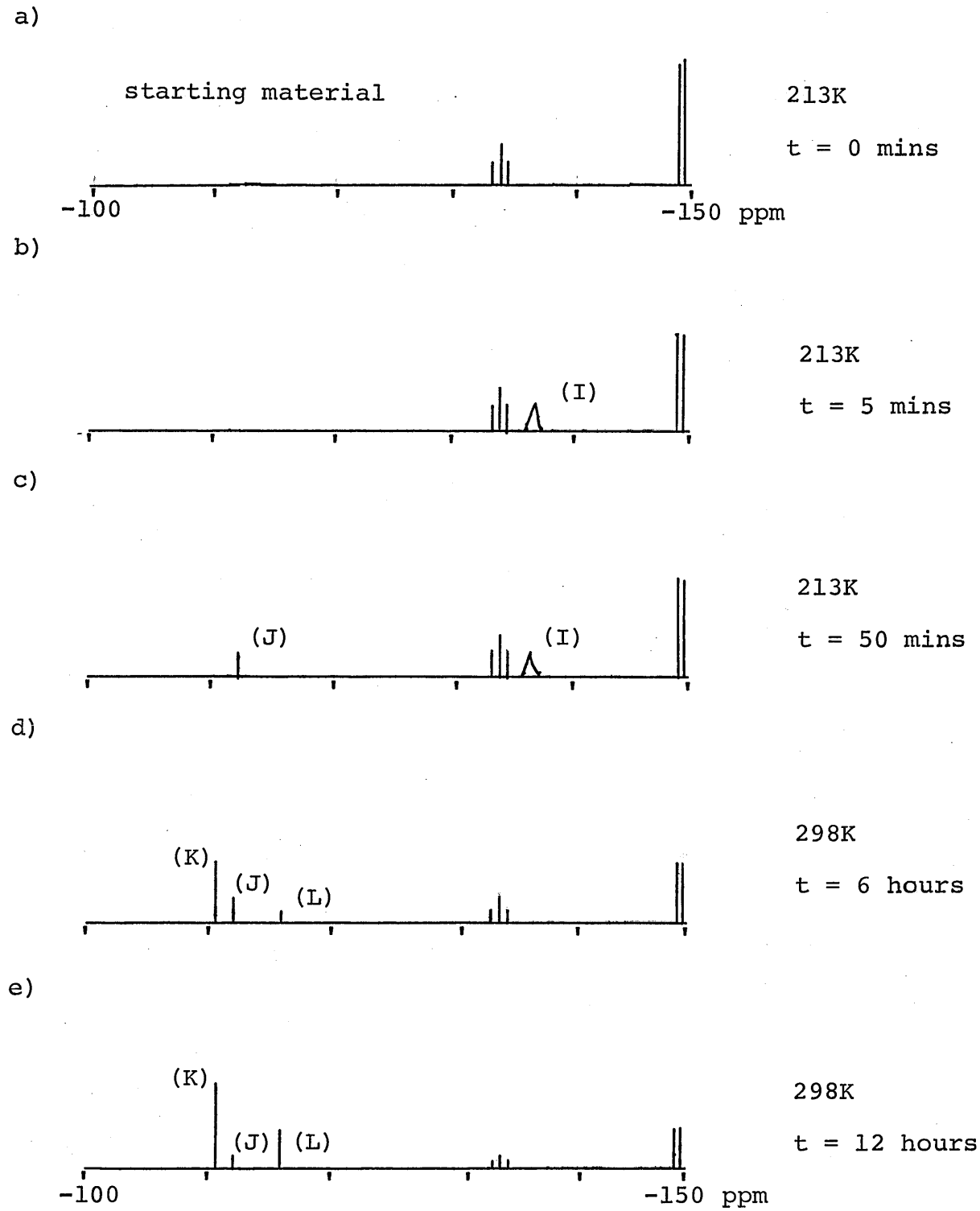

Figure (6.12) continued

f)

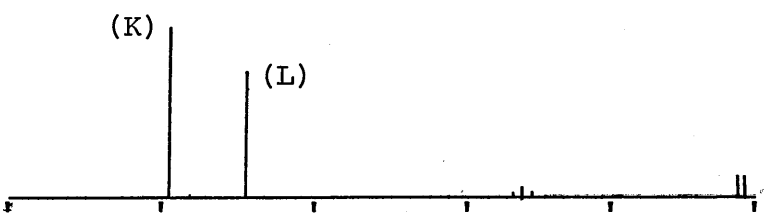

298K

t = 24 hours

g)

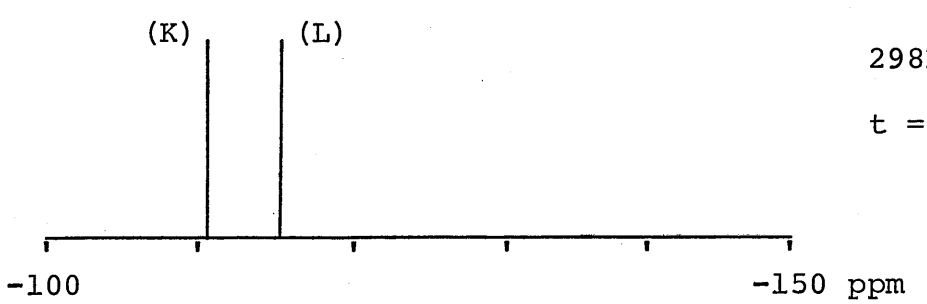

298K

t = 40 hours

analysis of (K) and (L).[24] One interesting point is the absence of a resonance due to the phosphonium salt $HPMe_2PhI$, and this may well be due to its insolubility in dme. A white product was seen to precipitate out on the sides of the NMR tube as the reaction proceeded.

TABLE (6.3): Assignments for Figure (6.12) (see later)

Signal	$\delta^{31}P$ (ppm)	Comments
P_3	-134.7(t) -149.6(d)	$[MoI_2(N_2H_2)(PMe_2Ph)_3]$
I	-136(br)	?
J	-112	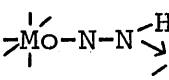 ?
K	-111	Final product
L	-116	Final product

6.4.5.2 ^{15}N NMR study

The ^{15}N NMR time course is shown in Figure (6.13). On addition of acid the spectrum of $[MoI_2(^{15}N_2H_2)(PMe_2Ph)_3]$ (M) is little changed with $\delta^{15}N_\alpha$(M) = -70.5 ppm and $\delta^{15}N_\beta$(M) = -241.4 ppm. Even after 20 minutes the proton decoupled spectrum (6.13b) shows little change. N_β(M) shows $^1J_{NN}$ ca. 12 Hz. After 90 minutes however several new sets of signals are observed. At lowest field are (N) = -14 ppm and (O) = -63 ppm. At highest field is (P) at -330 ppm. Signals (Q) are associated (vide infra), so the singlet at -84 ppm is N_α(Q) and N_β(Q) is an apparent doublet at -220 ppm, $^1J_{NH}$ = ca. 100 Hz. On proton decoupling all high field

Figure (6.13): ^{15}N NMR spectra of reaction of $[MoI_2(N_2H_2)(PMe_2Ph)_3]$ with HI in dme.

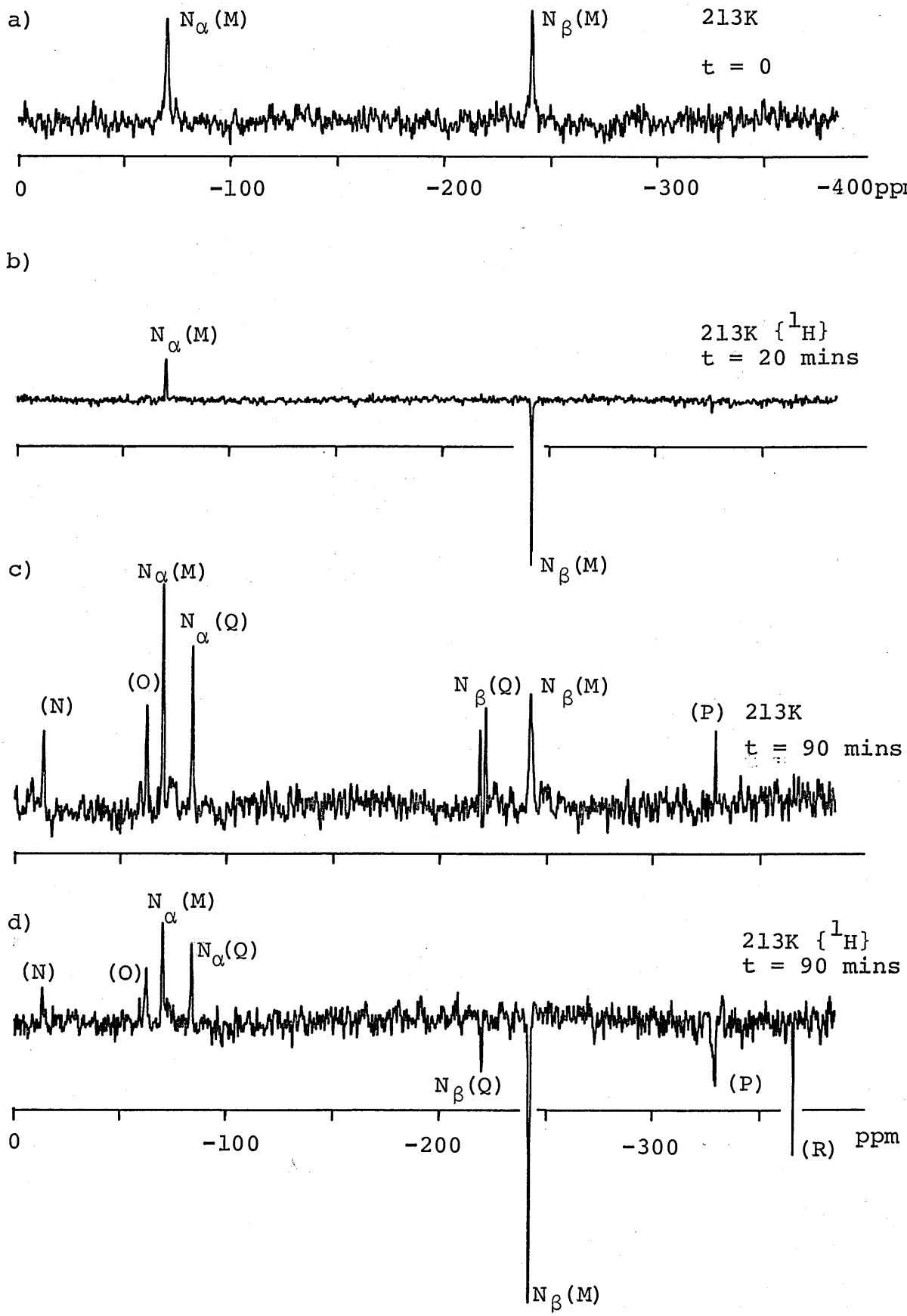

Figure (6.13) continued

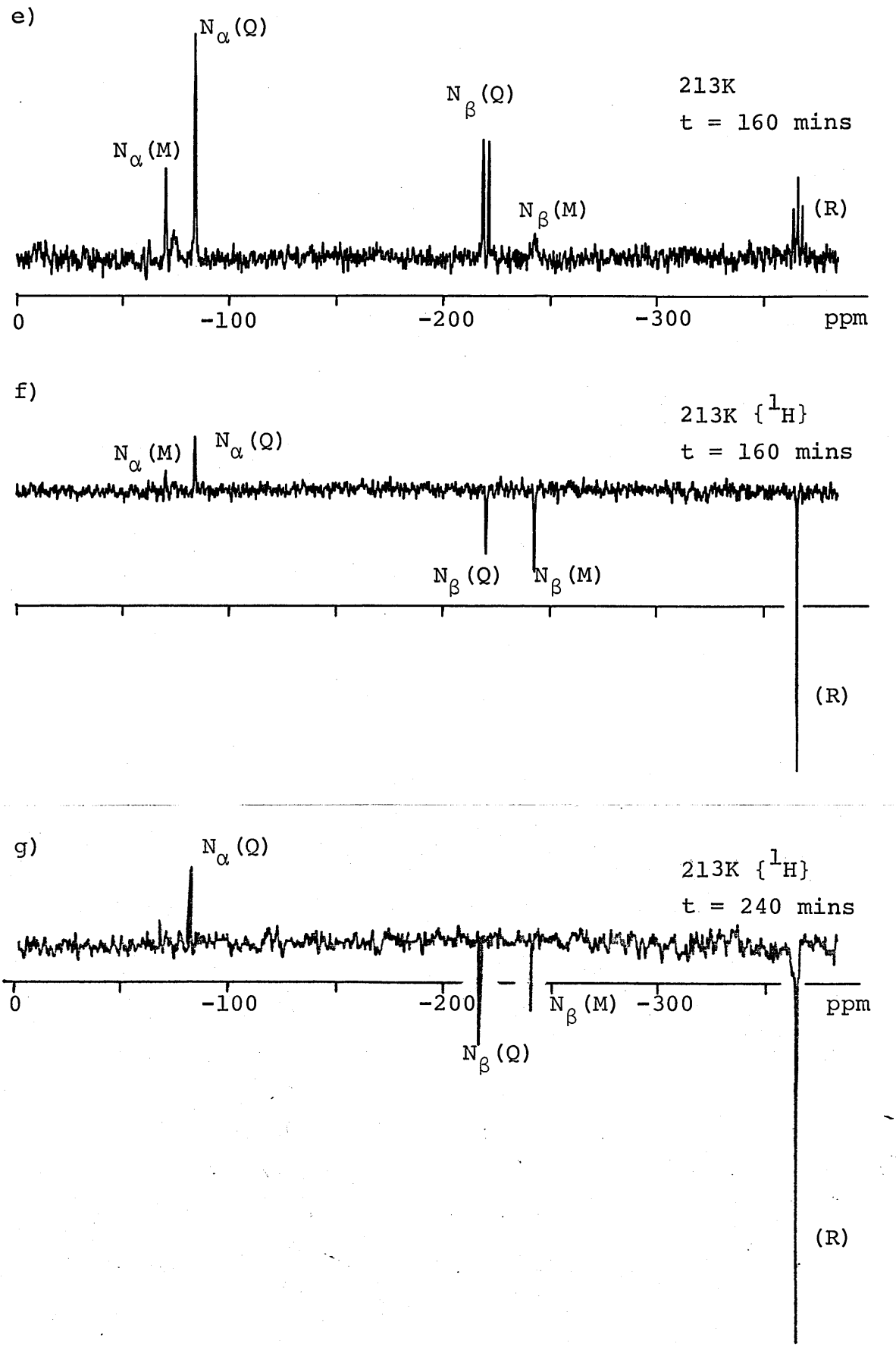

signals show NOE but the factor appears greater for $N_\beta(M)$ than $N_\beta(Q)$, a further indication of only one proton coupling to $N_\beta(Q)$ compared to the two on $N_\beta(M)$. (P) now shows a doublet with a coupling of ca. 18 Hz. Another signal is also detected on $\{^1H\}$, at -366 ppm (R), and is the highest field resonance detected.

A further spectrum at t = 160 mins shows the loss of signals (N), (O) and (P), reduction in intensity of (M) and increase in (Q) and (R). Interestingly, at this point $N_\beta(M)$ is broadened, showing exchange with free acid whereas (R) shows a quintet, $^1J_{NH}$ = 73 Hz. On proton decoupling [Figure (6.13f)] $N_\beta(M)$, $N_\beta(Q)$ and (R) are all inverted. A subsequent spectrum (6.13g) shows the gradual disappearance of (M) and increase in (R). After long periods of time only (R) is observed.

TABLE (6.4): Assignments for Figure (6.13)

Signal	$\delta^{15}N$ (ppm)	Comments
M	-70.5 -241.4	$[MoI_2(N_2H_2)(PMe_2Ph)_3]$
N	-14	?
O	-63	?
P	-330 ($^1J_{NN}$?=18Hz)	$-N-NH_x$?
Q	-84 -220 ($^1J_{NH}$=100Hz)	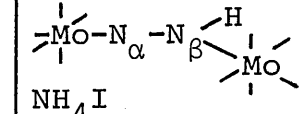 ?
R	-366 ($^1J_{NH}$=73Hz)	NH_4I

6.4.5.3 Discussion

In the absence of a detailed kinetic study and product analysis of this reaction, it is difficult to assign the various intermediates observed in the above experiments. Some general points can be made, however.

Over the reaction time course the starting material $[MoI_2(^{15}N_2H_2)(PMe_2Ph)_3]$ (M) is gradually degraded but without evolution of $^{15}N_2$ in contrast to the reaction performed in thf solution.[14] The final nitrogen-containing product (R) appears, by its coupling pattern and chemical shift, to be $^{15}NH_4I$. This is at odds with the product study[22] but it should be noted that the solubility of $^{15}N_2H_5I$ in dme is very low and may thus be below detection levels. The early stages of the reaction are complex, with the production and subsequent degradation of (N), (O) and (P). Resonance (P) is at a shift expected for $^{15}N_2H_5I$ but shows a coupling (ca. 18 Hz) and may thus be an aminophosphine. The nature of (N) and (O) are equally uncertain. The later stages seem to be somewhat clearer with degradation of starting material possibly via the intermediacy of (Q). The N_β resonance of (Q) is very interesting in that it shows apparent coupling to only one proton yet it is in the chemical shift range expected for hydrazido(2-)-complexes. The $^1J_{NH}$ coupling of ca. 100 Hz is also large for a hydrazido(2-)-ligand. The time scale suggests that signal (J) in the ^{31}P NMR spectrum is the equivalent of (Q) in the ^{15}N NMR spectrum.

The identity of (Q) can only be guessed at but it may involve a bridging structure of the type:

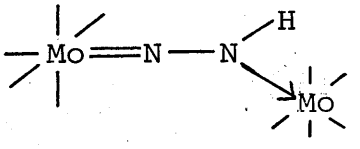

Although such proposals are highly speculative these preliminary ^{15}N and ^{31}P NMR experiments show that (Q) is relatively long-lived and suggest it may be possible to isolate it in future experiments. Such work in combination with detailed kinetic studies should be able to supplement the data already collected by NMR spectroscopy.

6.4.6 Protonation of cis-$[Mo(N_2)_2(PMe_2Ph)_4]$ with HI in dme

The title reaction was studied in an effort to check the generality of the early stages of protonation of dinitrogen complexes in various solvent/acid systems, to verify the presence of $[MoI_2(N_2H_2)(PMe_2Ph)_3]$, and to see if the reaction products were similar to those found in the protonation of the hydrazido(2-)-compound. This is important because Hidai et al. have reported[7] that the reaction of cis-$[Mo(N_2)_2(PMe_2Ph)_4]$ with HI in dme yields 0.53 mole NH_3 per Mo and only 0.01 moles of N_2H_4. Preliminary time courses studied by ^{31}P and ^{15}N NMR have been undertaken as described below.

6.4.6.1 ^{31}P NMR spectroscopy

When a limiting amount of HI (ca. 2 moles per Mo) was added to cis-$[Mo(N_2)_2(PMe_2Ph)_4]$, N_2 was evolved and the acid rapidly used up to give hydrazido(2-)-species after which the reaction stopped. A ^{31}P NMR spectrum shows the doublet and triplet signals assignable to $[MoI_2(N_2H_2)(PMe_2Ph)_3]$, a singlet assigned as trans-$[MoI(N_2H_2)(PMe_2Ph)_4]I$ (P_4) and free PMe_2Ph. No phosphonium $PhMe_2PH^+$ is observed, consistent with the absence of free acid. Addition of further acid (ca. 10 mole excess) at 213K produced the series of spectra shown schematically in Figure (6.14). Spectrum (6.14a) is essentially the same as that discussed above but the phosphine is protonated to give the phosphonium salt. This is interesting as no phosphonium salt was observed in the protonation of $[MoI_2(N_2H_2)(PMe_2Ph)_3]$. After 5 minutes reaction, the P_4 resonance is completely replaced by 2 sets of signals designated as (S). These are shown more clearly in Figure (6.14b), after 15 mins reaction time. Also observed at this stage is product (K). Further reaction shows increase of (S) peaks at the expense of $[MoI_2(N_2H_2)(PMe_2Ph)_3]$ and concomitant increase of (K). Interestingly the phosphonium band is broadening considerably over the reaction course. After 24 hours [Figure (6.14e)] both (K) and (L) are observed as in the protonation of the hydrazido(2-)-complex. No phosphonium signal can be seen.

Figure (6.14): Schematic ^{31}P NMR spectra of reaction of cis-$[Mo(N_2)_2(PMe_2Ph)_4]$ with HI in dme

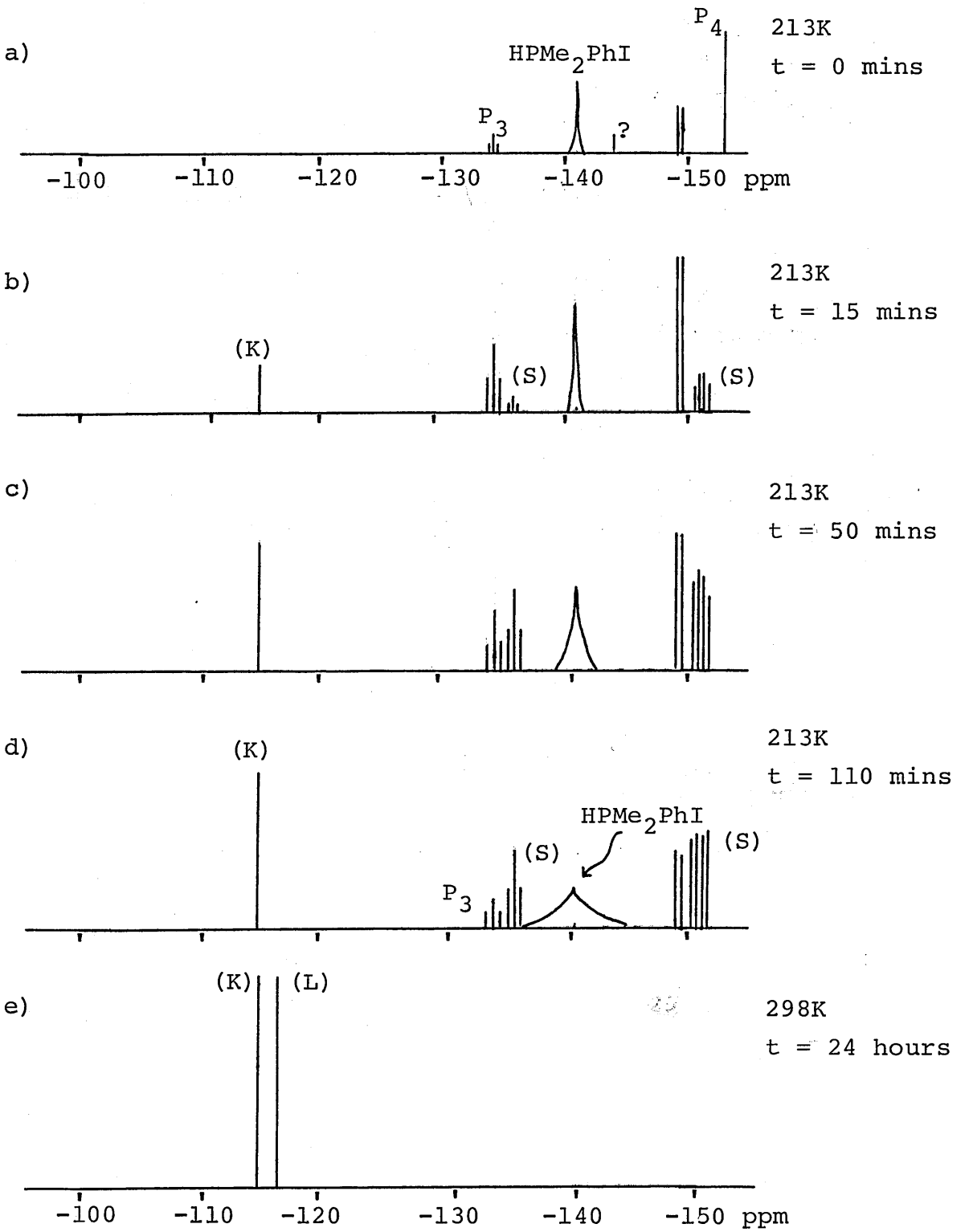

TABLE (6.5): Assignments for Figure (6.14)

Signal	$\delta^{31}P$ (ppm)		Comments
P_3	-134(t)	-150(d)	$[MoI_2(N_2H_2)(PMe_2Ph)_3]$
P_4	-153(s)		$[MoI(N_2H_2)(PMe_2Ph)_4]I$
S	-136(t)	-151(dd)	$[MoI(N_2H_2)(PMe_2Ph)_3(DME)]I$

6.4.6.2 ^{15}N NMR spectroscopy

Similar limiting acid conditions as used in the ^{31}P NMR experiment give two hydrazido(2-)-species in the ^{15}N NMR spectrum which do not react further. These species, as shown in Figure (6.15), have almost coincident N_α resonances (ca. -72 ppm) but the N_β signals are distinct triplets (exchange is prevented as there is no free acid). The high field triplet is close to the shift expected for $[MoI_2(^{15}N_2H_2)(PMe_2Ph)_3]$ (P_3) and $^1J_{NH}$ = 84 Hz. The other resonance is assigned to N_β of trans-$[MoI(^{15}N_2H_2)(PMe_2Ph)_4]I$ (P_4) with $^1J_{NH}$ = 88 Hz. Further acid (10 mole excess of HI) was added and the series of spectra shown in Figure (6.16) accumulated at 213K.

Figure (6.15): ^{15}N NMR spectrum of protonation of cis-$[Mo(^{15}N_2)_2(PMe_2Ph)_4]$ in dme with limiting HI

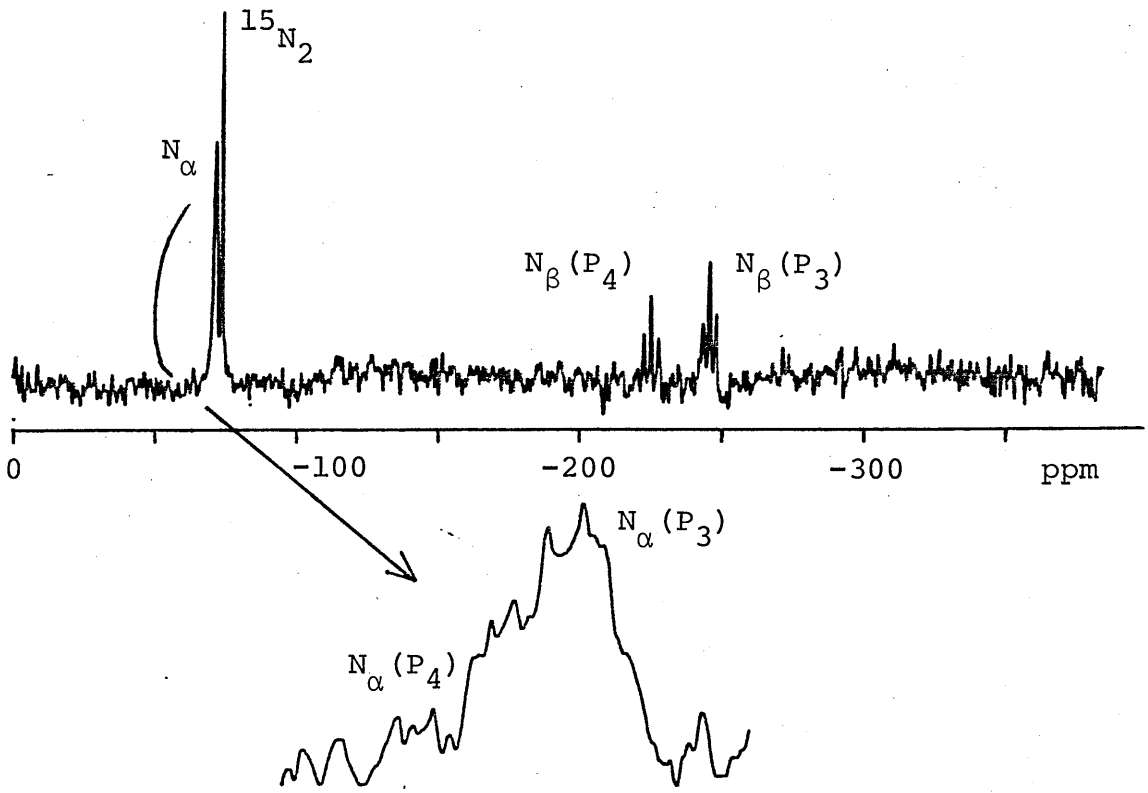

Spectrum (6.16a) shows inverted signals due to N_β of $[MoI_2(^{15}N_2H_2)(PMe_2Ph)_3]$ (P_3) and trans-$[MoI(^{15}N_2H_2)(PMe_2Ph)_4]I$ (P_4). After 15 minutes the spectrum (6.16b) shows a single N_β signal (T) with loss of the $N_\beta(P_4)$. (T) also shows a singlet in the undecoupled spectrum [Figure (6.16c)]. At t = 60 minutes, $^{15}NH_4^+$ and signal (P) have appeared. After further time, (P) was lost followed by (T) and finally only the signal due to $^{15}NH_4^+$ remained.

Figure (6.16): ^{15}N NMR spectra of further reaction of cis-$[Mo(N_2)_2(PMe_2Ph)_4]$ with an excess of HI in dme

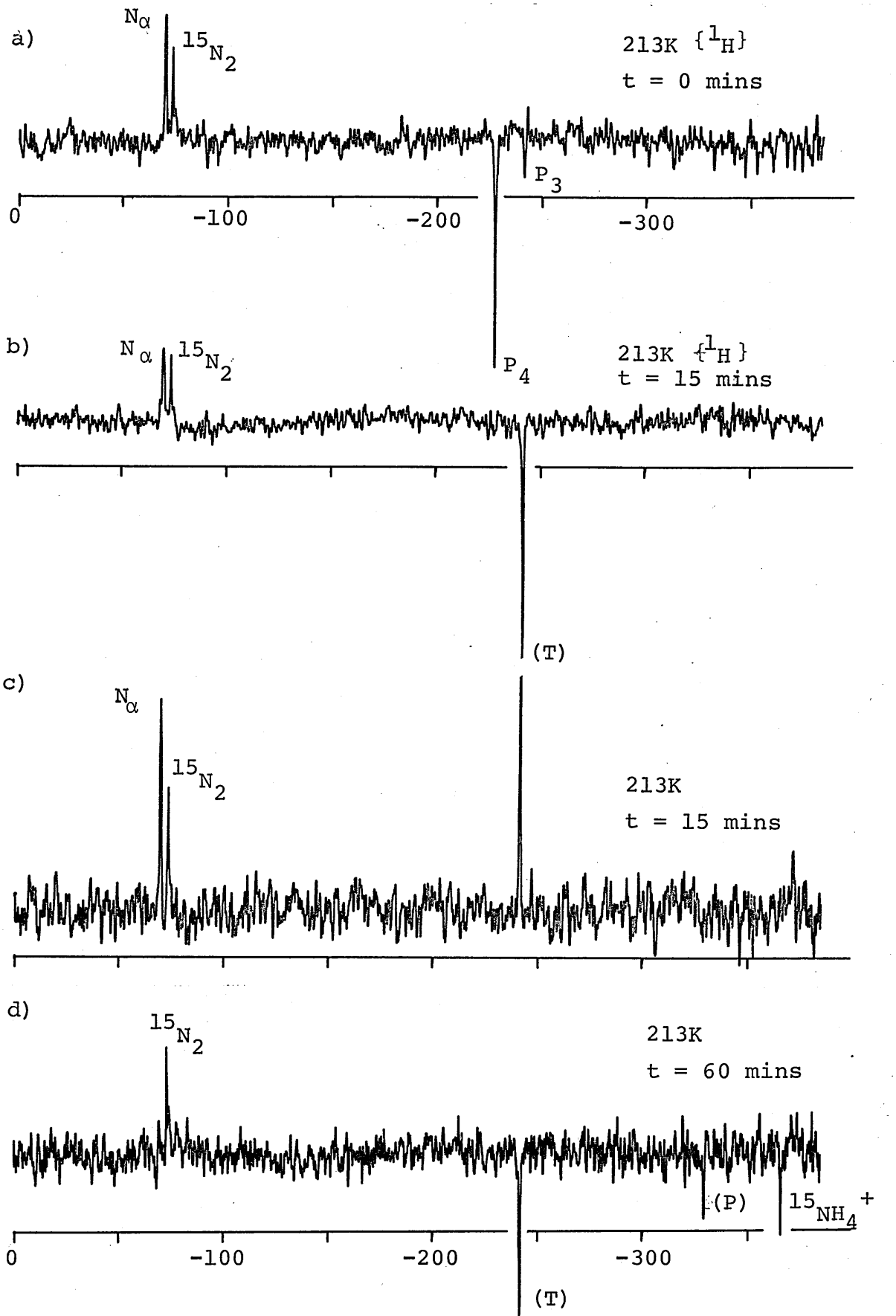

TABLE (6.6): Assignments for Figures (6.15) and (6.16) (vide infra

Signal	$\delta^{15}N$ (ppm)		Comments
P_3	-72	-243 (t) ($^1J_{NH}$=84Hz)	mer-$[MoI_2(N_2H_2)(PMe_2Ph)_3]$
P_4	-72	-226 (t) ($^1J_{NH}$=88Hz)	$[MoI(N_2H_2)(PMe_2Ph)_4]I$
T	-72	-243	$[MoI(N_2H_2)(PMe_2Ph)_3(DME)]I$

6.4.6.3 Discussion

The early stages of the protonation of cis-$[Mo(N_2)_2(PMe_2Ph)_4]$ involve the formation of two hydrazido(2-)-intermediates in a similar way to the PMe_3 dinitrogen complexes. However, in the latter case it appears that the tris-phosphine hydrazido(2-)-complex is not observed whereas both trans-$[MoX(N_2H_2)P_4]X$ and $[MoX_2(N_2H_2)P_3]$ are seen for P = PMe_2Ph and X = I. The above observations seem to indicate that the trans-P_4 species is short-lived for this system and quickly loses a PMe_2Ph ligand to form the P_3 species. From the ^{31}P spectrum it appears that P_3 isomerises to give (S) which has a more complicated spectrum. The pattern of resonances for (S) is consistent with there being a solvated hydrazido(2-)-complex as shown below:

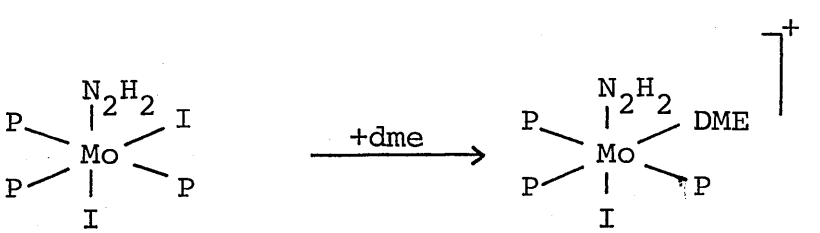

P_3

The spectrum of (S) shows a single triplet for the unique phosphine,as expected,but two doublets for the pair of equivalent phosphines. Similar behaviour has been observed for other substituted hydrazido(2-)-species of the type $[MX(N_2H_2)L(PMe_2Ph)_3]^+$ (e.g. M = W, X = Br and L = 2-methyl pyridine)[20] and has been interpreted as possibly due to the L ligand causing restricted rotation of the phosphines, forcing two distinct stereoisomers to form.[25] The ^{31}P spectra show both P_3 and (S) are present in solution during a period of the time course. The ^{15}N NMR spectrum shows only a single resonance (T) at this time and this may be due to overlapping of the P_3 and (S) species ^{15}N resonances. It seems it is the solvated hydrazido(2-)-species which goes on further to react.

(S) is not detected in the ^{31}P spectra of the reaction of isolated P_3 with acid described earlier (6.4.5.1). Another difference is the absence of intermediate (Q) in the protonation of cis-$[Mo(N_2)_2(PMe_2Ph)_4]$ which is significant because it may be the presence of this intermediate that determines whether hydrazine is formed. It is not immediately clear why the dinitrogen complex and the isolated P_3 hydrazido(2-)-complex should have different reaction paths. It may simply be the presence of excess phosphonium salt in the former case which determines the pathway. The phosphine containing end-products of both reactions appear to be the same.

6.5 ^{15}N NMR spectroscopy of mer-[Mo($^{15}N_2$)$_3$($PPr^n{}_2Ph$)$_3$]

The title complex has been structurally characterised and is unique in containing three dinitrogen ligands. No protonation studies have yet been attempted. As a preliminary, the ^{15}N NMR spectrum has been determined and is shown in Figure (6.17).

Figure (6.17): ^{15}N NMR spectrum of mer-[Mo($^{15}N_2$)$_3$($PPr^n{}_2Ph$)$_3$]

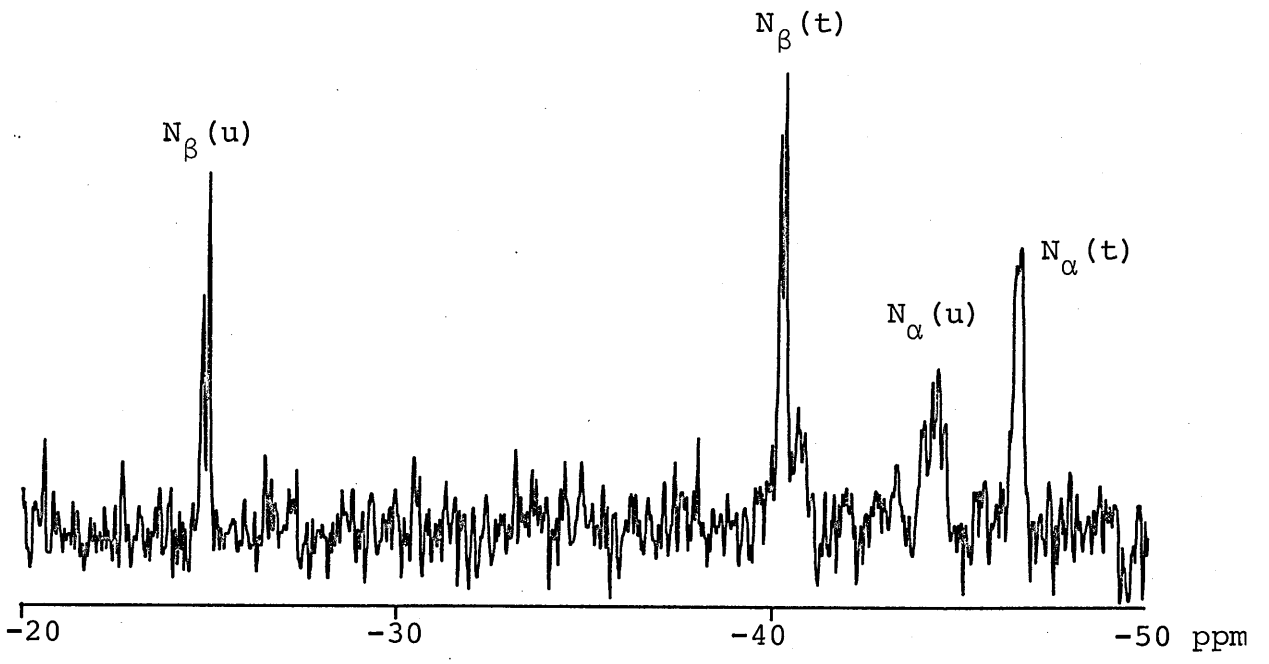

The chemical shifts and coupling constants in this system are:

$\delta^{15}N_\beta$(u) -25.0 ppm (d) $^1J_{NN}$ = 6Hz

$\delta^{15}N_\beta$(t) -40.3 ppm (d) $^1J_{NN}$ = 5Hz

$\delta^{15}N_\alpha$(u) -44.4 ppm (dd) $^2J_{NP}$ = 8Hz

$\delta^{15}N_\alpha$(t) -46.1 ppm (M)

u = unique N_2 ligand

t = trans N_2 ligands

This system should provide some very interesting results in the future when NMR studies of its protonation reactions are undertaken.

6.6 General conclusions

The NMR studies of protonation that have been discussed above show that such techniques can be a sensitive probe of reaction characteristics. The general pathway for protonation of dinitrogen has been given further support and it has been shown that the sequence:

$$M(N_2) \longrightarrow M(N_2H) \longrightarrow M(N_2H_2)P_4 \longrightarrow M(N_2H_2)P_3$$

seems to be the common feature. For the PMe_3 dinitrogen complexes, other short-lived hydrazido(2-)-species have been determined and the possible detection of a diazenido-species reported. The seemingly anomalous, low NH_3 yields of cis-$[W(N_2)_2(PMe_3)_4]$ have been explained by ^{15}N NMR spectroscopy, with detection of a long-lived acid-stable hydrazido(2-)-species.

Essential differences between the pathways for reduction of $[MoI_2(N_2H_2)(PMe_2Ph)_3]$ and cis-$[Mo(N_2)_2(PMe_2Ph)_4]$ have been highlighted and attempts made to assign intermediates after the hydrazido(2-)-stage.

Some of the results from these studies are not easy to interpret in isolation, but in conjunction with complementary studies, such as stopped-flow spectrophotometry and the isolation of intermediates, should lead to a better understanding of these protonation reactions. It is hoped that with further work in this area, detailed mechanisms of the

pathways by which N_2 is reduced at the metal site may be produced and the effect of variables such as acid and solvent rationalised. Such work may give clues to how dinitrogen is reduced at the enzymatic level by nitrogenase in the natural system.

CHAPTER 7

Concluding Remarks and Preliminary Studies of a Molybdo-Enzyme by ^{95}Mo NMR Spectroscopy

7.1 Study of the active site of Xanthine Oxidase

(In co-operation with R.C. Bray and G.N. George).

7.1.1 Introduction

(Reference: "Molybdenum and Molybdenum Containing Enzymes" Ed. M.P. Coughlan, Pergamon Press, 1980).

Xanthine oxidase is a much studied enzyme found widely distributed throughout the animal kingdom, including man, although its physiological role in mammals is still something of a mystery. The enzyme catalyses the hydroxylation of carbon atoms in certain compounds, especially the purines as shown below for xanthine [Reaction (7.1)].

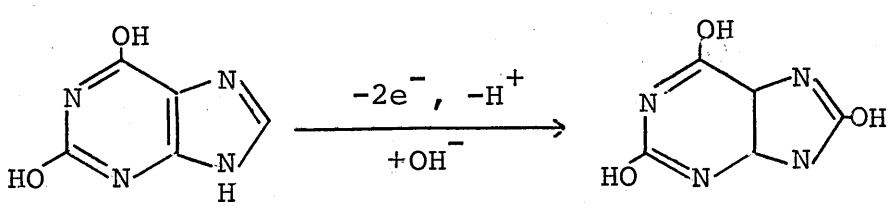

(7.1)

Xanthine Uric acid

The important feature of xanthine oxidase, in common with several other hydroxylase enzymes, is that it contains molybdenum at the active site in a cofactor (Moco). Various techniques including EPR and EXAFS have been used to probe the structure of the active site. The oxidised, active

enzyme centre appears to be Mo(VI) and it contains a S atom which may react with cyanide anion. Such observations coupled with EXAFS data give the proposed Scheme shown below:

Scheme (7.1):

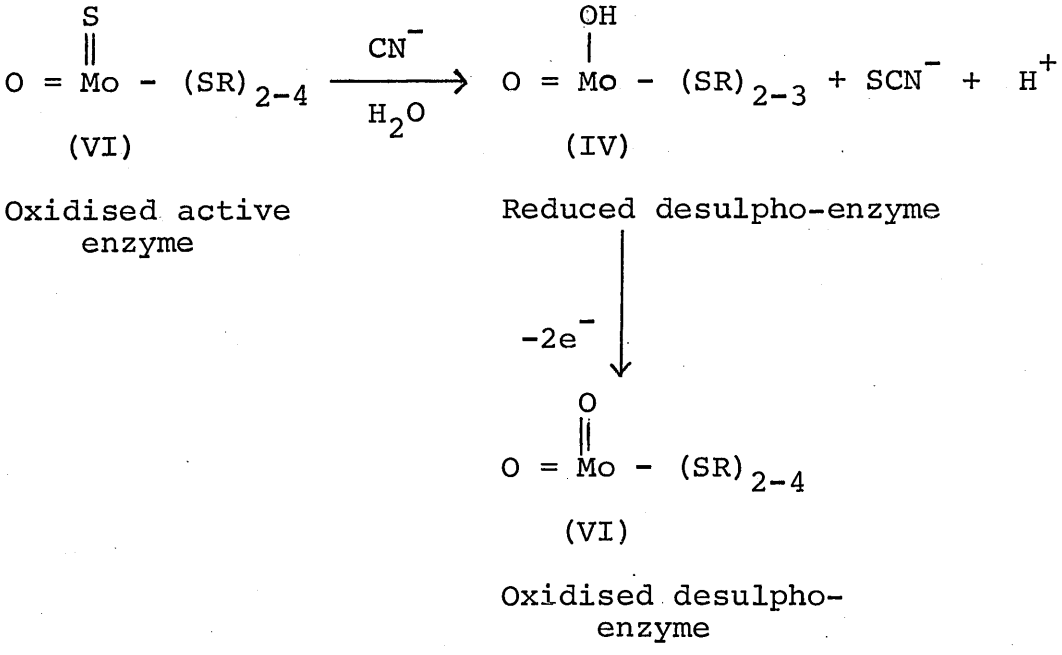

SR = thiol type ligand

During enzyme turnover, Mo cycles through the (IV), (V) and (VI) oxidation states. EPR may be used to study the d^1, Mo(V) state but no such probe exists for the even oxidation states.

At the beginning of Chapter 4 it was mentioned that several ^{95}Mo studies concerned with possible models of the xanthine oxidase active site have been undertaken. Associated with these have been various unsuccessful attempts to observe ^{95}Mo signals from the enzyme itself. Given below are details of our attempts to observe ^{95}Mo signals from enzyme enriched in ^{95}Mo.

7.1.2 ^{95}Mo NMR experiments

7.1.2.1 The enzyme

The high-power CXP300 NMR spectrometer was chosen for the study because of the RIDE facility which would be particularly important for the very broad signals expected from the enzyme.

A ^{95}Mo enriched sample of desulpho-xanthine oxidase ca. 50 mM in an aqueous buffer was run as detailed in the Experimental section. After many scans, no signals attributable to the enzyme were observed. (Spurious noise signals were generated but were discounted after running a control substance,which also gave such signals).

7.1.2.2 The cofactor

On treatment with 6M guanidinium chloride, the enzyme is denatured and unfolds to release the Moco in some form. The exact nature of solutions containing this "free" cofactor is unknown; such solutions are very air-sensitive but the concentration of Mo obtainable is larger than for intact enzyme. The spectrum of such a solution was accumulated for several extended periods but no assignable signals were observed. It should be stated, however, that in these preliminary experiments the NMR spectrometer was not operating under optimum conditions.

7.1.3 Discussion

The negative result obtained for the enzyme is not altogether surprising bearing in mind the low concentration of Mo, despite enrichment, and the large protein molecular weight leading to large correlation times and linewidths as discussed in Chapter 2. The "free" cofactor might be expected to have a smaller correlation time as it is likely to be "dangling" away from the bulk of the protein. This, coupled with the higher solubility, should provide much more favourable conditions for observation of a ^{95}Mo NMR signal. The failure to do so may be due to the instrumental problems and clearly further work with optimised conditions are required.

As an example of the type of signals the spectrometer system used can detect when optimised, the five-coordinate nitrosyl complex $[PPh_4][Mo(SAr)_4(NO)]$ (Ar = C_6H_4Cl-4) may be considered. A solution of this complex in CH_2Cl_2 gave a signal after an overnight accumulation with a $W_{\frac{1}{2}}$ of *ca.* 8000 Hz and a ^{95}Mo chemical shift of +1300 ppm.

Such results are encouraging and suggest that if Moco gives reasonable linewidths (<10 kHz), detection of ^{95}Mo signals should be possible.

7.2 Some general comments

The preliminary investigations above, although unsuccessful, demonstrate the potential information that could be obtained if the ^{95}Mo NMR spectroscopic technique

is developed far enough. The rapid advances over the past few years in the technique have been followed by periods of consolidation . The ^{95}Mo NMR studies in this thesis have shown that data obtained may be interpreted usefully, chemical shift regions have been defined reflecting ligand properties, especially of those ligands important to nitrogen fixation, such as dinitrogen.

In the field of ^{15}N NMR spectroscopy, the complexity and sensitivity of the ^{15}N chemical shift to ligand environment has been demonstrated, but even amid such complexity, some good predictive information has been obtained especially as regards ligand geometry. Another complicated area is the protonation work, and again, application of the NMR technique has supplied some answers and also, obviously, posed some interesting questions.

In the future, improvements in NMR spectrometer sensitivity, and particularly important for ^{95}Mo, improvements in the design of probes and receiver circuitry will increase the applicability of ^{15}N and ^{95}Mo NMR spectroscopy to problem solving. More information could be squeezed out of existing hardware using sophisticated pulse sequences as already demonstrated by INEPT and RIDE. Perhaps some of the greatest advances are to be made in the field of solid-state NMR, with study of ^{15}N becoming more widespread and "routine" high resolution solid-state ^{15}N NMR experiments are on the horizon. Some developmental work is required to extend this technique to ^{95}Mo, but in theory it is possible, with the attraction that solubility constraints disappear.

It is clear that ^{15}N and ^{95}Mo NMR spectroscopy will become increasingly useful tools in the study of nitrogen fixation in the future.

EXPERIMENTAL

General

Air-sensitive materials were handled, using standard Schlenk and vacuum-line techniques, under an inert atmosphere of dinitrogen or argon. ^{15}N-labelled dinitrogen complexes were handled under argon. Some very air-sensitive complexes were handled in a glove box under dinitrogen or a glove bag under argon. All solvents were dried over suitable agents and freshly distilled under dinitrogen before use.

Cyclic voltammetry was performed at ambient temperature in a three-electrode, two compartment cell containing 0.2M $[Bu_4N][BF_4]$ supporting electrolyte in thf under dinitrogen. Measurements were made with a Chemical Electronics waveform generator type RB1 and a potentiostat type TR70/2A and recorded on a Bryans XY recorder model 24000 A4 using a scan speed of 0.3 V s^{-1}. Voltammograms were refereneed internally using the trans-$[Mo(N_2)_2(dppe)_2]^{o/+}$ couple which has $E_{\frac{1}{2}}^{ox}$ = -0.16V versus s.c.e. in the above solvent/electrolyte system.

Infra-red spectra were measured as nujol or hexachlorobutadiene mulls on KBr plates, or in CH_2Cl_2 in a solution infra-red cell, using Pye-Unicam SP3-200 or SP2000 spectrophotometers.

U.V.-visible spectra were measured on a Perkin-Elmer Lambda-5 spectrophotometer in CH_2Cl_2 solution.

Microanalysis was performed by Mrs. G. Olney of the University of Sussex or by Mr. C.J. Macdonald of the Unit of Nitrogen Fixation.

Gas samples were analysed using an AEI MS10 mass spectrometer.

NMR spectroscopy

Chemical shifts should now be quoted as to high/low frequency of the reference but in accordance with common usage the high/low field terminology is used in this thesis. Positive chemical shift (δ) is to low field of the reference (read as high frequency) and vice versa.

^{1}H NMR spectra were run by the author or Mr. C.J. Macdonald in 5 mm tubes on a Jeol FX90Q spectrometer at 89.56 MHz.

^{31}P NMR spectra were similarly run in 10 mm tubes at 36.2 MHz using proton decoupling. Chemical shifts (±0.1 ppm) are referenced to trimethylphosphite (TMP) in C_6D_6 as lock in a 3 mm coaxial tube. TMP = -141 ppm versus 85% H_3PO_4 (the other commonly used reference). Protonation studies were carried out in modified tubes (see later) and shifts referenced to an absolute frequency determined from the external ^{7}Li lock signal.

^{15}N NMR spectra at 18.24 MHz were recorded by Mr. M. Cooper at P.C.M.U. Harwell on a Bruker WH180 spectrometer. Samples were run in special glass inserts in 25 mm tubes and referenced to CD_3NO_2 + $Cr(pd)_3$ (30 mg/ml) in a 5 mm O.D. coaxial tube which also acted as lock.

Typical accumulation parameters were:

pulse angle = 30°

acquisition time = 0.333 s.

^{15}N NMR spectra at 36.5 MHz were run by the author on the University of Sussex Bruker WM360 spectrometer. Samples were run in standard 10 mm tubes or in modified tubes [Figure E.1] used for very air-sensitive complexes and protonation reactions. Referencing and locking were achieved as above, by reference to free $^{15}N_2$ (-74 ppm v. $CD_3NO_2/Cr(pd)_3$) or by substitution. In the protonation reactions, lock was provided by the addition of a small amount of toluene-d^8. Chemical shifts are quoted ±0.1 ppm and unless otherwise stated are relative to $CD_3NO_2/Cr(pd)_3$ (0.12 M). Shifts may be converted to the neat nitromethane scale by the addition of 3.4 ppm.[1]

Typical accumulation parameters:

Data size = 32K

Total spectrum sweep width = 20 KHz (ca. 550 ppm)

Pulse angle = 22.5° (10 μs on WM360)

This gives an acquisition time of ca. 0.82 s and obviates the need for a relaxation delay.

Final spectrum resolution is 1.2 Hz per data point although this may be halved by adding 32K of zeros to the end of the FID and transforming the whole 64K (known as "zero filling" which also enhances the signal to noise ratio). It should be stressed, however, that the amount of information collected in an experiment depends on the initial data point resolution. Protonation reactions were run using 16K data points to decrease accumulation time.

Coupling constants were measured from the spectra (no signs were determined) and the limit of resolution typically imposes an uncertainty of at least ±0.5 Hz on J values.

Figure (E.1). Cross-section through modified tube used for very air-sensitive complexes and protonation reactions

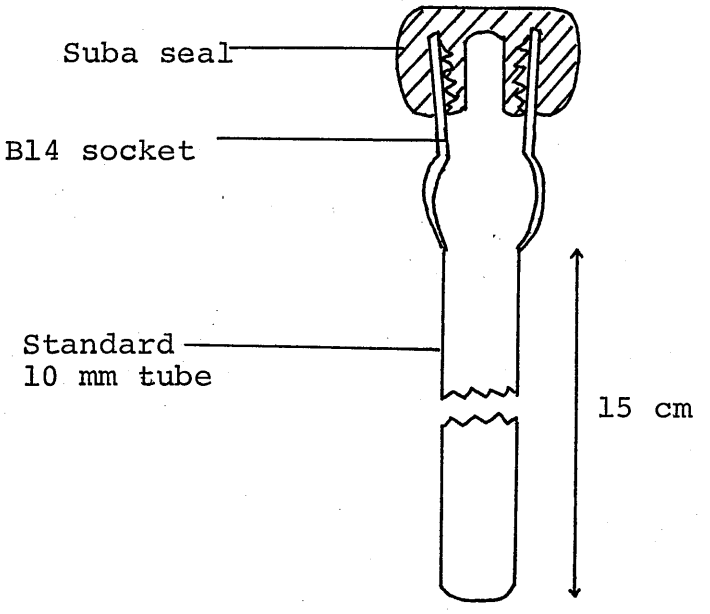

^{95}Mo NMR spectra at 5.80 MHz were measured by the author or Mr. C.J. Macdonald on a Jeol FX90Q spectrometer. Spectra were run externally locked (^{7}Li) as the field drift on electromagnet-type instruments may be large. All ^{95}Mo spectra run here and below were referenced to 2M aqueous Na_2MoO_4 at pH 11 by substitution and chemical shifts are quoted $\pm$ 1 ppm. The sample may be spun if desired but no significant improvement in resolution is observed. Typically pulse repetition rates of 0.1 s were used. Pre-acquisition delays in excess of 200 μs were used to minimise the effects of probe ringing. 90° pulses may be used without saturation.

^{95}Mo NMR spectra at 26.08 MHz were measured by the author or Dr. E.H. Curzon on the University of Warwick Bruker WH400 spectrometer. Pulse repetition rates of 0.01 s may be used for rapid accumulation but up to 0.05 s was

commonly employed. An example is an acquisition time of 0.017 s produced by a sweep width of 30 KHz (ca. 1000 ppm) in 1K data points. The inherent ring-down time of the low-frequency probe on this instrument means that only short pre-acquisition delays were required. Baseline distortion was removed by zeroing data points at the start of the FID. FID's were typically zero-filled up to 8 or 16K before transformation.

^{95}Mo NMR spectra at 23.46 MHz were run by the author on the University of Sussex Bruker WM360 instrument using similar parameters to those used on the WH400. However, the WM360 makes use of a high Q factor broad-band VSP probe which has very bad ring-down characteristics and pre-acquisition delays of up to 600 μs had to be used in some cases. The 90° pulse length was ca. 50 μs.

^{95}Mo NMR spectra at 19.54 MHz were measured by the author, Dr. P.S. Belton (AFRC Food Research Institute, Norwich) or Miss I.J. Cox (University of East Anglia) using the F.R.I. Bruker CXP300 spectrometer. In contrast to the above spectrometers, which have longitudinal probes and standard (or slightly modified) 10 mm tubes, the CXP300 has a transverse probe and short (ca. 5 cm) 10 mm diameter tubes must be used, which have a volume of ca. 2.5 cm^3. For air-stable complexes the tube design in Figure (E.2a) may be used but for sensitive complexes, tubes were flame sealed under vacuum [Figure (E.2b)].

Figure (E.2).

a)

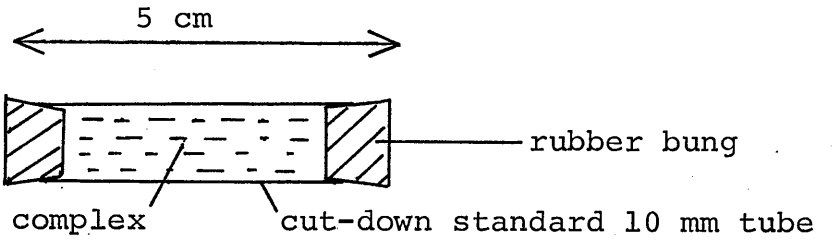

b)

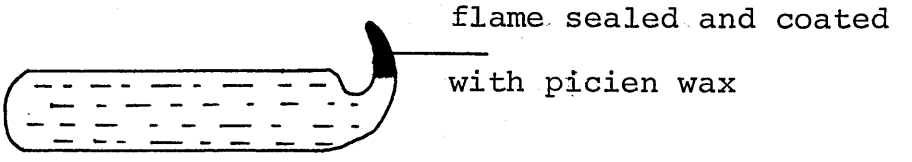

It is very difficult to seal the tubes without a bubble being trapped in the tube but fortunately this does not interfere with the NMR experiment. Short ring-down times were achieved using a version of the RIDE pulse sequence discussed in Chapter 2.

^{17}O NMR spectra at 48.82 MHz were measured by the author on the University of Sussex Bruker WM360 instrument. Complexes were run in standard 10 mm tubes without lock or spinning. All chemical shifts are quoted relative to H_2O measured by substitution. Shifts are ±1 ppm. Typical parameters for the ^{17}O spectra are:

90° pulse ca. 27 μs, sweep width 50 KHz (ca. 1000 ppm) using 1K data points giving a repetition rate of ca. 0.01 s. A pre-acquisition delay of 100 μs was employed to reduce baseline distortion.

Starting materials and labelled compounds

Unless otherwise stated, starting materials were prepared by standard, published methods.

Labelled materials: $^{15}N_2$ (95%), ^{15}NO (95%), $^{15}N_2H_4 \cdot H_2SO_4$ (95%), $Ph^{15}NH_2$ (95%) and $Na^{15}NO_2$ (98%) were obtained from Prochem Ltd.

All syntheses detailed below involving ^{15}N labelled materials were first performed, and in some cases optimised, using unlabelled compounds. References for particular syntheses may be found in the relevant Chapter unless otherwise indicated. ^{15}N labelled dinitrogen complexes were generally prepared by exchange reactions as detailed in reference 2.

Experimental details for Chapter 3

Nitrosyl complexes

trans-[MoBr(^{15}NO)(dppe)$_2$]

Triethylamine (0.064 ml, 1 mole equivalent) and thf (ca. 50 ml) were distilled *in vacuo* on to trans-[MoBr(N_2H_2)(dppe)$_2$]Br (0.5 g), prepared by the literature method[3], at -196°C. 2 mole equivalents of ^{15}NO gas were condensed on to the mixture which was then allowed to warm to ambient temperature and stirred overnight. The solution was refrozen and the amount of gas evolved measured via a Töepler system and identified by mass spectrometry (ca. 1 mole $^{14}N_2$ and traces of $^{15}N_2$). Solvent volume was reduced and on addition of MeOH a yellow solid precipitated. This was filtered and washed with H_2O, MeOH and Et_2O and dried. Recrysallisation from CH_2Cl_2/MeOH gave yellow crystals (0.27 g, ca. 60%).

trans-[Mo(NCMe)(^{15}NO)(dppe)$_2$][BF_4]

trans-[MoBr(^{15}NO)(dppe)$_2$] (0.25 g) was refluxed in MeCN (ca. 50 ml) with $TlBF_4$ (0.28 g, 5 mole excess) for 30 minutes. The mixture was filtered, solvent removed *in vacuo*, CH_2Cl_2 (10 ml) added, the resulting orange solution filtered, and Et_2O added to give orange crystals (0.24 g, 90%). This complex was converted into trans-[Mo(NCMe)(^{15}NO)(dppe)$_2$][BPh_4] by stirring in MeOH with ca. 2 mole excess of $NaBPh_4$, filtering and washing the brown-orange precipitate with MeOH and drying.

trans-[MoF(^{15}NO)(dppe)$_2$]

Reflux of trans-[Mo(NCMe)(^{15}NO)(dppe)$_2$][BF_4] (0.36 g) in thf/MeOH (1:1, ca. 50 ml) gave the fluoride complex but the yield was improved when KF (0.2 g, 10 mole equivalents) was added. After 2 hours solvent was removed, CH_2Cl_2 added, the solution filtered and addition of Et_2O gave yellow crystals (0.25 g, 75%).

trans-[MoX(^{15}NO)(dppe)$_2$] (X = I, NCO, SCN, N_3 or OPh)

These were all prepared in a similar manner and in similar yield, an example being trans-[Mo(NCO)(^{15}NO)(dppe)$_2$].

trans-[Mo(NCMe)(^{15}NO)(dppe)$_2$][BPh_4] (0.3 g) was refluxed overnight with KNCO (0.09 g, 5 mole excess) in thf/MeOH (1:1, 50 ml). After removal of solvent, CH_2Cl_2 was added, the solution filtered and MeOH added to give yellow crystals (0.15 g, 65%).

trans-[Mo(OH)(^{15}NO)(dppe)$_2$]

trans-[Mo(NCMe)(^{15}NO)(dppe)$_2$][BPh_4] (0.6 g) was stirred overnight in thf (∿50 ml) with Bu_4NOH (10 ml of a 0.1M solution in toluene/MeOH, ca. 2 mole excess). All solvent was removed and toluene added, the solution was then filtered and solvent removed. Stirring with MeOH produced a yellow solid which was filtered, washed with MeOH, pentane and then dried. Recrystallisation from CH_2Cl_2/MeOH gave yellow crystals (0.29 g, 66%).

trans-[MoQ(^{15}NO)(dppe)$_2$] (Q = CN or SPh)

Both complexes were prepared in a similar manner. trans-[Mo(CN)(^{15}NO)(dppe)$_2$] was prepared by refluxing trans-[Mo(OH)(^{15}NO)(dppe)$_2$] (0.15 g) overnight in thf (ca. 50 ml) with Me_3SiCN (0.1 ml, ca. 5 mole excess). MeOH (ca. 1 ml) was added with care to destroy unreacted Me_3SiCN and then all solvent removed. Addition of CH_2Cl_2/Et_2O gave orange crystals (0.09 g, 60%).

Diazenido-complexes

trans-[MoBr($^{15}N_2$Et)(dppe)$_2$] was made from trans-[Mo($^{15}N_2$)$_2$(dppe)$_2$] using the method published for unlabelled complex. Labelling was to ca. the 50% level.

trans-[Mo(NCMe)($^{15}N_2$Et)(dppe)$_2$][BPh_4]

trans-[MoBr($^{15}N_2$Et)(dppe)$_2$] (0.95 g) was refluxed for 2 hours in MeCN (ca. 50 ml) with $TlBF_4$ (0.5 g, ca. 2 mole excess). Solvent was removed, CH_2Cl_2 added and the solution filtered. Solvent was again removed, MeOH (ca. 50 ml) and $NaBPh_4$ (0.32 g, 1 mole equivalent) were added to give a green precipitate which was filtered off and washed with MeOH, Et_2O and then dried (0.9 g, 70%).

trans-[MoY($^{15}N_2$Et)(dppe)$_2$] (X = SCN, NCO or N_3)

These complexes were prepared in a similar manner. trans-[Mo(SCN)($^{15}N_2$Et)(dppe)$_2$] was synthesised by refluxing trans-[Mo(NCMe)($^{15}N_2$Et)(dppe)$_2$][BPh_4] (0.32 g) overnight

with NaSCN (0.1 g, ca. 5 mole excess) in thf/MeOH (1:1, ca. 50 ml). Solvent was removed, CH_2Cl_2 (10 ml) added and the orange solution filtered. Addition of Et_2O gave a red/brown powder which was filtered off, washed with Et_2O and dried (0.15 g, 60%).

trans-[Mo(NCR)($^{15}N_2$Et)(dppe)$_2$][BPh_4] (R=C_6H_4Z-4; Z=H, MeO or MeCO)

These complexes were prepared by a similar route. trans-[Mo(NCC_6H_5)($^{15}N_2$Et)(dppe)$_2$][BPh_4] was prepared by refluxing trans-[Mo(NCMe)($^{15}N_2$Et)(dppe)$_2$][BPh_4] (0.25 g) for 1 hour, with benzonitrile (0.25 ml, ca. 10 mole excess) in thf (ca. 40 ml). Solvent was removed and the solid produced washed with Et_2O (0.19 g, 70%).

Experimental details for Chapter 4

trans-$[Mo(N_2)_2(dArpe)_2]$ (Ar = C_6H_4Me-3 and C_6H_5) were synthesised by the author using standard methods and other complexes (Ar = C_6H_4Z-4; Z = MeO, Me, Cl or CF_3) were prepared by Miss H. Mohd-Ali.[4] PMe_3 dinitrogen complexes were kindly supplied by Professor E. Carmona, the ^{15}N labelled analogues were obtained by exchange as noted below. *trans*-$[Mo(N_2)_2(PMe_2Ph)(dppe)]$ and *cis*-$[Mo(N_2)_2(PMe_2Ph)_4]$ were prepared by Mr. F. O'Flaherty and *mer*-$[Mo(N_2)_3(PPr^n{}_2Ph)_3]$ was kindly supplied by Miss C. Shortman. *cis*-$[Mo(CO)_2(dArpe)_2]$ (Ar = C_6H_4Z-4; Z = H or OMe) were prepared by standard methods as were the other $[MoLL'(dppe)_2]$ complexes. *trans*-$[Mo(CO)_2(dppe)_2]$ was prepared for ^{95}Mo NMR spectroscopic study, just prior to use, by bubbling CO through a solution of *trans*-$[Mo(CO)(NCC_6H_4OMe\text{-}4)(dppe)_2]$. The complexes *trans*-$[MoL_2(PMe_3)_4]$ (L = CO_2 or C_2H_4) were kindly supplied by Professor E. Carmona.

Experimental details for Chapter 5

$[Ph^{15}N_2][BF_4]$ was made from $Ph^{15}NH_2$ and $Na^{15}NO_2$ using published procedures. The diazenido-complexes were made by methods given in the literature (as referenced in Chapter 5) using the appropriately labelled diazonium salt except for $[OsH(CO)(^{15}N_2Ph)(PPh_3)_2]$, $[RhCl(^{15}N_2Ph)(PMePh_2)_3][PF_6]$ and $[Ir(^{15}N_2Ph)(dppe)_2][PF_6]_2$ which were kindly supplied by Dr. B.L. Haymore as were $[ReCl_2(NO)(^{15}N_2HPh)(PPh_3)_2]$, $[ReHCl(NO)(^{15}N_2HPh)(PPh_3)_2]$ and $[ReBr_2(^{15}N_2Ph)(^{15}N_2HPh)(PPh_3)_2]$. The imido-complex cis-$[Mo(^{15}NPh)_2(S_2CNMe_2)_2]$ was prepared using the literature method employing labelled $Ph^{15}NNN$ prepared from $[Ph^{15}NN][BF_4]$. trans-$[ReCl(^{15}NPh)(S_2CNEt_2)_2]$ was synthesised as published using $Ph^{15}N{=}PPh_3$ prepared from $Ph^{15}NN$ and converted to trans-$[ReOEt(^{15}NPh)(S_2CNEt_2)_2]$.

The nitride complex trans-$[ReCl(^{15}N)(dppe)_2]Cl$ was synthesised by a literature method[5] from $[Re(^{15}N)Cl_2(PPh_3)_2]$ prepared following a published procedure[6] using $^{15}N_2H_6SO_4$. Crystals for X-ray analysis were grown from CH_2Cl_2/Et_2O. $[ReCl_2(^{15}N)(PEt_2Ph)_3]$ was also prepared from $[Re(^{15}N)Cl_2(PPh_3)_2]$ using the method for unlabelled complex;[6] ^{15}N NMR was run in the presence of an excess of PEt_2Ph to prevent formation of the bis-phosphine complex. trans-$[MoN_3(^{15}N)(dppe)_2]$ was prepared by stirring trans-$[MoBr(^{15}N)(dppe)_2]$, synthesised by Dr. W. Hussain,[7] in thf with an excess of $Bu_4N\ N_3$ for 30 mins; removal of solvent followed by addition of MeCN gave a yellow solid which was filtered, washed with pentane and dried [$\nu(N_3)$ = 2050 cm^{-1}, $\nu(Mo{\equiv}^{15}N)$ = 950 cm^{-1}].

The oxo-complexes $[MoOCl_2P_3]$ (P = PMe_2Ph or PEt_2Ph) were prepared by the published method[8] from $MoCl_5$, EtOH and the phosphine. The blue and green forms of $[MoOCl_2(PMe_3)_3]$ were kindly supplied by Professor E. Carmona.

Experimental details for Chapter 6

Protonation time courses

The NMR studies followed the same general pattern and were performed in the NMR tube shown in Figure (E.1). Typically, a suspension or solution of complex in the required solvent was introduced into the tube and this was then sealed with a suba-seal. Sufficient volume (>4 ml) was used to prevent vortexing when the tube was spun. Lock was provided by a deuterated solvent usually toluene d^8 but for ^{31}P NMR experiments the external lock facility could be utilised. Several methods of supplying acid were employed:

i) Me_3SiX was introduced by syringe through the suba-seal into a solution containing sufficient MeOH to generate HX *in situ*.

ii) Me_3SiX was introduced as above but directly to the reaction solution for which the solvent was MeOH, generating HX *in situ* as above.

iii) A standard solution of HX was made by reacting Me_3SiX with MeOH and an aliquot of this solution introduced via the suba-seal to the reaction mixture.

CARE! When working with dinitrogen complexes, on addition of acid, a rapid evolution of dinitrogen gas is produced and some of this should be allowed to purge from the tube to prevent excessive build-up of pressure.

Acid was usually introduced while the tube was cooled to *ca*. -60°C in a dry ice/industrial methylated spirit bath. Details of time courses are given in Chapter 6.

trans-[Mo$(N_2)_2$(triphos)(PPh_3)] was synthesised by the published method using a PARR-bomb and a pressure of ca. 8 atm of dinitrogen. Sodium amalgam had to be used as the reductant, as Mg proved ineffective in this preparation. trans-[Mo$(^{15}N_2)_2$(triphos)(PPh_3)] was prepared in a standard manner by exchange of unlabelled material in thf, over ca. 3 hours, using 1 atm of $^{15}N_2$ gas. Ca. 60% exchange was achieved: $\nu(^{14}N_2)_2$ = 1950 cm^{-1}, $\nu(^{14}N_2, ^{15}N_2)$ = 1930 cm^{-1} and $\nu(^{15}N_2)_2$ = 1885 cm^{-1}. Protonation was performed in thf with Me_3SiBr using method (i).

cis-[Mo$(^{15}N_2)_2(PMe_3)_4$], [Mo$(^{15}N_2)(PMe_3)_5$] and cis-[W$(^{15}N_2)_2(PMe_3)_4$] were made by the author, Mr. A. Galindo or Dr. R.L. Richards by exchange of the unlabelled complex as supplied by Professor E. Carmona.

^{15}N NMR spectra of the dinitrogen complexes in thf solution were accumulated, then solvent was removed in vacuo and MeOH added. Protonation using Me_3SiCl was performed by method (ii).

trans-[MoCl$(^{15}N_2H_2)(PMe_3)_4$]Cl synthesised by Mr. A. Galindo was protonated in a similar manner.

cis-[Mo$(^{15}N_2)_2(PMe_2Ph)_4$] was prepared in the standard way from unlabelled complex. [Mo$I_2(^{15}N_2H_2)(PMe_2Ph)_3$] was prepared by the published method using the labelled dinitrogen complex. Protonation reactions using Me_3SiI, on solutions in dme, were performed by method (iii).

Experimental details for Chapter 7

Bovine milk xanthine oxidase extracted from the milk of a cow fed on enriched $^{95}MoO_4^{2-}$, was supplied by Dr. R.C. Bray and Dr. G.N. George of Molecular Sciences, University of Sussex. Desulpho-xanthine oxidase for the ^{95}Mo NMR experiment was prepared as a saturated solution in BICINE [N,N-bis(2-hydroxyethyl)glycine] buffer and run in the tube type shown in Figure (E.2a).

The Moco solution was prepared by adding 6M guanidinium chloride to freeze-dried xanthine oxidase in BICINE buffer, under dinitrogen. The solution was run anaerobically in tube type (E.2b).

$[PPh_4][Mo(SC_6H_4Cl\text{-}4)_4(NO)]$ was kindly supplied by Mr. P.T. Bishop.

REFERENCES - EXPERIMENTAL

1. S. Donovan-Mtunzi, D. Phil. Thesis, University of Sussex, 1982.
2. M.E. Fakley, D. Phil. Thesis, University of Sussex, 1979.
3. J. Chatt, G.A. Heath and R.L. Richards, J.Chem.Soc. Dalton Trans., 1974, 2074.
4. H. Mohd-Ali, D. Phil. Thesis, University of Sussex, 1984.
5. N.P. Johnson, J.Inorg.Nucl.Chem., 1973, 35, 3141.
6. J. Chatt, C.D. Falk, G.J. Leigh and R.J. Paske, J.Chem.Soc.(A), 1969, 2288.
7. W. Hussain, G.J. Leigh and C.J. Pickett, J.Chem.Soc. Chem.Comm., 1982, 747.
8. A.V. Butcher and J. Chatt, J.Chem.Soc.(A), 1970, 2652.

Appendix 1. Relaxation mechanisms for spin $\frac{1}{2}$ nuclei (^{15}N)

There are two types of relaxation process: Spin-lattice or longitudinal relaxation characterised by a time T_1 and spin-spin or transverse relaxation characterised by a time T_2.

Spin-spin relaxation does not involve loss of energy, rather it involves loss of phase coherence between nuclear spins after the initial magnetisation. The T_2 value for this relaxation is determined by the interaction of the nuclear spins and also the inhomogeneity of the magnetic field.

Spin-lattice relaxation is the process by which energy is lost from the spins to the surroundings to achieve the equilibrium distribution. This process is dependent on interaction of nuclear spins with randomly fluctuating magnetic fields in the surroundings (the lattice) generated by the molecular motion of the spin-system and the lattice. There are several mechanisms by which this energy exchange is brought about.

"Extreme narrowing"

The efficiency of the exchange mechanism is determined by the intensity of fluctuations at the resonance frequency (ω_o in radians). As defined in Chapter 2, the correlation time τ_c defines the motion of a spin-system. Most efficient relaxation occurs when $\omega_o \tau_c = 1$ but the extreme narrowing condition occurs when $\omega_o^2 \tau_c^2 \ll 1$ and under this regime the motional part of relaxation equations are independent of the

applied field. It can be seen that the condition breaks down for long correlation times (macromolecules or viscous solutions) or at high fields. Under extreme narrowing $T_1=T_2$.

Contribution to T_1^{obs}

For a spin $\frac{1}{2}$ nucleus the observed spin-lattice relaxation time is a combination of contributions from different mechanisms:-

$$\frac{1}{T_1^{obs}} = \frac{1}{T_1^{DD}} + \frac{1}{T_1^{SA}} + \frac{1}{T_1^{SC}} + \frac{1}{T_1^{SR}} + \frac{1}{T_1^{e}} \qquad \text{(A1.1)}.$$

Dipole-dipole relaxation (DD)

There are three main types of DD relaxation:

a) Intramolecular one-bond interactions
b) Intermolecular interactions
c) Intermolecular long-range interactions

} usually via the proton

The intramolecular contribution to T_1 in extreme narrowing is given by

$$\frac{1}{T_1^{DD}(intra)} = \frac{\mu_o^2 \hbar^2 n_H \gamma_N^2 \gamma_H^2 r_{NH}^{-6} I(I+1) \tau_c}{12\pi^2} \qquad \text{(A1.2)}$$

r_{NH} → important only for directly protonated ^{15}N

μ_o = permeability of free space

n_H = number of protons at distance r_{NH}

The intermolecular DD relaxation rates is given by equation (A1.3).

$$\frac{1}{T_1^{DD}(\text{inter})} = \frac{\mu_o^2 \hbar^2 \gamma_N^2 \gamma_H^2 I(I+1)}{90\pi} \frac{N}{Da} \qquad \text{(A1.3)}$$

D = mutual translational diffusion constant

a = distance of closest approach

N = concn. of ^{15}N and ^{1}H spins

This mechanism can be important for ^{15}N, relaxation occurring via the protons of the solvent.

Shielding anisotropy relaxation (SA)

The shielding anisotropy is the difference between the parallel and perpendicular tensor elements, for an axial symmetric system. $\Delta\sigma = \sigma_{\parallel} - \sigma_{\perp}$

The equation for SA relaxation time is shown:

$$\frac{1}{T_1^{SA}} = \frac{2}{15} \gamma_N^2 B_o^2 (\Delta\sigma)^2 \tau_c (1+\omega_o^2 \tau_c^2)^{-1} \qquad \text{(A1.4)}$$

↑ not important for extreme narrowing

SA relaxation will be important at high fields and for nitrogen with large shielding anisotropy.

Scalar relaxation (SC)

SC relaxation of a nucleus A arises through the scalar J coupling to other nuclei. There are two types: the "first kind" occurs when J coupling is interrupted by exchange processes and the "second kind" results through the T_1 relaxation of a coupled quadrupolar nucleus X. This gives:

$$\frac{1}{T_1}_{SC} = \frac{8\pi^2}{3} J_{AX}^2 \, I_X(I_X+1) \quad \frac{\tau_{SC}}{1+(\omega_X-\omega_A)^2 \, \tau_{SC}^2} \qquad \text{(A1.5)}$$

τ_{SC} = scalar coupling correlation time $\approx T_1$ for X nucleus. This mechanism has an effect if $T_1(X) << (J_{AX})^{-1}$ and if the Larmor frequencies ω_X and ω_A are close. The mechanism is more important at low fields.

Other mechanisms

Spin-rotation (SR) is important for systems with rapid molecular rotation as in small molecules at high temperature or for freely rotating groups such as methyl substituents. The mechanism becomes more efficient as temperature is increased (c.f. DD and SA) and is dominant in the gas-phase. Relaxation via paramagnetic substances is particularly effective at reducing T_1 values.

References - Chapter 1

1. "Advances in Nitrogen Fixation" Proceedings of the 5th International Symposium on Nitrogen Fixation, Eds. C. Veeger and W.E. Newton, Nijhoff Junk, The Hague, 1984.
2. R.A. Henderson, G.J. Leigh and C.J. Pickett, Adv.Inorg. Chem.Radiochem., 1983, 27, 197.
3. "Nitrogen Fixation: The Chemical-Biochemical-Genetic Interface" Eds. A. Müller and W.E. Newton, Plenum Press, New York, 1983.
4. G.P. Roberts and W.J. Brill, "Ann.Rev.Microbiol", Eds. M.P. Starr, J.L. Ingraham and A. Balous, Vol.35, p.207, "Genetics and Regulation of Nitrogen Fixation", Annual Rev. Inc., 1981.
5. J.R. Postgate, "The Fundamentals of Nitrogen Fixation", Cambridge University Press, 1982.
6. B.E. Smith, R.A. Dixon, T.R. Hawkes, Y.C. Liang, P.A. McLean and J.R. Postgate, ref. 1, p.139.
7. B.M. Hoffman, J.E. Roberts and W.H. Orme-Johnson, J.Am.Chem.Soc., 1982, 104, 860.
8. B.E. Smith in ref. 3, p.23, and references therein.
9. R. Zimmerman and A.X. Trautwein in ref. 3, p.63 and references therein.
10. K.O. Hodgson in "Nitrogen Fixation" volume 1, p.261, University Park Press, Baltimore, 1980.
11. T.R. Hawkes, D.J. Lowe and B.E. Smith, Biochem.J., 1983, 211, 495.

12. D.J. Lowe, R.N.F. Thorneley and J.R. Postgate, in ref. 1, p.133.

13. R.N.F. Thorneley and D.J. Lowe, Biochem.J., in press.

14. A.E. Shilov in "New Trends in the Chemistry of Nitrogen Fixation" Eds. J. Chatt, L.M. da Câmara Pina and R.L. Richards, Chapter 5, Acad. Press, London 1980.

15. G.N. Schrauzer, ibid, Chapter 4.

16. C.J. Pickett in Proc. Cr, Mo, W Conference, University of Sussex, 1983.

17. B.E. Smith, D.J. Lowe, J.R. Postgate, R.L. Richards and R.N.F. Thorneley, "Current Perspectives in Nitrogen Fixation" Proc. Fourth Int.Symp. Nitrogen Fixation, Eds. A.H. Gibson and W.E. Newton, p.68. Australian Academy of Science, Canberra 1981.

References - Chapter 2

1. G.J. Martin, M.L. Martin and J-P. Gouesnard, "NMR Basic Principles and Progress" Ed. P. Diehl, E. Fluck and R. Kosfeld. Volume 18, "^{15}N-NMR Spectroscopy", Springer-Verlag, Berlin 1981.
2. G.C. Levy and K.R. Lichter, "^{15}N NMR Spectroscopy", Wiley, New York, 1979.
3. W. Witanowski, L. Stefaniak and G.A. Webb, "Annual Reports on NMR Spectroscopy", Ed. G.A. Webb, Vol. 11B, "Nitrogen NMR Spectroscopy", Academic Press, London, 1981.
4. a) J. Mason, Chem.Rev., 1981, 81, 205.
   b) Chem. in Brit., 1983, 654.
5. S. Donovan-Mtunzi, D. Phil. Thesis, 1982.
6. C. Brevard and P. Granger, "Handbook of High Resolution Multinuclear NMR", Wiley, 1981.
7. M.L. Martin, J-J. Delpvech and G.J. Martin, "Practical NMR Spectroscopy", Heyden, 1980.
8. D. Shaw, "Fourier Transform NMR Spectroscopy" 2nd Edn., Elsevier, Amsterdam, 1984.
9. K. Mullen and P.S. Pregosin, "Fourier Transform NMR Techniques: A Practical Approach", Academic Press, 1976.
10. T.C. Farrar and E.D. Becker, "Pulse and Fourier Transform NMR", Academic Press, London, 1971.
11. E. Fukishima and S.B.W. Roeder, "Experimental Pulse NMR. A Nuts and Bolts Approach", Addison-Wesley, 1981.
12. Y. Yamamoto and J. Uzawa, Chem.Lett., 1978, 1213.
13. W. Becker, W. Beck and R. Rieck, Z.Naturforsch.B., 1970, 25B, 1332.

14. M. Witonowski, L. Stefaniak, B. Kamienski, S. Biernat and G.A. Webb, J.Magn.Res., 1981, 43, 456.

15. R.K. Harris and B.E. Mann, "NMR and the Periodic Table", Academic Press, 1978.

16. R.G. Kidd, J.Magn.Res., 1981, 45, 88.

17. S.C.F. Au Yeong and D.R. Eaton, Can.J.Chem., 1983, 61, 2431.

18. J.W. Akitt and W.S. McDonald, J.Magn.Res., 1984, 58, 401.

19. A.F. Masters, R.T.C. Brownlee, M.J. O'Connor and A.G. Wedd, Inorg.Chem., 1981, 20, 4183.

20. E.C. Alyea, R.E. Lenkinski and A. Somogyrari, Polyhedron, 1982, 1, 130.

21. J.A. Gerlt, P.C. Demore and S. Mehdi, J.Am.Chem.Soc., 1982, 104, 2848.

22. T. Andersson, T. Drakenberg, S. Forsén, E. Tholin and M. Swärd, J.Am.Chem.Soc., 1982, 104, 576.

23. M.A. Freeman, F.A. Schultz and C.N. Reilly, Inorg.Chem., 1982, 21, 567.

24. M. Minelli, J.L. Hubbard and J.H. Enemark, Inorg.Chem., 1984, 23, 970.

25. P.S. Belton, I.J. Cox and R.K. Harris, in press.

26. B.P. Shehan, M. Kony, R.T.C. Brownlee, M.J. O'Connor, and A.G. Wedd, J.Magn.Res., in press.

27. S.F. Gheller, T.W. Hambley, R.T.C. Brownlee, M.J. O'Connor, M.R. Snow and A.G. Wedd, J.Am.Chem.Soc., 1983, 105, 1527.

28. D.I. Hoult, J.Magn.Res., 1984, 57, 394.

29. N.F. Ramsey, Phys.Res., 1950, 78, 699.

30. J. Mason, Adv.Inorg.Chem.Radiochem., 1976, 18, 197.

31. J. Mason, ibid., 1979, 22, 199.

32. R.G. Kidd, "Annual Reports on NMR Spectroscopy", Ed. G.A. Webb, Vol. 10A, "Nuclear Shielding of the Transition Metals", Academic Press, 1980.

33. A. Saika and C.P. Slichter, J.Chem.Phys., 1954, 22, 26.

34. M. Karplus and J.A. Pople, ibid., 1963, 38, 2803.

35. G.M. Bodner, M.P. May and L.E. McKinney, Inorg.Chem., 1980, 19, 1951, and references therein.

36. P.S. Braterman, D.W. Milne, E.W. Randall and E. Rosenberg, J.Chem.Soc. Dalton Trans., 1973, 1027.

37. O.A. Gansav, D.A. Schexuayder and B.Y. Kimura, J.Am.Chem.Soc., 1972, 94, 3406.

38. J.P. Hickey, J.R. Wilkinson, and L.J. Todd, J.Organomet. Chem., 1979, 179, 59.

39. J.W. Gleeson and R.W. Vaughan, J.Chem.Phys., 1983, 78, 5384.

40. W. Buchner and W.A. Schenk, J.Magn.Res., 1982, 48, 148.

41. W. Buchner and W.A. Schenk, Inorg.Chem., 1984, 23, 132 and references therein.

42. S. Donovan-Mtunzi, R.L. Richards and J. Mason, J.Chem. Soc. Dalton Trans., in press.

43. M. Sano, Y. Yoshikawa and H. Yamatera, Inorg.Chem., 1982, 21, 2521.

44. J. Chatt, C.T. Kan, G.J. Leigh, C.J. Pickett and D.R. Stanley, J.Chem.Soc. Dalton Trans., 1980, 2032.

45. A.M. Bond, S.W. Carr, R. Colton and D.P. Kelly, Inorg.Chem., 1983, 22, 989.

46. A.M. Bond communication to C.J. Pickett.

47. H.E. Toma, J.A. Vasin and J.M. Malin, Inorg.Chim.Acta, 1979, 33, C157.

48. T.H. Lowry and K.S. Richardson, "Mechanism and Theory in Organic Chemistry", Harper and Row, New York 1976.

49. T. Nakano, Bull.Chem.Soc.Jpn., 1977, 50, 661.

50. C.K. Jorgensen, "Absorption Spectra and Chemical Bonding in Complexes", Pergamon, Oxford, 1962.

51. R. Weiss and J.G. Verkade, Inorg.Chem., 1979, 18, 529.

52. J.S. Griffith and L.E. Orgel, Trans.Faraday Soc., 1957, 53, 601.

53. E.A.C. Lucken, K. Noak and D.F. Williams, J.Chem.Soc.A, 1967, 148.

54. D. Rehder, H-C. Bechtold, A. Kececi, H. Schmidt and M. Siewing, Z.Naturforsch, 1982, 37b, 631 and references therein.

55. F. Näizmann, D. Rehder and V. Park, Inorg.Chim.Acta, 1984, 84, 117.

56. D. Rehder and K. Ihmels, ibid, 1983, 76, L313.

57. M. Herbehold and H. Trampisch, Z.Naturforsch, 1982, 37b, 614.

58. R. Talay and D. Rehder, Inorg.Chim.Acta, 1983, 77, L175.

59. F. Calderazzo, E.A.C. Lucken and D.F. Williams, J.Chem. Soc.A, 1967, 154.

60. G.T. Andrews, I.J. Colqohoun, W. McFarlane and S.O. Grim, J.Chem.Soc. Dalton Trans., 1982, 2353.

61. J.M. Schulman and T. Venanzi, J.Am.Chem.Soc., 1976, 98, 6739.

References - Chapter 3

1. J. Chatt, A.J. Pearman and R.L. Richards, J.Chem.Soc. Dalton Trans., 1976, 1520.
2. C.T. Kan, P.B. Hitchcock and R.L. Richards, ibid, 1982, 79.
3. G.E. Bossard, D.C. Busby, M. Chang, T.A. George and S.D.A. Iske Jr., J.Am.Chem.Soc., 1980, 102, 1001.
4. D.C. Busby, T.A. George, S.D.A. Iske Jr., and S.D. Wagner, Inorg.Chem., 1981, 20, 22.
5. J. Mason, Chem.Rev., 1981, 81, 205.
6. G.A. Olah, B.P. Gupta and S.C. Narang, J.Am.Chem.Soc., 1979, 101, 5317.
7. W. Buchner and W.A. Schlenk, Inorg.Chem., 1984, 23, 132 and references therein.
8. R. Botto, B.W.S. Kolthammer, P. Legzdins and J.D. Roberts, Inorg.Chem., 1979, 18, 2049.
9. J.W. Gleeson and W.R. Vaughan, J.Chem.Phys., 1983, 78, 5385.
10. J. Mason, D.M.P. Mingos, J. Schaefer, D. Sherman and E.O. Stejskal, in press.
11. D.R. Lloyd and E.W. Schlag, Inorg.Chem., 1969, 8, 2544.
12. R. Hoffmann, M.M.L. Chen, M. Elion, A.R. Rossi and D.M.P. Mingos, Inorg.Chem., 1974, 13, 2666.
13. J.L. Hubbard and D.L. Lichtenberger, Inorg.Chem., 1980, 19, 3865.
14. S. Donovan-Mtunzi, R.L. Richards and J. Mason, ibid, 1984, 1329.

15. R.O. Duthaler, H.G. Förster and S.D. Roberts, J.Am.Chem. Soc., 1978, 100, 4974.

16. D.L. Dubois and R. Hoffmann, Nouv.J.Chim., 1977, 1, 479.

17. J. Chatt, C.T. Kan, G.J. Leigh, C.J. Pickett and D.R. Stanley, J.Chem.Soc. Dalton Trans., 1980, 2032.

18. B.L. Haymore and J.A. Ibers, Inorg.Chem., 1975, 14, 3060.

19. M. Minelli, J.L. Hubbard and J.H. Enemark, Inorg.Chem., 1984, 23, 970.

20. A.S. Pregosin and R.W. Kunz, "NMR Basic Principles and Progress", Eds. P. Diehl, E. Fluck and R. Kosfeld, Vol. 16 "^{31}P and ^{13}C NMR of Transition Metal Phosphine Complexes".

21. R. Grieves and J. Mason, unpublished work.

22. A.D. Buckingham and P.J. Stephens, J.Chem.Soc. London, 1964, 2747.

23. R.R. Dean and J.C. Green, J.Chem.Soc.A, 1968, 3047.

References - Chapter 4

1. J.H. Enemark in "Nitrogen Fixation: The Chemical-Biochemical-Genetic Interface" eds. W.E. Newton and A. Müller, Plenum Press, New York 1983.
2. R.T.C. Brownlee, J.H. Enemark, M. Minelli, M.J. O'Connor and A.G. Wedd, Coord.Chem.Rev., 1984 in press.
3. S.F. Gheller, P.A. Gazzana, A.F. Masters, R.T.C. Brownlee, M.J. O'Connor, A.G. Wedd, J.R. Rodgers and M.R. Snow, Inorg.Chim.Acta, 1981, 54, L131.
4. R.G. Kidd, "Annual Reports on NMR Spectroscopy", ed. G.A. Webb, Vol. 10A, "Nuclear Shielding of the Transition Metals" Acad. Press, 1980.
5. R. Talay and D. Rehder, Inorg.Chim.Acta, 1983, 77, L175.

6a. M. Minelli, J.H. Enemark, K. Wieghardt and M. Hahn, Inorg.Chem., 1983, 22, 3952 and references therein.

6b. M. Minelli, K. Yamanouchi , J.H. Enemark, P. Subramanian, B.P. Kaul and J.T. Spence, Inorg.Chem., 1984, 23, 2554.

7. S.F. Gheller, R.T.C. Brownlee, M.J. O'Connor and A.G. Wedd, "Proc. 4th Int.Conf. on the Chemistry and Uses of Molybdenum", eds. H.E. Barry and P.C.H. Mitchell, Climax Molybdenum Co., Ann Arbor, Michigan, 1982, p.67.
8. E.C. Alyea and A. Somogyvari, ibid., p.46.
9. A.F. Masters, G.E. Bossard, T.A. George, R.T.C. Brownlee, M.J. O'Connor, and A.G. Wedd, Inorg.Chem., 1983, 22, 908.
10. R. Grieves, unpublished work.

11. Y.J. LeGall, M.M. Kubicki, and F.Y. Petillon, J.Organomet.Chem., 1981, 221, 287.

12. R.T.C. Brownlee, A.F. Masters, M.J. O'Connor, A.G. Wedd, H.A. Kimlin and J.D. Cotton, Org.Mag.Res., 1982, 20, 73.

13. A.F. Masters, R.T.C. Brownlee, M.J. O'Connor and A.G. Wedd, Inorg.Chem., 1981, 20, 4183.

14. S. Dysart, J. Georgii and B.E. Mann, J.Organomet.Chem., 1981, 213, C10.

15. E.C. Alyea, R.E. Lenkinski and A. Somogyvari, Polyhedron, 1982, 1, 133.

16. J.T. Bailey, R.J. Clark and G.C. Levy, Inorg.Chem., 1982, 21, 2085.

17. G.T. Andrews, I.J. Colquhoun, W. McFarlane and S.O. Grim, J.Chem.Soc. Dalton Trans., 1982, 2353.

18. G.M. Gray and C.S. Kraihanzel, Inorg.Chem., 1983, 22, 2959 and references therein.

19. G.M. Gray and R.J. Gray, Organometallics, 1983, 2, 1026.

20. P. Jaitner and W. Wohlgenannt, Monatsh.Chem., 1982, 113, 699.

21. E.C. Alyea and A. Somogyvari, Inorg.Chim.Acta, 1984, 83, L49.

22. S. Donovan-Mtunzi, D. Phil. Thesis, Sussex University, 1982.

23. M. Minelli, J.L. Hubbard, K.A. Christensen and J.H. Enemark, Inorg.Chem., 1983, 22, 2652.

24. P.E. Hansen, "Ann. Revs. NMR Spect.", ed. G.A. Webb, Vol. 15, p.106, "Isotope Effects on Nuclear Shielding", Acad. Press, London 1983.

25. S.N. Anderson, D.L. Hughes and R.L. Richards, J.Chem. Soc.,Chem.Commun., 1984, 958.

26. D. Rheder, J.Magn.Res., 1980, 38, 419 and references therein.

27. M. Modh.Ali, D. Phil. Thesis, Sussex University, 1984.

28. P.S. Pregosin and R.W. King, "NMR Basic Principles and Progress", eds. P. Diehl, E. Fluck and R. Kosfeld, Vol. 16, "^{31}P and ^{13}C NMR of Transition Metal Phosphine Complexes".

29. R. Alvarez, E. Carmona, M.L. Poveda and R. Sanchez-Delgado, J.Am.Chem.Soc., 1984, 106, 2731.

30. E. Carmona, J.M. Marin, M.L. Poveda, J.L. Atwood and R.D. Rogers, J.Am.Chem.Soc., 1983, 105, 3014.

31. E. Carmona, personal communication.

32. J.W. Byrne, H.U. Blaser and J.A. Osborn, J.Am.Chem.Soc., 1975, 97, 3871.

33. J. Chatt, C.M. Elson, A.J.L. Pombeiro, R.L. Richards and G.H.D. Royston, J.Chem.Soc. Dalton Trans., 1978, 165.

34. M. Sato, T. Tatsumi, T. Kodama, M. Hidai, T. Uchida, and Y. Uchida, J.Am.Chem.Soc., 1978, 100, 4447.

35. D.R. Stanley, D. Phil. Thesis, Sussex University, 1980.

36. T. Tatsumi, H. Tominaga, M. Hidai and Y. Uchida, J.Organomet.Chem., 1980, 199, 63.

37. T. Tatsumi, H. Tominaga, M. Hidai, and Y. Uchida, Chem.Lett., 1977, 37.

38. P.M. Triechel, Adv.Organomet.Chem., 1973, 11, 21.

39. G.M. Bancroft, M.J. Mays, B.E. Prater and F.B. Stefanini, J.Chem.Soc.(A), 1970, 2146.

40. G.M. Bancroft, K.D. Butler, L.E. Manzer, A. Shaver and J.E.H. Ward, Can.J.Chem., 1974, 52, 782.

41. J.P. Crow, W.R. Cullen, F.G. Hessing, J.R. Sams and R.L. Tupping, Inorg.Chem., 1971, 10, 1616.

42. R.D. Feltham and P. Brant, J.Am.Chem.Soc., 1982, 104, 641 and references therein.

43. R. Alvarez, E. Carmona, E. Gutierrez-Puebla, J.M. Mavin, A. Monge and M.L. Poveda, in press.

44. J.G. Verkade, Coord.Chem.Rev., 1972/3, 9, 1.

45. D.S. Milbraith, J.G. Verkade and R.J. Clark, Inorg. Nucl.Chem.Lett., 1976, 12, 921.

References - Chapter 5

1. D.C. Dubois and R. Hoffmann, Nouv.J.Chim., 1977, 1, 479.
2. J.H. Enemark and R.D. Feltham, Coord.Chem.Rev., 1974, 13, 339.
3. R. Hoffmann, M.M.L. Chen, M. Elian, A.R. Rossi and D.M.P. Mingos, Inorg.Chem., 1974, 13, 2666.
4. R.A. Henderson, G.J. Leigh and C.J. Pickett, Adv.Inorg. Chem.Radiochem., 1983, 27, 197.
5. B.L. Haymore and J.A. Ibers, Inorg.Chem., 1975, 14, 2784.
6. B.L. Haymore and J.A. Ibers, ibid., 1975, 14, 3060.
7. D. Sutton, Chem.Soc.Rev., 1975, 443.
8. K.R. Laing, S.D. Robinson and M.F. Uttley, J.Chem.Soc. Dalton Trans., 1973, 2713.
9. J.A. Ibers and B.L. Haymore, Inorg.Chem., 1975, 14, 1369.
10. G.R. Clark, K.R. Grundy, W.R. Roper, J.M. Waters and K.R. Whittle, J.Chem.Soc.,Chem.Commun., 1972, 119.
11. M. Cowie, B.L. Haymore and J.A. Ibers, Inorg.Chem., 1975, 14, 2617.
12. B.L. Haymore and J.A. Ibers, J.Am.Chem.Soc., 1973, 95, 3052.

13a. K.D. Schramm and J.A. Ibers, J.Am.Chem.Soc., 1978, 100, 2932.

13b. K.D. Schramm and J.A. Ibers, Inorg.Chem., 1980, 19, 1231.

14. J.A. Ibers, M. Cowie and B.L. Haymore, J.Am.Chem.Soc., 1976, 98, 7608.

15. A.P. Gaughan, Jr., B.L. Haymore, J.A. Ibers, W.H. Myers, T.E. Nappier, Jr., and D.W. Meek, J.Am.Chem.Soc., 1973, 95, 6859.

16. R.E. Cobbledick, F.W.B. Einstein, N. Farrell, A.B. Gilchrist and D. Sutton, J.Chem.Soc. Dalton Trans., 1977, 373.

17. D.M.P. Mingos and J.A. Ibers, Inorg.Chem., 1971, 10, 1035.

18. G.W. Parshall, J.Am.Chem.Soc., 1965, 87, 2133.

19. S. Korsgrod and J.A. Ibers, Inorg.Chem., 1975, 14, 2298.

20. A. Gainsford and R. Mason, unpublished work.

21. J.R. Dilworth, D.Phil. Thesis, University of Sussex, 1970.

22. M.W. Bishop, G. Butler, J. Chatt, J.R. Dilworth and G.J. Leigh, J.Chem.Soc. Dalton Trans., 1979, 1843.

23. J.R. Dilworth, C.T. Kan, R.L. Richards, J. Mason and I.A. Stenhouse, J.Organomet.Chem., 1980, 201, C24.

24. J.R. Dilworth, S. Donovan-Mtunzi, C.T. Kan, R.L. Richards and J. Mason, Inorg.Chim.Acta, 1981, 53, L161.

25. R.L. Richards, unpublished work.

26. B.L. Haymore, unpublished results.

27. R.O. Duthaler, H.G. Forster and J.D. Roberts, J.Am.Chem. Soc., 1978, 100, 4974.

28. A.L. Blumenfeld, V.C. Lenenko, B. Lorentz, I. Mobins, M. Wahren, W.B. Shur and M.E. Volpin, Dokl.Akad.Nauk. S.S.S.R., 1980, 251, 611.

29. S. Donovan-Mtunzi, R.L. Richards and J. Mason, J.Chem. Soc. Dalton Trans., 1984, 469 and references therein.

30. D.L. Thorn, T.H. Tulip and J.A. Ibers, J.Chem.Soc. Dalton Trans., 1979, 2022.

31. S. Donovan-Mtunzi, R.L. Richards and J. Mason, J.Chem. Soc. Dalton Trans., 1984, 1329.

32. W. Witanowski, L. Stefaniak and G.A. Webb, "Annual Reports on NMR Spectroscopy", Ed. G.A. Webb, Vol. 11B, "Nitrogen NMR Spectroscopy", Acad. Press, London 1981.

33. J. Mason and W. van Bronswijk, J.Chem.Soc.(A), 1971, 791.

34. R.O. Duthaler and J.D. Roberts, J.Am.Chem.Soc., 1978, 100, 4969.

35. D.H. Evans, D.M.P. Mingos, J. Mason and A. Richards, J.Organomet.Chem., 1983, 249, 293.

36. L.K. Bell, J. Mason, D.M.P. Mingos and D.G. Tew, Inorg.Chem., 1983, 22, 3497.

37a. L.K. Bell, D.M.P. Mingos, D.G. Tew, L.F. Larkworthy, B. Sandell, D.C. Povey and J. Mason, J.Chem.Soc., Chem.Commun., 1983, 125.

37b. J. Bultitude, L.F. Larkworthy, J. Mason, D.C. Povey and B. Sandell, Inorg.Chem., in press.

38. L.O. Andersson, J. Mason and W. van Bronswijk, J.Chem. Soc.(A), 1970, 296.

39. J. Mason, Chem.Rev., 1981, 81, 205.

40a. C.F. Barrientos-Penna, F.W.B. Einstein, T. Jones and D. Sutton, Inorg.Chem., 1982, 21, 2578.

40b. F.W.B. Einstein, T. Jones, A.J.L. Hanlin and D. Sutton, ibid., 1982, 21, 2585.

41. J.R. Dilworth, S.A. Harrison, D.R.M. Walton and E. Schweda, Inorg.Chem., in press.

42. J.A. Carroll and D. Sutton, Inorg.Chem., 1980, 19, 3137.

43. C.F. Barrientos-Penna, C.F. Campana, F.W.B. Einstein, T. Jones, D. Sutton and A.S. Tracey, Inorg.Chem., 1984, 23, 363.

44. W.A. Nugent and B.L. Haymore, Coord.Chem.Rev., 1980, 31, 123.

45. G.V. Goeden and B.L. Haymore, Inorg.Chem., 1983, 22, 157.

46. B.L. Haymore, E.A. Maatta and R.A.D. Wentworth, J.Am.Chem.Soc., 1979, 101, 2063.

47. S.M. Rocklage and R.R. Schrock, J.Am.Chem.Soc., 1982, 104, 3077.

48. O.R. Chambers, M.E. Harrison, D.S. Rycroft, D.W.A. Sharp and J.M. Winfield, J.Chem.Res., 1977, (S) 150, (M) 1849.

49. J. Errington, personal communication to J. Mason.

50. M.R. Churchill and H.J. Wasserman, Inorg.Chem., 1982, 21, 223.

51. D.C. Bradley, M.B. Hursthouse, K.M. Abdul Malik, A.J. Nielsen, and R.L. Short, J.Chem.Soc. Dalton Trans., 1983, 2651.

52. J. Mason, D.M.P. Mingos, D. Sherman and R.W.M. Wardle, J.Chem.Soc.,Chem.Commun., 1984, 1223.

53. J. Mason, D.M.P. Mingos, J. Schaefer, D. Sherman and E.O. Stejskal, in press.

54. K. Dehnicke and J. Strähle, Angew.Chem.Intl.Ed.Engl., 1981, 20, 413.

55. B.L. Haymore, personal communication.

56. J.R. Dilworth, P.L. Dahlstrom, J.R. Hyde and J. Zubieta, Inorg.Chim.Acta, 1983, 71, 21.

57. M.B. Hursthouse and M. Motevalli, J.Chem.Soc. Dalton Trans., 1979, 1362.

58. E. Forsellini, V. Casellato, R. Graziani and L. Magon, Acta.Cryst., 1982, B38, 3081.

59. P.W.R. Corfield, R.J. Doedens, and J.A. Ibers, Inorg. Chem., 1967, 6, 197.

60. J. Chatt and B.T. Heaton, J.Chem.Soc.(A), 1971, 705.

61. D. Bright and J.A. Ibers, Inorg.Chem., 1969, 8, 709 and references therein.

62. E.I. Stiefel, Prog.Inorg.Chem., 1977, 22, 1.

63. L. Manojlovic-Muir, J. Chem.Soc.(A), 1971, 2796.

64. L. Manojlovic-Muir and K.W. Muir, J.Chem.Soc. Dalton Trans., 1972, 686.

65. A.V. Butcher and J. Chatt, J.Chem.Soc.(A), 1970, 2652.

66. E. Carmona, A. Galindo, L. Sanchez, A.J. Nielson and G. Wilkinson, Polyhedron, 1984, 3, 347.

References - Chapter 6

1. J. Chatt, A.J. Pearman and R.L. Richards, Nature, 1975, 253, 39.
2. J. Chatt, J.R. Dilworth, and R.L. Richards, Chem.Rev., 1978, 78, 589.
3. R.L. Richards, "New Trends in the Chemistry of Nitrogen Fixation", Ed. J. Chatt, L.M. da Camâra Pina and R.L. Richards, Acad.Press, London 1980.
4. R.A. Henderson, G.J. Leigh and C.J. Pickett, Adv.Inorg. Chem.Radiochem., 1983, 27, 197.
5. J. Chatt, A.J. Pearman and R.L. Richards, J.Chem.Soc. Dalton Trans., 1977, 1852.
6. "Current Perspectives in Nitrogen Fixation"(Proc. 4th Int.Symp. Nitrogen Fixation) Ed. A.H. Gibson and W.E. Newton, Australian Acad. Sci., Canberra, 1981.
7. T. Takahashi, Y. Mizobe, M. Sato, Y. Uchida and M. Hidai, J.Am.Chem.Soc., 1980, 102, 7461.
8. S.N. Anderson, M.E. Fakley, R.L. Richards and J. Chatt, J.Chem.Soc. Dalton Trans., 1981, 1973.
9. J.A. Baumann and T.A. George, J.Am.Chem.Soc., 1980, 102, 6154.
10. T.A. George and L.M. Koczon, ibid, 1983, 105, 6334.
11. G.E. Bossard, T.A. George, D.B. Howell and R.K. Lester, Proc.Int.Conf.Chem. Uses Molybd. 4th, 1982.
12. G.E. Bossard, T.A. George, D.B. Howell, L.M. Koczon and R.K. Lester, Inorg.Chem., 1983, 22, 1968.
13. T.A. George, personal communication to C.J. Pickett

14. S. Donovan-Mtunzi, R.L. Richards, and J. Mason, J.Chem.Soc. Dalton Trans., 1984, 1329.

15. R.A. Henderson and R.L. Richards, unpublished work.

16. S. Donovan-Mtunzi, R.L. Richards and J. Mason, J.Chem.Soc. Dalton Trans., 1984, 469.

17. E. Carmona, J.M. Marin, M.L. Poreda, J.L. Atwood, and R.D. Rogers, J.Am.Chem.Soc., 1983, 105, 3014.

18. R.L. Richards, unpublished work.

19. A. Galindo, unpublished work.

20. J. Chatt, A.J. Pearman and R.L. Richards, J.Chem.Soc. Dalton Trans., 1978, 1766.

21. J. Mason, Chem.Rev., 1981, 81, 205.

22. W. McFarlane and B. Wrackmeyer, J.Chem.Soc. Dalton Trans., 1976, 2351.

23. H.H. Sisler, A. Sankis, H.S. Ahuja, R.J. Drago and N.C. Smith, J.Am.Chem.Soc., 1959, 81, 2982.

24. R.A. Henderson, unpublished work.

25. A.J. Pearman, D. Phil. Thesis, University of Sussex, 1976.